ANALYTICAL DIAGNOSTIC MEASUREMENTS IN FLAMES
BY LASER EXCITED FLUORESCENCE SPECTROSCOPY

BY

MELANIE LOUISE ELDER

A DISSERTATION PRESENTED TO THE GRADUATE COUNCIL
OF THE UNIVERSITY OF FLORIDA IN
PARTIAL FULFILLMENT OF THE REQUIREMENTS
FOR THE DEGREE OF DOCTOR OF PHILOSOPHY

UNIVERSITY OF FLORIDA

1983

TABLE OF CONTENTS

                        iii

Abstract of Dissertation Presented to the Graduate
Council of the University of Florida in Partial
Fulfillment of the Requirements for the Degree
of Doctor of Philosophy

ANALYTICAL DIAGNOSTIC MEASUREMENTS IN FLAMES BY
LASER EXCITED FLUORESCENCE SPECTROSCOPY

By

Melanie Louise Elder

August 1983

Chairman: J.D. Winefordner
Major Department: Chemistry

The laser excited thermally assisted fluorescence
(THAF) technique has been reported to be a reliable method
for the measurement of spatially and temporally resolved
flame temperatures. THAF involves the monitoring of fluores-
cence from collisionally excited levels in the thermo-
metric seed (Tl, In, OH, etc.) upon laser excitation. Valid
THAF flame temperatures can be measured if, during the
laser pulse, a partial Boltzmann equilibrium over the col-
lisionally excited levels is established and steady state
fluorescence is measured.

The measurement of THAF flame temperatures as a func-
tion of the thermometric seed and the flame "quenching"
environment provided insight into the potential utiliza-
tion of THAF as an analytical diagnostic method. The
effect of the measurement procedure itself on the resulting

temperature determinations in terms of time-averaged detection of the fluorescence pulse vs. time-resolved detection of the peak fluorescence was also investigated.

THAF from the higher levels of Na was detected upon single-photon and two-photon resonance excitation. The Na atomic population distributions observed in the nine $C_2H_2/O_2/Ar$ or $C_2H_2/O_2/N_2$ flames that range in temperature from 2000 K to 2500 K indicated that partial Boltzmann equilibrium is not reached during the $\sim$ 5 ns laser pulse. Saturation curves constructed from measurements of time-averaged and time-resolved fluorescence indicate that steady state may not be reached for Na in the Ar-diluted flames and that Na under $\gtrsim$ 5 ns excitation will not provide valid local flame temperatures.

THAF measurements from Tl indicate that a partial Boltzmann equilibrium is attained during $\sim$ 5 ns laser excitation. Saturation curves from measurements of time-averaged and time-resolved fluorescence confirm that steady state is reached for Tl in both "quenching" and "nonquenching" flames.

Instantaneous single-shot THAF temperatures are reported for three $C_2H_2/O_2/Ar$ flames. Comparison with averaged THAF temperature measurements and reversal temperature values confirm the high accuracy and precision ($\gtrsim\pm$ 10 K) obtainable with single-shot THAF and its potential for use as a thermometric method for laboratory and turbulent flames.

INTRODUCTION

The development of the capability for local sensing
of flame parameters on a time-resolved basis continues to be
the principal impetus to the incorporation and application
of state of the art scientific techniques to flame diagnostics.
The major areas of investigation consist of measurements of
temperature, species concentrations, and gas velocities.

The modelling of combustion processes includes radical
recombination and energy releasing combustion reactions,
relaxation effects, production of thermal and nonthermal
radiation, inter- and intra-molecular energy transfer, ioni-
zation, excited state chemical reactions, dissociation and
atomization mechanisms, and particulate formation processes
[1-15]. Fundamental flame diagnostics have benefited through
contributions from physical and analytical spectroscopy,
physics, chemistry, and engineering flow dynamics. Flames
which range in type and nature from well-characterized
laboratory flames to three-dimensional, turbulent flames and
combustors and which range in temperature from < 1000 K to
> 3500 K need to be studied in detail.

The determination of the existence of local thermo-
dynamic equilibrium (LTE) throughout the flame is the neces-
sary first step in the characterization of virtually all dynamic

1

flame processes (see Appendix A) [2, 3]. Information derived from the flame "temperature" can be directly related to the concomitant profiles of species concentration, velocity and pressure fields, and particulate formation gradients axially and radially across the flame. The measurement of point temperatures (≤ 1 mm^3 probed volume) on the time scale of transient flame fluctuations ($\leq 10^{-6}$ s) [2, 6, 14] facilitates the complete understanding of combustion reaction phenomena, provides indications of design problems in practical combustion flames, and accordingly promotes the development of enhanced combustor efficiencies. In this vein, investigations by mechanical engineers are more generally directed toward the utilization of temperature measurements in the modelling of flame combustion on a macroscopic basis and toward their application in jet and internal combustion engines, reactors, and plasmas characterized by high temperatures, pressures, and significant external perturbation.

Physical spectroscopists are interested in the measurement of flame temperatures in order to evaluate temperature-dependent parameters such as reaction and collisional rates and cross sections, spectral line (band) intensities and profiles, population distributions within the atomic and molecular energy levels, and atomization efficiencies. These fundamental parameters are needed to describe the processes and interactions which occur within the flame and which include molecular dissociation, ionization, collisional population redistribution, radiative excitation-deexcitation of atoms and molecules at low and high source

intensities, and reactivity differences between ground
state and excited level flame species [2, 6].

Analytical spectroscopists are interested in flame tem-
perature measurements in order to optimize methods for sensi-
tive, analyte-specific spectroscopic detection. The use of
laboratory flames as atomizer cells in atomic absorption and
atomic fluorescence spectroscopy has delivered sub-part-per-
billion (< 10^2-10^8 atoms/cm^3 of solution) limits of detection
for many elements [1, 16-22]. In addition, the reducing
atmosphere, background emission, and temperature of the flame
can be continuously varied to achieve the lowest detection
limit and accordingly the highest signal-to-noise ratio for
each analyte element by adjusting the relative proportion of
the fuel, oxidant, and diluent gases and thus the chemical
composition of the flame [1, 2]. The flame type can also be
varied in order to alter the flame chemical environment, at
least with respect to the concentration of quenching species
[23-28]. Flame temperature and composition gradients affect
the analyte atomization processes [29-33], the excitation
(and therefore the ground state population) of the analyte
species [2, 18, 34], the radiative quantum efficiency (maxi-
mum fluorescence line intensities) [1, 2, 24], and the analyte
ionization or chemical reaction losses [2, 35, 36]. Knowledge
of the fundamental flame properties, which are generally tem-
perature sensitive, is required for the attainment of the
optimal operating conditions in terms of detection limit,
sensitivity, selectivity, accuracy, linearity of signal

response to analyte concentration, and freedom from spectral and chemical interferences by concomitants in the sample or by native flame species, whether stable or unstable.

The involvement of analytical spectroscopy in flame diagnostics consists primarily of investigations into new experimental techniques and procedures, development of improved theoretical models describing the interactions of incident source radiation with flame species, and applications of these analytical methods for temperature and species concentration measurements not only to laboratory flames, but also to combustors and fires.

Laser Combustion Probes

With the advent of tunable dye lasers, scattering spectroscopic techniques (fluorescence, Rayleigh scattering, Raman scattering, Coherent Anti-Stokes Raman Spectroscopy (CARS), etc.) have remarkably expanded the scope and potential of available analytical flame diagnostic methods [1, 6, 7]. The use of a laser for the excitation of atomic and molecular flame species has several important advantages over conventional (low-intensity) source excitation and emission-based methods for temperature and species concentration measurements:

(i)   due to the low divergence of the collimated laser beam, the spatial resolution of the probed flame volume can be enhanced below 1 mm^3, without the need for spatial deconvolution.

(ii)   in conjunction with a gated detector, a pulsed dye laser
       can provide temporally resolved measurements ($< 10^{-6}$ s
       time scale).

(iii) due to the high spectral radiance achievable with high
       resolution laser excitation, very weak processes like
       multiphoton ionization and nonlinear phenomena, such as
       CARS, can be exploited.

(iv)   saturation of the pumped optical transition in fluores-
       cence spectroscopy can result in improvements in detec-
       tion limits and linear dynamic range and insensitivity
       of the signal to fluctuations in source intensity and
       fluorescence efficiency [1, 2, 37, 38].

(v)   the flexibility of many laser-based methods can poten-
       tially allow the use of several laser systems for
       simultaneous, nonintrusive, nonperturbing, local tem-
       perature and species concentration measurements on a
       time-resolved basis with minor system redundancy [7].

Laser-based diagnostic methods enable the measurements
of flame parameters for various atomic and molecular species
over a wide range of conditions with high spatial and temporal
resolution; the latter advantages are especially important,
because significant concentration disturbances can occur over
a 0.1 mm distance in the flame in $\gtrsim 10^{-6}$ s [6, 7].
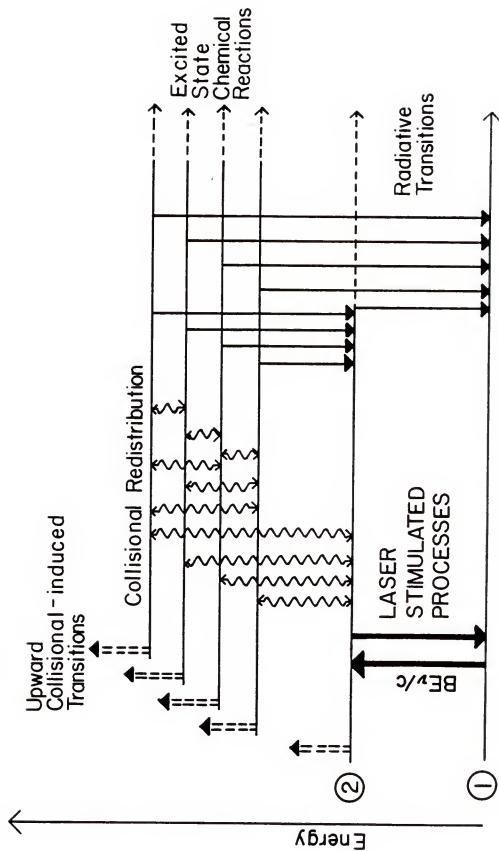
Most importantly, the attainment of <u>single-shot flame
temperatures</u> is required; specifically, a unique, local
temperature is measured during each laser pulse. The
achievement of single-shot temperatures at the highest

obtainable laser repetition rates will provide the most
specific and valuable information concerning the existence
of LTE in the flame and facilitates the complete character-
ization of even transient flame phenomena. The relaxation
times for the achievement of thermally equilibrated internal
energy distributions within each species and correspondingly
the lifetimes of the atomic and molecular energy levels are
on the order of 10^{-9}-10^{-7} s [2]. In contrast, the rates of
the combustion reactions which irreversibly perturb the
flame "equilibrium" and lead possibly to new "equilibrium"
states are on the order of $\gtrsim 10^{-6}$ s [2, 6, 7]. Therefore,
if single-shot temperatures can be measured during ~ 10^{-8} s
(excitation pulse length), the complex processes occurring
in the flame during the laser pulse will be apparently in
steady state. The attainment of this condition assumes no
significant secondary interactions, i.e., excited state
chemical reactions and collision induced ionization which
can disturb the thermalized internal energy distributions.

   Several laser-based diagnostic methods, including laser
saturated absorption, laser induced photoacoustic spectros-
copy, and laser Rayleigh scattering, are potentially applic-
able for flame temperature measurements (see Appendix A).
However, the most widely used techniques include laser
induced fluorescence (LIF), Raman scattering, and CARS.
LIF involves the sensitive detection of an emission transi-
tion arising from an upper electronic, vibrational, or rota-
tional energy state which had been radiatively excited via

Figure 1. Generalized diagram of the laser induced processes occurring within an atomic thermometric seed. Laser excitation of the electronic level 2 occurs from the ground state (level 1).

IONIZATION CONTINUUM

Energy

Upward Collisional-induced Transitions

Collisional Redistribution

Excited State Chemical Reactions

Radiative Transitions

LASER STIMULATED PROCESSES

BEν/c

②

①

absorption of one or more photons [1, 2]. Most atomic and many molecular species have electronic transitions amenable to laser excitation [6, 7]. Therefore, measurements of fluorescence within an internal degree of freedom can result in the determination of the corresponding population distribution and the Boltzmann or slope temperature [1, 2, 39, 40].

The fluorescence intensity is directly related to the fluorescence transition probability and is sensitive to competitive losses from collisional energy transfer to other levels, including the ground state, ionization, chemical reactions, molecular dissociation, and energy transfer to another molecule (see Fig. 1). These processes reduce the fluorescence by decreasing the efficiency of fluorescence transitions. However, collisions with major molecular species, such as N_2, can be exploited in temperature measurements via thermally assisted fluorescence (THAF) [40-44].

Thermally Assisted Fluorescence

Laser excitation promotes the population of atomic or molecular energy levels lying above the radiatively excited level to be far above thermal equilibrium (kT) values. A substantial fraction of the population of native flame species and thermometric seeds introduced into flames has been found to be redistributed among the higher levels (up to ~ 2 eV above the pumped level) as a result of laser excitation followed by collisions with flame gas species [36, 45-47]. If a partial Boltzmann population distribution can be established

over the excited levels during the laser pulse, then valid
excitation temperatures can be determined by THAF. THAF has
been successfully applied using Tl, Ga, and OH probes in
CH_4/air, gasoline/air, and C_2H_2/O_2/Ar flames [41-44].
Even if a partial Boltzmann equilibrium is not established
during the laser pulse, the relative excited state popula-
tion distribution can indicate deviations from LTE.

Information about the collisional processes which couple
the excited levels, including loss pathways, is required to
understand the laser excited fluorescence spectrum of the
thermometric species and to determine whether the excited
state population is in LTE or only rate-controlled. However,
because of the efficiency of energy transfer, emission prob-
abilities, etc., not every excited state which is collision-
ally populated will produce a detectable fluorescence signal
[2, 36]. Therefore, the observed fluorescence spectrum
characterizes the population of those levels which produce
detectable fluorescence and does not completely describe the
processes that the system undergoes during laser excitation.

Particularly in molecular species, the fluorescence
spectrum is often complicated by additional factors, e.g.,
vibrational and rotational relaxation in the upper and lower
electronic states, rotational energy transfer during the laser
pulse, differences in relative lifetimes, reactivities of the
lower and excited states, and the appearance of an interme-
diate metastable electronic state between two radiatively
pumped levels (see Appendix A) [6, 48-56]. In addition, the

molecular fluorescence spectrum is complicated by overlapping
of rotational lines from different vibrational bands at atmos-
pheric pressure [7, 9, 11]. In order to determine molecular
single-shot temperatures, the entire spectrum must be cap-
tured during a single laser pulse. Therefore, the utiliza-
tion of an atomic thermometric seed such as Tl, In, or Na
(via introduction of an inorganic salt) may provide valid
excitation temperatures avoiding the need for elaborate,
spectral isolation of vibrational and rotational fluores-
cence lines within selected bands and the evaluation of
vibrational-rotational relaxation effects.

Collisional Energy Transfer

When an electronically excited atom collides with
another flame species, an electronic transition may be in-
duced from the transfer of internal or relative transla-
tional energy between the collisional partners [2, 23, 52-57]:

$$A** + B* \rightleftarrows A* + B**$$
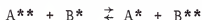
where

A** can be an electronically excited atom before collision,

B* is an excited or ground state collisional partner,

A* is the atom after collision in any other excited state
or in the ground state, and

B** is the collisional partner existing in another excited
energy state [58].

In general, different kinds of energy transfer, i.e.,
electronic energy $\leftrightarrow$ vibrational energy, vibrational energy

↔ translational energy, may occur to varying degrees of completeness in flames [2]. If A** is transferred to another excited state of the same multiplet, intramultiplet mixing (Na $3^2P_{3/2}$ ↔ Na $3^2P_{1/2}$) is said to occur [2, 58]. Inter-multiplet mixing refers to collisional transfer to another multiplet (Na $4^2P_{3/2}$ ↔ Na $3^2P_{3/2}$) [2, 58]. Quenching or mixing collisions are considered to be those collisions which transfer the excited state atom A** via nonradiative means to the ground state (Na $3^2P_{1/2}$ ↔ Na $3^2S_{1/2}$) or to another excited state (Na $5^2P_{1/2}$ ↔ Na $5^2S_{1/2}$) [2, 58, 59].

Most molecules, i.e., N_2, CO_2, CO, are very efficient quenchers because of the availability of many closely-spaced levels within the internal degrees of freedom in these molecu-lar collisional partners [2, 55, 60-63]. For most nonadiabatic mixing collisions, the collisional cross sections are on the order of 10^1-$10^2 \mathring{A}^2$ [2, 52-55, 58]. However, inert gas species, i.e., Ar, are especially inefficient in mixing or quenching energy transfer, most likely due to the nonavailability of suitable energy crossing points on the potential energy curves within the kT limit [2, 58]. Cross section upper limits of 10^2-$10^3 \mathring{A}^2$ have been suggested for inert gases [2, 64, 65]. Since the collisional rates are directly pro-portional to the reaction cross sections, it is apparent that the collisional rates for species collisions in inert gas-diluted flames are much smaller than the rates for spe-cies involved in collisions in N_2-based ("quenching") flames.

Excitation and deexcitation of flame species at atmospheric pressure occur predominantly by collisional interactions between the thermometric seed and either inert gas atoms or molecules and by photon emission and absorption. However, even for the most intense resonance transitions, the collisional rates are much larger than the spontaneous emission rates in flame gases consisting of efficient quenching species [1, 2]. Therefore, when pumped to a higher energy level via laser excitation, an atom may undergo various collisional, nonradiative transitions, directly to or in cascade to the lower lying levels and to the ground state. The resulting population distribution over all electronic levels therefore depends on sufficient collisions to partition available energy according to a partial Boltzmann equilibrium. If the collisional rates are insufficient to thermally redistribute the population in the laser excited level during the laser pulse, then the apparent measured flame temperature will not correspond to the LTE flame temperature (see Appendix A) [2, 36, 43]. Evaluation of the resulting THAF spectra for a particular species in flames having different quenching efficiencies should indicate the occurrence of nonLTE conditions. Non-Boltzmannian population distributions may be induced by weak collisional coupling and by perturbations in excited state-to-state collisional transfer (due to laser excitation) within the relaxation time needed to attain Boltzmann equilibrium.

Laser Enhanced Secondary Effects

Ionization

The ionization without external excitation of metals seeded in flames has been known for many years [2, 66-70]. It is well known that partial ionization of an analyte can produce a concave curvature in the analytical curve of growth at low analyte concentrations (< 30 ppm) [2, 71-73] and that hydrocarbon-based flames seem to stimulate the degree of ionization compared to hydrogen-based flames [71]; this effect is probably due to relative increases in the flame temperature and in the concentrations of free electrons and natural flame ions [2, 71]. The degree of ionization observed and its effect on atomic population distribution measurements depend strongly on the characteristics of the flame. Analyte ionization may interfere with the measurement and interpretation of energy transfer processes; the degree of perturbation depends on the "state" of thermal equilibrium existing in the flame and the effect of the measurement procedure itself on the phenomena being studied.

In addition to natural flame ionization occurring as a result of flame combustion, optogalvanic effects have been observed [2, 36, 74-79]. Laser enhanced ionization (LEI) consists of the detection of absorption spectra via measurement of current or flame conductivity changes. Several mechanisms have been proposed to explain LEI; however, it is generally agreed that LEI is due chiefly to photo-assisted ionization [2, 78, 79]:

$$A + h\nu \rightarrow A^* \qquad \text{resonance photon absorption}$$

$$A^* + M \rightarrow A^+ + e^- + M \quad \text{collisional ionization}$$

and

$$A^* + h\nu \rightarrow A^+ + e^- \qquad \text{radiative ionization.}$$

The latter process is unimportant in most cases.

The deexcitation, ionization, and recombination processes are assumed to be collision-dominated, at least for most molecular collision partners. As with electronic energy transfer collisions, noble gas atoms are highly inefficient in the excitation or ionization of thermometric seeds compared to molecular species such as N_2 or H_2O. The deviations from thermal equilibrium (as produced during the collisional ionization step) may be expected to be more severe in these Ar-diluted flames than in N_2-diluted flames, even for flames with temperatures near 2500 K [2].

Collisional ionization of the laser excited atoms will occur at an enhanced rate compared to the ionization of the thermal (kT) population of lower energy levels including the ground state. However, collisional energy transfer during laser excitation complicates the evaluation of the significance of flame ionization processes.

The ionization rate constant from each excited state is directly related to the energy difference between the laser excited state and the elemental ionization potential [74-77]. LEI is particularly significant for those atoms with lower ionization potentials and whose higher-lying atomic states

are excited. When saturation of the laser-excited transition occurs, the enhancement in the collisional ionization rate will affect the concentration of neutral atoms in the flame. Excited levels close (~ kT) to the ground state or to the ionization continuum should rapidly attain a new quasi-Saha-Boltzmann equilibrium distribution (see Appendix A) within 10^{-9}-10^{-10} s in atmospheric pressure flames [2, 36]. But the populations of those levels several kT above the ground state will suffer perturbing collisions which may not allow the attainment of Saha-Boltzmann equilibrium during the laser pulse or even after several microseconds [2]. If partial Saha equilibrium does not exist prior to the laser irradiation, deviations from the partial Boltzmann distributions for those levels (~ kT) near the ionization continuum may also occur. Therefore, LEI acts essentially as a physical disequilibrium process and may then influence the collisional population redistribution of the excited levels, whether or not deviations from Saha equilibrium occur prior to laser irradiation.

Chemical Reactions

Laser induced chemical interactions between the laser populated energy level and H_2 or H_2O flame constituents in atmospheric pressure, fuel rich flames (1700-2200 K) have been observed mainly for Na and Li [2, 80, 81]. During a ~ 1 µs laser pulse, within about 100 ns, a steady state redistribution can occur among the reactants and products (NaOH and NaH) such that the free atoms are drained into

metastable molecular sinks. However, unlike LEI which can still be significant during ~ 5 ns laser excitation, a short pulsed laser can be used to circumvent the problem of laser induced chemistry with native flame species [80].

Significance of Ionization and Excited State Chemistry

LEI and laser induced flame chemistry represent alternate collisional energy transfer processes which may compete with the sensitive detection of THAF. The determination of valid local flame temperatures may be affected, particularly if the actual achievement of LEI or the occurrence of excited state chemical reactions only during laser irradiation induces "losses" or perturbations to the population of the laser excited level and to the populations of neighboring collisionally excited levels. However, analyte ionization or chemical reactions may not affect the measurement of valid electronic temperatures if Saha-Boltzmann and mass-action equilibria can be reestablished during the laser pulse.

Collisional Population Redistribution in Na

The study of collisional energy transfer, particularly in Na, has centered mainly on the coupling between the first excited level and the ground state [23, 52-62]. Previous investigations have determined various collisional cross sections of the first excited state of alkali metals for specific collisional partners, primarily in molecular beam experiments [2, 82] and in vapor cells [2, 83-85, 86]. In order to evaluate the excitation and quenching mechanisms

and therefore the utility of Na as a fluorescence probe, Van Dijk et al. [36, 46] and Allen et al. [86] have extended these experiments to the study of the collisional interactions among the higher excited states in Na in $H_2/O_2/$ Ar and C_2H_2/air flames. They have evaluated population distributions under ~ 1 μs single-photon and two-photon resonance excitations.

The population redistribution among the upper excited states in flames is expected to be collision-dominated for two reasons:

(i)   the efficiency of several flame constituents (including residual quenching by flame decomposition products such as H_2O, CO, and CO_2) for inducing collisional energy transfer among higher levels is relatively larger than the efficiency for the quenching of the first excited state [2, 55, 65, 71, 87], and

(ii) the increased number of transfer possibilities among the excited states and the small energy differences between the levels should induce an efficient excited state population redistribution from the laser excited level [2, 36].

If these collisional rates among the excited levels, including the radiatively pumped level, are fast enough to redistribute thermally the laser excited population during the laser pulse, then a partial Boltzmann equilibrium should be observed and valid THAF temperatures could be measured. The population of other excited electronic levels of Na via two-photon excitation can be utilized to study the state-specific energy transfer processes.

From Na fluorescence measurements in a H_2/O_2 (1710 K) flame under ~1 μs excitation [36, 46], strong collisional coupling between neighboring levels was observed when pumping the 3S→3D, 3S→4D, and 3S→5S two-photon resonance transitions (see Fig. 2). A partial Boltzmann equilibrium was reached between the 5S and 6S levels, between the 5D and 6S levels, and between the 5S and 5D levels. However, this flame exhibited relative population inversions between the pumped level and lower-lying states. Large deviations from Boltzmann equilibrium occurred when the 3D, 4S, or 3P levels were considered. These experiments conducted with Na under ~1 μs laser excitation in a relatively low "quenching" flame do indicate that a partial Boltzmann equilibrium can only be reached for specific levels and valid THAF temperatures could be determined from these collisionally excited levels.

Excited state fluorescence from Na in a "quenching" C_2H_2/air flame was observed also under ~1 μs laser excitation [86]. More than 95% of the excitation energy of Na atoms was quenched via collisions with primarily N_2. Significant ionization and the formation of highly excited reaction products may be present. Specific levels were excited (3S→3P, 3S→3D, 3S→4D, 3S→4P, 3S→5S), but also only certain transitions were monitored under each excitation mode. Multistep collisional processes were observed, e.g., upper state deactivation to the 4P or 3P levels and then 3P→3S transfer, instead of direct single-step quenching to the ground state. An apparent thermal disequilibrium was

Figure 2.   Na partial energy diagram showing fluorescence
            transitions in nm. Heavy arrows indicate the
            laser excited level. The single-photon
            resonance transition corresponds to the 589.0
            nm line, while the two-photon resonance transi-
            tions correspond to the 578.7 nm and the 602.2
            nm lines.
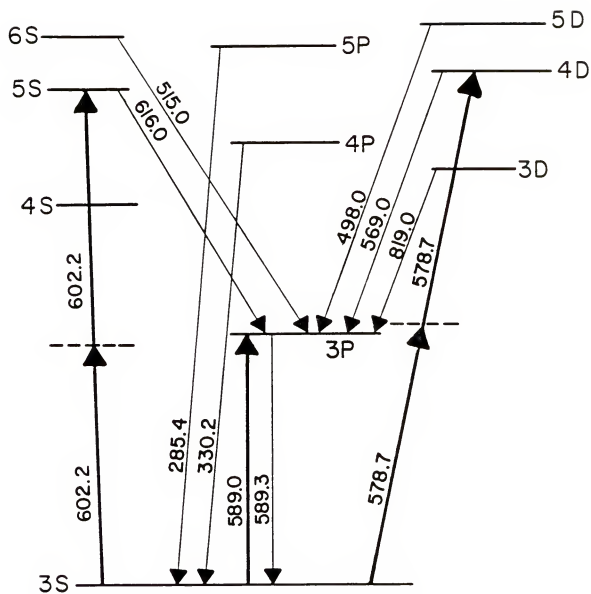
noted. However, even though a steady state population redistribution was assumed to be achieved, the observation that Na does not exhibit complete thermodynamic equilibrium under ~ 1 μs pulsed laser excitation is severely complicated by the occurrences of significant collision induced ionization and excited state chemical reactions. In addition, the effect of a change in collisional partner was not evaluated in either experiment.

Tl Thermally Assisted Fluorescence

Tl has been widely used in the past as a fluorescence thermometric seed (see Appendix A), particularly in the application of the two-line atomic fluorescence methods to flames ranging in temperature near 2500 K [39, 40, 88-90]. Tl has also been utilized for the measurements of THAF in CH_4/air, gasoline/air, and C_2H_2/O_2/Ar flames [41, 43, 44]. A partial Boltzmann equilibrium was observed for those upper levels above the laser excited level, particularly for the 6D, 7D, and 8S excited states (see Fig. 3). Intense laser excitation with ~ 5 ns and ~ 1 μs duration pulses produced detectable fluorescence ~ 1.9 eV above the laser excited level. Apparent steady state fluorescence was measured on a time-resolved basis (detection of peak fluorescence) and on a time-averaged basis (detection of fluorescence pulse within the boxcar averager gate). Some difficulties arose in the data interpretation due to relatively imprecise A (transition probability) values [43, 91-97].

Figure 3.   Tl partial energy diagram showing detected
             fluorescence transitions in nm. Heavy arrow
             indicates the laser excited 7S level at 377.6
             nm.
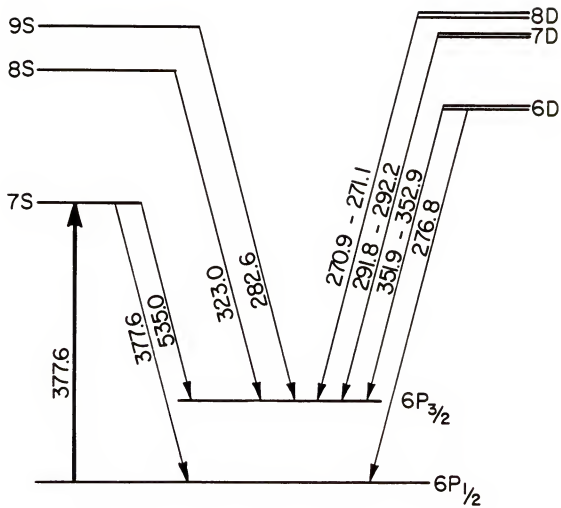
Fluorescence Measurement Methods

Time-resolved measurement of the peak fluorescence and time-averaging of the detected fluorescence pulse can produce different estimates of the relative population distributions and may therefore result in different apparent THAF temperatures [1, 48, 98-101]. The attainment of steady state fluorescence is required during the laser pulse for the determination of accurate THAF temperatures. However, the achievement of steady state level populations during the laser pulse is critically dependent upon the collisional and laser pumping rates and the lifetimes of the excited states [1, 98-106]. Consequently, the incident laser pulse which cannot be approximated as a time-independent step function produces fluorescence pulses whose time-averaged intensity will behave in a different way with laser power than the peak fluorescence intensity [1, 38].

The occurrences of steady state vs. transient level populations are reflected in relatively different onsets of saturation in saturation curves of fluorescence intensity vs. laser pulse energy (see Figs. 4 and 5) [18, 107-111]. Saturation occurs when the rates of deexcitation and excitation by stimulated absorption and emission become dominant over the collisional and spontaneous emission rates (see Fig. 4) [1, 2, 38]. However, if transient fluorescence is measured, the saturation curve constructed will deviate from the saturation curve corresponding to the detection of steady state fluorescence (see Fig. 5) [38, 111].

Figure 4.   Ideal saturation curve of log $B_{F_{steady\ state}}$ vs. log E_ν where B_F = fluorescence radiance ($J\ m^{-2}\ s^{-1}\ sr^{-1}$) and E_ν = incident laser spectral irradiance ($J\ m^{-2}\ s^{-1}\ Hz^{-1}$). Note that the equivalence between the magnitudes of the saturation irradiance, E_ν^s, at 50% $B_{F_{max}}$ and at the intersection of the linear and saturated ($B_{F_{max}}$) asymptotes.
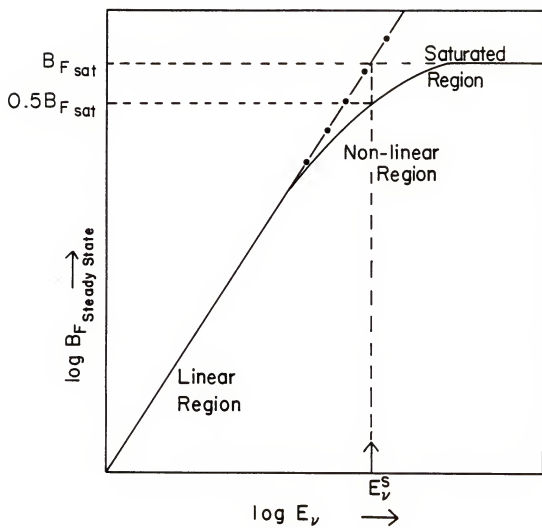
Figure 5. Saturation curves of log B_F (fluorescence radiance) vs. log E_ν (laser spectral irradiance) measured under ideal and nonideal experimental conditions.

Left: Saturation curve which corresponds to the detection of steady state fluorescence. Note the equivalence between the values of the saturation irradiance, E_ν^{sat}, at 50% B_{Fmax} and at the intersection of the linear and saturated asymptotes.

Right: Saturation curve which corresponds to the detection of transient fluorescence. Note the discrepancies between the values of E_ν^{sat} at 50% B_{Fmax} ($E_\nu^{sat}_{FS}$) and at the intersection of the linear and saturated asymptotes ($E_\nu^{sat}_{LA}$).

FLUORESCENCE RADIANCE, B_F

LASER IRRADIANCE, E_ν
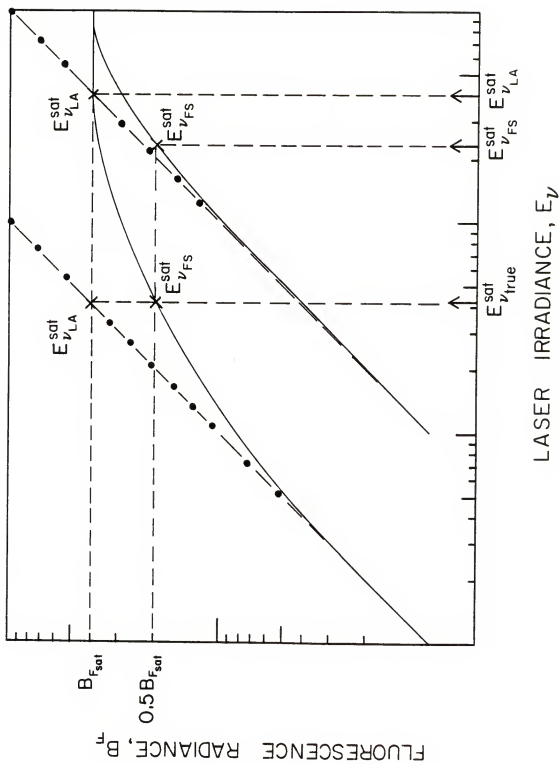
If complete saturation can be attained, two methods of determining the saturation parameter can be used [111]; the saturation parameter corresponds to the spectral irradiance required to obtain a steady state value of the excited state population which is 50% of the steady state saturation signal [111]. The saturation parameter (see Table 1) can be estimated by determining the laser power density at the fluorescence intensity which is 50% of the fully saturated intensity. In addition, the saturation parameter can be derived from the intersection of the linear and fully saturated asymptotes [111]. However, if the fluorescence detected corresponds to the measurement of transient excited state populations, the latter approach does not produce the same value as should be obtained from the fully saturated estimate. Technically, the saturation parameter evaluated from the experimental saturation curve under these conditions is meaningless, but the comparison between the two saturation parameter values, if saturation occurs and the experimental error is minimized, can be used to elucidate whether steady state is being established during the laser pulse [111]. As shown in Table 1, the saturation energy is proportional to the saturation parameter.

Table 1
Specific Terms and Relationships

I. E_ν = spectral irradiance (J m^{-2} s^{-1} Hz^{-1}),

   B_ν = spectral radiance (J m^{-2} s^{-1} Hz^{-1} sr^{-1}),

   ρ_ν = spectral energy density (J m^{-3} Hz^{-1}),

   ε = spectral energy per pulse (J).

II. $\rho_\nu = \dfrac{E_\nu}{c}$

   where c = speed of light (m/s).

   $\varepsilon = \rho_\nu \cdot \Delta V \cdot \Delta \nu$

   where ΔV = irradiated volume (m^{-3}),

      $\Delta \nu$ = laser bandwidth (Hz).

SPECIFIC AIMS

As observed from previous experiments [41-44], THAF from Tl, In, and OH can provide spatially and temporally resolved flame temperature measurements in certain flames. However, excitation temperatures which are dependent upon the attainment of steady state excited level populations in the thermometric seed and the emission of thermal radiation are highly sensitive to LTE perturbations occurring in the observed flame region. The detection of apparent nonthermal fluorescence may be due to deficiencies in the collisional energy transfer processes in the attainment of steady state Boltzmann equilibrium in the thermometric seed during the excitation and observation time periods. In effect, the optimal measurement of accurate and precise single-shot flame temperatures possessing ~ 5 ns temporal resolution requires the evaluation of THAF as functions of the thermometric seed, the flame environment, and the measurement method. Therefore, utilizing the theoretical basis for the measurement of THAF as described in the Theoretical Considerations section and according to the procedures described in the Experimental Measurements and Conditions section, the following studies were performed:

1. Na Thermally Assisted Fluorescence:

   i) Measurement of the excited state fluorescence spectra of Na under ~ 5 ns laser excitation in $C_2H_2/O_2/Ar$ and $C_2H_2/O_2/N_2$ flames by single-photon and two-photon resonance excitation.

   ii) Determination of the Na population distributions and the corresponding THAF temperatures.

   iii) Construction of saturation curves from time-resolved and time-averaged detection of fluorescence from radiatively and collisionally excited levels of Na and the estimation of the respective saturation energies.

2. Tl Thermally Assisted Fluorescence:

   i) Measurement of the excited state fluorescence spectra of Tl under ~ 5 ns resonance excitation in $C_2H_2/O_2/Ar$ and $C_2H_2/O_2/N_2$ flames.

   ii) Evaluation of the Tl population distributions and the determination of the corresponding THAF temperatures.

   iii) Analysis of the steady state excited level populations through construction of time-resolved and time-averaged saturation curves and the determination of the corresponding saturation energies.

   iv) Evaluation of several experimental approaches for the measurement of single-pulse THAF flame temperatures.

   v) Measurement of single-shot THAF temperatures with optimal precision and accuracy.

THEORETICAL CONSIDERATIONS

In this section, theoretical models are evaluated in order to describe the interactions of atoms dispersed within an atmospheric pressure flame ranging in temperature between 1500 K and 3000 K with external, high-intensity irradiation [1, 41, 43, 99]. Steady state solutions of the atomic level populations and possible solutions of the time-averaged non-steady state populations will be given. The effect of saturation on the fluorescence measurement is also described. The limiting assumptions will include

(i)   the analyte atoms are trace constituents in a gas of molecules and no self-absorption effects are present.

(ii)   the system is in local thermodynamic equilibrium such that the external radiation will not affect the atomic velocity distribution as described by the translational temperature (see Appendix A).

(iii) coherence effects between the absorbed and the emitted light are not present [1, 2, 111-113].

(iv)   polarization effects are not considered [1, 2].

(v)   the source radiation density is constant over the atomic absorption profile at the excitation wave-length so that the laser excitation bandwidth profile can be considered a spectrally quasi-continuum source [1, 98, 99].

The latter limitation implies that the monochromatic radia-
tion field interacts with all of the atoms within the atomic
absorption profile.

The spontaneous fluorescence radiance B_F measured as
a function of time during the laser pulse from any atomic
level is significantly dependent on the temporal atomic num-
ber density of the excited state from which the fluorescence
transition originates and upon the constants which charac-
terize the transition. The spontaneous fluorescence radi-
ance can be defined as

$$B_{F_j}(t) = n_j(t) \; \frac{\ell}{4\pi} \; A_{ji} \; h\nu_o \qquad\qquad (1)$$

where

$\quad B_{F_j}(t)$ = spontaneous fluorescence radiance at time t
$\qquad\qquad$ ($J \; s^{-1} \; m^{-2} \; sr^{-1}$),

$\qquad \ell$ = path length or depth of the fluorescing
$\qquad\qquad$ volume (m),

$\quad n_j(t)$ = atomic number density of the upper level j
$\qquad\qquad$ (m^{-3}),

$\qquad A_{ji}$ = Einstein coefficient of spontaneous emission
$\qquad\qquad$ for the transition j→i (s^{-1}),

$\qquad \nu_o$ = frequency of fluorescence transition j→i (Hz),

$\qquad h$ = Planck constant (J s),

$\qquad 4\pi$ = number of steradians in a sphere and indicates
$\qquad\qquad$ the isotropic, unpolarized properties of spon-
$\qquad\qquad$ taneous fluorescence.

Depending on the desired parameter, i.e., temperature, peak fluorescence, etc., and on the measurement conditions, i.e., saturation of the transition, time-resolved measurement vs. time-integrated measurement of the fluorescence, etc., specific rate equation models can be constructed in order to explain the interaction of the atomic system with laser irradiation [1, 38, 111, 113]. The use of rate equations in the description of the time-dependent behavior of an atomic system under laser irradiation is considered valid when the laser pulse rises more slowly than the collisional dephasing rate [2, 111]; in atmospheric pressure flames, this condition occurs for laser rise times on the order of 1 ns [111, 112].

Two Level Model

The resonance fluorescence measured from the laser excited level which is produced from highly saturating laser irradiation can be evaluated for a two level model in which the atom is considered to possess only two (significant) levels (see Fig. 6) [1, 99, 111]. Laser radiation may radiatively pump atoms in the lower energy level 1 to the upper energy level 2 at a rate proportional to $B_{12} \rho_\nu(\nu_o,t)$ by absorption of a photon of energy corresponding to the frequency of the transition from level 1 to level 2, ν_o (Hz), where B_{12} (m^3 J^{-1} s^{-1} Hz) is the Einstein coefficient of stimulated absorption for the transition 1→2 and $\rho_\nu(\nu_o,t)$ is the time-dependent spectral power density (J m^{-3} Hz^{-1}) of

Figure 6.   Diagram of generalized two level atomic system consisting of the ground state 1 and the laser enhanced level 2. The laser excitation transition is indicated by the heavy arrow.

② ━━━━━━━━━━━━━━━━━━━━━ E_2

$B_{12}E\nu_{12}/c$ $B_{21}E\nu_{12}/c$ A_{21} k_{21} k_{12}

$E_2 - E_1 = h\nu_0$

① ━━━━━━━━━━━━━━━━━━━━━ E_1
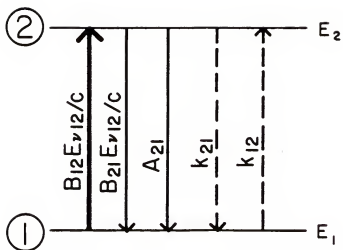
the laser irradiation at ν_o (see Table 1). Collisions of atoms in level 1 with other species may also excite those atoms to level 2 at a collisional rate k_{12} (s^{-1}). Once in the excited level, the atom may be deactived to level 1 by

(i)   collisions with other flame species without the emission of radiation at a rate k_{21} (s^{-1}),

(ii) spontaneous emission of radiation at a rate described by A_{21}, or

(iii) induced stimulated emission of radiation by the laser in the same direction as the incident radiation, at a rate described by $B_{21}\rho_\nu(\nu_o,t)$ where B_{21} $(m^3\ J^{-1}\ Hz\ s^{-1})$ is the Einstein coefficient of stimulated emission for the radiationally induced transition $2 \rightarrow 1$.

For a closed system in local thermal equilibrium, detailed balance dictates the equality of the number of downward transitions to the number of upward transitions; this condition is needed to define the relationships among A_{21}, B_{21}, and B_{12} as

$$\frac{A_{21}}{B_{21}} = \frac{8\pi h\nu_o^3}{c^3} \tag{2}$$

where

    c = the speed of light (m/s)

and

$$B_{12}g_1 = B_{21}g_2 \tag{3}$$

where

g$_1$ = statistical weight of level 1 (dimensionless),

g$_2$ = statistical weight of level 2 (dimensionless).

In equilibrium, collisions can also induce detailed balance of the collisional rates (v) of the upward and downward transitions between levels 1 and 2 [1, 2] such that

$$(v_{12})^{eq}_{coll} = (v_{21})^{eq}_{coll} = (n_1 k_{12})^{eq} = (n_2 k_{21})^{eq} \qquad (4)$$

where

$(v_{12})^{eq}_{coll}$ and $(v_{21})^{eq}_{coll}$ = equilibrium collisional rates of the radiationless transitions between levels 1 and 2 $(m^{-3} s^{-1})$,

n_1 and n_2 = atomic number densities in levels 1 and 2 (m^{-3}).

In addition, if LTE exists, then the Boltzmann equation can describe the atomic number densities in levels 1 and 2:

$$(k_{12})^{eq} = (k_{21})^{eq} \frac{g_2}{g_1} \exp (-h\nu_0/kT) \qquad (5)$$

where

k = Boltzmann constant $(J \ K^{-1})$,

T = flame temperature (K).

For transitions in the ultraviolet and visible spectral regions and for T $\leq$ 3000 K, k$_{12}$ << k$_{21}$ [1, 2].

In a flame at atmospheric pressure, the temperature-dependent <u>collisional rate constant</u> is given by [1, 2]

$$k_{21} = \sum_s n_s \ \sigma_{21} \ (8kT/\pi\mu)^{1/2} \qquad (6)$$

where

n_s = density of quenching species s (m^{-3}),

σ_{21} = effective quenching cross section (m^2),

μ = reduced mass of species s (dimensionless).

Typically, k_{21} is $\sim 10^8$-10^9 s^{-1} [1, 2, 4].

The density of atoms, n_2, spontaneously, radiatively decaying per unit time t to level 1 is defined as

$$\frac{dn_2}{dt} = -A_{21}n_2 = \frac{-n_2}{\tau_{sp}} \qquad (7)$$

where

τ_{sp} = spontaneous or radiative lifetime of level 2 (s).

Atoms in level 2 may also decay to level 1 via only collisions such that

$$\frac{dn_2}{dt} = -n_2 \left(\frac{1}{\tau_{coll}}\right) \qquad (8)$$

where

τ_{coll} = collisional or nonradiative lifetime (s).

The <u>effective fluorescence lifetime</u> τ (s) of the excited level is determined through spontaneous radiative decay and collisional deexcitation:

$$\tau \equiv \tau_{sp} + \tau_{coll} \equiv \left[A_{21} + k_{21}\right]^{-1}. \qquad (9)$$

The <u>fluorescence quantum efficiency</u> Y_{21} of the transition $2 \rightarrow 1$ is defined as the fractional probability that the

excited atom loses its energy by radiative emission:

$$Y_{21} = \frac{A_{21}}{A_{21}+k_{21}} = \frac{\tau}{\tau_{sp}} .$$ (10)

The rate of population of the excited level 2 by the excitation and deexcitation processes is summarized in Fig. 6 as

$$\frac{dn_2(t)}{dt} = n_1(t) \, B_{12}\rho_\nu(\nu_o,t) - n_2(t) \, B_{21}\rho_\nu(\nu_o,t) -$$
$$n_2(t)[A_{21} + k_{21}]$$ (11)

where

$n_1(t)$ and $n_2(t)$ = time-dependent atomic number densities
of levels 1 and 2 (m^{-3})

and $k_{12} \approx 0$.

By assuming that the total atomic number density n_T (m^{-3}) is distributed between the two levels, then

$$n_T = n_1(t) + n_2(t).$$ (12)

In terms of n_T, the rate of population of level 2 is

$$\frac{dn_2(t)}{dt} = n_T \, B_{12}\rho_\nu(\nu_o,t) - n_2(t)[B_{21}\rho_\nu(\nu_o,t) +$$
$$B_{12}\rho_\nu(\nu_o,t)] - n_2(t)[A_{21} + k_{21}].$$ (13)

Under experimental conditions, $dn_2(t)/dt$ can be evaluated for two cases: Case (1) in which a steady state population of the excited level 2 is achieved during the laser pulse (laser pulse duration >> fluorescence lifetime τ of

the excited level 2) and Case (2) in which steady state is not achieved during the duration τ_o of the laser pulse ($\tau_o \leq$ fluorescence lifetime τ). In Case (1), the change in population of the excited level is negligible [1, 99] such that

$$\frac{dn_2(t)}{dt} = 0 \qquad (14)$$

and

$$n_2^{ss} = n_T\, B_{12}\, \left(\frac{\rho_\nu(\nu_o,t)}{\rho_\nu(\nu_o,t)(B_{12}+B_{21}) + A_{21} + k_{21}}\right) \qquad (15)$$

or

$$n_2^{ss} = \frac{n_T\, B_{12}}{B_{12}+B_{21}}\left(\frac{\rho_\nu(\nu_o,t)}{\rho_\nu(\nu_o,t) + \dfrac{A_{21}+k_{21}}{B_{12}+B_{21}}}\right) \qquad (16)$$

where

n_2^{ss} = steady state number density in level 2 (m^{-3}).

Therefore, under steady state conditions, the population of the excited level increases nonlinearly with the peak irradiance $\rho_\nu(\nu_o,t)$, such that as $\rho_\nu(\nu_o,t)$ increases, the term $(A_{21}+k_{21})/(B_{12}+B_{21})$ becomes more negligible [1, 99]. Under saturation of level 2, the population of level 2 is dependent only on the Einstein coefficients of stimulated absorption and emission for that transition and not on the quenching characteristics of the flame:

$$n_{2_{sat}}^{ss} = \frac{n_T\, B_{12}}{B_{12}+B_{21}} \qquad (17)$$

where

$n_{2_{sat}}^{ss}$ = steady state number density of saturated level 2 (m^{-3}).

Since from Eqn. 3, $g_1 B_{12} = g_2 B_{21}$, the maximum ratio of excited atoms in level 2 to the total number of atoms is given by

$$\frac{n_{2_{sat}}^{ss}}{n_T} = \frac{n_T}{n_T} \left[\frac{B_{12}}{B_{12} + \frac{g_1}{g_2} B_{12}} \right] = \frac{g_2}{g_1 + g_2} \; . \tag{18}$$

If $g_1 = g_2$, then

$$n_{2_{sat}}^{ss} = \frac{n_T}{2} \; . \tag{19}$$

The <u>saturation spectral energy density</u>, $\rho_{\nu_o}^s$ (J m^{-3} Hz^{-1}), (see Table 1) is the value of $\rho_\nu(\nu_o, t)$ where $\rho_\nu(\nu_o, t) = (A_{21} + k_{21})/(B_{12} + B_{21})$ and therefore,

$$n_{2_s}^{ss} = \left(\frac{n_T \, B_{12}}{B_{12} + B_{21}} \right) \frac{1}{2} = \frac{n_{2_{sat}}^{ss}}{2} \; . \tag{20}$$

When the incident spectral energy density $\rho_\nu(\nu_o, t)$ reaches the value $\rho_{\nu_o}^s$, the excited state density $n_{2_s}^{ss}$ will be 50% of the maximum $n_{2_{sat}}^{ss}$ under complete saturation.

In Case (2) under nonsteady state transient irradiation, the <u>time-dependent population of level 2</u> during one laser pulse is given by [1, 99, 113]

$$n_2(t) = \frac{n_T \, B_{12} \rho_\nu(\nu_o,t)}{(A_{21}+k_{21}) + \rho_\nu(\nu_o,t)(B_{12}+B_{21})} \; \times$$

$$\left[1 - \exp\,-(A_{21} + k_{21} + \rho_\nu(\nu_o,t)(B_{12} + B_{21}))t\right]$$

$$(21)$$

or at any time t as [1, 113]

$$n_2(t) = n_T \, B_{12}\rho_\nu(\nu_o,t) \, t_r[1 - \exp(-t/t_r)] \qquad (22)$$

where

$$t_r = [\rho_\nu(\nu_o,t)(B_{12}+B_{21}) + A_{21} + k_{21}]^{-1} \qquad (23)$$

t_r = response time of system (s).

If the pumping time of the system defined as [1]

$$t_p = [(B_{12}+B_{21})\rho_\nu(\nu_o,t)]^{-1} \qquad (24)$$

is much greater than $[A_{21} + k_{21}]^{-1}$, i.e., the spontaneous emission and collisional decay rates, then the temporal behavior of the population of level 2 is governed by the pumping time, such that

$$t_r \simeq [\rho_\nu(\nu_o,t)(B_{12}+B_{21})]^{-1}. \qquad (25)$$

The magnitude of the spontaneous fluorescence is directly proportional to the excited state population as given in Eqn. 1. The temporal behavior of the fluorescence pulse should correspond to the transient excited level population produced during the laser pulse. For laser pulses on the order of 1-10 μs, a gated detector can be easily used to monitor only the steady state excited level population.

However, for laser pulses less than 40 ns, it is often easier experimentally to measure the average fluorescence produced over a specified time interval [99] than to measure the peak fluorescence due to instrumental limitations and the difficulty in maintaining a short gate width ($\gtrsim 1$ ns) at the peak signal. A boxcar integrator can be used as a gated detector to measure the time-averaged fluorescence.

It is apparent that due to the finite rise time of the excited level population (as given by the response time) to its steady state value, an accurate, steady state fluorescence is not measured, even under saturation conditions, but rather a rate-controlled averaged density of the excited level [1, 99-101]. It is therefore necessary to determine the difference in magnitude between the steady state fluorescence and the averaged fluorescence signals.

The average density $\overline{n_2}$ (m^{-3}) of the excited level 2 during the laser pulse (assuming that the rise time and decay of $\rho_\nu(\nu_o,t)$ is faster than any time constant in the two level model) can be calculated as [99]

$$\overline{n_2} \quad = \overline{n_2(t)} = \frac{1}{t_o} \int_o^{t_o} n_2(t)dt \qquad (26)$$

and therefore

$$\overline{n_2} = n_T \, B_{12} \, \frac{\rho_\nu(\nu_o,t)}{\rho_\nu(\nu_o,t)(B_{12}+B_{21}) + A_{21} + k_{21}} \times$$

$$\left[1 - \frac{1 - \exp\left(-\left(A_{21}+k_{21}+\rho_\nu(\nu_o,t)(B_{12}+B_{21})\right)t_o\right)}{(A_{21}+k_{21}+\rho_\nu(\nu_o,t)(B_{12}+B_{21}))t_o} \right]$$

$$(27)$$

where

t_o = laser pulse duration = boxcar gate width (s).

The time-integrated fluorescence signal is not simply proportional to the gate width nor to

$$\frac{n_T \; \rho_\nu(\nu_o,t)}{\rho_\nu(\nu_o,t)(B_{12}+B_{21})+A_{21}+k_{21}}$$

but contains additional dependencies on $\rho_\nu(\nu_o,t)(B_{21}+B_{12})$ [99, 111]. The fluoresence pulse has a finite rise time and decay time even if the laser pulse is considered a rectangular step function; the rise and decay time constants $(B_{12}+B_{21})\rho_\nu(\nu_o,t)$ + k_{21} + A_{21} do not compensate for each other when the time averaged population is measured [99, 113].

Under saturation conditions, $\overline{n_2}$ still depends on the quenching characteristics of the flame [99, 111, 113]:

$$\overline{n_2}^{sat} = n_T \; \frac{g_2}{g_1+g_2}\left(t_o \; + \; \frac{1}{A_{21}+k_{21}}\right) \tag{28}$$

which is in contrast to the steady state value of $n_{2_{sat}}^{ss}$ as given by Eqn. 20. Only if the duration of the laser pulse $t_o \gg [A_{21}+k_{21}]^{-1}$ and the boxcar gate duration $\gtrsim t_o$, does $\overline{n_2}^{sat} = n_{2_{sat}}^{ss}$ [36, 99, 113]. In contrast, if $t_o \gtrsim [A_{21}+k_{21}]^{-1}$, then the averaged, saturated value of n_2 will still depend on the spontaneous emission and collisional decay rates. Therefore, for values of the boxcar gate $\gtrsim$ the laser pulse duration, t_o, the excited level population $\overline{n_2}$ will rise with increasing $\rho_\nu(\nu_o,t)$ toward the saturation value at a rate determined by the exponential term and therefore by t_o, A_{21} + k_{21}, and

$(B_{12}+B_{21})\rho_\nu(\nu_o,t)$. The extent of departure of $\overline{n_2}^{sat}$ from $n_{2_{sat}}^{ss}$ decreases as t_r increases toward t_p. However, the saturation parameter or the saturation spectral energy density (see Table 1) measured for the averaged nonsteady state value at 50% of $\overline{n_2}^{sat}$ will be higher than $n_{2_s}^{ss}$ by the factor $(1 + [A_{21}+k_{21}]^{-1})$. Saturation is therefore harder to achieve for atomic populations that vary with time significantly during the laser pulse, i.e., $t_r \gtrsim [A_{21}+k_{21}]^{-1}$. The difference between the observed $n_{2_s}^{ss}$ and $\overline{n_2}$ and thus the shape of the saturation curve at high $\rho_\nu(\nu_o,t)$ will also depend on the gate width and position.

In summary, at lower $\rho_\nu(\nu_o,t)$ where the rates of spontaneous fluorescence and collisional decay are comparable to the rates of induced absorption and emission, n_2^{ss} will vary linearly with $\rho_\nu(\nu_o,t)$ and the effective fluorescence lifetime of the level. At low spectral irradiances, $\overline{n_2}$ will also increase linearly with $\rho_\nu(\nu_o,t)$ and the fluorescence lifetime only if $t_o > \tau$. At high spectral irradiances, $\overline{n_2}^{sat}$ will be identical to $n_{2_{sat}}^{ss}$ if

$$t_o \gg [\rho_\nu(\nu_o,t)(B_{12}+B_{21})] \qquad (29)$$

and

$$[\rho_\nu(\nu_o,t)(B_{12}+B_{21})] \gg (A_{21}+k_{21}) . \qquad (30)$$

Otherwise, $\overline{n_2}^{sat}$ varies nonlinearly with t_o and $(B_{12}+B_{21})\rho_\nu(\nu_o,t)$ and is dependent on $A_{21} + k_{21}$.

Four Level Model

In the measurement of THAF from Na upper excited states above the radiatively pumped level, it is necessary to evaluate minimally a four level model for Na in which the total atomic number density is given by [41-43]

$$n_T = n_1(t) + n_2(t) + n_3(t) + n_4(t) \qquad (31)$$

where

$n_1(t)$, $n_2(t)$, $n_3(t)$, $n_4(t)$ = respective time-dependent atomic number densities in levels 1, 2, 3 and 4 (m^{-3}).

Level 2 corresponds to the coalesced Na-D doublet lines. The laser irradiance resonantly pumps ground state atoms in level 1 to level 2 according to the rate $B_{12}\rho_\nu(\nu_o,t)$ (see Fig. 7). A ground state atom can be collisionally excited to level 2, but due to the relatively large energy difference between levels 1 and 2 as compared to kT, $k_{12} = 0$. Excited state atoms in levels 2, 3, and 4 may be excited and deexcited to other levels by mixing collisions at rates k_{23}, k_{32}, k_{42}, k_{34}, etc. Corresponding to the two level model, four level atoms in level 2 may radiatively decay to the ground state by stimulated emission according to $B_{21}\rho_\nu(\nu_o,t)$, spontaneously emit fluorescence to induce a radiative transition to level 1 at a rate A_{21}, and decay to level 1 through quenching collisions with major flame species at a rate k_{21}. In addition, atoms in the laser excited level 2 may become involved in mixing collisions to be excited to levels 3 and 4. Atoms

Figure 7.   Diagram of generalized four level system for
            a Na-type atom. Heavy arrow indicates the
            laser excitation transition. Level 2 can
            correspond to the coalesced Na-D doublet lines.
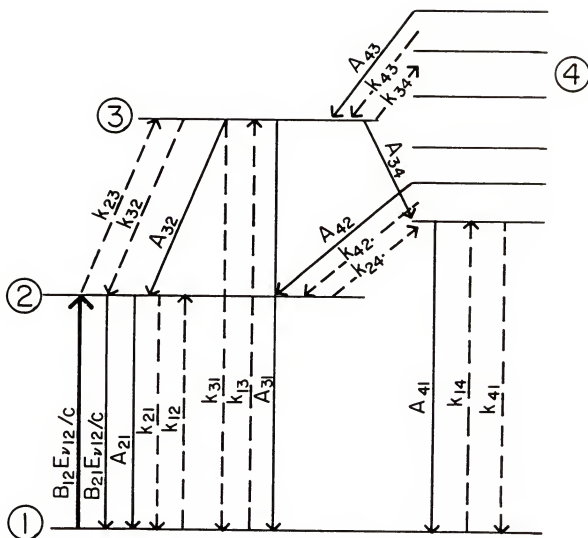
in levels 3 and 4 may also radiatively decay through spontane-
ous emission to levels 2 and 1. Quenching collisions which
promote the deexcitation of atoms in the excited levels to
level 1 in a single step may also occur, but are considered
to be less probable than mixing collisions because of the
small energy differences among the upper levels as compared
to the energy differences between the excited levels and
level 1. Correspondingly, collisions which excite ground
state atoms to levels 3 and 4 are considered quite improbable.
Therefore, the rates of population of levels 2, 3, and 4 can
be evaluated as [41-44]

$$\frac{dn_2(t)}{dt} = n_1(t)[B_{12}\rho_\nu(\nu_o,t) + k_{12}] + n_3(t) (A_{32}+k_{32}) +$$
$$n_4(t) (A_{42}+k_{42}) - n_2(t)[A_{21}+k_{21}+B_{21}\rho_\nu(\nu_o,t) +$$
$$k_{23} + k_{24}], \tag{32}$$

$$\frac{dn_3(t)}{dt} = n_1(t)k_{13} + n_2(t)k_{23} + n_4(t) (A_{43}+k_{43}) -$$
$$n_3(t) (A_{32}+k_{32}+A_{31}+k_{32}+k_{34}), \tag{33}$$

$$\frac{dn_4(t)}{dt} = n_1(t)k_{14} + n_2(t)k_{24} + n_3(t)k_{34} -$$
$$n_4(t) (A_{41}+k_{41}+A_{42}+k_{42}+A_{43}+k_{43}) \tag{34}$$

where

$$k_{12} = k_{13} = k_{14} = 0.$$

Under steady state conditions,

$$\frac{dn_2(t)}{dt} = \frac{dn_3(t)}{dt} = \frac{dn_4(t)}{dt} = 0. \tag{35}$$

If the main path for the thermal population of levels 3 and 4 is from the laser excited level, $2 \rightarrow 3$ and $2 \rightarrow 4$, and not directly from the ground state, $k_{13} = k_{14} = 0$ and the collisional deactivation rates are much larger than the rates for spontaneous emission from each level [1, 2, 41], laser irradiation at $\nu_{o_{12}}$ should not perturb the relative populations of levels 3 and 4. Therefore, the measured THAF temperature should be equivalent to the slope temperature derived from emission measurements (see Appendix A) [2]; i.e., the THAF temperature should be independent of the laser irradiance. The steady state population ratio of levels 3 and 4 with respect to the laser excited level 2 can be given as [41-44]

$$\frac{n_3}{n_2} \approx \frac{k_{23}}{k_{32}} \left(\frac{k_{32}}{k_{32}+k_{31}} \right) \left(\frac{k_{32}+K_3}{k_{32}+K_3 K_5} \right) \tag{36}$$

and

$$\frac{n_4}{n_2} \approx \frac{k_{24}}{k_{42}} \left(\frac{k_{42}}{k_{42}+k_{41}} \right) \left(\frac{k_{42}+K_4}{k_{42}+K_4 K_6} \right) \tag{37}$$

where

$$K_3 = \frac{k_{34}k_{42}}{k_{41}+k_{42}+k_{43}} \tag{38}$$

$$K_4 = \frac{k_{43}k_{32}}{k_{31}+k_{32}+k_{34}} \tag{39}$$

$$K_5 = \frac{1 + (k_{41}/k_{42})}{1 + (k_{31}/k_{32})} \tag{40}$$

$$K_6 = \frac{1 + (k_{31}/k_{32})}{1 + (k_{41}/k_{42})} = \frac{1}{K_5} . \tag{41}$$

The exact solution for the ratio of atomic number densities in the thermally assisted excited levels 3 and 4 can be derived as [43]

$$\frac{n_3}{n_4} = \frac{[(R_{24}^* R_{43}^* + R_{23}^* R_4) + R_{14}(R_{23}^* \frac{R_{42}^*}{R_{12}} + R_{43}^* \frac{R_2}{R_{12}} + R_{13}(R_4 \frac{R_2}{R_{12}} - R_{24}^* \frac{R_{42}^*}{R_{12}})]}{[(R_{23}^* R_{34}^* + R_{24}^* R_3) + R_{14}(R_3 \frac{R_2}{R_{12}} - R_{23}^* \frac{R_{32}^*}{R_{12}}) + R_{13}(R_2 \frac{R_{34}^*}{R_{12}} + R_{24}^* \frac{R_{32}^*}{R_{12}})]} \tag{42}$$

where

$$R_2 = R_{21} + R_{23} + R_{24} + R_{12},$$

$$R_3 = R_{31} + R_{32} + R_{34} + R_{13},$$

$$R_4 = R_{41} + R_{42} + R_{43} + R_{14},$$

$$R_{32}^* = R_{32} - R_{12},$$

$$R_{42}^* = R_{42} - R_{12},$$

$$R_{43}^* = R_{43} - R_{13},$$

$$R_{23}^* = R_{23} - R_{14},$$

$$R_{24}^* = R_{24} - R_{14},$$

$$R_{34}^* = R_{34} - R_{14},$$

$$R_{12} = B_{12}\rho_\nu(\nu_o,t) + k_{12} \ (s^{-1}),$$

$$R_{21} = B_{21}\rho_\nu(\nu_o,t) + k_{21} + A_{21} \ (s^{-1}),$$

$$R_{13} = k_{13} \ (s^{-1}),$$

$$R_{31} = k_{31} + A_{31} \ (s^{-1}),$$

$$R_{14} = k_{14} \ (s^{-1}),$$

$$R_{41} = k_{41} + A_{41} \ (s^{-1}),$$

$$R_{23} = k_{23} \ (s^{-1}),$$

$$R_{32} = k_{32} + A_{32} \ (s^{-1}),$$

$$R_{24} = k_{24} \ (s^{-1}),$$

$$R_{42} = k_{42} + A_{42} \ (s^{-1}),$$

$$R_{34} = k_{34} \ (s^{-1}),$$

$$R_{43} = k_{43} \ (s^{-1}).$$

At high $\rho_\nu(\nu_o,t)$, the rate due to induced absorption, $B_{12}\rho_\nu(\nu_o,t)$, and the rate due to induced emission, $B_{21}\rho_\nu(\nu_o,t)$, will be much larger than the corresponding collisional rates k_{12} and k_{21}. In addition, $R_{13} = R_{14} = 0$. Neglecting the spontaneous emission rates A with respect to the collisional rates k and assuming detailed balance between the levels such that [43]

$$\frac{k_{24}k_{32}}{k_{34}} = \frac{k_{23}k_{42}}{k_{43}}, \tag{43}$$

the population rates between levels 3 and 4 can be re-stated as

$$\frac{n_3}{n_4} = \frac{k_{43}}{k_{34}} \; \frac{1 + \dfrac{k_{41}}{K_7}}{1 + K_8 \dfrac{k_{41}}{K_7}} \tag{44}$$

where

$$K_7 = k_{42} + \frac{k_{43}}{k_{23}} (k_{23} + k_{24}) \tag{45}$$

$$K_8 = \frac{k_{42}/k_{41}}{k_{32}/k_{31}} \; . \tag{46}$$

As indicated by Alkemade et al. [2] (see Appendix A), under LTE, the population of the electronic levels will be distributed according to the Boltzmann equation as

$$\frac{n_3}{n_4} = \frac{g_3}{g_4} \exp \; (-\Delta E_{34}/kT) \tag{47}$$

where

ΔE_{34} = energy difference between levels 3 and 4 (J).

From the relationship between the steady state atomic number density and the corresponding fluorescence stated in Eqn. 1,

$$\frac{n_3}{n_4} = \frac{\dfrac{B_{F_{3i}}}{h\nu_{o_{3i}} A_{3i}}}{\dfrac{B_{F_{4j}}}{h\nu_{o_{4j}} A_{4j}}} = \frac{g_3}{g_4} \exp \; (-\Delta E_{34}/kT) \tag{48}$$

where

$B_{F_{3i}}$ = fluorescence radiance for transition from level 3 to i (J s^{-1} m^{-2} sr^{-1}),

$B_{F_{4j}}$ = fluorescence radiance for transition from level 4 to j ($J\ s^{-1}\ m^{-2}\ sr^{-1}$),

A_{3i} = Einstein coefficient of spontaneous emission for transition from level 3 to i (s^{-1}),

A_{4j} = Einstein coefficient of spontaneous emission for transition from level 4 to j (s^{-1}),

$\nu_{o_{3i}}$ = frequency of 3→i transition (Hz),

$\nu_{o_{4j}}$ = frequency of 4→j transition (Hz).

The local temperature T can then be evaluated for any population ratio, i.e., particularly level 3 to level 4, as

$$T = \frac{\Delta E_{34}/kT}{\ln\left[\dfrac{B_{F_{4j}}}{B_{F_{3i}}}\right] + \ln\left[\dfrac{A_{3i}g_3}{A_{4j}g_4}\right] + \ln\left[\dfrac{\lambda_{4j}}{\lambda_{3i}}\right] + \ln\ \left(\dfrac{1}{D}\right)} \qquad (49)$$

where

λ_{4j} = wavelength of fluorescence transition from level 4 to level j (m),

λ_{3i} = wavelength of fluorescence transition from level 3 to level i (m),

and

$$D = \frac{1 + \dfrac{k_{41}}{K_7}}{1 + K_8\dfrac{k_{41}}{K_7}}\ . \qquad (50)$$

The local temperature T evaluated from the above expressions can correspond to a partial Boltzmann distribution among the excited levels if D, which is the factor which indicates the deviation of the population ratio from a

partial Boltzmann equilibrium, is equal to unity. Therefore, a valid T is measured if, as assumed, the mixing collisional rates among the upper levels are much larger than the collisional rates to or from level 1:

$$k_{41} = k_{31} = 0 \tag{51}$$

or

$$\frac{k_{42}}{k_{41}} = \frac{k_{32}}{k_{31}} \ . \tag{52}$$

Five Level Model

In order to measure THAF from collisionally excited levels in Tl-type atoms, a five level model is minimally needed. In Tl, the laser irradiation pumps ground state atoms to level 3 while level 2 acts as a metastable sink in which no radiative transitions are allowed between levels 2 and 1 (see Fig. 8). In the same format as the Na four level model, the rates of population of levels 4 and 5 can be derived as

$$\frac{dn_4(t)}{dt} = n_1(t)k_{14} + n_2(t)k_{24} + n_3(t)k_{34} + n_5(t)k_{54} -$$
$$n_4(t)(A_{41}+k_{41}+A_{42}+k_{42}+A_{43}+k_{43}+k_{45}) \tag{53}$$

$$\frac{dn_5(t)}{dt} = n_1(t)k_{15} + n_2(t)k_{25} + n_3(t)k_{35} + n_4(t)k_{45} -$$
$$n_5(t)(A_{51}+k_{51}+A_{52}+k_{52}+A_{53}+k_{53}+k_{54}) \ . \tag{54}$$

Figure 8. Diagram of generalized five level system for Tl-type atom. Heavy arrow indicates the laser excitation transition.

⑤ ④ ②

K_{15}
K_{51}
A_{51}
K_{41}
A_{41}
K_{24}
K_{42}
A_{42}
K_{25}
K_{52}
A_{52}
K_{12}
K_{21}

K_{45}
K_{54}
A_{54}

K_{23}
K_{32}
A_{32}

K_{43}
K_{34}
A_{43}

K_{35}
K_{53}
A_{53}

K_{13}
K_{31}
A_{31}

$B_{31} E_{v13}/C$
$B_{13} E_{v13}/C$

③ ①
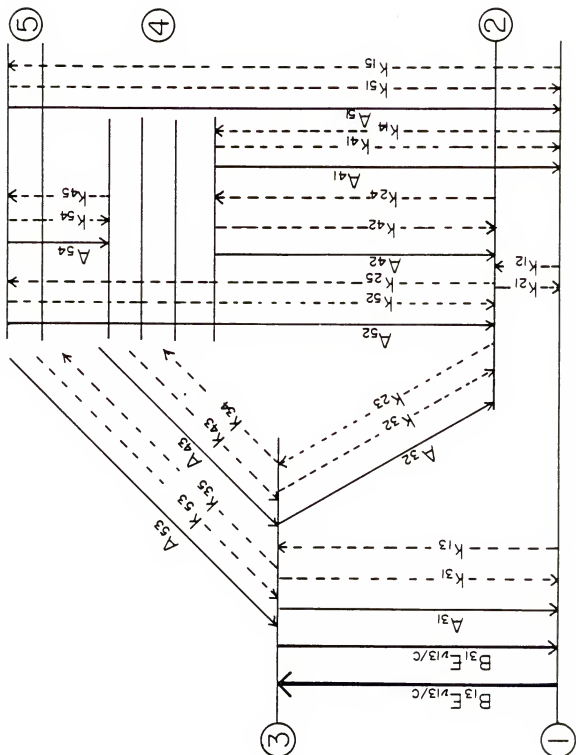
Under steady state conditions

$$\frac{dn_2(t)}{dt} = \frac{dn_3(t)}{dt} = \frac{dn_4(t)}{dt} = \frac{dn_5(t)}{dt} = 0. \tag{55}$$

Under the assumptions that

$$k_{12} = k_{13} = k_{14} = k_{15} = 0 \tag{56}$$

and that the collisional mixing rates among the upper levels are greater than the quenching rates to the ground state or to the laser excited state,

$$\frac{n_4}{n_5} = \frac{k_{54}}{k_{45}} = \frac{1 + \dfrac{k_{51}}{K_9}}{1 + \dfrac{k_{41}}{K_{10}}} \tag{57}$$

where

$$K_9 = k_{53} + k_{54}\left(1 + \frac{k_{35}}{k_{34}}\right) \tag{58}$$

$$K_{10} = k_{43} + k_{45}\left(1 + \frac{k_{34}}{k_{35}}\right). \tag{59}$$

Since k_{51} and k_{41} are not balanced by upwards collisional rates k_{15} and k_{14}, the ratio n_4/n_5 is Boltzmannian only if

$$k_{51} \ll K_9 \tag{60}$$

and

$$k_{41} \ll K_{10}. \tag{61}$$

Therefore, it is feasible to measure a valid THAF temperature from the ratio of atomic number densities in the thermally assisted levels 4 and 5 if

$$\frac{n_4}{n_5} \approx \frac{k_{54}}{k_{45}} \ .$$

(62)

The THAF temperature can also be determined from the slope of a plot of

$$\ln(B_{F_{j12}} \lambda_j / g_j A_j) \text{ vs. } \Delta E_j / k$$

(63)

where

$B_{F_{j12}}$ = spontaneous fluorescence radiance from level j upon laser excitation of level 2 from level 1 (J s^{-1} m^{-2} sr^{-1}),

λ_j = wavelength of transition from level j (m),

g_j = statistical weight of level j (dimensionless),

A_j = Einstein coefficient of spontaneous emission from level j (s^{-1}),

ΔE_j = energy difference of any level j and level 2 (J).

Multilevel Model

In summary (see Fig. 9), a multilevel atomic system under pulsed laser excitation reaches a new population distribution during the laser pulse, because the laser enhanced population of level e is partially transferred via collisions with major flame species to other excited levels j. The following relationships between the population of the laser enhanced level, n_e, and the populations of the collisionally excited levels, n_c, and between the population of only one excited level, n_i, to the total population of the collisional manifold, n_c, can be stated as [48, 114]

Figure 9.   Diagram of generalized multilevel atomic sys-
             tem consisting of the ground state and the laser
             enhanced level e (laser excitation transition
             indicated by the heavy arrow) and a manifold
             of j upper levels, c, whose total population
             n_c is produced from the collisional redistri-
             bution of the laser excited level. Any
             individual level within the thermally assisted
             group of levels is indicated by i. The dashed
             lines indicate collisional and radiative path-
             ways of rate R (s^{-1}).
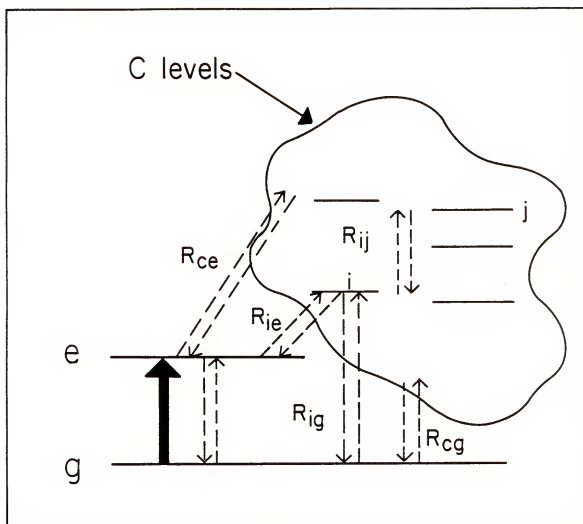
$$\frac{\sum\limits_{j} n_j}{n_e} = \frac{n_c}{n_e} = \left(\frac{n_c}{n_e}\right)_{Bolt} \frac{R_{ce}}{R_{ce}+R_{cg}} \tag{64}$$

$$\frac{n_i}{n_c} = \left(\frac{n_i}{n_c}\right)_{Bolt} \frac{\dfrac{R_{ie}/R_{ig}}{R_{ce}/R_{cg}} + \dfrac{\sum\limits_{j}(R_{ij}+R_{ie})}{R_{ig}}}{1 + \dfrac{\sum\limits_{j}(R_{ij}+R_{ie})}{R_{ig}}} \tag{65}$$

where

$\sum\limits_{j} n_j$ = total atomic number density in the collisionally excited levels j (m^{-3}),

n_i = atomic number density in any excited level i within the collisional manifold (m^{-3}).

The average 2nd order collisional rates ($m^3 \ s^{-1}$) for quenching of the excited level manifold to the laser pumped level e or to the ground state g are given respectively by [42, 114]

$$\overline{R_{ce}} = \frac{\sum\limits_{j} R_{je}}{\sum\limits_{j} n_j} \tag{66}$$

and

$$\overline{R_{cg}} = \frac{\sum\limits_{j} R_{jg}}{\sum\limits_{j} n_j} \quad . \tag{67}$$

The individual collisional rates, R_{ie} and R_{ig} (s^{-1}), represent collisional energy transfer of any excited level i within the collisional manifold c to or from the laser enhanced level e or the ground state g, while the collisional

mixing rates among the thermally assisted excited levels
are given by $\sum_j R_{ij}$.

Equation 64 indicates that the laser excited level e
is overpopulated with respect to the partial Boltzmann dis-
tribution of the level populations as given by the local
flame temperature (without external source excitation of g→e),
while the total population of the collisionally excited levels,
n_c, should be partially thermalized. The deviation from par-
tial Boltzmann equilibrium which is indicated when consider-
ing the ratio of the population of the laser enhanced level,
n_e, to the population of the collisionally excited levels,
n_c, is dependent upon the significance of the average quench-
ing to the ground state $\overline{R_{cg}}$ and to the laser enhanced level
$\overline{R_{ce}}$. A partial Boltzmann equilibrium will be established
among the upper excited levels, c, and the laser enhanced
level, e, if the population distribution over these levels
is collision-dominated.

An individual level i can deviate from the average
Boltzmann distribution of the collisionally excited levels
c according to Eqn. 65 if the quenching rates R_{ie} and R_{ig}
are significantly different from the average quenching rates
$\overline{R_{ce}}$ and $\overline{R_{cg}}$ of the manifold so as to indicate collisional
imbalance to or from the lower lying levels. Therefore,
collisionally excited levels, c, for which $R_{ie}/R_{ig} \sim R_{ce}/R_{cg}$
will be in partial Boltzmann equilibrium within the colli-
sional manifold and valid THAF temperatures should be
measured. However, levels which are strongly coupled with

the radiatively pumped level e as given by $R_{ie}/R_{ig} \gg R_{ce}/R_{cg}$
will be overpopulated with respect to the partial Boltzmann
distribution, while levels with energies considerably above
or below e so that $R_{ie}/R_{ig} \ll R_{ce}/R_{cg}$ will be underpopulated.
Upper levels for which $\sum_j (R_{ij}+R_{ie})/R_{ig} \gg (R_{ie}/R_{ig})/(R_{ce}/R_{cg})$
and $\gg 1$ will maintain a partial Boltzmann distribution upon
laser excitation. For those levels which are mainly popu-
lated by multiple (thermal) collisions from neighboring
levels and do not suffer extensive quenching collisions
(to the ground state), the laser excited level e can be con-
sidered a pseudo-ground state and a new thermal distribution
under laser excitation will be achieved.

Nonsteady State (Transient) Fluorescence

As described previously for the two level model, if a
boxcar averager is used to measure the THAF signals produced
during the laser pulse which is <u>comparable to or shorter than</u>
<u>the effective fluorescence lifetime of the upper excited state</u>
from which the fluorescence originates, the rate of change in
the population of the excited level [$dn_2(t)/dt$, $dn_3(t)/dt$, etc.]
can not be ignored [1, 99, 113]. The transient populations of
the THAF excited levels have been evaluated, assuming a con-
stant $\rho_\nu(\nu_o,t)$ (laser power density) step function for a
three level system as [100]

$$n_2(t) = C_1 \exp(-\xi_1 t) + C_2 \exp(-\xi_2 t) + Q_2/B \qquad (68)$$

$$n_3(t) = C_1 \frac{(R_2-\xi_1)}{R_{32}^*} \exp(-\xi_2 t) + C_2 \frac{(R_2-\xi_2)}{R_{32}^*} \; x$$

$$\exp(-\xi_2 t) + Q_3/B \qquad\qquad (69)$$

where the coefficients and relations used are listed in Table 2. The accurate determination of the appropriate saturation parameters (see Table 1) requires an evaluation of the transient level populations and a temporal shape of the laser pulse in the excitation of level $1 \rightarrow 2$. These derivations are beyond the scope of this dissertation. However, it is apparent that saturation of the radiatively excited and the thermally assisted levels will depend significantly upon the effective lifetime of the excited state and the duration and shape of the laser excitation pulse. In addition, even for relatively poor collisional coupling between the laser excited level and the upper states under low incident irradiance, a partial Boltzmann population redistribution could be achieved within $\sim 10^{-8}$ s [49, 100].

Table 2
Coefficients and Relations for the Temporal
Behavior of a Three Level System

$R_2 = R_{21} + R_{23} + R_{12}$

$R_{23}^* = R_{23} - R_{13}$

$Q_2 = R_{12}R_3 + R_{32}^* R_{13}$

$B = R_2 R_3 - R_{23}^* R_{32}^*$

$\xi_1 = \dfrac{(R_3 + R_2)}{2} - \sqrt{\dfrac{(R_3 + R_2)^2}{4} - B}$

$k_1 = \dfrac{[Q_2/B - n_{2th}]}{(\xi_2 - \xi_1)} (R_2 - \xi_1)$

$RR = (R_2 - \xi_2)/(R_2 - \xi_1)$

$C_1 = k_1 RR - k_2/R$

$C_2 = -k_1 + k_2/R$

$R_{12} = k_{12}$

$R_{21} = k_{21}$

$R_{13} = B_{13}\rho_\nu(\nu_{013}, t) + k_{13}$

$R_3 = R_{31} + R_{32} + R_{13}$

$R_{32}^* = R_{32} - R_{12}$

$Q_e = R_{13}R_2 + R_{12}R_{23}^*$

$\xi_2 = \dfrac{(R_3 + R_2)}{2} + \sqrt{\dfrac{(R_3 + R_2)^2}{4} - B}$

$k_2 = \dfrac{[Q_3/B - n_{3th}]}{(\xi_2 - \xi_1)} (R_2 - \xi_2)$

$R = (R_2 - \xi_2)/R_{32}^*$

$C_3 = k_1 R - k_2$

$C_4 = -k_1 R + k_2$

$R_{23} = k_{23}$

$R_{32} = k_{32} + A_{32}$

$R_{31} = B_{31}\rho_\nu(\nu_{031}, t) + k_{31} + A_{31}$

EXPERIMENTAL MEASUREMENTS AND CONDITIONS

General

Due to its tunability, extremely high peak power (~ 10 to 100 kW), spatial and temporal coherence, and spectral selectivity, the pulsed dye laser can be used to advantage in analytical flame diagnostics. The N_2- and excimer-pumped dye lasers enjoy high pulse energies ($\gtrsim$ 1 - $\gtrsim$ 2 mJ per pulse) and a wide tunability range (360-950 nm). However, the laser pulse duration (~ 6-8 ns) is on the order of the collisional relaxation times of the atomic energy states. Under certain conditions which are dependent on the thermometric seed employed and the flame quenching characteristics, steady state of the level populations may not be reached during the laser pulse and the choice of the measurement procedure becomes critical. Interestingly, flashlamp-pumped dye lasers also possess high pulse energies, but in contrast, the tunability range is more limited (435-750 nm). However, because of the longer pulse durations (~ 1 μs), attainment of steady state during the laser pulse most certainly occurs and the necessity for time-resolved detection of the THAF fluorescence is not as great [36, 38, 111]. In contrast, ionization of atoms and excited state chemical reactions become more important on the ~ 1 μs time

scale [2]. The signal-to-noise ratio of the detected fluor-
escence may also decrease under longer pulse irradiation and
correspondingly wider gate widths, because of the increase in
detected noise due to flame background emission and detector
shot noise.

The observation of the atomic excited state fluorescence
spectrum under optimal and reproducible experimental condi-
tions is therefore required. Inaccurate or crude experi-
mental procedures may result in the nondetectability of
fluorescence from weak transitions and speculation concern-
ing the extent or significance of ionization or excited state
chemical reactions in the interpretation of the measured
spectrum. In addition, several atomic and molecular species
have absorption transitions which are amenable to laser exci-
tation only through two-photon absorption processes (with
cross sections 10^{-9}-10^{13} times smaller than the single-
photon absorption process) or frequency doubling of the
visible laser output to achieve the UV excitation wavelength
needed. Therefore, much of the experimentation performed
and the instrumentation and procedures employed are results
of attempts to derive as much information as possible from
the optimal and accurate measurement of the analyte excited
state fluorescence spectrum. Rather elaborate measurement
systems are often required to obtain fundamental parameters
on a spatially and temporally resolved basis.

Flame Composition

Acetylene/oxygen (C_2H_2/O_2) flames were utilized through-
out these experiments in THAF fluorescence measurements, be-
cause they are popular analytical flames as well as being
interesting flames for diagnostic studies [1, 4, 24-28]. The
requirements for successful utilization of specific flames in
analytical spectroscopy include the capability to vaporize
and to atomize efficiently the analyte, low background emis-
sion, and sufficient reducing atmosphere to prevent further
oxidation reactions of the analyte species. C_2H_2/O_2 flames
generally satisfy the above conditions [1, 28, 32, 33, 115-117].
These flames typically possess higher temperatures than
hydrogen/oxygen (H_2/O_2) flames which may increase the atomi-
zation efficiencies for certain analytes [28]. However, the
background spectra which are produced from the emission of OH
(260.0-320.0 nm region), C_2 (435.0-580.0 nm region), CH (390.0-
435.0 nm region) and CN (350.0-425.0 nm region) are more sig-
nificant than the spectra of hydrogen-based flames which pro-
duce only OH emission, but are less significant than the
spectra of acetylene/nitrous oxide and hydrogen/nitrous oxide
flames [1-3, 28]. In addition, if the acetylene-based flames
are diluted with N_2 ($C_2H_2/O_2/N_2$), the flame temperature is
decreased while the increased concentration of quenching
species may significantly decrease the fluorescence quantum
efficiency. In contrast, Ar-diluted acetylene/oxygen flames
($C_2H_2/O_2/Ar$) are generally ~ 200 K hotter than the correspond-
ing $C_2H_2/O_2/N_2$ flames of equivalent fuel to oxidant ratio and

provide ~ five times the improvement in limits of detection of many elements because of the relative increase in quantum efficiency [1, 28]. The analytical growth curves (linear dynamic range) have not been found to change with variation in flame composition for either $C_2H_2/O_2/Ar$ or $C_2H_2/O_2/N_2$ flames [1, 2, 28]

Because of the widely varying quenching characteristics of $C_2H_2/O_2/N_2$ and $C_2H_2/O_2/Ar$ flames, these flames are often employed for diagnostic purposes. The inefficient energy transfer collisions reported in the Ar-diluted flames [2, 36] can result in the nonattainment of steady state population distributions under short laser pulse excitation. In addition, the fluorescence intensities may vary with changes in the fuel-to-oxidant ratio from the stoichiometric proportion. Conveniently, the temperature of $C_2H_2/O_2/Ar$ flame mixtures can be easily varied over a wide range (~ 500 K) while maintaining the same flame shape and external characteristics. $C_2H_2/O_2/N_2$ flames are less easily manipulated.

Analytical Calibration Curves

Growth curves for the observed fluorescence transitions in Na and Tl were constructed for the 2465 K $C_2H_2/O_2/Ar$, 2315 K $C_2H_2/O_2/Ar$, 2200 K $C_2H_2/O_2/Ar$, and 2220 K $C_2H_2/O_2/N_2$ reversal temperature flames to determine if self-absorption of the emitted fluorescence as it traversed the inner seeded flame occurred at the concentrations of the thermometric seeds used for the temperature measurements, 1000 ppm NaCl and 3000 ppm $TlNO_3$ [2, 118-124]. At low metal concentrations, the log of the integrated fluorescence intensity is linearly

related to the log concentration introduced into the flame, while at higher seed concentrations, where the flame is considered "optically thick," the relationship becomes nonlinear and a plateau is produced at succeedingly higher concentrations as is expected for a quasi-continuum source. The bend-over is due to primary absorption and self-absorption which occurs when the photon emitted by the analyte atoms undergoing a downward transition x→y is reabsorbed by atoms in state y. Self-absorption effects are mainly observed for atomic resonance lines [2].

Solutions from 10^{-1}-10^4 ppm of the analyte were introduced into the flame and the corresponding fluorescence intensity at each concentration was measured. The self-absorption correction factor was derived by extrapolating to zero concentration and measuring the difference between the linear slope and the experimental plateau [2, 36].

Saturation Curves

Plots of relative fluorescence intensity vs. relative laser pulse energy or laser density (see Table 1) were constructed for fluorescence transitions arising from the radiatively pumped level and from many of the collisionally excited levels in Na and Tl for each of the acetylene-based flames used in these experiments. Calibrated neutral density filters were used to attenuate the laser beam so as to prevent variations in the temporal, spatial, or spectral properties of the laser pulse associated with adjustments to the laser driving power. To reduce reflections of the beam from

the face of the filter back into the laser cavity, the filters were placed at ~ 20° angle with respect to the laser beam. Attenuations of the laser beam energy of up to 10^5 from the initial laser irradiance energy were measured.

The accuracy of the observed saturation energy which is proportional to the saturation parameter (see Table 1) is dependent upon several factors [2, 18, 110, 125, 126]. To avoid spatial inhomogeneities across the flame viewing region and post-filter effects, only the homogeneous central spot of the laser beam was allowed to irradiate the whole inner seeded flame. A diffuser which maximized the spatial uniformity of the beam was not utilized, due to the $\gtrsim 10^2$ times decrease in laser pulse energy reaching the flame [110]. In addition, temporally-resolved measurement of the peak steady state fluorescence was required, because the laser pulse could not be approximated as a rectangular step function, but instead rose and decayed gradually over time. Therefore, as discussed previously, the saturation energy corresponded to a higher laser pulse energy when time-integrated detection of the fluorescence was employed. Since a longer pulse length laser could not be employed for analyte excitation, both time-resolved and time-integrated fluorescence measurements were performed.

Experimental Apparatus

The instrumentation employed in the experiments consisted of an excitation source (tunable dye laser), a flame of reproducible composition and temperature as an atomizer, a detection

and signal processing system, and a readout mechanism. The
block diagrams for each experiment are shown in Figs. 10-12.

The major random errors in the measurements of fluores-
cence intensity were due to pulse-to-pulse variations in laser
flux, Rf noise, boxcar drift, and nebulizer irregularities in
spray rate, droplet size, and efficiency. For many fluores-
cence signals, the limiting noise was felt to be due to flame
background emission. Systematic errors in the determination
of the fluorescence intensity levels resulted, in general,
from the measurement procedure.

Flames

The nine experimental acetylene/oxygen flames were pro-
duced on a multihole, Méker-type, brass burner which provided
an inner seeded flame and an outer, mantle (unseeded) flame
[59, 71]. An additional, inert gas sheath was not used to
surround the outer flame. The flame mantle minimized infu-
sion of ambient air into the inner flame and other edge
effects such as radial temperature and concentration gradi-
ents across the inner flame [2, 127].

The burner consisted of a rectangular grid of 96 holes
arranged in an 8 x 12 format 0.033 inches in diameter and
spaced 0.045 inches apart. Flame gases reached the burner
head through either 32 (4 x 8) channels which produced the
inner flame or through two rows of 64 holes arranged around
the inner flame grid to produce the outer flame. The height
of the primary combustion cones in the laminar, homogeneous,
and stable flames was approximately 2 mm [2, 59].

Figure 10. Experimental setup for measurement of Na THAF temperatures with ~ 5 ns pulsed laser excitation.
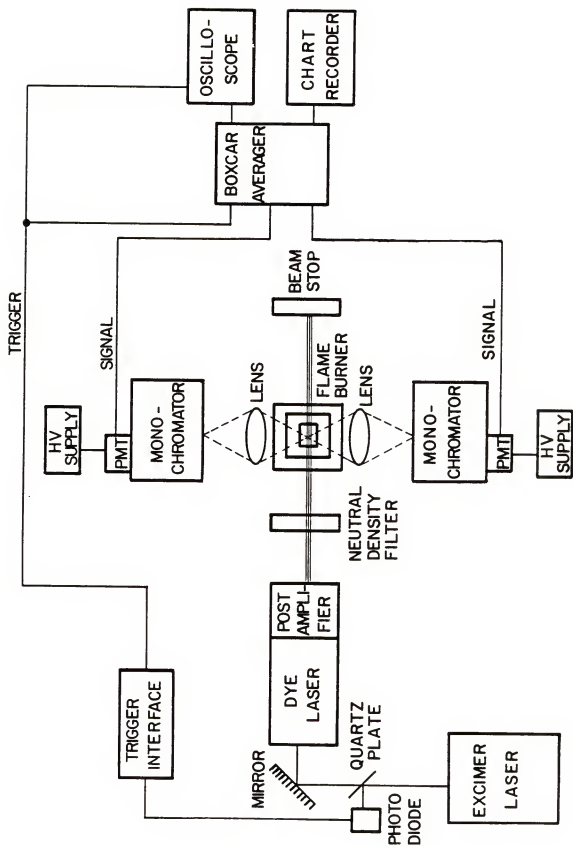
Figure 11. Experimental setup for measurement of single-shot THAF temperatures using Tl as the thermometric seed and ≈ 5 ns pulsed laser excitation.
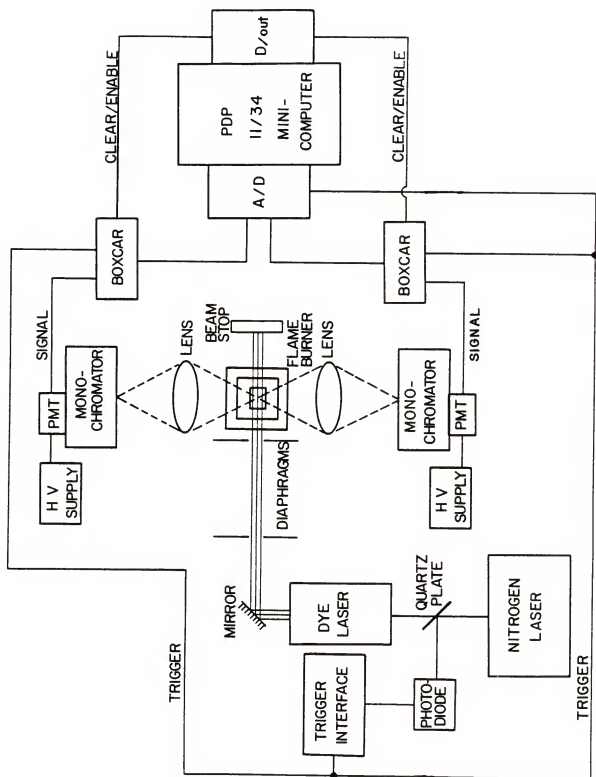
The metering of gas flows consisted of three stages: tank pressure regulation, intermediate gas pressure gauge regulation, and final stage rotameter flow control. Separate flow systems were employed for the inner and outer flame gases. The fuel and oxidant flows were split into two streams downstream from the high pressure storage tanks and prior to the intermediate gauge controls. The diluent gas (Ar or N_2) was divided into four streams: inner flame, outer flame, nebulizer (carrier) gas, and outer sheath. The input pressure of each flow stream to the limiting flow rotameters was regulated by crude neoprene pressure gauges to $\leq$ 30 psig. This stage acted as a reducing valve to ensure constant working pressure across the rotameters and to the flame. The rotameters provided precise, calibrated flow adjustment; the rotameter volumetric flow rate was roughly independent of the variable resistance from pressure changes downstream. A change in the size of the tube allowed the metering of considerably different flow rates needed for the development of flames of differing composition. An adequate precision of 3 to 5% was routinely achieved without constant system recalibration. The rotameters were calibrated for each gas using a linear mass flow meter (Hastings ALK-50K).

The flow rates of the unburnt gases producing the nine experimental flames are listed in Table 3. Throughout these experiments, the fuel was C_2H_2 and the oxidant was O_2. The diluent gas was either Ar or N_2. The flame temperatures ranged from ~ 2000 K to ~ 2500 K. The flames were selected by

Table 3
Flame Gas Composition and Reversal Temperatures
of the Nine Experimental C_2H_2/O_2 Flames

Flame	C_2H_2 (l/min) Inner	Outer	O_2 (l/min) Inner	Outer	(l/min) Inner	Outer	Reversal Temperature (K)
1	0.98	1.25	0.98	1.25	3.95	5.00	2465 ± 10 [a]
2	1.10	1.40	1.0	1.05	4.20	4.70	2450 ± 15 [a]
3	0.76	1.11	1.10	0.95	3.98	5.42	2315 ± 12 [a]
4	0.63	1.15	1.82	1.25	4.59	6.32	2275 ± 15 [a]
5	0.76	1.15	1.33	1.40	4.80	7.75	2200 ± 14 [a]
6	0.63	1.15	1.20	1.40	4.80	7.75	2080 ± 11 [a]
7	1.28	1.70	1.56	1.96	5.27	7.37	2220 ± 14 [a]
8	0.91	1.29	1.10	1.47	4.35	6.67	2140 ± 15 [a]
9	0.98	1.68	0.98	1.93	6.0	7.75	2050 ± 12 [a]

Columns under (l/min): Ar for flames 1–4, N_2 for flames 5–9.

[a] Error in reversal temperature measurement obtained by determining the temperature range over which net detectable Na emission or absorption was not observed.

carefully adjusting the gas flow rates until each flame was near as possible in appearance (shape of flame and height of combustion cones) to the 2465 K stoichiometric $C_2H_2/O_2/Ar$ flame. The variation in observed overall flame height was particularly significant only for the 2080 K $C_2H_2/O_2/Ar$ flame and the 2140 K and 2050 K $C_2H_2/O_2/N_2$ flames. However, in all flames the observation height was 3 cm above the burner head and always appeared to traverse the stable equilibrium zone.

Nebulizer

To minimize Mie scattering of the incident source radiation by solution droplets within the flame viewing region, ultrasonic nebulization of aqueous salt solutions produced a reproducible aerosol which was carried into the inner flame by ~ 0.5 ml/min diluent carrier gas flow [128, 129]. The nebulizer consisted of an ultrasonic transducer (1.4 MHz) seated in the center of a Teflon collar in the middle of the nebulizer body (laboratory constructed by Dr. C. A. Van Dijk). Distilled water cooled the backside of the crystal while a peristaltic pump introduced the sample through a stainless steel capillary tube onto the front of the crystal face. The nebulizer was tilted at 45° to ensure minimum pooling of the solution at the bottom of the crystal and maximum aerosol production. Two carrier gas inlets in front of the crystal swept the aerosol into the inner flame gas stream.

Ultrasonic nebulization has been reported to possess a high aerosol production efficiency which is rather independent of the carrier gas and sample concentration. This factor is

especially important because the degree of aerosol formation and the subsequent analyte atomization efficiency has a direct influence on the sensitivity of the technique and the extent of interference effects [1, 2]. However, contamination by the solution (memory effects) can be quite severe; adequate rinsing is often required, e.g., every 30 min.

Reversal Temperature Measurement

The flame temperatures were (initially) determined using the Na line reversal technique (see Appendix A) [2, 9, 130]. A 6 V, 18 A tungsten microscope lamp (GE EPS-1121) served as the continuum source and provided a higher, maximum operating temperature ($\geq$ 2600 K) than the conventionally used tungsten strip lamp ($\leq$ 2400 K). The microscope lamp was calibrated for operating current vs. brightness temperature at 655 nm and allowed the determination of reversal temperatures of all the flames according to the desired null method. The reflection losses from the lenses ($\gtrsim$ 10%) compensated for the correction factor needed to adjust the brightness temperature to the apparent temperature at the Na 589.0 nm line [9, 11]. A solution of 1000 ppm Na was used in the temperature measurements and resulted in significant self-absorption of the Na resonance line.

The lamp was focused slightly past the flame so that the lamp radiation completely filled the inner seeded flame. This alignment minimized the measurement of an apparently high reversal temperature due to detection of flame emission not within the focusing region of the lamp. A second lens

focused the light onto the monochromator entrance slits (Jarrell Ash 63-000). Two diaphragms were utilized at the focal plane of each lens in order to limit the light (source plus flame emission) viewed by the detector (Hamamatsu R777), to eliminate the detection of emission from the combustion cones, and to equalize the solid angle of light detected to the solid angle of incident source radiation.

As the lamp current (and subsequently, the brightness temperature) was increased, the 589.0 nm Na line was wavelength scanned in order to observe the spectrum of the lamp background continuum plus the superimposed, net Na emission or absorption. The lamp current was continually increased until the Na emission just disappeared. Then at a lamp current corresponding to an initially higher temperature (net Na absorption) the lamp current was decreased until no net signal (null point) was observed. The error in the reversal temperature measurement was indicated by determining the current (and thus the temperature) range over which no noticeable Na emission or absorption occurred. The reversal temperatures are listed in Table 3.

Laser

An excimer-pulsed tunable dye laser (Lumonics TE 861S excimer laser, Molectron DLII dye head with DL 222 post amplifier) was employed for the Na THAF measurements. The excimer fill gas was 40 torr XeCl in 40 psi balance He and lased at 308 nm at a 20 Hz repetition rate (chosen for optimal signal-to-noise ratio). Rhodamine 6G dye (5 x 10^{-3} M in absolute ethanol) was pumped at ~ 1.0 mJ total pulse energy. Separate

flowing dye systems including reservoir and cuvette were used for both the oscillator stage of the primary dye head and the postamplifier stage in order to increase the dye lifetime and to therefore produce laser pulses of reproducible constant energy. No intermediate amplifier stage was needed because of the observation that this stage minimally increased the pulse energy while having introduced significant background dye fluorescence. The total pulse energy was measured by a calibrated energy meter (Molectron J3-05DW).

The tuning range of R6G permitted Na excitation in three modes (see Fig. 2): single-photon resonance absorption at 589.0 nm (3S→3P) and two two-photon resonance absorption modes at 578.7 nm (3S→4D) and 602.2 nm (3S→5S). The 602.2 nm pulse energy was significantly lower than the other modes (~ 0.5 mJ). The laser pulse duration was ~ 5 ns.

For measurement of Tl THAF fluorescence, a N_2-pumped tunable dye laser (Molectron UV-24 laser with DL II dye head) was utilized to pump BBQ dye (3.5 x 10^{-3} M in 50% toluene/50% absolute ethanol) at 377.6 nm ($6P_{3/2}$→7S) at 0.2 to 1.6 mJ total pulse energy (see Fig. 3). The laser, operated at a 20 Hz repetition rate, produced ~ 5 ns laser pulses. Quartz cuvettes fitted with Brewster windows were used in the oscillator and amplifier stages. The dye lifetime was approximately 1½ hours.

In order to minimize spatial inhomogeneities across the laser beam and post-filter effects, no lenses were used to focus the laser beam. One 2 mm diameter diaphragm (~ 1 m from

dye head to burner) was employed to limit the usable area of
the excimer dye laser beam to the central, more homogeneous
beam "hot spot." However, two 2 mm diameter diaphragms,
~ 3 m from the laser head to the first aperture and separated
by ~ 1 m, were needed to limit the N_2-pumped dye laser beam.
Each excitation beam completely filled the inner flame. In
contrast to single-photon Na resonance excitation, a 5 cm
focusing lens was required to tightly focus the laser beam
for two-photon resonance excitation of Na and to observe the
THAF fluorescence.

Optical and Electronics Setup

The fluorescence fluxes resulting from the ~ 3 mm^3 laser
probed flame volume 3 cm above the burner top were collected
at right angles to the beam and focused with 2 inch diameter,
3 inch focal length lenses onto the entrance slits of two,
f = 3.5 throughput monochromators (Instrument SA Jobin-Yvon
H 10 UV) (see Figs. 10-12) in a 2f-to-2f arrangement. A band-
pass of 8.0 nm was utilized for the Na time-integrated measure-
ments while a 4.0 nm bandpass was used for the Na time-resolved
measurements. Accordingly, a 4.0 nm spectral bandpass was
observed for the Tl time-integrated and time-resolved fluo-
rescence detection. Even though spatial constraints necessi-
tated the use of small focal length lenses which resulted in
the overfilling of the monochromators, the large diameter of
the lenses increased the solid angle of fluorescence detected
and therefore increased the fluorescence signals observed.
The dark currents of the fast-wired photomultipliers were

~ 7 to 10 nA; calibrated neutral density filters (Corion) were required to prevent photomultiplier saturation.

The relative spectral response from 250 to 700 nm of each monochromator and photomultiplier were calibrated using a tungsten strip lamp (GE EPUV 1068). On a DC emission basis, the response at each wavelength was recorded.

Signal Processing

For time-averaged fluorescence measurement, the photomultiplier current signals (which were, typically, electronically delayed by 90 to 120 ns) were fed into 50 Ω input impedance inputs of a boxcar averager (PAR 162 with 164 gated integrator modules). Two boxcars were utilized in the Tl single-shot THAF measurements. For the typical "signal averaged" method of measuring Tl and Na THAF, only one detection channel was used and the fluorescence from the two transitions were sequentially detected. The following boxcar parameters were used: 1.0 μs input time constant in exponential averaging, 0.5 μs aperture range, nominal 5 ns gate width, 0.1 ms output time constant, and external (20 Hz) triggering. To compensate for timing jitter from erratic laser triggering, an optical trigger (laboratory constructed by Dr. E. Voigtman) was used to trigger the boxcar. A small fraction of the pump laser beam (split off by a 90% beam splitter) was detected by a fast photoelectric detector. The TTL compatible signal was utilized for boxcar, oscilloscope, and computer interrupt triggering.

The output signal (0.1 to 1.0 V) from the boxcar was observed on a strip chart recorder (Fisher Products Quanti-graph) or was fed directly to a PDP 11/34 minicomputer system (Digital Equipment Corporation) via ± 1 V 12-bit A/D converter inputs of the LPS11 laboratory peripheral interface. The photomultiplier signals were displayed on a fast storage oscilloscope (Tektronix 7834 using 7A26 and 7B80 plug-ins) in order to facilitate the correct timing of the boxcar triggering and the signal integration.

Time-resolved Detection

The measurement of time-resolved fluorescence (gate < pulse duration) required an elaborate detection and signal processing system (see Fig. 12). The 1S1 sampling head of the Tektronix 549 oscilloscope provided a 350 ps rise time gate which was <u>scanned</u> across the fluorescence pulse ($\leq$ 2 V input) at a rate of < 0.01 Hz (each sweep was a culmination of > 2400 laser shots). A DC offset was externally applied in order to sweep only the fluorescence pulse within the ~ 15 ns range. An x→y chart recorder (BBN Plotamatic) was used to record the scan of the THAF signals.

Because the 1S1 sampling head did not provide time-resolved detection of just one pulse (unlike a transient digitizer system), the recorded output was dependent on the reproducibility of the fluorescence pulse intensity and shape. As shown in Fig. 13, the irregularities in laser excitation pulse shape and duration (ringing after pulse)

Figure 12. Experimental setup for time-resolved measurement of peak fluorescence induced by ∿ 5 ns pulsed laser excitation.
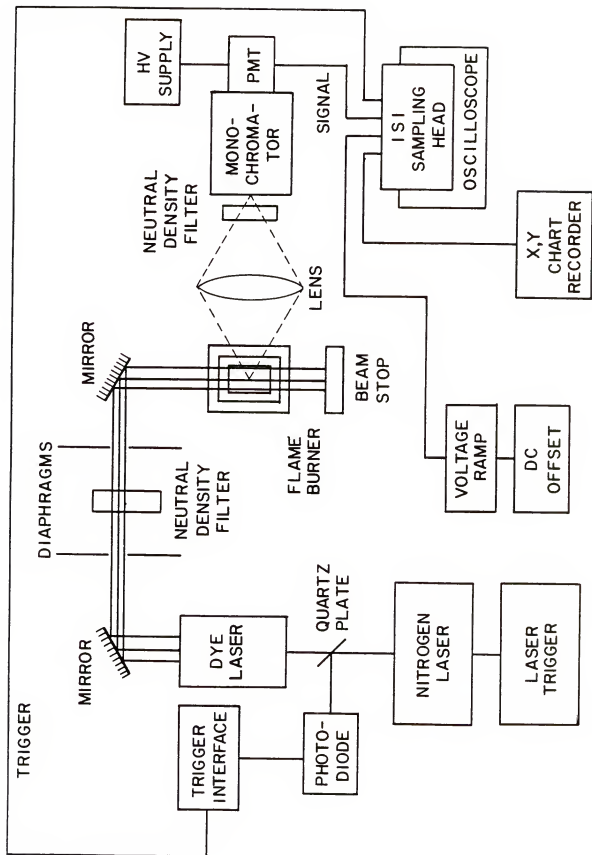
Figure 13. Laser excitation pulses produced from Rhodamine
6G (top) and BBQ (bottom) laser dyes. The
apparent rise time of each laser pulse is the
convolution of the true laser rise time and the
impulse response of the photomultiplier. The
pulse duration corresponding to the pulse
half width is estimated as $\sim$ 6 ns for Rhodamine
6G and $\sim$ 5 ns for BBQ. The two pulses depicted
for BBQ indicate the irreproducibility in
amplitude and shape observed for the laser
excitation pulses. The ringing at the end of
each pulse is most likely due to the detection
electronics.
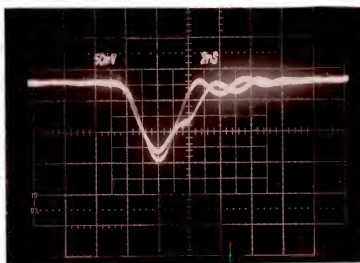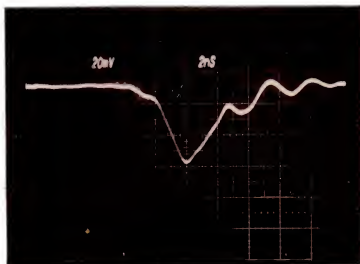
are evident. However, the shape and intensity of the 1S1
output sweeps were consistently reproducible within the 10%
experimental error.

   The experimental calibration factors, wavelengths,
transition probabilities, etc., for the Na and Tl fluores-
cence transitions are listed in Tables 4 and 5.

Table 4

Na Experimental Parameters

THAF Transition Wavelength λ (nm)	THAF Transition	Energy of Upper Level (cm⁻¹)	g^a (dimensionless)	A^b (s⁻¹)	$\dfrac{\lambda}{\Sigma gA}$ (nm s)	$S_{\lambda i}^{\,c}$ (au)	$S_{\lambda j}^{\,d}$ (au)
589.3	$3P_{3/2} \to 3S_{1/2}$	16965	4	61.0	1.61	1000	760
	$3P_{1/2} \to 3S_{1/2}$		2	61.2			
330.2	$4P_{3/2} \to 3S_{1/2}$	30270	4	3.58	15.4	76	27
	$4P_{1/2} \to 3S_{1/2}$		2	3.54			
285.4	$5P_{3/2} \to 3S_{1/2}$	35042	4	0.92	51.0	17	6.2
	$5P_{1/2} \to 3S_{1/2}$		2	0.94			
	$5D_{5/2} \to 3P_{1/2}$		6	4.73			
498.0	$5D_{3/2} \to 3P_{1/2}$	37037	4	3.96	10.5	1150	690
	$5D_{3/2} \to 3P_{3/2}$		4	0.79			

[a] Statistical weight of upper level of fluorescence transition (dimensionless).

[b] Einstein coefficient of spontaneous emission for fluorescence transition (s⁻¹).

[c] Relative response of detection channel i at wavelength of transition (arbitrary units).

[d] Relative response of detection channel j at wavelength of transition (arbitrary units).

Table 5

Tl Experimental Parameters

TlAF Transition Wavelength λ (nm)	TlAF Transition	Energy of Upper level (cm⁻¹)	g^a (dimensionless)	A^b (s⁻¹)	$\lambda_{E_{jk}}$ (nu s)	$S_{\lambda i}^{\,c}$ (au)	$S_{\lambda j}^{\,d}$ (au)
377.6	$7S_{1/2} \rightarrow 6P_{1/2}$	26478	2	0.6203	304.4	240	95
535.0	$7S_{1/2} \rightarrow 6P_{3/2}$	26478	2	0.6994	382.5	1220	800
323.0	$8S_{1/2} \rightarrow 6P_{3/2}$	38747	2	0.2147	752.2	64	22
292.0	$7D_{5/2} \rightarrow 6P_{3/2}$	42030	6	0.4836			
	$7D_{3/2} \rightarrow 6P_{3/2}$		4	0.0867	89.9	23	8
352.5	$6D_{5/2} \rightarrow 6P_{3/2}$	36159	6	1.2975			
	$6D_{3/2} \rightarrow 6P_{3/2}$		4	0.2148	40.8	132	52
276.8	$6D_{3/2} \rightarrow 6P_{1/2}$	36118	4	1.2479	55.5	12.5	4.8
282.6	$9S_{1/2} \rightarrow 6P_{3/2}$	43166	2	0.1000	1413.0	16	5.8
271.0	$8D_{5/2} \rightarrow 6P_{3/2}$	44683	6	0.1990			
	$8D_{3/2} \rightarrow 6P_{3/2}$		4	0.0427	198.6	10	4.2

[a] Statistical weight of upper level of fluorescence transition (dimensionless).

[b] Einstein coefficient of spontaneous emission for fluorescence transition (s⁻¹).

[c] Relative response of detection channel i at wavelength of transition (arbitrary units).

[d] Relative response of detection channel j at wavelength of transition (arbitrary units).

Na THERMALLY ASSISTED FLUORESCENCE

Experimental Results

THAF Measurement

With time-averaged detection of Na THAF signals under
single-photon and two-photon resonance excitation modes,
fluorescence could be observed for the 3P→3S (589.3 nm),
4P→3S (330.2 nm), 5P→3S (285.4 nm), and 5D→3P (498.0 nm)
transitions [36, 131]. The fluorescence signals from the
5S→3P (616.0 nm) and 4D→3P (569.0 nm) transitions could not
be resolved from the laser background. The 6S→3P (515.0 nm)
transition fluorescence could not be detected while the ob-
served signal from the 3D→3P (819.0 nm) transition was due
to spurious laser dye emission and not to Na fluorescence.
The random errors ranged from ~ 1% for the hotter flames to
~ 10% for the coolest Ar- and N_2-diluted flames. The fluo-
rescence signal-to-noise ratio degraded significantly as the
flame temperature decreased.

The fluorescence signals were measured by carefully
scanning across the fluorescence wavelength and by subtracting
the background produced by the natural flame emission. The
fluorescence from each transition was sequentially detected
using one detection channel (monochromator plus boxcar). In
order to verify the accuracy of the optical calibration, the
fluorescence from the 2465 K $C_2H_2/O_2/Ar$ flame was initially

measured with two detection channels (each monochromator oriented at 90° with respect to the other). If the temperature determined from the intensities of any pair of levels with one detection channel was the same as that determined using the other channel, then the optical calibration was assumed to be reliable (see Tables 4 and 5). The THAF temperatures from measurements using one detection channel for the 2465 K flame were within 0.5% of those determined with the other channel.

The THAF temperatures for all of the observed transitions of Na in the nine flames under each excitation mode are listed in Table 6. In Figs. 14 and 15, typical Na atomic population distributions are shown for the 2465 K Ar-diluted and 2220 K N_2-diluted flames. As indicated in Eqn. 1, atomic level populations are proportional to the normalized fluorescence intensities $B_F\lambda/gA$ originating from the excited levels. The population distributions observed were consistent for each type "quenching" flame and for each excitation mode. The intensity ratios for the 2050 K N_2-diluted flame did show some anomalies compared to the other flames (see Table 6); one possible reason was the excessively poor signal-to-ratio obtained for two (5P→3S and 5D→3P) of the four transitions observed in this flame.

In general, under 3S→3P, 3S→4D and 3S→5S excitations, the Na 3P level possessed the largest population which ranged from 4.5 x 10^3 to 5 x 10^6 times greater than the populations of any of the upper levels under 3S→3P excitation, from 80 to 2.5 x 10^4 times larger under 3S→4D excitation,

Table 6

Na Thermally Assisted Fluorescence (THAF)
Temperatures for the Experimental Flames

THAF Transition Ratio (K)	2465 K Ar (K)	2450 K Ar (K)	2315 K Ar (K)	2275 K Ar (K)	2200 K Ar (K)	2080 K Ar (K)	2220 K N₂ (K)	2140 K N₂ (K)	2050 K N₂ (K)	2170 (K)
5P→3S 4P→3S	-3350[a] -9060[b] -6930[c]	-4050	-2970 -2.2×10^4	-3090	-2830 -1.9×10^4	----	3120 7060	4370 -2320	-2265	2170
5P→3S 5D→3P	730[a] 540[b] 500[c]	1110	750 580	880	800 630	----	1340 510	1620 260		
5P→3S 3P→3S	3090[a] 5910[b] 5870[c]	2640	2950 5990	2410	2830 2740	----	1980 4195	2180 ----	1740	
4P→3S 5D→3P	5000[a] 2140[b] 2070[c]	1.1×10^4	6410 2090	9240	8420 2320	4090	2240 1470	2910 1190	5130	
4P→3S 3P→3S	1825[a] 3680[b] 3510[c]	1650	1710 4090	1460	1630 1930	1460	1740 3640	1840 ----	1610	
5D→3P 3P→3S	2350[a] 2980[b] 2860[c]	2330	2295 3120	2060	2270 2060	1880	1990 2450	2120 ----	2120	

[a] resonance 3S→3P excitation; [b] 3S→4D two-photon excitation; [c] 3S→5S two-photon excitation.

Figure 14.   Boltzmann plots of ln ($B_F\lambda/gA$) vs. the energy
             of the upper level involved in the Na fluores-
             cence transition for the 2465 K $C_2H_2/O_2/Ar$
             flame under three excitation modes: a. 3S→3P,
             b. 3S→4D, and c. 3S→5S. The dashed lines
             indicate the reversal temperature and are
             plotted using the pair of levels closest to the
             reversal temperature. The arrow indicates the
             laser excited level. All B_F values are
             expressed in the same, but arbitrary units (au).
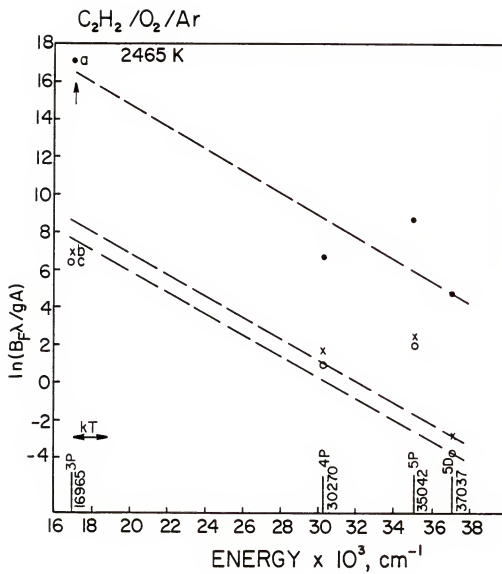
Figure 15. Boltzmann plots of ln ($B_F\lambda/gA$) vs. the energy of the upper level involved in the Na fluorescence transition for the 2220 K $C_2H_2/O_2/N_2$ flame under three excitation modes: a. 3S→3P, b. 3S→4D, and c. 3S→5S. The dashed lines indicate the reversal temperature and are plotted using the pair of levels closest to the reversal temperature. The arrow indicates the laser excited level. All B_F values are expressed in the same, but arbitrary units (au).

$C_2H_2/O_2/N_2$

2220 K
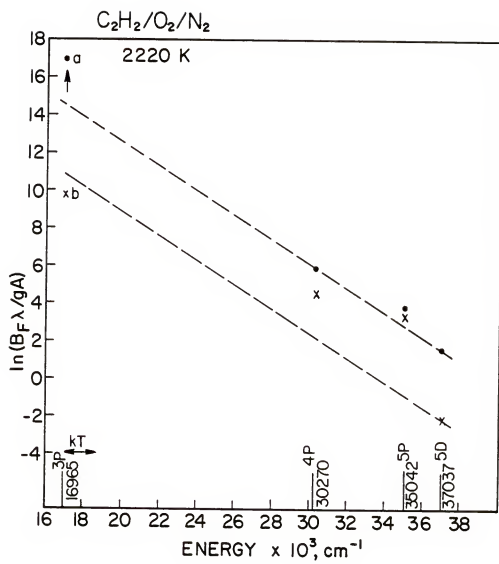
and from 85 to 2.5 x 10^4 times larger under 3S→5S excitation. The 3P level was overpopulated with respect to the upper states under 3S→3P laser excitation for all flames; the sole exception occurred for the relatively more overpopulated 5P level in the Ar-diluted flames as seen in Fig. 14. Overpopulation refers to the condition where for certain levels, $B_F\lambda/gA$ values are higher than the matching points on the $B_F\lambda/gA$ vs. ΔE curve corresponding to the flame reversal temperature. In contrast, under 3S→4D and 3S→5S excitation modes, the 3P level was relatively underpopulated with respect to the 4P, 5P, and 5D levels.

The weakest fluorescence intensities for those transitions producing detectable fluorescence under all excitation modes originated consistently from the 5D level which is ~ 2.5 eV above the 3P level. The next weakest lines observed under single-photon and two-photon resonance excitations were the 4P→3S (350.2 nm) transition for the N_2-diluted flames and the 5P→3S (285.4 nm) transition for all of the Ar-diluted flames. The 2140 K N_2-diluted flame also showed a stronger 5P→3S transition than the 4P→3S transition under 3S→4D excitation.

All of the Ar-diluted flames consistently indicated a large
population inversion between the 4P and 5P levels, especially
under 3S→3P excitation, while the N_2-diluted flames showed
only significant deviations from partial Boltzmann equilibrium.

The dashed lines in Figs. 14 and 15 indicate the reversal
temperature slope and were plotted using the pair of levels
which produced the fluorescence ratio closest to the Boltzmann
value at the flame reversal temperature. The THAF temperature
closest to the reversal temperature always resulted from the
ratio of fluorescence intensities from the 3P→3S and 5D→3P
transitions.

Saturation curves (relative fluorescence vs. relative
laser pulse energy) were constructed for all of the flames
from the fluorescence observed from the 3P radiatively pumped
level and from the thermally assisted 4P level. In addition,
plots of fluorescence originating from the 5P and 5D levels
were also determined for the 2465 K Ar-diluted flame (see
Figs. 16 and 17). The slopes at low laser energies for the
fluorescence transitions involving the excited levels under
3S→3P excitation match closely within 5% the initial slope
of the saturation curve for the 3P→3S transition. In contrast
to the $C_2H_2/O_2/N_2$ flames, the slopes for the $C_2H_2/O_2/Ar$ flames
at low laser energies, within the 10% experimental precision,
are significantly less than unity.

Time-resolved THAF measurements

Using the N_2-pumped tunable dye laser, time-resolved
detection of the peak fluorescence using the 1S1 sampling

Figure 16.   Saturation curves of relative fluorescence
              intensity vs. relative laser pulse energy for
              Na in the 2465 K $C_2H_2/O_2/Ar$ flame showing
              four transitions of interest: a. 3P→3S
              (589.3 nm), b. 4P→3S (330.2 nm), c. 5D→3P
              (498.0 nm), and d. 5P→3S (285.4 nm). The
              time-averaged fluorescence intensities are
              expressed in the same, but arbitrary units
              (au). The laser energies (measured in mJ
              per pulse) are recorded in the same, but
              arbitrary units (au). Note that there is no
              significance attached to the absolute signal
              magnitudes of each saturation curve.

Figure 17.   Saturation curves of relative fluorescence
              intensity vs. relative laser pulse energy
              for Na in the 2220 K $C_2H_2/O_2/N_2$ flame showing
              two transitions of interest: a. 3P→3S
              (589.3 nm) and b. 4P→3S (330.2 nm). The
              time-averaged fluorescence intensities are
              expressed in the same, but arbitrary units
              (au). The laser energies (measured in mJ
              per pulse) are recorded in the same, but
              arbitrary units (au). Note that there is
              no significance attached to the absolute
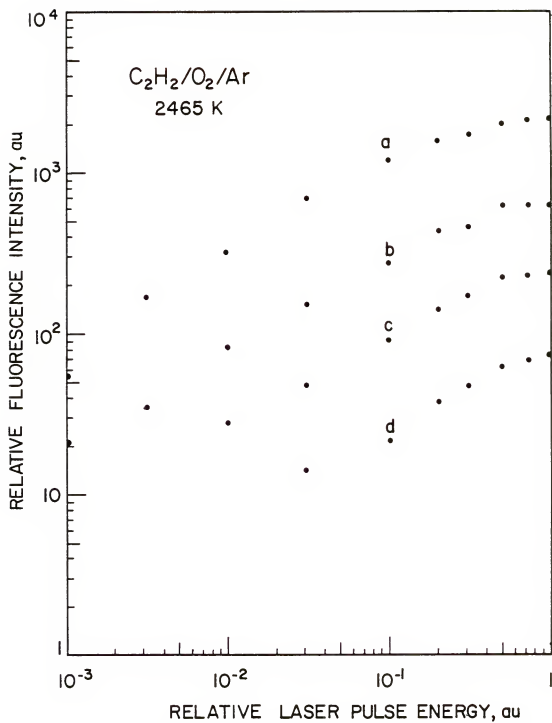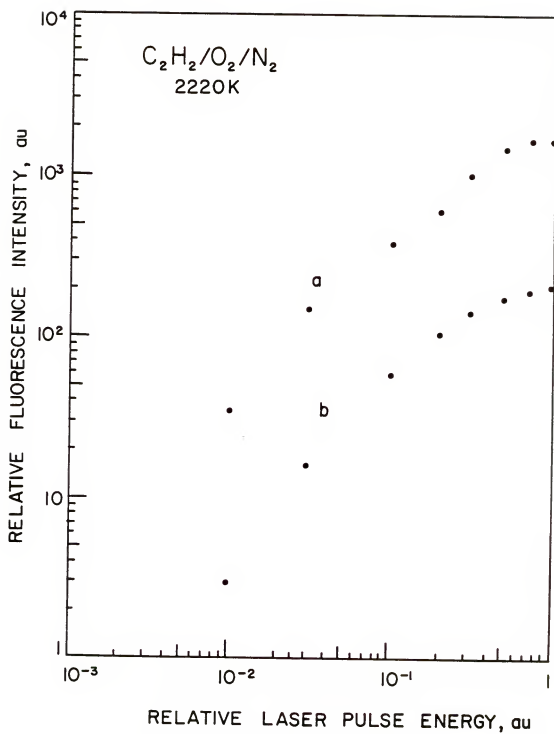   signal magnitudes of each saturation curve.

$C_2H_2/O_2/N_2$
2220K

RELATIVE FLUORESCENCE INTENSITY, au

RELATIVE LASER PULSE ENERGY, au

head as well as time-averaged measurements using the boxcar
averager were performed. The fluorescence originating from
the 3P→3S, 4P→3S, 5P→3S, and 5D→3P transitions was detected
for both the 2465 K Ar- and 2220 K N_2-diluted flames (see
Figs. 18 and 19). The THAF temperatures are listed in Table
7. Again, as corresponding to the time-averaged measurements
for all nine C_2H_2/O_2 flames, the pair of levels which produced
the ratio of fluorescence closest to the reversal temperature
was consistently the 5D and 3P levels.

Typically, the 3P level again possessed the largest pop-
ulation under 3S→3P, 3S→4D, and 3S→5S excitation modes. The
3P level time-resolved population magnitude ranged from 6 x 10^3
to 4 x 10^5 times larger than the populations of any of the
other excited levels under 3S→3P laser excitation; however,
only the fluorescence from the 3P→3S and 4P→3S transitions
under the two-photon excitations was detected. The 3P level
was relatively overpopulated with respect to the thermally
assisted levels under 3S→3P excitation except for the 5P
level in both the 2465 K Ar- and 2220 K N_2-diluted flames.

Consistent with the previous results obtained under
time-averaged detection, the 2465 K $C_2H_2/O_2/Ar$ flame showed
a relative population inversion between the 4P and 5P levels
under time-resolved detection, although the magnitude of the
inversion as indicated by the 5P/4P population ratio was
smaller than that observed previously by a factor of 4.
As indicated with prior time-averaged measurements, the 2220
K $C_2H_2/O_2/N_2$ flame showed only a deviation from partial Boltz-
mann equilibrium for those levels.

Table 7
Comparison of Time-Resolved and Time-Averaged Na THAF Temperatures for the 2465 K C_2H_2/O_2/Ar and the 2220 K $C_2H_2/O_2/N_2$ Flames under 3S→3P Resonance Excitation

Transition Ratio	2465 K C_2H_2/O_2/Ar		2220 K $C_2H_2/O_2/N_2$	
	Time-Resolved (K)	Time-Averaged (K)	Time-Resolved (K)	Time-Averaged (K)
$\frac{5P \rightarrow 3S}{4P \rightarrow 3S}$	-5660	-1.1×10^4	4.9×10^7	5940
$\frac{5P \rightarrow 3S}{5D \rightarrow 3P}$	775	865	1340	1590
$\frac{4P \rightarrow 3S}{5D \rightarrow 3P}$	2035	3600	4250	3290
$\frac{5P \rightarrow 3S}{3P \rightarrow 3S}$	4330	2815	2610	2345
$\frac{4P \rightarrow 3S}{3P \rightarrow 3S}$	1930	1940	1950	1925
$\frac{5D \rightarrow 3P}{3P \rightarrow 3S}$	2330	2300	2390	2240

Figure 18.   Boltzmann plots of ln $(B_F\lambda/gA)$ vs. the energy
of the upper level involved in the Na fluores-
cence transition for the 2465 K $C_2H_2/O_2/Ar$
flame. Time-averaged fluorescence detection
is indicated by the dot, while time-resolved
detection of peak fluorescence is indicated
by the x. The arrow indicates the laser
pumped level. All B_F values are expressed
in the same, but arbitrary units (au).
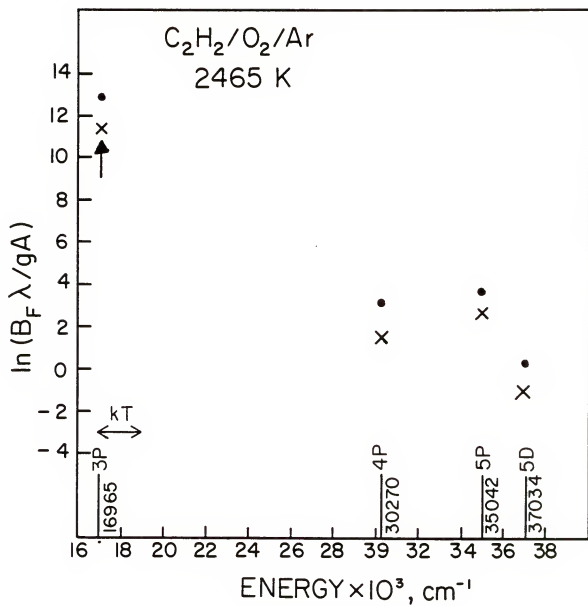
Figure 19. Boltzmann plots of ln $(B_F\lambda/gA)$ vs. the energy
of the upper level involved in the Na fluores-
cence transition for the 2220 K $C_2H_2/O_2/N_2$
flame.   Time-averaged fluorescence detection
is indicated by the dot, while time-resolved
detection of peak fluorescence is indicated
by the x. The arrow indicates the laser
pumped level. All B_F values are expressed
in the same, but arbitrary units (au).

$C_2H_2/O_2/N_2$

2220K

$\ln(B_F\lambda/gA)$

kT

3P
16965

4P
30270

5P
35042

5D
37037

ENERGY×10^3, cm^{-1}
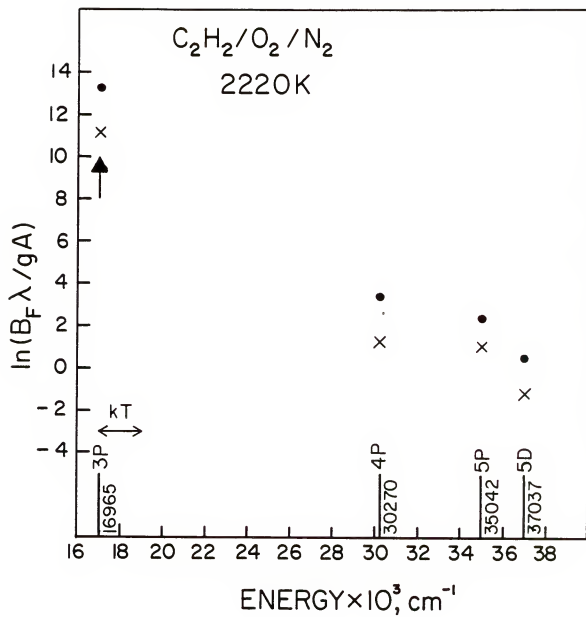
Saturation curves of time-resolved and time-averaged fluorescence vs. laser pulse energy (see Figs. 20 and 21) were constructed using fluorescence corresponding to the laser excited 3P level and to the collisionally populated 4P and 5D levels. The incident laser pulse energies (prior to the atten-uation via neutral density filters) were ~ 0.57 mJ per pulse for the $C_2H_2/O_2/Ar$ flame and ~ 1.35 mJ per pulse for the $C_2H_2/O_2/N_2$ flame. The initial slopes of the saturation curves at low laser energies corresponded to ~ 1.0 ± 0.05. Three important features are apparent:

(i)   for each flame, the shape of each curve constructed from the time-averaged fluorescence from the collisionally excited states closely follows the saturation curve of the time-averaged fluorescence produced from the laser excited level.

(ii)   for each flame, the time-resolved fluorescence saturation curves appear to be consistently equivalent.

(iii) the onset of fully saturated fluorescence appears to occur at relatively lower laser pulse energies for the Ar-diluted flame than for the N_2-diluted flame.

The saturation energy (corresponding to the saturation param-eter) was calculated for each saturation curve by two estimation approaches: the laser pulse energy which corresponds to 50% of the fully saturated laser energy and the pulse energy which corresponds to the intersection of the linear and saturated aymptotes.

Figure 20.   Saturation curves of relative fluorescence
             intensity vs. relative laser pulse energy for
             Na in the 2465 K $C_2H_2/O_2/Ar$ flame showing
             three transitions of interest: a. $3P \rightarrow 3S$
             (589.3 nm), b. $4P \rightarrow 3S$ (330.2 nm), and c.
             $5D \rightarrow 3P$ (498.0 nm).   All fluorescence inten-
             sities are expressed in the same, but
             arbitrary units (au).   The laser energies
             (measured in mJ per pulse) are recorded in
             the same, but arbitrary units (au).   Time-
             averaged fluorescence detection is indicated
             by the dot, while time-resolved detection
             of peak fluorescence is indicated by the x.
             Note that there is no significance attached
             to the absolute signal magnitudes of each
             saturation curve.

Figure 21.   Saturation curves of relative fluorescence
             intensity vs. relative laser pulse energy
             for Na in the 2220 K $C_2H_2/O_2/N_2$ flame showing
             three transitions of interest: a.   3P→3S
             (589.3 nm), b.   4P→3S (330.2 nm), and c.
             5D→3P (498.0 nm).   All fluorescence inten-
             sities are expressed in the same, but
             arbitrary units (au).   The laser energies
             (measured in mJ per pulse) are recorded in
             the same, but arbitrary units (au).   Time-
             averaged fluorescence detection is indicated
             by the dot, while time-resolved detection
             of peak fluorescence is indicated by the x.
             Note that there is no significance attached
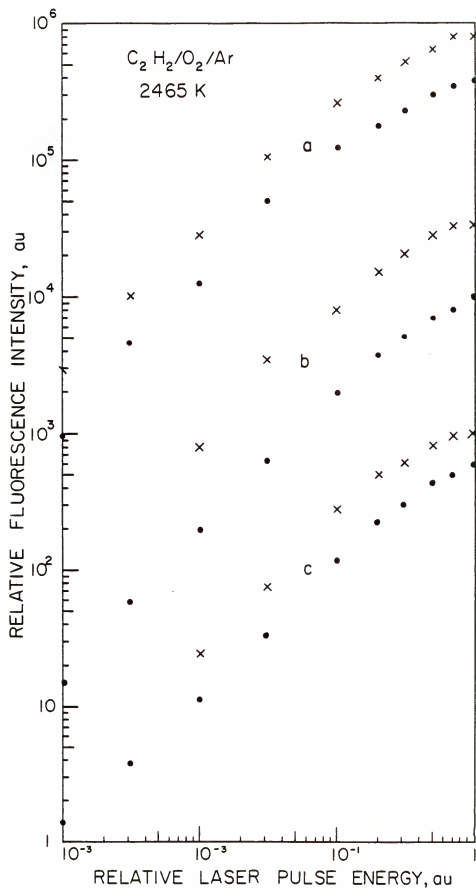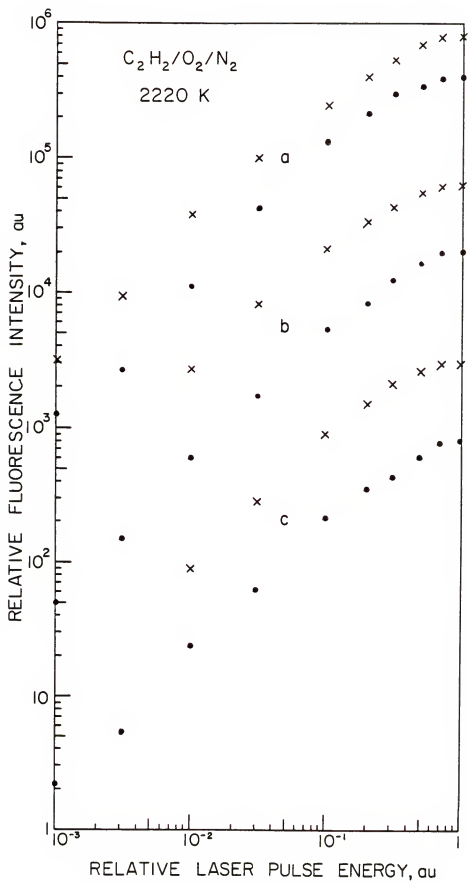   to the absolute signal magnitudes of each
             saturation curve.

$C_2H_2/O_2/N_2$

2220 K

RELATIVE FLUORESCENCE INTENSITY, au

RELATIVE LASER PULSE ENERGY, au

The saturation energies determined for each flame and the relative comparison between the values reached by each method are listed in Table 8. The estimated error for the 50% saturation method was approximately ± 5-10%. However, the asymptotic method is critically dependent on the accurate measurement of fluorescence of low signal-to-noise ratio at low laser energies. The best-fit line must possess the least error in its slope to result in a highly accurate saturation parameter determination; the estimated error in the asymptotic measurement was ~ 10-25%. As can be seen from Table 8, the time-resolved measurements in the $C_2H_2/O_2/N_2$ flame provided quite consistent estimates of the saturation energy for the 3P→3S, 4P→3S, and 5D→3P fluorescence transitions of 0.21 ± 0.2; the slightly higher value of 0.32 as determined by the relatively more inaccurate asymptotic method for the 4P→3S transition may not be significant. However, the time-averaged measurements provided two estimates of the saturation energy for each transition; in addition, the resulting determinations by the relatively more accurate 50% saturation method for the collisionally excited 4P and 5D levels do appear to be slightly higher than the 3P→3S transition saturation energy.

In contrast, the time-resolved saturation energy measurements for the $C_2H_2/O_2/Ar$ flame show disparate results depending on the estimation method. However, the 50% saturation approach does provide consistently lower values as can be observed for each flame, each transition, and each measurement method. The saturation energy determined for the 4P→3S and 5D→3P transitions

Table 8
Comparison of Time-Resolved and Time-Averaged
Saturation Energies for Na in the 2465 K
$C_2H_2/O_2/Ar$ and the 2220 K $C_2H_2/O_2/N_2$ Flames

Flame	Saturation Energy (mJ per pulse)		
Measurement Method	$3P{\rightarrow}3S$ (589.0 nm)	$4P{\rightarrow}3S$ (330.2 nm)	$5D{\rightarrow}3P$ (498.0 nm)
2465 K $C_2H_2/O_2/Ar$			
Time-averaged	0.11[a] 0.12[b]	0.21[a] 0.38[b]	0.21[a] 0.37[b]
Time-resolved	0.084[a] 0.087[b]	0.11[a] 0.16[b]	0.11[a] 0.15[b]
2220 K $C_2H_2/O_2/N_2$			
Time-averaged	0.20[a] 0.35[b]	0.27[a] 0.35[b]	0.24[a] 0.32[b]
Time-resolved	0.20[a] 0.23[b]	0.20[a] 0.32[b]	0.20[a] 0.22[b]

[a] Saturation energy estimated from 50% fully saturated intensity.

[b] Saturation energy estimated from intersection of linear and saturated asymptotes.

are higher than the 3P→3S transition saturation energy and those values estimated by each method are significantly not equivalent. The saturation energies derived from the time-averaged results are even more variable. Significantly, the values determined for the 3P→3S laser excited transition by each measurement approach are only slightly larger than those obtained by the time-resolved measurements not only in the $C_2H_2/O_2/Ar$ flame but also in the $C_2H_2/O_2/N_2$ flame. In contrast, the saturation energies determined for the 4P→3S and 5D→3P transitions are considerably greater than the 3P→3S value and vary significantly (by roughly a factor of 1.8) between measurement methods.

Discussion

It is readily apparent from Figs. 14 and 15 that partial Boltzmann equilibrium over the collisionally and radiatively excited levels of Na under ~ 5 ns pulsed laser excitation was not attained. Both $C_2H_2/O_2/Ar$ and $C_2H_2/O_2/N_2$ type flames exhibited significant deviations from thermally assisted (Boltzmann) population distributions. In itself, the over-population of the Na 3P level under 3S→3P laser excitation with respect to the other excited states at the reversal temperature is not particularly unexpected; the fast laser pumping rate not only promoted saturation of the 3P level, but under these saturation conditions, was predictably much larger than any collisional redistribution rate which induced population of other excited states. Therefore, the ratio of

population of any other level to the population of the 3P
level was quite insensitive to changes in flame temperature.
The converse relative underpopulation of the 3P level with
respect to other collisionally and radiatively excited states
under 3S→4D and 3S→5S two-photon laser excitations was also
not unexpected [36]. The 3P level serves as an intermediate
for many downward transitions and its depopulation rate is a
comparatively fast process; therefore, the 3P population may
have been due only to downward collisional cascade, unless the
3P level was additionally populated via a single-photon wing
mechanism under two-photon excitation of the 4D or 5S level.
One-photon excitation has been theoretically predicted [132],
and previously, the Na 3P level (in a $H_2/O_2/Ar$ flame) had
been observed to be populated via some 3P wing absorption
as well as via a two-photon (3S→4D or 3S→5S) process with
subsequent cascading deexcitation [36].

The saturation curves depicted in Figs. 16 and 17 can
be used to indicate whether indirect radiative excitation of
any upper state above the laser pumped 3P level was present.
As shown in Fig. 22, the 4D or 5S level (under Na 3S→3P
pumping) could be excited either through a simultaneous
two-photon <u>absorption</u> process or through a two step <u>excitation</u>
process with the 3P level serving as a real intermediate [2,
38]; the latter may occur if the duration and intensity of
the laser pulse is sufficient to result in the sequential
absorption of two photons by a Na atom whose 3P excitation
energy has been perturbed by flame molecules to become

Figure 22. Simplified level diagram depicting possible pathways for two step, two-photon excitation of the upper levels of Na. The energetically shifted Na 3P level is involved as the intermediate state in the sequential two-photon excitation of the 4D or 5S levels. The heavy arrow indicates the laser excited levels; the thin arrows indicate collisional transitions; the dashed lines indicate the energy of the laser photons (detuning not to scale), while the dots indicate line broadening collisions.
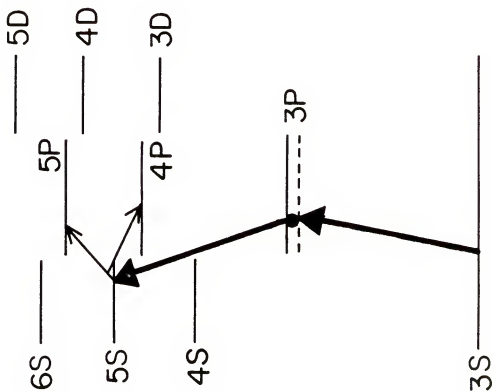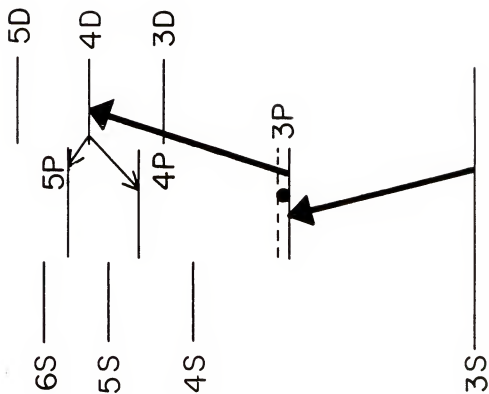
comparable to the incident photon energy [16, 38, 133, 134].
Therefore, under these conditions, a Na atom could be excited
to the 4D or 5S states via the energetically shifted 3P level.
Even though no detectable fluorescence from the 4D or 5S
levels was observed, saturation curves of fluorescence from
other collisionally excited levels may perhaps be utilized to
determine if additional radiative excitation of the upper
states above the 3P level was occurring. It can probably be
correctly assumed that the mixing collisional rates among the
4D, 5S, 4P, and 5P levels were fast enough (especially since
no 4D or 5S level fluorescence was detected and small energy
differences exist between the levels) to transfer adequately the
radiatively excited population to the 4P or 5P levels. Satur-
ation curves plotted for levels which are radiatively excited
from either of the two-photon processes or from the collisional
cascade from these levels should have   initial slopes at low
laser energies two times larger than the slope observed for
a one-photon pumped transition [38]. As can be seen from
Figs. 16 and 17 for the 2465 K $C_2H_2/O_2/Ar$ and the 2220 K
$C_2H_2/O_2/N_2$ flames, the slopes at low laser energies for fluo-
rescence transitions involving the excited levels under 3S→3P
excitation are comparable within 5% to the initial slope for
the 3P→3S transition. Therefore, collisional processes were
most likely dominating in the excitation of the upper states.
However, within the 10% experimental precision, the slopes
for the Ar-diluted flames are less than unity; the laser pulse
energy was perhaps too high to achieve the linear fluorescence
vs. laser pulse energy relationship [38].

Another important feature that can be seen from the Na "Boltzmann" plots in Figs. 14 and 15 is the difference in the relative populations among the excited levels resulting from the change in diluent gas; this effect is especially apparent for the two flames with approximately the same temperature: 2200 K Ar-diluted and 2220 K N_2-diluted flames. N_2 was a more effective redistributing agent of Na level population, since a more Boltzmann-like distribution was approached as reflected in Tables 6 and 7 and Figs. 14 and 15; in contrast, a population inversion was observed between the 4P and 5P levels in the Ar-diluted flames under 3S→3P, 3S→4D, and 3S→5S excitations [135, 136]. Even though CO and CO_2 are effective quenching species [2], N_2 is rather more abundant and has been observed to be the predominant quenching species in C_2H_2/air flames [2, 55]. The Na-D doublet lifetime in these flames was measured to be 0.72 ns at atmospheric pressure [63], a significant decrease compared to the natural radiative lifetime of 16.2 ns [62, 137]. However, Ar is a rather poor quencher with a collisional cross section of $\leq 10^{-2}$ $\AA^2$ [2, 52-55]. Even though this cross section has been predicted to increase upon collision with higher states of Na [65, 87] and is somewhat temperature dependent [53], the residual decomposition products CO and CO_2 are probably the major quenching species in Ar-diluted flames [65, 84]. However, since these species are not as abundant as Ar in Ar-diluted flames, it is possible that the collisions which Na underwent in these flames were so inefficient in redistributing the population of the

radiatively excited levels according to a partial Boltzmann distribution that steady state was not being reached in the Ar-diluted flames, but may have been reached in the N_2-diluted flames under ~ 5 ns laser excitation.

As depicted in Figs. 20 and 21, saturation curves constructed from time-resolved and time-averaged fluorescence can be used to evaluate whether steady state or transient atomic level populations were being measured. In the $C_2H_2/O_2/N_2$ flames, the commensurable values for the time-resolved saturation energies corresponding to saturation of the 3P→3S, 4P→3S, and 5D→3P transitions indicated that steady state populations (and therefore steady state detected fluorescence) were attained during the laser excitation pulse. However, the disparate results obtained for the time-averaged measurements of fluorescence in terms of the slightly higher values of the saturation energy determined for each transition and the differing results obtained by each estimation method indicate that steady state fluorescence was not being measured, but rather fluorescence proportional to the time-averaged, transient level populations. This particular effect was a result of two factors: the nonuniform temporal behavior of the laser excitation pulse and significant (with respect to the rise and decay rates of the laser pulse) effective lifetimes of the upper states which minimized the ability of the level populations (fluorescence pulse shape) to follow effectively the incident laser pulse intensity (laser pulse shape). In addition, as explained by Alkemade [2, 38], the duration

of the laser pulse increases with increasing laser energy.
Therefore, the time-averaged fluorescence intensity will also
increase with increasing laser intensity. In contrast, time-
resolved peak fluorescence will not be so affected [38]. In
effect, the resultant measurement of the transient excited
level population (dependent on the lifetime of the level) via
time-averaged detection explains the different results obtained
by the two saturation energy calculation methods (see Figs. 20
and 21) due to the change in shape of the saturation curves.
Higher incident pulse energies are required to saturate a
time-varying transition when the peak, steady state fluores-
cence is not being measured. In addition, the onset of sat-
uration (as reflected by the changes in the shape of the
saturation curve with increasing pulse energy) is much sharper,
since the absolute magnitude of the saturated level population
is the same, regardless of the measurement method, if <u>steady
state</u> is being attained during the laser pulse. As can be
seen from Table 8, the slightly higher saturation energies
measured by the 50% fully saturated method for the $4P \rightarrow 3S$ and
$5D \rightarrow 3P$ transitions in comparison with the respective time-
resolved values (by a factor of ~ 1.35) were most likely
caused by slightly longer effective lifetimes (dependent on
the relative magnitudes of the collisional rates) of the col-
lisionally excited levels in comparison with the 3P pumped
level. However, these apparent lifetimes in the $C_2H_2/O_2/N_2$
flames must have been significantly shorter than the ~ 5 ns
laser pulse duration; otherwise, steady state would not have

been approached during the laser pulse and would have been reflected in much higher saturation energy estimates.

The $C_2H_2/O_2/Ar$ flames exhibited quite different saturation behavior with increasing laser intensity. For the time-averaged as well as the time-resolved fluorescence measurements, significantly different results were obtained depending on the saturation energy estimation approach, particularly for the 4P→3S and 5D→3P transitions. Transient fluorescence intensities were detected even under time-resolved fluorescence measurements. This result indicates that at least for the collisionally excited level, steady state was not being reached during the laser pulse. The time-averaged measurements of the saturation energies continue to reinforce this possibility: significantly variable and higher results were obtained for each estimate for the 4P→3S and 5D→3P transitions. Slightly higher values (in comparison to the time-resolved values) were observed for the 3P→3S transition; as with the collisionally excited levels in the $C_2H_2/O_2/N_2$ flames, the effective 3P level lifetime must have been increased in the $C_2H_2/O_2/Ar$ flames relative to the apparent lifetime in the $C_2H_2O_2/N_2$ flames (see Figs. 23 and 24). This result is consistent with the concomitant decrease in quenching efficiency of Ar in comparison to N_2. However, it is likely that steady state was attained for the 3P→3S transition in the Ar-diluted flames even during the ~ 5 ns laser pulse.

Interestingly, even though steady state level populations consistently occurred in the N_2-diluted flames and for the 3P→3S transition in the Ar-diluted flames, partial Boltzmann

Figure 23. Laser induced fluorescence produced from Na in the 2465 K $C_2H_2/O_2/Ar$ flame under ∿ 5 ns laser excitation. The fluorescence pulse (top) at 589.3 nm corresponds to the resonance fluorescence transition, while the fluorescence pulse (bottom) at 330.2 nm corresponds to the THAF transition from the 4P level of Na.
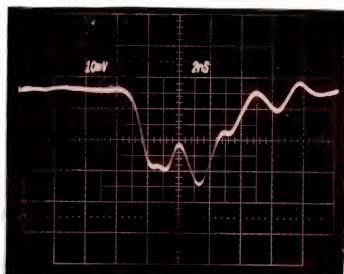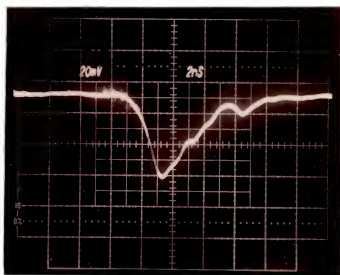
Figure 24. Laser induced fluorescence produced from Na
            in the 2220 K $C_2H_2/O_2/N_2$ flame under $\sim$ 5 ns
            pulsed laser excitation. The fluorescence
            pulse (top) at 589.3 nm corresponds to the
            resonance fluorescence transition, while
            the fluorescence pulse (bottom) at 330.2 nm
            corresponds to the THAF transition from the
            Na 4P level.

135
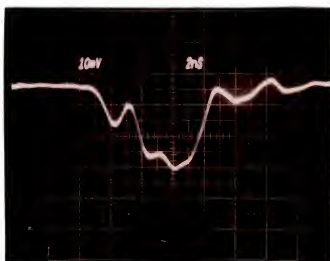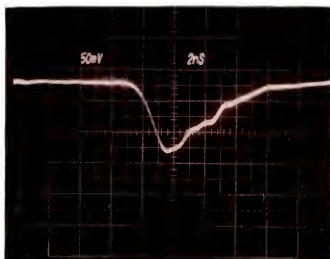
equilibrium was not achieved. It may be likely that the non-thermal radiation was due to state-specific ionizing collisions and excited state chemical reactions which promoted excitation "losses" from the relative level populations, at least for the "quenching" N_2-diluted flames. Thermal radiation as characterized by partial Boltzmann equilibrium is generally produced when physical and chemical processes invoke detailed balance between the excited levels. Since slow relaxation in the attainment of steady state level populations prior to ex-ternal radiation was not likely to occur at the observation height utilized, it must be assumed that the laser irradiation perturbed the relative Boltzmann distribution and the colli-sional rates, especially in the Ar-diluted flames, were unable to initiate Boltzmann equilibrium during the laser pulse. In addition, the attainment of thermally assisted populations is based upon the critical assumption that the collisional mixing rates among the higher levels were much larger than the down-ward quenching rates (whether via single-step or multistep pathways); the quenching rates were not balanced by upward excitation collisional rates due to the severe endoenergicity of these collisional transfer reactions. Since several of the transitions which produced nonthermal radiation terminated in the 3S ground state, it can be speculated that downward collisional rates were not negligible. Interestingly, the two fluorescence transitions which provided the closest tem-perature to the reversal flame temperature were the 3P→3S and 5D→3P transitions.

In summary, the following features of collisional redistribution of Na radiatively excited population in C_2H_2/O_2 flames under ~ 5 ns laser excitation are [138]

(i)   compared to the reversal temperature (dashed line) distributions in Figs. 14, 15, 18, and 19, the 3P level was generally overpopulated under 3S→3P excitation; however, the measured THAF temperature which was closest to the reversal temperature involved the 3P→3S and 5D→3P transitions.

(ii)   the mechanisms responsible for the relative underpopulation of the 3P level with respect to the 5P level and the deviations of the upper level populations from the reversal temperature distribution are unknown; the processes populating the excited states, at least under 3S→3P excitation, were probably entirely collisional.

(iii) Ar-diluted flames consistently showed a population inversion between the 4P and 5P levels under all excitation modes, while the N_2-diluted flames exhibited only large deviations from partial Boltzmann equilibrium for those levels; this result may indicate that steady state was not being reached during the ~ 5 ns laser pulse in the Ar-diluted flames.

(iv)   when considering the limited number of transitions observed, partial Boltzmann equilibrium was not being established during the laser pulse.

(v)   Na, which has been widely used in the past as a tempera-
       ture probe (see Appendix A), does not provide meaningful
       flame temperatures for methods based upon fluorescence
       under ~ 5 ns pulsed laser excitation.

T1 THERMALLY ASSISTED FLUORESCENCE

Experimental Results

THAF Measurement

In order to optimize the determination of single-shot THAF temperatures, time-averaged and time-resolved measurements of THAF were obtained for the 2465 K $C_2H_2/O_2/Ar$ and 2220 K $C_2H_2/O_2/N_2$ flames (see Figs. 25 and 26). The time-averaged and time-resolved methods utilized only one detection channel such that the fluorescence from the T1 radiatively and collisionally excited levels was sequentially detected. As can be seen from Figs. 25 and 26, fluorescence from eight T1 transitions could be observed after laser excitation at 377.6 nm ($6P_{1/2} \rightarrow 7S_{1/2}$ pumping), including the fluorescence from the radiatively excited 7S level at 377.6 nm ($7S_{1/2} \rightarrow 6P_{1/2}$) and at 535.0 nm ($7S_{1/2} \rightarrow 6P_{3/2}$). THAF from the collisionally excited levels was observed from the $8S_{1/2} \rightarrow 6P_{3/2}$ (323.0 nm), $9S_{1/2} \rightarrow 6P_{3/2}$ (282.6 nm), $6D_{3/2} \rightarrow 6P_{1/2}$ (276.8 nm), $6D_{5/2,3/2} \rightarrow 6P_{3/2}$ (351.9-352.9 nm), $7D_{5/2,3/2} \rightarrow 6P_{3/2}$ (291.8-292.2 nm), and $8D_{5/2,32} \rightarrow 6P_{3/2}$ (270.9-271.1 nm) transitions. The radiatively pumped 7S level was generally overpopulated with respect to the other excited levels. The $7S_{1/2} \rightarrow 6P_{3/2}$ (535.0 nm) transition fluorescence generally indicated some overpopulation of the 7S level which ranged from a factor of ~ 1.5 in the 2465 K Ar-diluted flame to a factor of ~ 2.7 in the 2220 K N_2-diluted flame. However,

139

Figure 25.   Boltzmann plots of ln ($B_F\lambda/gA$) vs. the energy
              of the upper level involved in the Tl fluores-
              cence transition for the 2465 K $C_2H_2/O_2/Ar$
              flame. Time-averaged fluorescence detection
              is indicated by the dot, while time-resolved
              detection of peak fluorescence is indicated
              by the x. The arrow indicates the laser
              pumped level. All B_F values are expressed in
              the same, but arbitrary units (au). The
              dashed lines indicate the slope temperatures
              derived from the THAF measurements. The
              time-averaged THAF slope temperature is 2481 K.
              The time-resolved THAF slope temperature is
              2482 K.
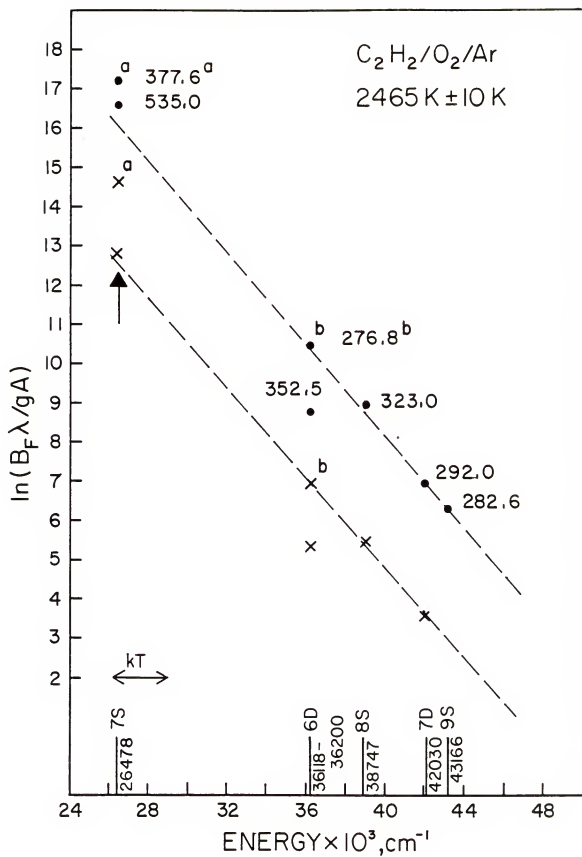
Figure 26.   Boltzmann plots of ln ($B_F\lambda/gA$) vs. the energy
of the upper level involved in the Tl fluores-
cence transition for the 2220 K $C_2H_2/O_2/N_2$
flame.   Time-averaged fluorescence detection
is indicated by the dot, while time-resolved
detection of peak fluorescence is indicated
by the x.   The arrow indicates the laser
pumped level.   All B_F values are expressed in
the same, but arbitrary units (au).   The
dashed lines indicate the slope temperatures
derived from the THAF measurements.   The time-
averaged THAF slope temperature is 2242 K.
The time-resolved THAF slope temperature is
2208 K.
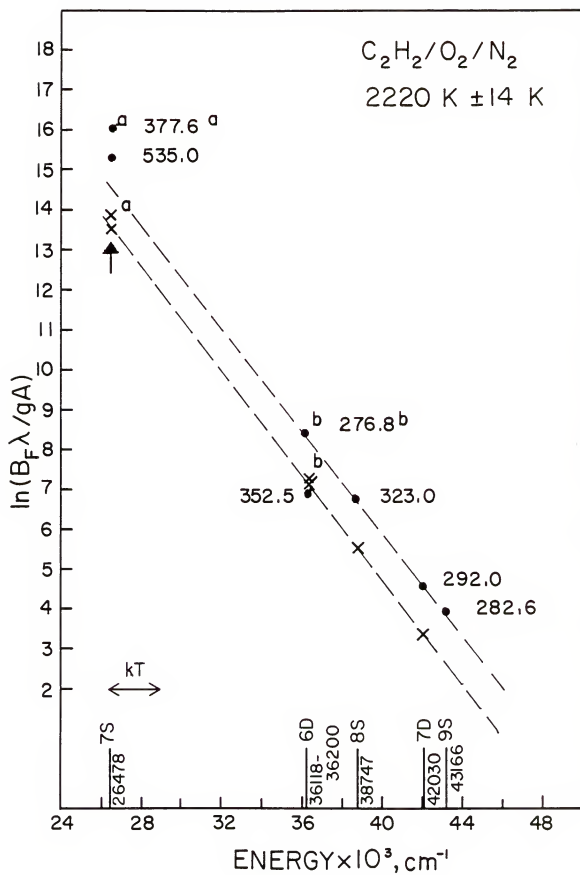
the resonance fluorescence at 377.6 nm ($7S_{1/2} \rightarrow 6P_{1/2}$ transition) indicated a significant overpopulation of the 7S level which ranged from a factor of ~ 3.3 in the 2465 K Ar-diluted flame to a factor of ~ 4.0 in the 2220 K N_2-diluted flame; this result could be due to the detection of Rayleigh scattering signals and spurious laser light at 377.6 nm.

In addition, even though detectable fluorescence was observed for the 282.6 nm and 270.9-271.1 nm transitions, a rather poor signal-to-noise ratio was observed for the fluorescence corresponding to these transitions in the lower quantum efficiency N_2-diluted flame (see Fig. 26). The fluorescence observed from the 351.9-352.9 nm transition from the 6D level also could not be conveniently utilized because of the difficulty in determining the maximum signal within the 4.0 nm monochromator bandpass, assuming the A values are correct [41]. This inaccuracy resulted in $B_F\lambda/gA$ values relatively lower than the Boltzmann value (see Figs. 25 and 26). However, the fluorescence detected from three transitions: 276.8 nm from the 6D level, 291.8-292.2 nm from the 7D level, and 323.0 nm from the 8S level, provided routinely accurate ($\gtrsim$ 2%) and precise ($\gtrsim$ 2%) THAF temperatures and were used for the single-shot THAF temperature measurements.

Table 9 lists the saturation energies determined for several radiatively and collisionally excited Tl levels in the 2465 K C_2H_2/O_2/Ar flame and the 2220 K $C_2H_2/O_2/N_2$ flame by each estimation approach. The fluorescence from the laser excited 7S level was monitored at 535.0 nm in order to avoid

Table 9
Comparison of Time-Resolved and Time-Averaged
Saturation Energies for T1 in the 2465 K
$C_2H_2/O_2/Ar$ and the 2220 K $C_2H_2/O_2/N_2$ Flames

Flame	Saturation Energy (mJ per pulse)		
Measurement Method	7S $6P_{3/2}$ (535.0 nm)	6D $6P_{1/2}$ (216.8 nm)	6D $6P_{3/2}$ (352.5 nm)
2465 K $C_2H_2/O_2/Ar$			
Time-averaged	0.15[a] 0.18[b]	0.15[a] 0.17[b]	0.16[a] 0.19[b]
Time-resolved	0.052[a] 0.053[b]	0.052[a] 0.054[b]	0.052[a] 0.055[b]
2220 K $C_2H_2/O_2/N_2$			
Time-averaged	0.21[a] 0.30[b]	0.22[a] 0.32[b]	0.23[a] 0.24[b]
Time-resolved	0.19[a] 0.20[b]	0.20[a] 0.20[b]	0.19[a] 0.21[b]

[a] Saturation energy estimated from 50% fully saturated value.
[b] Saturation energy estimated from the intersection of the linear and saturated asymptotes.

detection of Rayleigh scattering at the resonance 377.6 nm
wavelength. The incident laser pulse energy was ~ 1.6 mJ
per pulse. Consistent with the previous results obtained with
Na, the time-resolved saturation curves for the thermally as-
sisted levels (see Figs. 27 and 28) closely follow the curves
corresponding to the fluorescence from the radiatively excited
7S level for both the Ar-diluted and the N_2-diluted flames.
However, the onset of fully saturated fluorescence (as mea-
sured via time-resolved detection) appears to occur at signifi-
cantly lower pulse energies for the Ar-diluted flame (~ 0.053
mJ per pulse saturation energy) than for the N_2-diluted flame
(~ 0.20 mJ per pulse saturation energy).

It is readily apparent from Table 9 that the saturation
energies observed for the $6D_{5/2,3/2} \rightarrow 6P_{3/2}$ (352.5 nm) transi-
tion under both time-resolved and time-averaged fluorescence
measurements in the $C_2H_2/O_2/N_2$ flame are essentially
equivalent. The fluorescence observed from the $7S_{1/2} \rightarrow 6P_{3/2}$
(535.0 nm) and the $6P_{3/2} \rightarrow 6P_{1/2}$ (276.8 nm) transitions also
provides comparable results for the time-resolved saturation
energy, but there is an apparent discrepancy between the
values of the saturation energy estimated by the 50% fully
saturated and linear asymptotic methods: ~ 0.21 mJ per pulse
vs. ~ 0.31 mJ per pulse energies.

The time-resolved saturation energies observed for each
of the fluorescence transitions in the $C_2H_2/O_2/Ar$ flame are
completely equivalent (~ 0.053 mJ per pulse energy). In addi-
tion, consistent saturation energies are also obtained for

Figure 27.   Saturation curves of relative fluorescence
             intensity vs. relative laser pulse energy
             for Tl in the 2465 K $C_2H_2/O_2/Ar$ flame showing
             three transitions of interest: a. $7S \rightarrow 6P_{3/2}$
             (535.0 nm), b. $6D_{5/2, 3/2} \rightarrow 6P_{3/2}$ (352.5 nm),
             and c. $6D_{3/2} \rightarrow 6P_{1/2}$ (276.8 nm).   All fluores-
             cence intensities are expressed in the same,
             but arbitrary units (au).   The laser energies
             (measured in mJ per pulse) are recorded in
             the same, but arbitrary units (au).   Time-
             averaged fluorescence detection is indicated
             by the dot, while time-resolved detection of
             peak fluorescence is indicated by the x.
             Note that there is no significance attached
             to the absolute signal magnitudes of each
             saturation curve.

$C_2H_2/O_2/Ar$

2465 K

a

b

c

RELATIVE FLUORESCENCE INTENSITY, au

RELATIVE LASER PULSE ENERGY, au
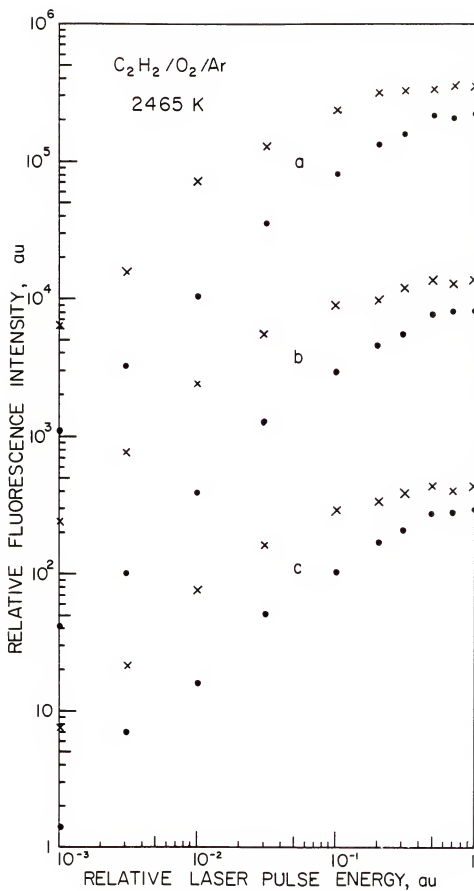
Figure 28.   Saturation curves of relative fluorescence
             intensity vs. relative laser pulse energy for
             Tl in the 2220 K $C_2H_2/O_2/N_2$ flame showing
             three transitions of interest: a. $7S \to 6P_{3/2}$
             (535.0 nm), b. $6D_{5/2, 3/2} \to 6P_{3/2}$ (352.5 nm),
             and c. $6D_{3/2} \to 6P_{1/2}$ (276.8 nm). All fluores-
             cence intensities are expressed in the same,
             but arbitrary units (au). The laser energies
             (measured in mJ per pulse) are recorded in the
             same, but arbitrary units (au). Time-averaged
             fluorescence detection is indicated by the
             dot, while time-resolved detection of peak
             fluorescence is indicated by the x. Note that
             there is no significance attached to the
             absolute signal magnitudes of each saturation
             curve.

$C_2H_2/O_2/N_2$

2220 K
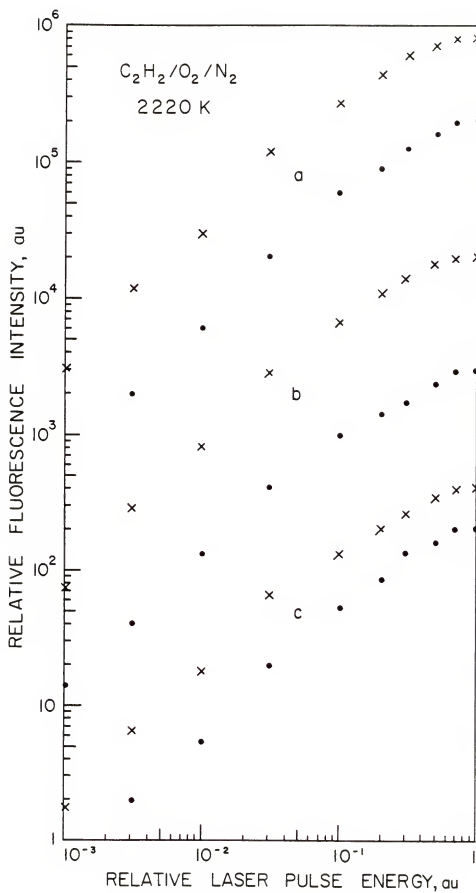
each fluorescence transition measured under time-averaged
measurement; however, the value of the time-averaged satura-
tion energy is ~ 0.17 mJ per pulse which is a ~ 220% increase
over the time-resolved values.

The Boltzmann plots of the population distributions for
the Ar-diluted and N_2-diluted flames are depicted in Figs.
25 and 26 under both time-resolved and time-averaged detection.
The THAF temperatures, obtained from the slopes of the plots
of ln $(B_F\lambda/gA)$ vs. ΔE of the excited level, for the 2465 K
$C_2H_2/O_2/Ar$ flame were 2482 K (time-resolved measurement)
and 2481 K (time-averaged detection). The 2220 K $C_2H_2/O_2/N_2$
THAF slope temperatures were 2208 K for time-resolved measure-
ment and 2242 K for time-averaged measurement.

Single-Shot Temperature Measurements

In order to measure single-shot THAF temperatures, two
detection channels (monochromator and boxcar averager signal
processing unit) were required to detect simultaneously fluo-
rescence from two thermally assisted transitions. Each boxcar
averager was operated in the summation (linear) mode under
1.0 μs input time constant and nominal ~ 5 ns gate. To mea-
sure single-shot temperatures for each and every shot of a
specific number of laser pulses, the output from each boxcar
was fed directly to two ± 1 V 12-bit A/D converter inputs of
the LPS11 laboratory peripheral interface of the PDP 11/34
minicomputer system (Digital Equipment Corporation) for
subsequent data processing by the minicomputer. Using

digital I/O lines, the boxcar was cleared and then reenabled for the next signal after each laser shot. Triggering of the boxcars and LPS11 interface (external Schmitt trigger) was accomplished using the N_2-laser optical trigger. Real time (interrupt-driven) computer control of the experiment was therefore allowed.

The sensitivity in fluorescence response of one detection channel to the other channel was calibrated in the following manner:

(i)   the fluorescence signals from each observed transition (see Fig. 29) were simultaneously detected for each channel.

(ii) each signal was corrected for photomultiplier response at that wavelength.

(iii) the ratio of detection channel j to detection channel i was determined for each transition.

(iv) the average ratio was computed and produced a sensitivity calibration factor of 10.0 ± 0.1.

The following experimental procedure was followed for the THAF single-shot measurements:

(i)   background measurements of the average of 100 shots (laser irradiation, no Tl in the flame) for each channel were determined.

(ii) 100 single-shot THAF measurements were collected.

(iii) the average background value was subtracted from each single-shot count.

Figure 29.   Boltzmann plot of ln (B$_F\lambda$/gA) vs. the energy
of the upper level involved in the Tl fluores-
cence transition for the 2465 K C$_2$H$_2$/O$_2$/Ar flame.
The arrow indicates the laser excited level.
All B$_F$ values are expressed in the same, but
arbitrary units (au). The dashed line indicates
the slope temperature derived from time-
averaged THAF measurements.
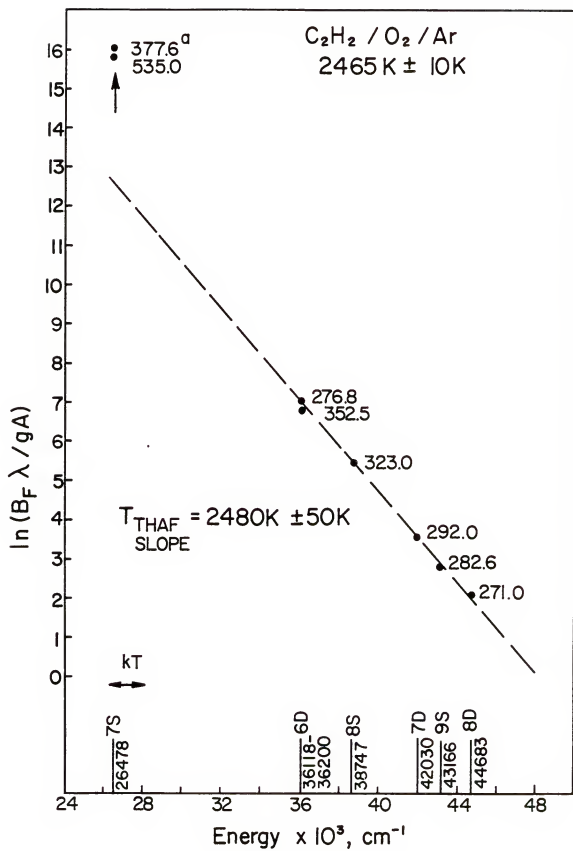
(iv) the single-shot temperature was calculated for each laser pulse.

(v) the average temperature and the standard deviation of the 100 shots measurement set for each flame was computed using the scientific subroutine for our PDP 11/34 computer.

Earlier attempts to obtain accurate THAF single-shot temperatures involved the use of a current-integrating 11 bit, ± 2 V analog-to-digital converter interface of the CAMAC crate system. The photomultiplier signals were fed directly (50 Ω input impedance) to the ADC. However, due to the nominal 30 ns gate, the ratio of the unamplified fluorescence from the 276.8 nm and 323.0 nm transitions resulted in a THAF temperature of 3120 K ± 32 K for the 2465 K $C_2H_2/O_2/Ar$ flame. In order to maintain the simplicity of this experimental approach, pulse stretching of the THAF fluorescence (see Fig. 30) produced ~ 10 µs pulses (time resolution was thereby lost). However, only the high (> 50) signal-to-noise ratio fluorescence transitions (377.6 nm, 535.0 nm, and 276.8 nm fluorescence) resulted in reproducible pulse stretching; the other THAF signals when stretched produced very noise, unusable signals.

In Fig. 29, the Boltzmann plot for the 2465 K $C_2H_2/O_2/Ar$ flame is shown; two fluorescence signals were detected simultaneously and the output of each boxcar was fed to a two-channel recorder instead of the minicomputer in order to verify

Figure 30.   Detection and signal processing system for
             the single-shot THAF measurements using the
             CAMAC charge-integrating A/D converter inter-
             face. The SIGNAL refers to the photomulti-
             plier current, while the TRIGGER refers to
             the laser optical trigger.
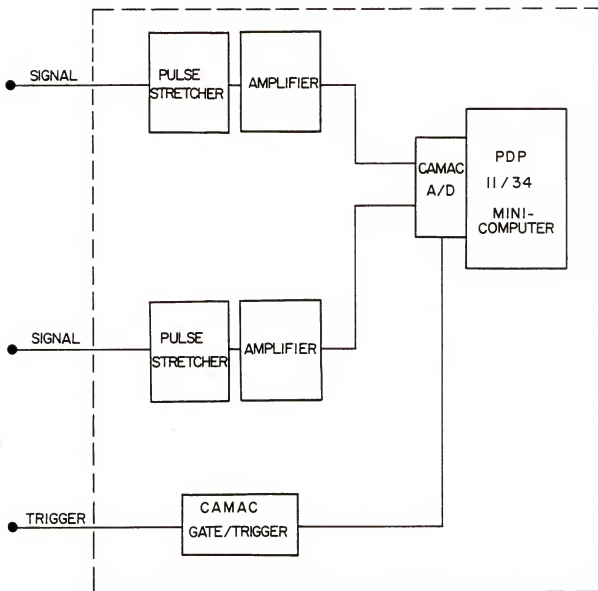
the accuracy of the optical calibration in terms of sensitivity and wavelength response. The resultant THAF slope temperature was 2480 K ± 50 K. The only significant difference between this population distribution and the distribution obtained previously in Fig. 25 was the apparent larger overpopulation of the radiatively excited 7S level. "Averaged" measurements of THAF from the 276.8 nm, 292.0 nm, and 323.0 nm transitions were obtained for the 2465 K, 2315 K, and 2200 K Ar-diluted flames (see Table 10).

In Fig. 31 a typical histogram of the temperature probability (number of occurrences vs. temperature interval) is shown. The histogram was obtained from a set of 100 subsequent single-shot measurements for the 2465 K flame when measuring the ratio of fluorescence from the 276.8 nm to the 292.0 nm transition pair. In spite of the small number of samples (100), a peaked distribution with an average temperature of 2470 K was obtained. The THAF temperature measured was in very good agreement with the Na line reversal temperature previously measured. The data shown in Fig. 31 is summarized in Table 11. The maximum, minimum, and averaged signal counts detected by channel i (276.8 nm line) and by channel j (292.0 nm line) with standard deviations and percentual errors of their statistical distributions are reported together with the pertinent temperature values. The signal counts tabulated for each channel were the products of the actual count measured for the fluorescence signal and the reciprocal of the attenuation factor needed to maintain the

Table 10
Comparison of Thermally Assisted Fluorescence Temperatures Obtained in
"Averaged" and "Single-Shot" Modes for Three $C_2H_2/O_2/Ar$ Flames

Flame	276.8 nm-292.0 nm	276.8 nm-323.0 nm	323.0 nm-292.0 nm
2465 K ± 10 K			
averaged[a]	2440 K ± 50 K[c]	2439 K ± 45 K[c]	2447 K ± 100 K[c]
single-shot[b]	2470 K ± 11 K	2475 K ± 30 K	2456 K ± 32 K
2315 K ± 12 K			
averaged[a]	2308 K ± 30 K[c]	2326 K ± 50 K[c]	2316 K ± 130 K[c]
single-shot[b]	2308 K ± 14 K	2301 K ± 36 K	2310 K ± 61 K
2200 K ± 14 K			
averaged[a]	2212 K ± 60 K[c]	2241 K ± 72 K[c]	3319 K ± 720 K[c]
single-shot[b]	2225 K ± 17 K	2215 K ± 25 K	3542 K ± 313 K

[a] "Averaged" temperatures obtained by sequentially monitoring THAF fluorescence over time.

[b] Temperatures given are the average of 100 separate single-shot temperature measurements.

[c] Standard deviation of the "averaged" temperature measurements determined by evaluating the standard deviation of the signal for each fluorescence signal and calculating the resulting temperature precision. The standard deviation of sixteen temperatures determined over a time period corresponding to 2400 laser shots.

Figure 31. Probability histogram of the 100 single-shot THAF temperature measurements reported for the 2465 K C2H2/O2/Ar flame using the Tl 276.8 nm - 292.0 nm line pair.

$C_2H_2/O_2/Ar$
2465 K ± 10K

$T_{THAF} = 2470$ K ± 11K
SINGLE-SHOT

Number of Occurrences
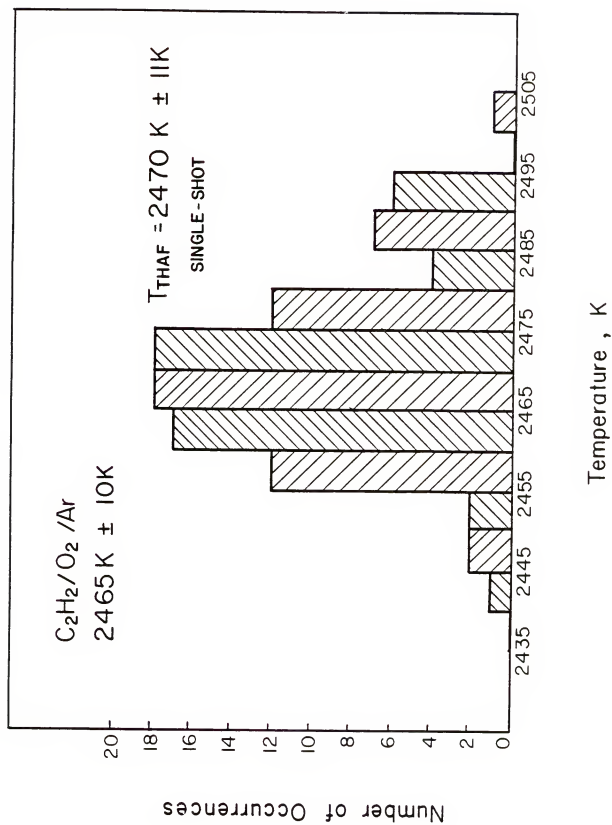
Temperature , K

Table 11
Summarizing Parameters of the Statistical Distributions
for the 276.8 nm-292.0 nm Line Pair in the 2465 K
$C_2H_2/O_2/Ar$ Flame

	Channel 1 (counts)[a]	Channel 2 (counts)[a]	Single-Shot THAF Temperature (K)
Minimum	25670	6595	2443
Maximum	27187	6840	2501
Average	26572	6701	2470
Std. Dev.	327.7	58.4	11.3
Rel. Std. Dev.	1.2%	0.9%	0.46%

[a]Counts given are the product of the actual ADC count value and the reciprocal of the fluorescence attenuation needed for a signal within ± 1 V.

signal within ± 1 V. As can be seen, for the 2465 K rever-
sal temperature flame, a standard deviation of 11.3 K and a
precision of 0.46% were obtained for the THAF temperature of
2470 K. The same analysis for the other flames and other line
pairs investigated gave similar results (see Table 12). Com-
parison of temperatures obtained in the "averaged" and single-
shot modes for the three flames investigated are reported in
Table 10 [114,139].

Discussion

THAF Measurements

As can be readily seen from Figs. 25 and 26 and Table 10,
the THAF signals detected corresponded closely to a partial
Boltzmann equilibrium over the collisionally excited Tl levels;
the slope temperatures obtained from the fluorescence from the
276.8 nm, 292.0 nm, 323.0 nm, and 282.6 nm transitions in the
2465 K, 2315 K, and 2200 K Ar-diluted flames and in the 2200
K N_2-diluted flame were consistently in good agreement with the
corresponding reversal temperatures values.

The saturation energies from time-resolved measurements
of peak fluorescence and time-averaged measurements of the
complete THAF fluorescence pulse indicate that steady state
level populations were attained during the ~ 5 ns excitation
pulse for both the $C_2H_2/O_2/Ar$ and $C_2H_2/O_2/N_2$ flames. Particu-
larly for the high quenching efficiency N_2-diluted flame,
there appears to be very little difference between the satura-
tion energies obtained under time-resolved and time-averaged
measurements. The slightly higher values of the time-averaged

Table 12
Relative Standard Deviations of the
THAF Single-Shot Temperature Measurements

$C_2H_2/O_2/Ar$ Flame	276.8 nm[a]–292.0 nm[b]			276.8 nm[a]–323.0 nm[b]			323.0 nm[a]–292.0 nm[b]		
	% RSD i[a]	% RSD j[b]	% RSD Temp.	% RSD i[a]	% RSD j[b]	% RSD Temp.	% RSD i[a]	% RSD j[b]	% RSD Temp.
2465 K	1.2	0.9	0.46	2.8	2.6	1.2	1.5	4.8	1.3
2315 K	1.9	1.1	0.6	5.0	3.0	1.6	7.3	4.5	2.7
2200 K	3.1	1.2	0.8	4.6	1.2	1.1	3.1	8.4	8.8

[a]Channel i
[b]Channel j

Figure 32. Laser induced fluorescence produced from Tl
in the 2465 K $C_2H_2/O_2/Ar$ flame under $\sim$ 5 ns
pulsed laser excitation. The fluorescence
pulse (top) at 535.0 nm corresponds to the
Stokes direct-line fluorescence transition
from the laser excited 7S level, while the
fluorescence pulse (bottom) at 276.8 nm
corresponds to the THAF transition from
the 6D level of Tl.
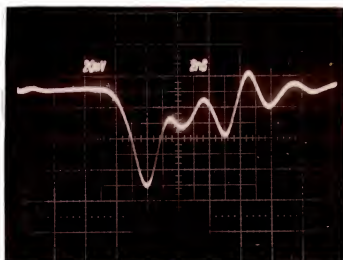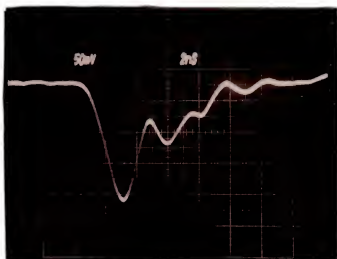
Figure 33. Laser induced fluorescence produced from Tl
in the 2220 K $C_2H_2/O_2/N_2$ flame under $\sim$ 5 ns
pulsed laser excitation. The fluorescence
pulse (top) at 535.0 nm corresponds to the
Stokes direct-line fluorescence transition
from the laser excited 7S level, while the
fluorescence pulse (bottom) at 276.8 nm
corresponds to the THAF transition from the
6D level of Tl.
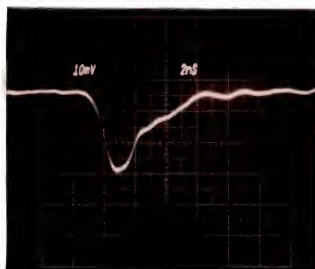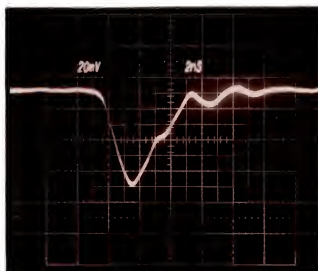
saturation energies determined for the $7S_{1/2} \to 6P_{3/2}$ (535.0 nm) and the $6D_{3/2} \to 6P_{1/2}$ (276.8 nm) transitions from the linear asymptotic method over that obtained from the 50% fully saturated approach were most likely due to experimental errors in the measurements of the fluorescence signal levels at low laser pulse energies and the resulting errors in the linear asymptotic slopes. Consistent with this assumption are the equivalent values of the saturation energies obtained by both methods for the 352.5 nm fluorescence from the same upper level (6D) as the 276.8 nm transition. The effective lifetimes of the investigated thermally assisted excited states must have been significantly shorter than ~ 5 ns in the $C_2H_2/O_2/N_2$ flame such that the excited state populations could closely follow the laser pulse (see Figs. 32 and 33). Otherwise, the saturation energies determined would have been significantly larger than the time-resolved values. As with the Na measurements, these comparisons between the time-resolved and time-averaged results assume relatively good experimental accuracy in the fluorescence signal detection.

Steady state fluorescence also appears to have been detected from the THAF transitions in the $C_2H_2/O_2/Ar$ flame (see Table 9 for saturation energies). However, the significantly higher saturation energy values for the time-averaged results indicate that although steady state level populations were achieved in the Ar-diluted flame, the effective lifetimes of the thermally assisted excited levels in this high quantum efficiency/low quenching efficiency flame must have been

longer than the respective lifetimes in the N_2-diluted flame.
With detection of the time-varying population exemplified by
the duration of the fluorescence pulses in Figs. 32 and 33,
higher laser pulse energies were required to saturate the
transitions. In addition, the lower laser energy of ~ 0.053
mJ needed to obtain time-resolved detection of a fully satura-
ted level population confirms this observation, predicted
theoretically, than the onset of saturation occurs when the
stimulated absorption and emission rates dominate over the
collisional excitation-deexcitation and spontaneous emission
rates and therefore will occur at lower laser powers for
higher quantum efficiency flames (Ar-diluted flames). The
excitation of the thermally assisted levels from the laser
pumped level is therefore a linear process which is completely
collision-dominated. When the saturation of the laser excited
level occurs, the fluorescence from the thermally assisted
levels will subsequently correspond to an apparent saturation
of that level and will be reflected in equivalent saturation
energies if steady state is achieved and time-resolved detec-
tion of fluorescence is measured. From the results obtained,
it is apparent that the determination of THAF excitation tem-
peratures with ~ 5 ns pulsed laser excitation and with time-
averaging of the fluorescence signals over the boxcar gate
appeared to be a reasonably valid procedure, even in Ar-
diluted flames; for the N_2-diluted flames, however, a higher
laser power was needed to achieve optimal (saturated) signal-
to-noise ratio fluorescence signals.

<u>Single-Shot Temperature Measurements</u>

From Table 10, the single-shot temperature results determined for the 2465 K, 2315 K, and 2200 K Ar-diluted flames can be evaluated with respect to the fluorescence line pairs being utilized. Different transitions were detected with different fluorescence signal-to-noise ratios. In general, the 276.8-292.0 nm pair produced the best results in terms of accuracy and precision while the 323.0-292.0 nm pair produced the worst results. In the case of the 2200 K flame, the 323.0-292.0 nm pair gave an anomalous temperature value, mainly due to the poor signal-to-noise ratio of the fluorescence measurements, as indicated by the large standard deviations. Apart from this particular case, comparison of the temperatures obtained with the THAF technique in the "averaged" and single-shot modes and the line reversal technique shows excellent agreement for all the different experimental conditions investigated. Moreover, the temperature precision (see Tables 10 and 11) was better than the precision obtained in either channel (based upon counts) indicating that THAF temperature measurements were not influenced appreciably by laser power fluctuations or other errors from Rf noise variations and nebulizer irregularities in aerosol production. However, systematic errors in the measurements of the fluorescence intensities due to boxcar drifts in signal levels and in triggering which may have occurred more significantly for one detection channel than for the other and to nonlinearity of each of the ADC channels at low levels of signal response could have still

influenced the temperature precision reported. However, the
results in Table 11 for the 2465 K C_2H_2/O_2/Ar flame confirm
that no appreciable drifts in the experimental conditions
were present during one set of 100 measurements.

   In summary, the first single-shot temperature measure-
ments in flames using a laser excited fluorescence technique
have been performed. Care used in calibrating the experimental
setup and in performing the experiments resulted in sets of
measurements with very high accuracy and precision which con-
firm the THAF technique as a useful method for temperature
measurements even for turbulent combustion studies. With a
new experimental apparatus which uses a longer pulse length
laser, better optical collection, a native flame species
thermometric seed such as OH, and more sensitive electronic
equipment, further improvements in temperature precision
could be obtained.

CONCLUSION

Thermally assisted fluorescence (THAF) promises to be an exceptionally versatile technique for flame temperature and population distribution measurements on a spatially and temporally resolved basis. As is apparent from the THAF observed from Tl radiatively and collisionally excited levels, single-shot temperatures are more than just possible; the experimental approach evaluated in this dissertation could be easily applied even to turbulent flames. Pulsed laser excitation on the ~ 5 ns time scale is desirable due to the minimization of ionization and excited state chemical reaction losses and the increase in achievable temporal resolution. However, ~ 5 ns excitation induces difficulties in the attainment and measurement of steady state fluorescence on this time scale in quenching and nonquenching flames. As can be seen from the Na results, not every flame species can be utilized ubiquitously as a fluorescence thermometric seed. Each potential thermometric species must be rigorously evaluated within the desired flames. The measurement of saturation energies (from fluorescence saturation curves) can help elucidate the behavior (in terms of relative steady state population distributions) of the flame species. However, accurate determinations of collision cross sections, excited state effective lifetimes, and saturation

173

energies via time-resolved and time-averaged fluorescence detection are required to provide unambiguous information concerning the temporal responses of the collisionally excited levels in the thermometric seed under ~ 5 ns pulsed laser excitation. Therefore, increasingly more complex and sophisticated data processing instrumentation is required to obtain the precise results needed. The transient fluorescence rate equations and models must also be developed.

In summary, the THAF technique can provide the most accurate and precise flame temperature measurements which are quite sensitive to even subtle temperature variations throughout the flame. However, correct A (transition probability) values must be obtained and most importantly, the relative population distributions observed within the thermometric species must correspond to a partial Boltzmann equilibrium under the excitation and measurement conditions utilzed in order that the flame temperature measurements possess physical validity.

APPENDIX A
FLAME TEMPERATURE MEASUREMENTS

I. Introduction

In this review, the meaning and validity of temperature,
established flame temperature techniques and other potential
approaches, and their relative comparisons for use in differ-
ent flames will be discussed (see Table A-1 and Fig. A-1).
Laser-based techniques will be especially emphasized not
only because laser methods can often provide nonintrusive,
spatially and temporally resolved temperatures, but also
because of the laser power produced and the capability to
achieve high resolution excitation, very weak processes
and nonlinear phenomena can be exploited. The simultaneous
detection or measurement of several desired flame parameters
in a wide range of flame environments could be accomplished
by several integrated, laser-based techniques. Therefore,
this review will emphasize a broad range of temperature
measurement approaches able to be utilized with high degrees
of success by scientists and engineers.

Table A-1
Potential Flame Temperature
Measurement Techniques

I. Intrusive Probe Methods.

    A. Thermocouples.
    B. Resistance thermometry.
    C. Cooled Film probes.
    D. Pneumatic probes.
    E. Ultrasonic thermometry.
    F. Optical fiber thermometry.
    G. Gas sampling/pressure sampling probes.

II. Nonintrusive Methods.

    A. Gas density-based methods.

        1. Particle tracking photography.
        2. Schlieren and shadowgraph photography.
        3. Interferometry.
        4. Radiation absorption methods.
        5. Sound velocity (photoacoustic) methods.

    B. Radiation pyrometry.

        1. Spectral emission-absorption methods.
        2. Integrated emission-absorption methods.
        3. Color temperature method.
        4. Line-reversal method.

    C. Spectrophotometry.

        1. Emission methods.
        2. Absorption methods.
        3. Elastic (Rayleigh) scattering.
        4. Spontaneous Raman scattering.
        5. Near-resonant enhanced Raman scattering.
        6. Coherent anti-Stokes Raman scattering.
        7. Stimulated Raman gain/loss spectroscopy.
        8. Fluorescence methods.
        9. Spectrophotometric translational temperature
           methods.

Figure A-1. Generalized diagram of potential approaches to flame temperature measurement. Intrusive techniques refer to probe thermometry methods. Nonintrusive techniques refer to spectroscopic line-of-sight, single beam, and multiple beam methods.

I. INTRUSIVE TECHNIQUES
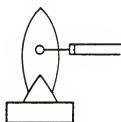
II. NON-INTRUSIVE TECHNIQUES

line of sight methods (Absorption , Emission)
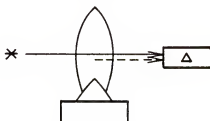
single beam methods (Raman, Fluorescence, Scatter)
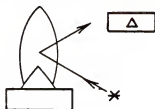
multiple beam methods (CARS)
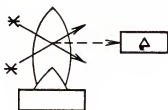
II. Meaning of Temperature

A. Thermodynamic Equilibrium

A state of thermodynamic equilibrium [2, 3, 9, 130, 140-143] will be attained by an undisturbed closed system when surrounded by a heat bath at uniform temperature, T [2, 9]. As detailed by Alkemade et al. [2], the thermodynamic state of a pure, monoatomic gas is defined by its pressure and volume, but a system that is composed of particles (atoms, ions, molecules) can possess energy in various modes (electronic, vibrational, rotational, and translational degrees of freedom), can ionize, dissociate, and become involved in chemical reactions, and can emit and absorb discrete lines of radiation. The single parameter T for a system in thermodynamic equilibrium characterizes the distributions of energy over the various internal degrees of freedom (thermal equilibrium), the distributions of dissociation and ionization products (chemical equilibrium), and the spectral distribution of radiant energy (radiation equilibrium). The laws (see Table A-2) which govern these distributions that are independent of the nature or rate of the actual interactions which promote the exchange of energy between the various modes are listed in Tables A-2 and A-3. The thermodynamic equilibrium distributions are functions only of T and the species within the system. The parameter T can be interpreted in terms of each distribution and, if complete thermodynamic equilibrium exists, each temperature value which describes each energy distribution will be equivalent to the thermodynamic T.

In thermodynamic equilibrium, the available energy is partitioned among the translational and internal degrees of freedom. For gaseous systems, the translational energy (or kinetic energy) can be considered classsically. Maxwell's law of velocity distribution (see Table A-3) determines the fraction of particles with a velocity component along one of three axis of a volume element and can be extended to determine the average absolute velocity of the particles. The average translational energy follows from the distribution of absolute velocity and kinetic energy. The translational or kinetic temperature is an index of the kinetic energy distribution of the gas particles and is an interpretation of the thermodynamic T of the system.

If the internal energy states of a particle are in thermodynamic equilibrium, they will be distributed according to the Maxwell-Boltzmann law (see Table A-3) which gives the fractional population over the various internal energy levels. The number of particles (of a specific particle type) in specific energy levels (the Boltzmann distribution of these species) will determine the statistical temperature. The internal degrees of freedom are nearly independent of each other and will possess their own particle energy distribution. Therefore, neutral or ionized atoms will possess characteristic electronic "temperatures" at each T, while molecules will possess vibrational, rotational, and electronic "temperatures."

Table A-2
Thermodynamic Equilibrium Requirements

A unique value of T must describe:

I. <u>Maxwell's Law</u>: The velocity distribution function of all gas particles.

II. <u>Boltzmann's Equation</u>: The population distribution of the excited energy states.

III. <u>Saha-Eggerts' Equation</u>: The distribution of atomic and ionization products.

IV. <u>Mass-Action Law</u>: The distribution of molecules and their dissociation products.

V. <u>Planck's Law</u>: The distribution of the electro-magnetic radiation energy.

Table A-3
Thermodynamic Equilibrium Equations

I. <u>Maxwell Equation</u>

    A. Velocity distribution of particles:

$$f(v_x)dv_x = \text{fractional population with a velocity component } v \text{ along the x axis (dimensionless),}$$

$$m = \text{mass of particle (g),}$$

$$k = \text{Boltzmann's constant } (J\,K^{-1}),$$

$$T = \text{translational temperature (K).}$$

$$f(v_x)dv_x = (m/2\pi kT)^{1/2} \exp(-mv_x^2/2kT)dv_x$$

    B. Average translational energy of particle ensemble

$$f(E_K)dE_K = (2/\pi^{1/2})E_K^{1/2}/(kT)^{3/2} \exp x$$

$$(-E_K/kT)dE_K$$

$$f(E_K)dE_K = \text{fractional population with energy between } E_K \text{ and } E_K + dE_K \text{ (dimensionless)}$$

II. <u>Boltzmann Equation</u>

$$f(E_j) = g_j \exp(-E_j/kT)/Q$$

$$f(E_j) = \text{fractional population at energy } E_j \text{ (dimensionless),}$$

$$E_j = \text{energy of jth level with respect to the ground state (J),}$$

$$g_j = \text{statistical weight of jth level (dimensionless),}$$

$$Q = \text{internal partition function added to normalize equation (dimensionless):}$$

$$\sum_{i=0}^{\infty} f(E_i) = 1,$$

$$Q = \sum_{i=0}^{\infty} g_i \exp(-E_i/kT)$$

Table A-3 continued

$$\frac{n_i}{n_j} = \frac{f(E_i)}{f(E_j)} = \frac{g_i}{g_j} \exp (E_j - E_i)/kT$$

n_i and n_j = number density of particles in ith and jth
   level (m^{-3}),

T = excitation temperature (rotational, vibra-
   tional, electronic) (K).

III. Saha-Eggerts' Equation

$$K_i(T) = [A^+][e^-]/[A]$$

for ionization/recombination process:

$$A \rightleftarrows A^+ + e^-$$

$K_i(T)$ = ionization constant (m^{-3}),

$[A^+]$ = number density of ions (m^{-3}),

$[A]$ = number density of neutral species (m^{-3}),

$[e^-]$ = number density of electrons (m^{-3}).

$$K_i(T) = 2(2\pi m_e kT/h^2)^{3/2} (Q_{A^+}/Q_A) \times \exp (-E_{ion}/kT)$$

m_e = electron mass (g),

Q_{A^+} = internal partition function in terms of rota-
   tional, vibrational, and electronic degrees
   of freedom for ion (dimensionless),

Q_A = internal partition function for neutral
   species (dimensionless),

h = Planck's constant (J s),

k = Boltzmann's constant $(J\ K^{-1})$,

E_{ion} = energy of ionization continuum of species (J),

T = ionization temperature (K).

$$K_i(T) = 4.83 \times 10^{15}\ T^{3/2}\ (Q_{A^+}/Q_A) \times 10^{-5040\ E_{ion}/T}\ (cm^{-3}).$$

Table A-3 continued

IV. <u>Mass-action Law</u>

$$K_d(T) = n_A n_B / n_{AB}$$

for dissociation reaction:

$$AB \rightleftarrows A + B$$

$K_d(T)$ = dissociation constant (m^{-3}),

n_A = number density of species A (m^{-3}),

n_B = number density of species B (m^{-3}),

n_{AB} = number density of species AB (m^{-3}).

$$K_d(T) = (2\pi kT/h^2)^{3/2} (m_A m_B / m_{AB})^{3/2} x$$

$$(Q_A/Q_B/Q_{AB})(S_{AB}/S_A S_B) \exp x (-D_o/kT)$$

m_A = mass of particle A (g),

m_B = mass of particle B (g),

m_{AB} = mass of particle AB (g),

Q_A = internal partition function of A (dimensionless),

Q_B = internal partition function of B (dimensionless),

Q_{AB} = internal partition function of AB (dimensionless).

V. <u>Planck Radiation Law</u>

$$B_\lambda^b (\lambda,T) = 2hc^2 \lambda^{-5}/(\exp (hc/\lambda kT)-1)$$

$B_\lambda^b (\lambda,T)$ = spectral radiance of a blackbody $(\text{erg s}^{-1}\text{sr}^{-1}\text{cm}^{-2}\text{\AA}^{-1})$,

h = Planck constant (Js),

Table A-3 continued

c = speed of light (m s^{-1}),

λ = light wavelength (m),

T = temperature at radiative equilibrium (K).

The Saha law (see Table A-3) relates the concentration of neutral species to those of the ionized products in thermodynamic equilibrium. For each ionization-recombination process, including ones which involve the detachment of electrons from negative ions, the ionization constant as functions of T and the ionization energy of the ion, E_{ion}, will be equal to the ratio of products to reactants. If all the ionization processes in the gaseous system possess ionization temperatures corresponding to the thermodynamic T, then Saha equilibrium exists. Thermal ionization exists for each individual ionization process, if for that process, the ionization temperature is equivalent to T.

The mass-action law (see Table A-3) relates the concentration of the products to those of the reactants in equilibrium. The dissociation constant for each reaction is dependent only on the properties of the individual species and T and not on the nature or rate of the actual reaction process; i.e., single-step vs. multistep reactions, branching reactions, etc.

The distribution of radiant energy is governed by the Planck radiation law (see Table A-3) for a blackbody radiator which releases unpolarized and isotropic radiant energy solely due to its T.

Thermodynamic equilibrium implies that the system cannot be perturbed (to a nonequilibrium state) from the "outside" and that the system has relaxed to its equilibrium state if not in that state initially. The distribution

laws detailed above are considered to be valid for any
energy mode if the energy exchange processes within a
degree of freedom or between degrees of freedom proceed
according to the law of microscopic reversibility [2,3];
thermodynamic equilibrium can only be attained if the for-
ward process (radiative or collisional) corresponds exactly
to the reverse process, whether referring to rotational and
vibrational transitions or to ionization processes and chem-
ical reactions. Detailed balance must exist such that the
rate of the forward process is exactly equivalent to the
reverse process. Therefore, in principle, if the energy
distribution of one degree of freedom is disturbed, then the
other distributions are also affected and the existence of
a thermodynamic system T loses its validity.

B. Deviations from Thermodynamic
Equilibrium

The determination of whether thermodynamic equilibrium
can exist in a flame is necessary for the interpretation of
the flame temperature. These difficulties in applying the
concept of thermodynamic equilibrium to a flame system are
listed in Table A-4. A flame is a free flowing system com-
posed of mainly high temperature gaseous species with con-
tinuous energy release input (perturbation) into the system
at the base and diffusion of hot gases into the surrounding
atmosphere. A flame is composed of several regions, or
zones, which are highly characteristic and sensitive to the
total gas pressure (low pressure, atmospheric pressure, high

Table A-4
Flame Deviations from Thermodynamic Equilibrium

I.   Absence of boundaries (open system).

II.   Net transfer of heat, mass, and energy.

III. Temperature and concentration gradients in vertical
      and radial directions.

IV.   Radiative disequilibrium (not blackbody radiator).

V.   Nonthermal radiation (chemiluminescence from metals,
      OH, C_2, CH, etc., in reaction zone).

pressure flames), the flame composition (H_2/air, C_2H_2/air, CH_4/NO_2, gasoline/air flames, etc.), the type of flame mixing and flow (laminar, turbulent, premixed, diffusion flames), the mixing ratio of gases (fuel-rich, stoichiometric, fuel-lean flames), and the burner type (Bunsen, Méker, flat, etc.). For example, a rather simple, premixed laminar flame produced on a Bunsen burner has been described by Alkemade et al. [2, 144] to be composed of the following regions (see Fig. A-2): 1) primary reaction zone in which most of the combustion reactions take place [2, 11, 12, 130, 144]; 2) equilibration zone in which equipartition of the chemical energy tends to occur and is characterized by steep temperature gradients with height above the primary reaction zone; 3) secondary reaction zone in which O_2 can be entrained from the atmosphere (edge effects) to induce further oxidation reactions such as CO and H_2 to CO_2 and H_2O; 4) disturbed area which is characterized by the occurrence of diffusive mixing with the surrounding atmosphere and the appearance of turbulent flow [71, 130, 144]; and 5) near-homogeneous, local equilibrium region termed the interzonal region, in which a near-thermodynamic equilibrium state is suspected to occur [71]. These zones are not as nearly distinct in more turbulent flames and combustors [145-153] which possess multidimensional flow, fluctuating vortices, and severe diffusive mixing.

Chemiluminescence which may lead to nonthermal radiation if the reaction partners are not in chemical and physical

Figure A-2.   Depiction of flame zones within a premixed
              flame produced on a Bunsen burner.

outer (diffusive mixing) zone

LTE ? zone

equilibration zone

secondary reaction zone

primary reaction zone

interconal (premixing) zone
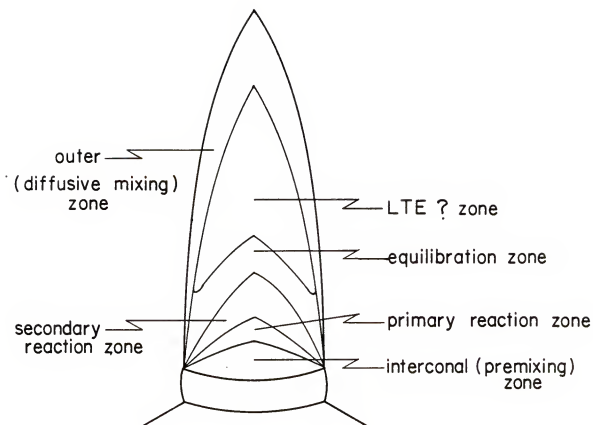
equilibrium [2] has been noted in the primary reaction zone, mainly from metal additives, OH, and CO [2, 10-12, 154-163]. Ions and radicals, such as H, OH, CH, and C_2, are formed in the excited state and in supraequilibrium concentrations in the reaction zone, while a more chemically equilibrated distribution of flame species (except for soot and other particulates) is found to occur above this zone [2, 130, 164-177]. Therefore, severe concentration and temperature gradients occur in the flame as well as local regions of nonequilibrium distributions of atomic, ionic, and molecular species (in concentration and in internal energy modes) which produce a net transfer of heat, mass, and radiation throughout the flame.

The flame is not optically thick, except at the center of strong, self-absorbing resonance lines and in some portions of the infrared spectral region, and therefore, the spectral radiance emitted from most spectral regions is far below the Planck value at kT [2, 23, 52, 124, 144, 178-181]. Also, it is well known that excited species can release their excitation energy through emission of radiation which is not balanced by absorption of radiation, unless an external source is used (radiative disequilibrium). However, if the attainment of thermal equilibrium for the flame species is collision-dominated, such that the collisional decay rates of the excited states are much larger than the radiative deexcitation rates, then the significance of the

radiative disequilibrium effect is quite negligible (at least for atmospheric pressure flames).

C. Achieving Thermodynamic Equilibrium

Thermodynamic equilibrium is achieved via collisions with other species, chemical reactions, and the emission and reabsorption of radiation [2]. The system relaxes to an equilibrium state, to a first approximation according to the gas-kinetic collision frequency, ν_c. For a flame at 1 atm pressure, ν_c is on the order of 10^{10}-10^9 s^{-1} [2, 3]. The number of collisions, N_c, necessary to distribute the chemical energy from strongly perturbed thermodynamic states (flame system) has been experimentally and theoretically estimated for each degree of freedom [3] and is listed in Table A-5. These values vary drastically from one species to another, but it is apparent that thermodynamic equilibrium is not readily achieved in the flame reaction (combustion) zone. The gas species do not spend adequate time (gas rise velocity ~ 10^3 cm s^{-1}) to suffer sufficient collisions to promote the distribution of combustion energy among the various modes. The equilibrium of the translational and rotational degrees of freedom for most flame species should occur almost immediately (within a few mm above the burner). Disequilibrium over the vibrational and electronic degrees of freedom should not persist over a height interval of 10^{-1} cm [2, 3]. However, most importantly, a general state of thermodynamic equilibrium characterized by a single T cannot generally exist in a flame.

Table A-5
Equilibrium Relaxation Times

Degrees of Freedom*	Number of Collisions, N_c
Translational	10
Rotational	10^3
Vibrational	10^5
Electronic, dissociation	10^7
Ionization	10^9

*For system at atmospheric pressure with 3×10^6 average number of collisions per cm.

D. Local Thermodynamic Equilibrium

The concept of local thermodynamic equilibrium (LTE) [2, 142, 182] characterized by a local T which describes the velocity particle distribution and the distributions of internal energy states can be considered to be valid in a flame, if at specific points in the flame, the rates of the transport processes are slow with respect to the rates at which energy is locally partitioned over the various degrees of freedom (see Table A-6). The LTE principle can be applied even if different local regions have different local T's as long as thermal equilibrium is established at each point in the flame. However, even locally, it is possible that complete chemical equilibrium is not achieved; i.e., the degree of ionization or dissociation of a species-specific process does not conform to the mass-action and Saha relations. Partial chemical equilibrium may be established when the chemical reaction products participate in other reactions such that the forward process does not balance the reverse process or the rate of the reverse process is much slower (defect of microscopic reversibility-detailed balanced principles). Partial physical equilibrium with respect to a species may exist even if all of a particle's internal energy distributions do not correspond to the local T. The exchange of energy between the degrees of freedom may not be fast enough to insure energy partitioning. The energy redistribution over the states of each mode may also not be sufficiently fast to produce a Maxwell-Boltzmann

Table A-6
Local Thermodynamic Equilibrium Considerations

I.   Local T - describes particle velocity distribution
       and energy distributions over degrees of
       freedom corresponding to Boltzmann law.

II. Radiation LTE not necessary.

III. Existence of temperature gradients acknowledged.

IV. Transient local T possible.

V.   Different "temperatures" for different degrees of
       freedom in any one species considered.

Table A-7
"Degrees of Freedom" Temperatures

Species	Temperature
Atom	Excitation - electronic
Ion	Excitation - ionization
Free electron	Recombination - electron
Molecule	Rotational Vibrational (vibrational-rotational) Electronic (vibrational-rotational-electronic)
Moving particle	Translational (kinetic)

energy distribution. Therefore, the "temperatures" measured for each degree of freedom (see Table A-7) for each species may not be identical and accordingly correspond only to the distribution of which they describe: translational, rotational, vibrational, and electronic "temperatures" (as well as ionization and mass-action "temperatures"). However, in LTE, the "temperatures" closely coincide, generally except for the radiation temperature. Because the number of collisions needed to achieve translational equilibrium is small and there is only one translational "temperature," the translational energy distribution is often the desired flame "temperature" to be measured in each flame zone.

As indicated by Tourin [9], a state of nonequilibrium in a particular flame region exists for the conditions listed in Table A-8. For the first two cases, an effective translational temperature could be measured or if the disequilibrium exists for a specific species, the temperature measured from other energy distributions of another species could be monitored. In the last case, the temperature concept is meaningless. Nonequilibrium can occur when the situations in Table A-9 exist [2, 9]. Exacting information about the flame processes is often required to determine whether a true state of non-thermodynamic equilibrium is actually occurring or is due to the temperature measurement procedure [2, 183-186].

Table A-8
Nonequilibrium Conditions

I. Different degrees of freedom for a particular species
    have different "temperatures".

II. Energy distribution of an internal degree of freedom
    is not Boltzmannian.

III. Velocity distribution of particles is not Maxwellian.

Table A-9
Nonequilibrium Perturbations

I. Energy input or extraction rate >> equilibrium relax-
    ation rate.[a]

II. Weak interaction between degrees of freedom.[b]

III. Measurement of temperature within equilibrium relaxa-
    tion time.[c]

[a]Nonthermal (chemical or electrical) excitation of particles
   in flame or radiative input or output rate >> collisional
   energy transfer to restore equilibrium.

[b]Very low densities (insufficient collisions).

[c]Measurement rate too fast.

III. Temperature Methods Based on Intrusive Probes

A. Probe Thermometry

Probe thermometry [1, 187] covers the range of thermo-
couple and thermometer devices widely used in laboratories
and in industry (see Tables A-10 and A-11). Probe thermom-
etry is the simplest and most direct method for the determina-
tion of local translational temperatures in flames. The two
basic requirements for use are the probes must be small with
respect to the thickness of the flame front and they must be
rugged enough to withstand the high temperature, corrosive
environments of many flames and combustors.

B. Thermocouple Thermometry

Thermocouples [188-212] are based on the development
of a thermoelectric potential (EMF) at a junction of two
dissimilar conductors which are maintained at two differ-
ent temperatures, i.e., flame and room temperature. The
potential developed is a reproducible function of the mater-
ials as long as no appreciable temperature gradient exists
across the junction. The sensing diameter of the thermo-
couple tip can be widely varied to provide small flame
volume sensing (bead diameters $\leq$ 0.01 mm). The composition
of popular wires for thermocouples in terms of temperature
durability are listed in Table A-12. For use in turbulent
flames, the thermocouples need to be larger and made of a
more durable material in order to follow the temporal mean

Table A-10

Figures of Merit of Thermometric Probes

Method	Type of Temp. [a]	Temperature Range (K)	Temperature Precision (K)	Spatial Resolution [b] (mm³)	Temporal Resolution [c] (s)	Sensitivity [d]	Selectivity [e]	Cost [f]	Time [g]	Overall Rating [h] in Flames		
										Laminar	Turbulent	Sooty
Thermocouple	TR	< 3000	10-100	< 0.1	10^{-4}-1	H	E	VL	S	G	F	F
Hot Wire Anemometry	TR	< 3000	20-100	< 0.1	10^{-4}-1	H	E	VL	S	G	F	F
Resistance Thermometer	TR	< 3000	≳ 200	< 1.0	10^{-3}-1	H	E	VL	S	F	F	F
Cooled Film Probe	TR	< 2000	≳ 200	< 10.0	≲ 10^{-3}	H	E	VL	S	F	F	F
Pneumatic Probe	TR	< 2500	40-100	< 10.0	~ 3	H	E	VL	S	F	P	P
Ultrasonic Thermometer	TR	< 3125	≳ 50	< 1.0	~ 10^{-6}	H	E	VL	S-M	G	G	G
Optical Fiber Thermometer	TR	< 2300	1-20	< 1.25	10^{-2}-1	H	E	VL	M	G	F	F
Gas Sampling/Pressure Sampling Probes	TR	< 2500	≳ 200	≳ 10.0	--	L	F	L-M	L	P	P	P

-- = not applicable

[a] Temperature measured: TR = translational, RA = radiational, E-El = electronic excitation, E-El* = electronic excitation, vibrational excitation or rotational excitation temperature.

[b] I = inversion methods not needed to obtain radially resolved temperature.

[c] Temporal resolution refers to the time interval in which the measurement can be made, not to the frequency of measurement, cw = continuous wave measurement.

[d] Sensitivity of measurement: H = high, M = moderate, L = low.

[e] Selectivity refers to freedom from spectral interferences: E = excellent, F = fair.

[f] Cost = equipment cost: VH = very high (> \$100,000), H = high, M = moderate, L = low, VL = very low (< \$10,000).

[g] Time = time to set up system and time for proper operation: L = long, M = moderate, S = short.

[h] Overall rating = capability to provide reproducible, accurate, and precise temperature measurements in laminar, turbulent, and sooty flames; E = excellent, G = good, F = fair, P = poor.

Table A-11

Probe Thermometry Advantages and Disadvantages

Method	Advantages	Disadvantages
Thermocouple (Hot wire anenometry)	i) High precision typical of electrical measurements ii) Small sensing volume iii) Applicable to a wide variety of flames iv) Quick, routine use v) Translational temperature obtained	i) Radiation/conduction losses ii) Catalytic effects iii) Wake effects/flame front disturbances iv) Slow temporal response v) Thermocouple in LTE with flame? vi) Limited temperature working range vii) Can't use in primary reaction flame zone viii) Intrusive technique
Resistance Thermometer	i) Approximately linear relationship of temperature with resistance ii) Small sensing volume iii) Translational temperature obtained	i) Same as above ii) Use not as general as thermocouple devices iii) Relatively poor precision compared to thermocouple
Cooled Film Probe	i) Velocity - independent temperature ii) Capability for time-resolved measurement iii) Translational temperature obtained	i) Poor accuracy and precision ii) Sample species segregation effects iii) Intrusive technique
Pneumatic Probe	i) Concomitant spatial temperature and composition gradients ii) Translational temperature obtained	i) Sensitivity decrease with temperature increase ii) Non-isokinetic effects iii) Temperature is flame composition dependent iv) Intrusive technique

Table A-11 continued

Method	Advantages	Disadvantages
Ultrasonic Thermometer	i) Good precision and accuracy ii) Real-time two dimensional (and three-dimensional) temperature profiles	i) Not yet applied to flames ii) Thermometer in LTE with flame? iii) Intrusive technique
Optical Fiber Thermometer	i) Very good precision (NBS standard) and accuracy ii) Radiation pyrometry-based comparison of flame with blackbody iii) Higher accuracy and faster time response than thermocouple iv) Lower heat transfer losses v) Translational temperature obtained	i) Limited temperature range ii) Relatively poor spatial resolution iii) Intrusive technique
Gas Sampling/ Pressure Sampling Probes	i) Readily used in turbulent flames and combustors ii) Translational temperature obtained	i) Reaction perturbations within probe sampler before actual measurements ii) Flame combustion disturbances iii) Temperature indirectly determined from species concentrations iv) Relatively poor precision and reproducibility v) Intrusive technique

Table 13
Temperature Ranges of Thermocouples

Base Metals	Temperature Range (K)	Potential (Emf) (mv)
Cu/Constantan	90-672	-5.284-20.805
Fe/Constantan	90-1150	-7.52-50.05
Chromel/Constantan	273-1260	0-75.12
Chromel/Alumel	90-1535	-5.51-51.05
Platinel 1813/ Platinel 1530	273-1575	0-5.11
Pt 10% R/Pt	273-1815	0-15.979
Pt 13% R/Pt	273-1870	0-18.636
Pt 30% R/Pt 6% Rh	310-2075	0.007-13.499
Ir/Ir 60% R 40%	1670-2100	7.30-9.55
W/Rh	280-2475	0.064-29.47
W 5% Rh/W 20% Rh	273-3000	0-38.45
W/W 20% Rh	290-3100	0.042-43.25

temperature of the flame and not the instantaneous, fluc-
tuation temperatures characteristic of turbulent flame
environments.

The assumptions inherent in the use of thermocouple de-
vices are the thermocouple junction tip is in equilibrium
with the flame gases, the thermal conductivity of the gas
and the gas velocity is uniform over the sensing region,
since gradients in velocity would induce temperature gradi-
ents across the junction due to changes in heat transfer to
the wire, and the errors to be discussed below can be cor-
rected very accurately (within 1 K). Systematic errors in-
clude radiation and conduction losses, catalytic effects,
and the effects of the probe itself on the flame. The radi-
ation errors are due to the thermal effect of the probe when
acting as a heat sink such that an apparently low temperature
is measured [187-190, 205]; the magnitude of the error is a
function of the temperature difference between the flame and
the thermocouple. The conductive heat transfer increases as
the diameter of the wires is decreased and therefore most
thermocouples are made as small as possible within limits of
mechanical strength as well as to decrease the sensing volume.
However, larger wires need to be used in steep temperature
gradients. Radiation losses (up to 300 K at 2000 K) can also
be reduced if shields are used around the couple (suction
pyrometry), but they promote severe disturbances in the probed
flame region [11]. Catalytic effects on the thermocouple
surface lead to anomalously high temperatures

(up to 200 K differences) which are particularly signifi-
cant for the reaction zone. Hysteresis in temperature
profiles is commonly observed [187, 192-196]. These
effects (usually conversion of CO and O_2) are principal
causes of error in thermocouple flame temperature measure-
ments. Even at low temperatures, e.g. 300 K, bare metal
junctions, especially Pt surfaces, can suffer catalytic
effects. These errors have been found to be reduced if
the junction is coated with a thin layer of ceramic:
zirconia, silica, or magnesium oxide. Silica and mag-
nesium oxide form quite uniform coatings, but tend to
vaporize; silica can also react with Pt at high tempera-
tures ($\geq$ 2000 K). The thermocouples may also disturb the
flame front by inducing a mass-burning velocity-dependent
wake behind the wire, alterations to the flow field, heat
and mass transfer, and perturbations to the homogeneous
and heterogeneous rate process [196]. These temperature
distortions are less severe in high pressure flames and
more severe in fast, highly nonequilibrated flame reaction
zones [196, 211]. The question of whether the thermocouple
is in equilibrium with the local flame gases is not trivial
nor obvious and must be determined empirically (via compari-
son with line reversal measurements [11, 187, 204]).

Radiation errors can be compensated by using thermo-
couples of different diameters and extrapolating to zero
diameter [3, 188-190, 205] or by electrically heating the
wires until the thermocouple is roughly the same temperature

as the flame (hot wire anemometry) [3, 11, 194-205]. These hot wire methods are generally not appropriate for reaction zone measurements, while being more suitable for large industrial flames and furnaces [187, 206]. Thermocouples need to be optically calibrated by heating in a furnace whose temperature has been measured [11, 187, 201]. For use in turbulent flames, the thermocouple may be placed in a reference flame such as a premixed, laminar H_2/air flame (N_2 sheath) and temperature calibrated against the Na line reversal value [187, 204]. Errors in applying the thermocouple to turbulent flames would include differences in thermal conductivity, viscosity, and gas densities between the reference and test flames.

Thermocouple probes have been used in a wide variety of flames with good (< 2%) precision, e.g., CH_4/air flat diffusion flames, CH_4/O_2/Ar diffusion flames, propane air Bunsen flames, turbulent H_2/air flames, etc. Temperature profiles throughout the flame, including the reaction zone (mainly for low pressure flames), have been accomplished by traversing the wire across the flame and measuring the time-averaged (weighted with respect to time response) temperature fluctuations [194, 198, 204]. The movement and vibration of the probe can cause turbulent burning of the flame gases, usually in regions of steep temperature gradients where heavier and shorter wires are required [11, 187].

C. Resistance Thermometry

Resistance thermometry [11, 187, 213-215] can be used to determine a local translational flame temperature via the development of an electrical resistance through conducting wires (noble metals) from the sensing of changes in the flame temperature. Resistance thermometry is related to thermocouple thermometry and the relationship of resistance to T is relatively linear. The potential use of resistance thermometry, because it also utilizes metal wires, is limited by catalytic effects and disturbances to flame flow patterns and equilibrium states. The use of resistance thermometry is not as widespread as the use of thermocouples, being mainly confined to low pressure, hydrocarbon-based flames, but resistance thermometry also provides good accuracy (if corrections are adequate) and precision. A source of constant current and a wire resistance-measuring apparatus is required [187, 205].

D. Cooled Film Probes

Cooled film probes [216, 217] have been applied to premixed, turbulent flames by Ahmed [216]. These probes are essentially heat flux transducers and can be used to obtain time-resolved probe measurements ($< 10^{-3}$ s) in flames. Even though their accuracy is not great ($< 10\%$), their potential for use as spatial profile probes is quite good, because they can be made independent of velocity and velocity fluctuations characteristic of turbulent flames. Errors

due to disturbances in concentration profiles of different species can be severe.

E. Pneumatic Probes

Pneumatic probes [187, 206, 218-221] measure the pressure drop across two orifices, such that the temperature and pressure of the flow at each orifice can be related by

$$T_1 = K T_2 \left(\frac{P_1}{P_2}\right)^2 \tag{70}$$

where

T_1 = unknown local translational temperature (K),

T_2 = reference temperature (K),

P_1 = pressure drop across the first orifice (Pa),

P_2 = pressure drop across the second orifice (Pa),

K = a constant assuming constant molecular weight and specific heat ratio and is a function of the Reynolds number (dimensionless) at each orifice.

If the orifices are too small, the Reynolds number will increase and K will not be constant with temperature; however, if the orifices are too large, spatial resolution is lost. The pressure drop is measured with a diaphragm gauge or a Hg manometer. The probe is usually quartz and the precision obtainable is dependent on the flame temperature. The main errors are due to the possible occurrence of large radical and atom concentrations which may recombine before reaching the second orifice and thus, alter the molecular weight and specific heat ratios, and to isokinetic (flame

gases measured at gas stream velocity) gradients between
the orifices. The orifices should be operated in only con-
tinuum flow flames. The pneumatic probe can record instan-
taneous temperature fluctuations (~ 3 s) in moderate
temperature regions (~ 2000 K).

F. Ultrasonic Thermometry

Ultrasonic thermometry [222] was developed mainly to
measure high translational temperatures ($\leq$ 3125 K) in
reactor beds, but could be applied to flames. The thermom-
eter consists of a magnetostrictive Fe-Co head welded to a
W wire whose tip possesses small notches (acoustic reflectors)
at regular intervals (20 mm diameter sensor wire, 1 cm inter-
val notches). The thermometer measures changes in sound
velocities as indicators of temperature changes at points
along the sensor wire (the average temperature measured be-
tween the notches). An electromagnetic coil is wrapped
around the thermometer head to produce 60 Hz 1 μs length
acoustic pulses. Each notch reflects a small part of each
pulse back to the coil and the velocity of the reflected
pulses is dependent on the wire temperature. Three-
dimensional temperature profiles could be obtained with
a helical sensor wire. The precision measured from exper-
iments in reactor beds is quite good: ± 1 K at > 1275 K
and ± 50 K at < 900 K, since the time differences between
pulse arrival times can be measured accurately to < 2 ns.

G. Optical Fiber Thermometry

The higher temperature (~ 2300 K) optical fiber ther-
mometer [223] has been developed by the NBS as a new temp-
erature standard. The thermometer is a single-crystal
sapphire (A1O) whose tip is coated with thin films of Ir
and A1O to create a blackbody cavity (1 mm to 30 cm long
crystal rod, 0.25 to 1.25 mm tip diameter). In high temp-
erature gas flows, the Ir cavity emits blackbody irradiation
which is transmitted to a remote detector which is sensitive
to the 0.6 μm and 0.7 μm wavelength bands by the crystal fiber.
With proper selection of the cavity length-to-diameter ratio,
the emissivity can be made constant over an entire tempera-
ture range, up to 2300 K. The thermometer responds eight
times faster than thermocouple devices, has lower heat
transfer losses, and can measure temperatures in lower vel-
ocity gas streams with a precision of ± 0.05%.

H. Gas Sampling/Pressure Sampling Probes

The combination gas sampling and pressure probes [187,
220] have been used to determine the flame translational
temperature from the concentrations of species sampled (CO_2,
CO, and total hydrocarbon species) at known total gas stream
pressure. The major disadvantages are typical of all con-
centration probe sampling techniques [224-230]: 1) reacting
gases in the sample must be "quenched" completely (reactions
stopped) in order to prevent continued reaction in the sam-
ple vessel; 2) disturbances in multiphase samples may occur;

3) water often condenses in the probe; and 4) the probe often disturbs the flow dynamics of the flame such that it is quite difficult to obtain a representative sample and to interpret the sample composition qualitatively and quantitatively. Most sample probes used sample the flame gases isokinetically, producing many physical and compositional disturbances; however, the quartz microprobe [187] samples the flame at sound velocities such that the pressure drop through the orifice is so severe that the reactions are quenched immediately (< 100 μs) without the necessity of water-cooling the probe, thereby decreasing the bulk and disturbance potential of the probe. This probe has been shown to provide sampling results independent of the sample pressure, the size of the orifice, the probe orientation, or the detailed construction. The sampling bias is very small [220].

The sample can be defined via gas chromatographic separation and/or mass spectrometric analysis [231-238]. IR and UV spectroscopic methods have also been utilized for stable species analysis. All concentration probe techniques are less suitable for unstable species (atoms, free radicals, ions) because of their high reactivity and low concentrations (10^{-2} to 10^{-8} mole fraction). However, continued developments in chemical scavenging analysis [239] for radical determinations and most importantly, in molecular beam mass spectrometry (collisionless flow inlet system) [229] and in ion mass spectrometry [187, 233, 238] may provide possibilities for accurate (< 10%) compositional analysis.

I. Concluding Remarks

Probe thermometry can be routinely utilized in most flames with relatively good precision and accuracy (see Table A-11). Most problems in use, at least for thermocouples and thermometers, can be corrected relatively easily if the other parameter distributions which characterize the flames are known, i.e., pressure and velocity streamlines and compositional gradients. The optical fiber thermometer appears to be a potentially excellent technique in terms of accuracy and mode of detection (radiation pyrometry), but a compromise between precision and minimum disturbance to the flame must be achieved. The ultrasonic thermometer also possesses the potential for the measurement of excellent flame temperatures, since the method could provide fairly precise temperature profile information on a real time basis. As for the other probe techniques, especially the sampling probe methods, the thermometer may cause flame flow and combustion reaction perturbations which must be experimentally investigated and corrected for. The most important consideration continues to be whether the probe is in equilibrium with the flame such that the temperatures measured or the gases sampled are locally representative of the flame.

IV. Temperature Methods Based On
Nonintrusive Probes

A. Methods Based on Gas Density

1. Basis of approach

The ideal gas law relates the temperature of a low density, high temperature gaseous system to its density:

$$T = \frac{P\overline{M}}{\rho R} \qquad\qquad (71)$$

where

P = pressure (Pa),

R = gas constant (Pa m^3/mol K),

$\overline{M}$ = average molecular weight of gas molecules (kg mol^{-1}),

ρ = gas density (kg/m^3),

T = mean translational temperature of the gas (K).

The measurement of the local gas density (10^{-3} cm spatial resolution in flames) in flames can be accomplished with varying degrees of success by the methods [11, 187, 240] listed in Tables A-13 and A-14. The mean translational temperature is determined and the measurements are thus rather insensitive to small local disequilibrium effects and to temperature and composition gradients at the flame edges. The small flame thickness can result in quite insensitive measurements of the flame density gradients, and therefore, often significant imprecision in the apparent temperatures obtained. The main disadvantage to many temperature methods based upon measurement of flame gas density gradients is thus the need for composition and temperature edge corrections.

Table A-13
Figures of Merit of Gas Density-based Methods

Method	Type of Temp.[a]	Temperature Range (K)	Temperature Precision (K)	Spatial Resolution[b] (mm)	Temporal Resolution[c] (s)	Sensitivity[d]	Selectivity[e]	Cost[f]	Time[g]	Overall Rating[h] in Flames Laminar	Turbulent	Sooty
Particle Tracking	TR	≳ 4000	50-200	≲ 0.01	10^{-2}-10	H	E	VL	M	F	P	P
Deflection Mapping -Schlieren/shadography	TR	--	100-500	> 1.0-I	cw	L	F	M	M	F	P	P
-Moire deflectometry	TR	--	?	> 1.0-I	≲ 10^{-3}	L	F	H	M-L	G	F	F
Radiation Absorption	TR	--	50-200	> 3.0-I	cw	H	F	H	M	F	F	P
Interferometry -Conventional	TR	≳ 5000	20-100	> 1.0-I	≲ 10^{-1}-cw	L	F	M-H	M-L	G	F	F
-Holography	TR	≳ 5000	50-100	> 1.0-I	≲ 10^{-6}-cw	L	F	H	L	G	G	F
Sound Velocity Methods (photoacoustic technique)	TR	--	15-50	> 1.0	≲ 10^{-8}	H	E	H	L	E	G	G

-- = not applicable

[a] Temperature measured: TR = translational, RA = radiational, E-El = electronic excitation, E-VB = vibrational excitation, E-RT = rotational excitation, E:El* = electronic excitation, vibrational excitation or rotational excitation temperature.

[b] I = inversion methods not needed to obtain radially resolved temperature.

[c] Temporal resolution refers to the time interval in which the measurement can be made, not to the frequency of measurement, cw = continuous wave measurement.

[d] Sensitivity of measurement: H = high, M = moderate, L = low.

[e] Selectivity refers to freedom from spectral interferences: E = excellent, F = fair.

[f] Cost = equipment cost: VH = very high (> $100,000), H = high, M = moderate, L = low, VL = very low (< $10,000).

[g] Time = time to set up system and time for proper operation: L = long, M = moderate, S = short.

[h] Overall rating = capability to provide reproducible, accurate, and precise temperature measurements in laminar, turbulent, and sooty flames: E = excellent, G = good, F = fair, P = poor.

Table A-14
Gas Density-based Temperature Methods
Advantages and Disadvantages

Method	Advantages	Disadvantages
Particle Tracking	i) Complete flame flow streamlines visualized ii) Flame gases themselves used as thermometer iii) Translational temperature obtained	i) Introduction of foreign particles which may not have same aerodynamic characteristics as flame gases ii) Temperature dependent on knowledge of composition gradients and species molecular weights iii) Knowledge of position of final flame temperature and gas velocity required iv) Insensitive to small fluctuations in temperature v) Edge effects vi) Laborious data reduction
Schlieren and Shadowgraph Photography (Deflection Mapping Techniques)	i) Complete flame density gradients visualized ii) Capability to measure temperature in reaction zone iii) Sensitive to very sharp temperature gradient fluctuations iv) Translational temperature obtained	i) Temperature and composition flame edge effects ii) Temperature dependent on knowledge of composition gradients and species molecular weights iii) Greatest accuracy for planar reaction zones, symmetric flames iv) Generally, only stationary flames can be visualized v) Diffraction effects can distort the results vi) Laborious data reduction (need Abel inversion methods)

Table A-14 continued

Method	Advantages	Disadvantages
Moire Deflectometry	i) Three-dimensional temperature profiles visualized ii) Moire pattern notaffected by high background radiation or particle incandescence iii) Laser or incoherent white light source can be utilized iv) Translational temperature obtained	i) Knowledge of spatial distribution of flame chemical composition required ii) Radially resolved temperatures require Abel inversion techniques
Radiation Absorption	i) Temperature independent of molecular composition or gradients ii) Most suitable for flame edge temperature iii) Translational temperature obtained	i) Generally, foreign tracerspecies must be introduced into the flame ii) Flame edge thickness must be known iii) Not good for temperature profiling
Interferometry -Conventional (Mach-Zehnder)	i) Two-dimensional temperature profiling of laminar and turbulent flames obtained ii) Translational temperature obtained	i) Refraction errors at flame boundaries ii) Defined optical path and proper alignment generally required iii) Low sensitivity to sharp temperature fluctuations iv) Inversion methods needed v) Must interpret fractional shifts in interference fringes quantitatively

Table A-14 continued

Method	Advantages	Disadvantages
Interferometry - Holography	i) Complete temperature profiles for multi-dimensional flames can be obtained ii) Transient flame temperature fluctuations visualized iii) No requirement for very high optical quality components--reference and test beams compared in time iv) Translational temperatures obtained	i) Knowledge of compositional gradients required ii) Tomography requires Abel inversion methods iii) Contrast in interference fringes not as bright as Mach-Zehnder interferometry
Sound Velocity (Photoacoustic Technique)	i) Abel inversion techniques not required ii) Instantaneous (single-shot) temperature measurements possible iii) Applicable to "quenching" flames iv) Insensitivity to background luminescence or particle incandescence v) Translational temperature obtained with excellent precision	i) Composition gradients, average molecular weight of species, and average ratio of specific heats required ii) Relatively poor accuracy iii) Turbulence in flame or at edges can distort the sound waves or laser beams iv) Poor spatial resolution

2. Particle tracking photography

The particle tracking method [11, 33, 241-248] is used to obtain velocity and density gas flow streamlines which can be interpreted in terms of a temperature profile. The flame gases themselves can be used as the flame thermometer, through the integrated density profile. The disadvantages include laborious data reduction, the necessity to know $\overline{M}$, and the need to correct for edge effects.

Some early studies [241-246] involved the measurements of streak pictures of density streamlines under prolonged illumination by a controlled spark system or by photoflash photography under the assumption that the velocity function is parallel to the flame front [11]. Magnesium oxide particles (20 to 40 μm diameter range) may be introduced into the flame in order to visualize the flow, but difficulties arise from particle drag and inertial forces and the reliance on the assumption that the introduced particles travel at the same velocity and along identical streamlines as the flame gases [33, 247, 248]. Incorrect temperature maxima which have been observed in the apparent temperature distributions are due to several reasons: 1) failure of the flame to possess a velocity component parallel to the flame front, 2) failure of $\overline{M}$ to follow a simple pattern in the flame which corresponds to the density gradients, and 3) the incorrect assignment of the position of the final temperature (temperature due solely to products of the combustion reactions) in the temperature profile [246].

Later work [249-252] resulted in improved particle tracking methods which utilize repetitive illumination of the flame at 10 ms intervals by a high-pressure Hg lamp. Direct measurements of both velocity components could be made. Glowing particles of aluminum (AlCl) and colloidal clay particles (1-10 μm diameter range) can be introduced into the flame instead of MgO in order that a more reproducible range of particle sizes is obtained and the errors due to inertial forces are more easily controlled. The particles must not be too small (< 1 μm) or Brownian motion may produce local errors and the intensity of reflected light needed to visualize the flow decreases with particle radius$^{1/4}$. Even though these particles can be used in slower flame gas streams, the significance of particle asphericity, the effects of particles on flame reactions, and the optical inhomogeneities in the photography must be evaluated. Time-of-fall experiments can provide corrections for particle velocity lag, while probe measurements can indicate changes in $\bar{M}$ [246].

The primary data needed for particle track analysis is the measurement of the position and time (knowledge of gas velocity required) relation for each particle observed in the field of focus. With the assumption that

$$\rho v A = \text{constant} \tag{72}$$

where

ρ = gas density (g/ℓ),

v = gas velocity (cm/s),

A = cross sectional area (cm) of volume element gener-
ated by rotating area between two adjacent velocity
streamlines at a position i in the photograph, the
local temperature can be evaluated from

$$T_i = T_o[v_i/v_o][r_i/r_o][\overline{M}_o/\overline{M}_i] \tag{73}$$

where

T_i = local temperature (K),

T_o = initial flame temperature (K),

v_i = velocity at position i (m/s),

v_o = initial velocity (m/s),

r_i = horizontal distance from axis of flame (m) at
position i,

r_o = horizontal distance (m) at initial position of
stream tube,

$\overline{M}_o$ = average molecular weight of initial flame
reactants (g/mol),

$\overline{M}_i$ = average molecular weight of species at position i
in flame (g/mol).

Even though the potential spatial resolution can be below
0.01 mm, it is necessary to measure accurately the average
molecular weights (composition gradient) throughout the
flame as well as the initial flame temperatures.

3. Schlieren and shadowgraph photography

Schlieren and shadowgraph method [253-262] are mainly used for the visualization of flame structure and geometry resulting from the observation of the irregular deflections of incident light passing through the flame as functions of changes in the refractive index throughout the flame. The measured deflections of narrow light beams can be related to the refractive index gradient in Schlieren photography and to the first derivative of the refractive index gradient in shadowgraphy:

$$\theta = \frac{-dn}{dy} \cdot D = \frac{-dS}{dy} \cdot D \qquad (74)$$

where

θ = angle of ray deflection (degrees),

n = refractive index (dimensionless),

D = distance light travels perpendicular to flame front (cm),

S = n-1 (dimensionless),

and

$$S = S_0 T_0 / T \qquad (75)$$

where

S_0 = n-1 of initial flame reactants (dimensionless),

T_0 = initial flame temperature (K),

T = flame temperature at position D above the flame burner.

It is apparent from Eqn. 74 that at low flame temperatures (< 1000 K), a small change in T corresponds to a large change in S, while at high temperatures (< 2000 K), a large change in T corresponds to only a small change in S. The first derivative of Eqn. 75 (Schlieren photography) indicates that a change in S is due to a change in T and is inversely proportional to the square of the absolute T:

$$dS = -S_0 T_0 \left(\frac{dT}{T^2}\right) \tag{76}$$

The first derivative of Eqn. 76 (shadowgraphy) at $\left(\frac{d^2 S}{dy^2} = 0\right)$ maximum deflection can be given by

$$T\left(\frac{d^2 T}{dy^2}\right) = 2\left(\frac{dT}{T}\right)^2 \tag{77}$$

which again indicates the dependence on the need for accurate measurement of the refractive index gradient. An incident collimated light wavefront will be bent due to the resulting velocity distribution of the light, if the refractive index gradient has a component perpendicular to the direction in which the wave front propagates. The deflections are visualized most simply by introducing a slit or knife edge after the flame and before the screen or photographic plate [254-260], such that without the flame present, the incident light will be just blocked by the slit. When the flame is introduced before the slit, the deflection of the light toward the cooler regions of the flame will cause some of

the light to pass the slit and be recorded. If the super-
imposed diffraction pattern produced by the slit or knife
edge can be minimized, a curved light image can be detected;
the greatest deflection will occur within the flame zone
where the refractive index variation with respect to compo-
sition changes are negligible and the temperature changes
are the most significant. The deflection at any point is
equal to the vertical displacement from the straight slit
image at that point divided by the distance to the screen
beyond the flame. Inaccuracies in the deflection mapping
may arise if the incident light beam is not parallel with
respect to the flame (highest accuracy therefore obtained
when deflection mapping is utilized in flat flames) and if
the refraction of the rays as they leave the flame into the
surrounding atmosphere is not severe; this error is in addi-
tion to the errors due to flame edge effects. Difficulties
in interpreting the data also occur because the value of D
varies along the slit with respect to the detector. The
quantitative spatial resolution can be increased if an addi-
tional slit inclined at ~ 45° is placed before the flame
[263-268]. If the slit is placed horizontally, the deflec-
tions will be measured as only intensity distributions. If
the slit is placed vertically, the radial variation cannot
be measured.

A coarse (Ronchi) grating can be used in place of the
slit after the flame [253, 255, 269]. The image of the
front slit is focused onto one of the gaps in the grating

so that the detector is uniformly illuminated. When the flame is placed between the slit and the grating, a series of contour lines will be recorded. Different color filters can be used in front of the grating and with color photography, the pattern can be more easily interpreted [11, 253, 270, 271]. If it is desired to record the refractive index distribution throughout the whole flame field, many slits can be used parallel to each other (radial distribution mapping). In addition, the use of multiple slits can correct for deviations from flame flatness.

In shadowgraphy, the positions of maximum and minimum intensities can be related to the maximum and minimum d^2S/dy^2 in the flame <u>only</u> if the detection plate is placed very close to the flame. With larger distances from the flame, the shadow pattern is complicated by ray crossing from different regions of the flame. Even though both Schlieren photography and shadowgraphy require knowledge of the initial temperature, because of the difficulties in interpreting the shadow pattern, shadowgraphy is not generally used for temperature profile measurements [253, 261]. Shadowgraphy is thus mainly used for simple visualization of flames: shadow methods are more sensitive to steep refractive index changes than Schlieren methods, but are less sensitive to gradual changes in refractive index [253]. Most importantly, both shadow and Schlieren methods promote difficult and laborious quantitative interpretation of the recorded patterns for temperature measurement.

Except for the one Schlieren deflection mapping method that utilizes a coarse grating, only stationary phenomena can be observed with most deflection mapping techniques, since the mapping of the flame generally requires moving the slits vertically above the burner. However, with the Ronchi grating method, nonsteady fluctuations in the re-fractive index gradients can be measured, because the radial distributions at several levels above the burner can be simultaneously recorded [255]. Considerable difficulties can arise because of severe defraction effects with the simultaneous mapping of the deflections from multiple slits. An improvement in this method, Moire deflectometry, has been developed [272-274] which utilizes two Ronchi gratings, mutually rotated by an angle θ. The distance between the grating is adjusted so that the fringe pattern is sharpened and diffraction effects are minimized [275]. The collimated light beam is produced from a He-Ne laser and the Moire pattern is recorded via a video camera and visualized instantaneously on TV. The Moire pattern is not affected by the hostile environment of the flame or the presence of hot particles.

However, Abel inversion techniques are still required for three-dimensional mapping (see Appendix C) and thus, an axially symmetric flame must be used [9, 276, 277].

4. Interferometric methods

   a. Conventional interferometry. Interferometric meth-
ods for investigation of combustion phenomena are mainly
utilized for the continuous temperature profiling of lam-
inar and two-dimensional (turbulent) flames. The accurate
evaluation of temperature gradients and heat transfer
necessitates minimally an interferometer (typically a
Mach-Zehnder interferometer [253, 278-281] and a photo-
graphic plate for recording the interferometric fringe
pattern. Typically, a collimated light beam is split into
two beams, the reference and test beams, and are then re-
combined after travelling separate optical paths. The
flame is placed in the path of the test beam. Assuming
the flame refractive index gradient does not refract the
light rays, the refractive index gradient will produce
distortions in the interference fringes produced under the
conditions existing when neither the reference nor the test
beam passes through a distorting medium. The shift in the
interference fringe pattern can be observed and the measure-
ment of the shifts is related to the product of the flame
thickness and the refractive index change [253, 282]:

$$S(x,y) = \frac{\ell}{\lambda}[n(x,y) - n_r] \qquad (78)$$

where

   $S(x,y)$ = fringe shift in the x-y plane perpendicular
             to the light path (dimensionless),

      ℓ = change in path length due to flame (m),

λ = wavelength of incident light (m),

$n(x,y)$ = index of refraction in the flame (dimensionless),

n_r = index of refraction of medium in the reference path (dimensionless).

If ℓ is known (by optical methods, generally), then $n(x,y)$ can be quantitatively determined from the interference pattern [253, 285].

The paths of the light beams must be well defined. Inaccuracies in temperature determination may occur because the inherent wavelength spread about λ decreases the resolution and thus the sensitivity of the technique because of changes in fringe spacing with λ. Deviations in the linearity of the optical path often occur during traversal of the light through the flame due to severe refraction and displacement errors in steep refractive index gradients. The strict requirements for proper alignment and defined optical path length often require very good optical components and a laser to be used as the light source. Interferometry, in contrast to deflecting mapping, generally possesses low sensitivity for sharp but small changes in the refractive index gradient. Classical Mach-Zehnder interferometric methods have been used to some extent in combustion studies, primarily for long optical path length flames in order to achieve maximum sensitivity and for those flames (including curved flames) with less severe edge effects [253].

Multiwavelength interferometry can be used for analysis of flames for both composition and temperature [284-286]. Characteristically, in flames, the value of n increases as λ decreases, the rate of increase is greater the shorter λ used, and the larger initial n, the greater the rate of change in n. Because the wavelength spread is limited by the transparency range of the interferometer optical components, generally, only two wavelengths can be used, but two may be sufficient to provide maximum sensitivity over a wide range of n existing in the flame. In practice, however, an undesirable compromise in resolution (due to scatter) observed in attempts to record nonsteady refractive index gradients in turbulent flames is often encountered [253].

Alternative interferometric systems include the two- and four-transmission diffraction grating systems [253, 287-289]. Inexpensive replica gratings can be used to split the incident light into its constituent wavelengths, to change its direction, and to recombine the beams (with respect to the first-order diffraction pattern). The advantages of these systems are the insensitivity to misalignment and the necessity for only relatively simple, inexpensive mounts. However, because only the interference fringes from the first-order spectra are recorded, more light is wasted compared to the classical interferometer techniques.

b. Holographic interferometry. This type of inter-
ferometry [290-295] provides the capability to measure the
complete temperature profiles associated with an unsteady,
multidimensional flame at several instants in time (see
Table A-15). Because of the considerable reduction in
image quality resulting from the use of an incoherent
source which possesses little spatial and temporal
coherence [296-298], lasers (generally when operated in
single-mode emission) possess much greater spatial and
temporal coherence and are generally used in holographic
applications [11, 298-303]. The optimal increase in fringe
resolution and visibility is desired. The advantage of
holographic interferometry over classical interferometry
is there is no requirement for very high optical quality
components, because the wavefronts propagated along the
test path are compared in time and not the wavefronts which
have propagated along two different paths (test and refer-
ence beams) [302, 303]. In contrast, classical and holo-
graphic interferometry do share a requirement for knowledge
of the compositional gradients, $\bar{M}$, throughout the flame.
The sources of holographic image distortion include coherent
noise and speckle, if diffuser surfaces are used (see below),
motion during holographic exposure, nonuniform reference
beam illumination on the hologram which results in only
portions of the hologram being properly exposed, and the
use of polychromatic light as the source [300].

Table A-15
Holographic Interferometry Techniques

I. Double Exposure:

    - first hologram made of sample volume (without flame
      ignition) to record the interference between the
      reference and object waves.

    - second hologram recorded interference between refer-
      ence and object waves passing through disturbed
      volume (flame ignited).

    - appropriately used for instantaneous recording of
      ignition and flame propagation temperatures.

II. Time Lapse Exposure:

    - two holograms of same flame volume recorded at two
      different times.

    - most suitable for premixed, laminar flames.

III. Real Time Exposure:

    - wave field of flame illuminates a previously re-
      corded hologram of flame such that differences in
      the "state" of the flame are observed interfero-
      metrically, in real time.

IV. Long Time Exposure:

    - Illumination of flame volume for long intervals.

Holographic differential interferometry [302-304] in the double-exposure mode can be used to obtain path-integrated two-dimensional phase information (line-of-sight refractive index gradient measurement) about the flame. An Abel inversion, and therefore, an axially symmetric flame, is needed to reconstruct the radial temperature distribution. Modifications in the inversion algorithm to account for ray refraction through the flame has resulted in more accurate temperature profiling [304-306].

Three-dimensional phase information may be obtained by placing a diffuser [302, 303, 307] behind the flame so that the incident laser light will be scattered in many directions (180° viewing range) from each point of the diffuser. Therefore, no matter from what direction the flame is viewed, the light incident on the flame will be back-illuminated by the diffuser. The fringe patterns obtained from the multidirectional holographic interferometric method represents the same information which could be obtained from many Mach-Zehnder interferograms, each recorded at a different viewing orientation. Most importantly, unlike single-direction holography, multidirectional interferometry can be used to analyze asymmetric flames, if the fast Fourier transforms at several points along the set of radial lines across the flame are obtained [308, 309]. To minimize the severe dependence of temperature on the generally unknown value of $\bar{M}$, the wavelength of the incident laser can be

tuned to nearly coincide with a resonant absorption line
of only one flame species [310]. However, all interfero-
metric methods, in contrast to Moire deflectometry, require
strict mechanical stability, even with the use of pulsed
lasers ($< 10^{-6}$ s pulse length) and generally coherent laser
light, while being relatively unable to be adjusted for
optimal sensitivity [278]. Spatial resolution via deflec-
tion mapping or interferometry does require mathematical
inversion techniques, but tomographic flame temperature
measurements are definitely possible.

5. Radiation absorption methods

Radiation absorption methods have been used for flame
temperature measurements because the scattering of α par-
ticles and neutrons [11, 187, 311, 312] from nuclei is
independent of the molecular composition or gradients
throughout the flame. The temperature within less than
a cm path length can be measured from the ionization of
the particles. Difficulties for very high temperature
flames (> 2000 K) may arise from severe reductions in gas
density due to dissociation of certain flame species.
Soft x-rays (Fe^{55} source) [313, 314] have also been util-
ized, but all these methods do appear to be more suitable
for plasma investigation. Border flame temperature mea-
surements have been made with the addition of a highly
absorbing tracer gas like Xe [187]. Hg vapor and O_2 [315]
have also been studied as potential tracer species, but

problems with reactivity and spectral interference have
limited their use to shock tubes [312].

6. Sound velocity methods

In ideal gases, the passage of a pressure disturbance
is essentially an adiabatic and reversible process directly
related to the translational temperature [11, 187] as well
as to the average ratio of specific heats of the gas par-
ticles and to the average molecular weight:

$$c = \left(\frac{\gamma RT}{\overline{M}}\right)^{1/2} \qquad\qquad (79)$$

where

    c = velocity of sound (m/s),

    γ = ratio of specific heats at constant pressure and
       volume (dimensionless),

    R = gas constant (J K^{-1} mol^{-1}),

    T = translational temperature (K),

    $\overline{M}$ = average molecular weight (g/mol).

The main requirements are $\overline{M}$ and γ must be known or assumed
constant (for temperature profiling) and the sound frequency
must not be high enough to alter γ because of molecular
vibrational effects.

Schlieren and shadow photography of sound waves (with
an instantaneous spark flash) can be obtained, but the
spatial resolution is relatively poor [292, 319]. If the
ratio of $\overline{M}$ to γ is assumed constant, then exact knowledge
of the compositional gradients is not required. These

methods probably could not be applied to turbulent flames because of flame edge and reaction zone effects which may cause anomalous distortions in the sound velocity-based photographs.

The photoacoustic technique could be used to obtain translational temperatures [317-320], especially if a pulsed dye laser ($\leq$ 1 μs) is used to excite an internal energy state of a specific flame species (atom or molecule) such that the energy released in the quenching of the ex- cited state by the flame gases produces a sound wave which can be detected by a condenser microphone (~ 1 cm from the flame). The photoacoustic process occurs from a transfer of electronic energy into the vibrational modes of a flame species ($E \rightarrow V \rightarrow T$ process). The photoacoustic method can be used for high pressure flames because collisions of the excited species with other quenching species, like N_2, only enhance the optical energy to acoustic energy conversion process.

The speed of sound is determined by the measurement of the arrival time of the pressure wave produced at a par- ticular point in the flame. The laser beam can be moved within the flame (< 1 cm) and the arrival time from that location is measured. The difference in arrival times to the microphone and the distance between the two laser paths in the flame can be determined and the speed of sound calculated. For instantaneous time resolution, the inci- dent laser beam could be split into two or three components

and the difference in arrival times could be measured on a single-shot basis. The disadvantages to this photoacoustic method are the slow rise times of the microphones (< 10 µs), which limit the time resolution and the capability to follow transient temperature phenomena, and inaccuracies in the apparent temperature due to the necessity for the acoustic waves to cross the turbulent flame boundaries [317].

A significant development in the photoacoustic technique has been reported by Zapka et al. [321]. Three laser beams which are coplanar, parallel, and sufficiently displaced by a known distance are focused inside the flame. The excitation pulsed laser beam (~ 10 ns pulse duration) is used to produce an acoustic pulse from plasma breakdown within the flame. The difference in arrival times of the propagating transient signals as indicated by the transient deflections of the two probe beams is used to determine the acoustic velocity (deflection rise time ~ 0.2 µs). The flame temperature measured corresponds to the averaged temperature over the region defined by the focused volumes of the probe beams. For the highest accuracy, the probe beams cannot be generally closer than 1 cm to the excitation beam or nonlinear acoustic effects from the large amplitude acoustic pulse will be produced; the probe beams can be placed less than 10 mm apart (precision < 3%), but generally they are separated by ~ 1 cm (resulting precision of < 1-5%). The heights of the laser beams can be varied in order to obtain a flame temperature profile that agrees well with

a thermocouple-derived profile. The optoacoustic laser-beam deflection (OLD) method is the first known <u>nonspectroscopic</u>, laser-based, <u>noncontact</u> method to directly measure the local translational flame temperature. The advantages of OLD are insensitivity to background luminescence or particle incandescence, no requirement for detailed knowledge of the laser beams' spatial or temporal profiles, and the instrumentation needed is simple (no requirement for tunable, narrow-band lasers or critical beam matching and overlap). As will be shown, the spatial resolution obtained is relatively poor compared with laser-based spectroscopic techniques, but the potential precision and accuracy may be greater.

B. Radiation Pyrometry

1. Methods

Radiometric methods as defined by Tourin [9] involve the measurement of radiant energy without knowledge of the microscopic mechanisms of emission and absorption of radiation or the energy distributions of the gas species, but rather, depends on the Planck radiation law. These techniques listed in Tables A-16 and A-17 do not disturb the system and do not have a high temperature limit as many of the probe thermometric methods possess.

2. Spectral emission-absorption methods

The spectral emission-absorption methods [9, 11, 322-325] which include the Schmidt method, infrared brightness and

Table A-16
Figures of Merit of Radiation Pyrometry

Method	Type of Temp.[a]	Temperature Range (K)	Temperature Precision (K)	Spatial Resolution[b] (mm)	Temporal Resolution[c] (s)	Sensitivity[d]	Selectivity[e]	Cost[f]	Time[g]	Overall Rating[h] in Flames Laminar	Turbulent	Sooty
Spectral Emission-Absorption	E-VB (E-EL)	--	> 50-200	> 1.0-I	10^{-3}-CW	H	E	L-M	S-M	G	P	P
Integrated Emission-Absorption	RA	--	> 200	> 1.0-I	CW	H	F	L-M	S-M	P	P	F
Color Temperature	RA	--	50-200	> 1.0-I	CW	H	F	L-M	S-M	P	P	F
Line-Reversal	E-EL	> 1000	≤ 5	> 1.0-I	10^{-2}-CW	H	E	M	M	E	G	F

-- = not applicable

[a] temperature measured: TR = translational, RA = radiational, E-EL = electronic excitation, E-VB = vibrational excitation, E-RT = rotational excitation, E-El* = electronic excitation, vibrational excitation or rotational excitation temperature.

[b] I = inversion methods not needed to obtain radially resolved temperature.

[c] temporal resolution refers to the time interval in which the measurement can be made, not to the frequency of measurement, cw = continuous wave measurement.

[d] Sensitivity of measurement: H = high, M = moderate, L = low.

[e] Selectivity refers to freedom from spectral interferences: E = excellent, F = fair.

[f] Cost = equipment cost: VH = very high (> $100,000), H = high, M = moderate, L = low, VL = very low (< $10,000).

[g] Time = time to set up system and time for proper operation: L = long, M = moderate, S = short.

[h] Overall rating = capability to provide reproducible, accurate, and precise temperature measurements in laminar, turbulent, and sooty flames: E = excellent, G = good, F = fair, P = poor.

Table A-17

Radiation Pyrometry Advantages and Disadvantages

Method	Advantages	Disadvantages
Spectral emission-absorption	i) Knowledge of flame chemical composition not required ii) No high temperature limit iii) Flame temperature need not be the same as the source brightness temperature iv) Source modulation allows the sequential detection of emission and absorption-- rapid temperature determination	i) Line-of-sight temperature ii) Strong absorber (IR) required iii) Concentration and temperature gradients errors iv) Inaccuracy in temperature due to nonhomogeneous spectral gas absorption v) Calibrated lamp required; at least at one temperature and spectral region
Integrated emission-absorption	i) Good for sooty flames ii) Simple approach	i) Same as above ii) Flame edge temperature generally measured iii) Flame must be graybody and temperature must not be measured at banded (CH, H_2O, etc.) emission spectral regions
Color Temperature	i) Good for sooty flames ii) Measurements made in emission only iii) Relatively simple temperature method	i) Same as above ii) Flame must be optically thick or the color temperature at three wavelengths must be determined
Line Reversal	i) Excellent precion and accuracy obtained at null point (no net emission or absorption) ii) No data analysis needed iii) Several thermometric species can be utilized iv) Applicable to all flame zones of particular flames v) Time resolution can be increased over other radiation pyrometry methods	i) Line-of-sight temperature ii) Calibrated source required iii) Temperature and concentration gradients introduce errors iv) Very good optical alignment required v) Apparent temperature dependent on excitation energy of thermometric species

infrared monochromatic radiation methods, and the Planck-Kirchoff method are based on the measurements of spectral radiance and absorption at one specific wavelength. The spectral radiance emitted by a blackbody at any wavelength depends solely on its temperature, while the spectral radiance emitted by a flame in any region depends on its local temperature, composition, pressure, and geometry. The absorption can be determined by using a background source (globar, carbon arc, Xe high-pressure arc, flash discharge tube, or W strip lamp) which has a much higher brightness temperature than the flame so that the flame emission can be neglected. The emissivity of the flame can be measured by using Kirchoff's law (emissivity equals absorptivity for gases in thermodynamic equilibrium [326, 327]. Typically, a monochromator or spectrometer is needed to isolate the wavelength region being observed. The absorption and emission signals can be monitored by a photocell, bolometer, or photomultiplier detector (see Appendix B for equations).

The spectral emission-absorption method is generally used in the infrared spectral region where most combustion gas radiation occurs (H_2O at 2.3 to 3.4 μm, CO_2 at 4.1 to 4.9 μm and CO at 4.5 to 5.4 μm) [324, 328, 329] or at the center of strong self-absorbing resonance lines like the Na-D lines [324, 331]. For most practical applications, CO_2 appears to be the most feasible for the temperature range 800-3500 K, since with Na-D lines, erroneous results may be obtained due to the measurement of an average absorption and emissivity over

the contour of the Na-D line. Elaborate procedures are
therefore required to deconvolute the contour of the line
to obtain the true temperature [332].

   An alternative to using a monochromator or spectrometer
is the use of a color filter so that a pyrometer will view
the flame and the comparison source directly [322]. The
accuracy of this method can be adequate if the flame spectrum
is continuous over the wavelength range transmitted by the
flame.

   Particularly useful for luminous flames and those flames
which possess time-varying temperature distributions is the
two-path method of measuring the absorption. In this ap-
proach, the ratio of the radiation detected after one pass
through the flame to the sum of the radiation detected after
one pass and the radiation reflected back through the flame
by a mirror of known reflection is determined.

   Interestingly, a chopped light detection system [9, 323]
can be used for luminous flames, turbulent flames, and those
flames whose temperature is comparable to the brightness
temperature of the source lamp. A light chopper is intro-
duced between the background light source and the flame and
the photomultiplier amplifier circuit is tuned to the chop-
ping frequency. Potentially, a lock-in amplifier with
phase-sensitive detection could be used. The photomulti-
plier then only detects the fluctuating signal and not the
steady flame emission. The absorption can therefore be
determined by measuring the difference in signals with and

without the flame present. The flame emission, B(em), can be measured by observing the signal recorded without the background source present. The spectral absorption of the flame, $\alpha(\nu, T_f)$, is given by

$$\alpha(\nu, T_f) = 1 - B_s'(\nu)/B_s(\nu) \tag{80}$$

where

T_f = flame temperature (K),

ν = frequency being detected (Hz),

$B_s(\nu)$ = incident source radiance (J m^{-2} s^{-1} sr^{-1}),

$B_s'(\nu)$ = source radiance transmitted through the flame (J m^{-2} s^{-1} sr^{-1}).

The ratio of the emission signal to the absorption signal can be used to determine the Planck temperature from the Kirchoff-Planck relations:

$$\frac{B(em)}{\alpha(\nu, T_f)} = B_\nu^b(\nu, T_b) \tag{81}$$

where

$B_\nu^b(\nu, T_b)$ = spectral radiance of blackbody source at ν and T_b (J s^{-1} m^{-2} sr^{-1}),

T_b = brightness temperature of source (K)

and

$$B_\nu^b(\nu, T_b) = \frac{c}{4\pi}\left(\frac{8\pi h\nu^3}{c^3}\right)\left(\frac{1}{\exp(h\nu/kT_b)-1}\right) \tag{82}$$

where

h = Planck constant (J s),

k = Boltzmann constant (J K^{-1}),

c = speed of light (m/s).

No information about the detailed chemical composition of the flame is needed; the only requirement is that a suitable wavelength for the absorption-emission measurements is found. For most flames at temperatures below 3000 K, a strong IR emitter could be introduced into the flame [333, 334]. The source may be hotter, cooler, or at the same temperature as the flame and only one wavelength is needed. If a temperature gradient exists over the line-of-sight (spatial resolution determined by volume illuminated), then the apparent temperature measured will be weighted to higher values at wavelengths of lower absorption and to lower values at wavelengths of higher absorption. The practical limit to the temperature measurement by these methods depends on the relative absorption of the wavelength being used. An absorption of at least 5% is required for a 10% precision in temperature, but > 20% absorption will significantly increase the precision and accuracy of the average temperature measured. Inaccuracies in the apparent temperature (see Appendix B) are due to concentration gradients, self-absorption of the resonance line, nonhomogeneous gas absorption across the spectrum, and temperature gradients [332-337].

Therefore, the spectral emission-absorption method gives an electronic excitation "temperature" when applied to atomic resonance lines, and a vibrational excitation "temperature" when applied to the infrared bands of molecules.

An Abel inversion procedure (see Appendix C) is needed to obtain radially resolved temperature distributions.

3. Integrated emission-absorption method

The integrated emission-absorption or the modified Schmidt method [9] can be used for sooty flames in which the soot acts as a graybody to absorb, but not to scatter the incident source radiation. The flame will only act as a graybody if it is heavily charged with soot, so that the emissivity is essentially invariant with wavelength. The accuracy of the method therefore depends on the validity of the flame as a graybody; the effect of temperature gradients on the temperature measurement is unknown [332, 338]. However, it is probable that the surface temperature at the flame edge is being measured.

4. Color temperature method

The color temperature of a sooty, luminous flame can also be measured through the comparison of the contour of the flame emission spectrum to the contour of the blackbody emission spectrum over a range of temperatures or through the location of the maximum in the contour and the calculation of the color temperature from the Wien displacement law [9, 11, 192, 339-342]. These methods, especially the

latter, provide only rough estimates of the mean transla-
tional flame temperature because the contour shape and
the location of the relatively broad maximum are rather
insensitive to temperature changes; the resulting preci-
sion is at least 6%.

The flame color temperature can also be determined
from the measurement of relative brightness at two isolated
wavelengths, if the spectral absorption is assumed constant
across the spectral range [192, 343-345]. Typically, the
temperature measured can be up to 10% lower than the Na
line reversal temperature measurement, but this result may
be due equally as much to the use of the line reversal
method for temperature measurement in sooty, luminous
flames (see Appendix B). The advantage of this method
lies only in the fact that there is no need for explicit
knowledge of the spectral absorption or the use of an
external source; the measurements are made in emission only.

However, if the flame is not optically thick, then the
spectral absorption will vary significantly with wavelength.
The color temperature can still be evaluated if the relative
brightness (emission) is measured at three selected wave-
lengths [11, 15, 338]. Generally, this method is applicable
only to the visible region, because the spectral absorption
varies linearly in this region, but varies quite nonlinearly
in the IR region; also, the wavelengths whose emissions are
being detected must be a portion of the graybody spectrum
and not be banded emission (H_2O, CH, C_2, etc.).

5. Line reversal method

One of the methods most generally used for flame temperature measurement is the line reversal method. At the reversal point, the flame temperature in terms of the excitation temperature of the thermometric species (either introduced or native) is equivalent to the brightness temperature of the source background lamp at the excitation wavelength [130, 346-360]. The equations which can be used to determine the reversal temperature are given in Appendix B for flames under isothermal, nonisothermal, and concentration gradient conditions within the line-of-sight probed volume (see Table A-18). There is no criterion for the existence of LTE; however, at the reversal temperature, the line emission intensity follows a Boltzmann distribution of the upper excited level with respect to the ground state. The resonance line used for the thermometric species, Na, Tl, Pb, K, Li, Rb, Fe [349, 361], OH, O_2 [362], CO_2, and H_2O [348], must have a high oscillator strength in order to obtain the highest precision and accuracy ($\leq$ 2 K at 2600 K), although the transition probability data is not required for the explicit temperature determination. As detailed in Table A-18 and Appendix B, the apparent reversal temperature depends upon the excitation energy of the upper level; as the excitation energy is increased toward the ultraviolet, the reversal temperature will be anomalously high. In isothermal flames, the accuracy of the method is not affected by self-absorption of the excitation line, since the emission and absorption line

Table A-18
Spectroscopic Flame Temperatures

The line-of-sight spectroscopic flame temperature is
equivalent to:

1. The measurement of the total population ratio of thermo-
   metric species within the spectrometer's viewing field,
   and

2. The Boltzmann temperature that corresponds to this ratio.

This line-of-sight spectroscopic flame temperature is depen-
dent on:

1. The temperature profile witin the probed flame volume,

2. The concentration gradient of the thermometric species,
   and

3. The excitation energies of the levels whose transition
   is being measured:

   a. At low values of E_i and E_j for the transition from
      levels $j \rightarrow i$, the species number densities in levels
      i and j will be relatively large in the flame regions
      where the thermometric species are present, and the
      temperature measured is due to the whole probed
      flame volume,

   b. At higher values of E_j (or E_i), only the highest
      temperature regions will have detectable number
      densities in levels i and j; therefore, the appar-
      ent temperature measured will more closely approach
      the temperature of the higher temperature regions,
      and

   c. At the highest values of E_i and E_j, the apparent
      temperature will correspond to the maximum flame
      temperature if the transitions from these levels
      can be detected.

profiles are affected in the same way, in contrast to the profiles measured in nonisothermal flames. If the concentration of the thermometric species is too low, the line will be difficult to detect above the background over a wide range of source temperatures. If the concentration is too high, the apparent temperature measured will correspond to the temperature at the flame edges [127, 130, 363]. Anomalously high excitation temperatures have been observed in the reaction zones of certain premixed hydrocarbon/air (O_2) flames, methyl alcohol flames, cyanogen flames, and in hydrogen/nitrous oxide flames [12].

Other systematic and random errors are listed in Table A-19. Other difficulties can arise due to the presence of particulates. Soot can reflect and scatter the light, and therefore weaken the background continuum radiation and emission from the back of the flame (with respect to the viewing surface); an anomalously high flame temperature will be measured. In smaller laboratory flames, this error may be less significant [364]. Generally, it is most advantageous to use a source which can provide brightness temperatures equivalent to the flame temperature. If the flame temperation is ≳ 500 K higher than the maximum source temperature, the reversal temperature can still be measured by modulating the flame emission inefficiently by chopping the emission with a 10% "off" and 90% "on" chopper between the flame and detector, while modulating the absorption at the same frequency with a normal 50% "off"/"on" chopper

Table A-19
Errors in the Line-Reversal Method*

A. Systematic errors due to the apparatus ($\leq$ 5 K)

    1. Too high temperature (favoring flame emission) when solid angle of lamp radiation is less than the detected flame radiation solid angle,

    2. Reflection losses at optical surfaces ($\sim$ 5%),

    3. Emissivity corrections at resonance line wavelength for strip lamp material ($\sim$ 5% for Na-D doubletlines),

    4. Too low temperature when emission radiated from flame is reflected back into lamp solid angle,

    5. Stray light from flame toward detector, and

    6. Anomalous temperature due to depopulation of upper level of transition when used in low quenching flame.

B. Random errors ($\leq$ 5 K)

Detectability of weak signal on strong background continuum.

*see ref. 130.

placed between the background source and the flame. There-
fore, the flame emission measurement is decreased while
keeping the absorption constant. The advantages of the
line reversal method include rapid, convenient use, and no
need for data analysis, unless radially resolved temperatures
which require Abel inversion methods are desired.

To increase the time resolution, a vibrating mirror or
quartz plate can be used for fast, repetitive wavelength
scanning about the central frequency, f_o, (~ 100 Hz) [2, 365].
Phase-sensitive detection of the signal at $2f_o$ will indicate
the occurrence of net emission, net absorption, or the re-
versal point.

Other approaches have been developed for the study of
transient phenomena [366-369], including a double-beam sys-
tem in which two photomultipliers view two background sources
at effectively different brightness temperatures, T_1 and T_2,
and the flame and source radiation at the Na-D line [367].
If the flame temperature is between T_1 and T_2, it may be
possible to linearly interpolate between T_1 and T_2 to deter-
mine the flame temperature on a time scale of ~ 2 μs with a
precision of ± 30 K.

C. Spectrometric Methods

1. Basis of technique

Spectrometric temperature methods include measurements
of the spectral radiances [9] corresponding to transitions
(emission, absorption, fluorescence) from populated levels
of the internal energy distributions within the atomic or

molecular species   as   functions of the collisional and
radiative processes which produce the observed spectra.
These approaches to temperature determination depend on
measurements of a single line or band or on some relation
(Maxwell velocity and Boltzmann distributions) between the
spectral lines. Spectrometric methods have no high tempera-
ture limit, but do assume LTE within the probed flame volume
and negligible self-absorption of the measured lines (see
Tables A-20 and A-21).

2. Emission methods

    a. Absolute measurement. The measurement of single
line or band emission radiances [370] requires the absolute
intensity calibration of the spectrometric detection system
and the integration of the line radiance over the full width
of the line:

$$B(em) = \frac{c}{4\pi} \ell \, A_{ji} \, h\nu_{ji} \, n_j \qquad (83)$$

where

    $B(em)$ = integrated emission radiance of transition
         from level j to i ($J \, s^{-1} \, m^{-2} \, sr^{-1}$),

    ℓ = path length (m),

    n_j = number density of atoms in upper level j (m^{-3}),

    A_{ji} = Einstein coefficient of spontaneous emission
         for transition j→i (s^{-1}),

    ν_{ji} = frequency of transition j→i (Hz).

and

$$B(em) = \frac{hc}{4\pi} \, \ell \, \frac{A_{ji}}{\lambda_{ji}} \, \frac{g_j}{Q} \, n_j \, exp^{-E_j/kT} \qquad (84)$$

where

E_j = energy of the upper energy level j (J),

g_j = statistical weight of level j (dimensionless),

Q = partition function, $Q = \sum\limits_{j} g_j \, exp^{-E_j/kT}$ for

      upper levels (dimensionless),

λ_{ji} = wavelength of transition j→i (m),

T = flame temperature (K).

This procedure is applicable to any spectral line or band to which valid values of λ_{ji}, A_{ji}, g_j, and E_j can be assigned. In practice, a plot of B(em) vs. T for each measured line is constructed, and assuming the instrumental calibration does not change, a measured value of B(em) will correspond directly to T. Because this technique, like all emission spectrometric methods, involves line-of-sight measurement of B(em), the path length ℓ is defined as the distance within the flame between two points at which the detected radiance is virtually zero. The line or band used must not be overlapped by any other line or band; this requirement necessitates high spectrometer resolving power, since at atmospheric pressure, many lines suffer severe overlapping. As indicated in Appendix B, self-absorption of the lines and concentration and temperature gradients will invalidate the accuracy of the apparent temperature. If

Table A-20

Figures of Merit for Spectrophotometric Techniques

Method	Type of Temp.[a]	Temperature Range (K)	Temperature Precision (K)	Spatial Resolution[b] (mm³)	Temporal Resolution[c] (s)	Sensitivity[d]	Selectivity[e]	Cost[f]	Time[g]	Overall Rating[h] in Flames Laminar	Overall Rating[h] in Flames Turbulent	Overall Rating[h] in Flames Sooty
Absolute Line Radiance												
-Emission	E-El*	≤ 1500	≤ 100	< 1.0-I	cw	H	F	L-M	S-M	F	P	P
-Absorption	E-El*	--	≤ 100	< 1.0-I	cw	H	E	L-M	M	F	P	P
-Fluorescence	E-El*	--	≤ 100	< 1.0	cw	H	E	M	M	F	P	P
Two-line/band Radiance Ratio (emission)	E-El*	≤ 1500	50-200	< 1.0-I	cw	H	F	L-M	L	F	F	P
Boltzmann Slope Method (emission)	E-El*	≤ 1500	≤ 50	< 1.0-I	cw	H	F	L-M	L	F	F	P
Absorption												
-Conventional	E-El*	--	≤ 50	< 1.0-I	10^{-4} cw	H	E	M	L	G	P	F
-Laser Saturated	E-El*	--	?	< 1.0	≤ 10^{-8}	H	E	H	L	G	F	F
PROBE	E-El*	--	?	< 1.0	≤ 10^{-8}	H	E	H-VH	L-H	E	G	G

-- = not applicable

[a]Temperature measured: TR = translational, RA = radiational, E-El = electronic excitation, E-VB = vibrational excitation, E-RT = rotational excitation, E-El* = electronic excitation, vibrational excitation, rotational excitation temperature.

[b]I = inversion methods not needed to obtain radially resolved temperature.

[c]Temporal resolution refers to the time interval in which the measurement can be made, not to the frequency of measurement, cw = continuous wave measurement.

[d]Sensitivity of measurement: H = high, M = moderate, L = low.

[e]Selectivity refers to freedom from spectral interferences: E = excellent, F = fair.

[f]Cost = equipment cost: VH = very high (> $100,000), H = high, M = moderate, L = low, VL = very low (< $10,000).

[g]Time = time to set up system and time for proper operation: L = long, M = moderate, S = short.

[h]Overall rating = capability to provide reproducible, accurate, and precise temperature measurements in laminar, turbulent, and sooty flames: E = excellent, G = good, F = fair, P = poor.

Table A-21
Spectrophotometry Advantages and Disadvantages

Method	Advantages	Disadvantages
Single line/band radiance	i) Applicable to any well-characterized spectral line from any thermometric species (atomic or molecular) ii) No high temperature limit iii) No external source needed	i) Absolute intensity calibration of detection system required ii) A (transition probability) values needed iii) Line-of-sight temperature iv) Susceptible to interferences from overlapping lines or bands v) Temperature and concentration gradients introduce errors vi) Self-absorption errors vii) Temperature must be high enough to detect emission
Two line/band radiance ratio (emission)	i) Same above ii) Applicable to atomic and molecular species emissions iii) Can provide accurate temperature measurements throughout most flames (dependent on thermometric species) iv) No external source needed	i) Line-of-sight temperature ii) Assumes LTE (Boltzmann distribution of excited level population) iii) Sensitive to temperature and concentration gradients errors iv) Need A (transition probability) values or relative ratio v) Sensitivity dependent on excitation energies of emission lines and flame composition vi) Temperature must be high enough to detect emission
Boltzmann slope Method (emission)	i) Same as above ii) Various approaches available to measure molecular rotational temperatures in optically thick flames	i) Same as above ii) Relatively more accurate than two-line method because not as susceptible to small fluctuations from LTE and calibration errors may be less severe

Table A-21 continued

Method	Advantages	Disadvantages
Absorption - Conventional Absorption	i) Applicable to optically thin and thick flames ii) Many thermometric species can be used (dependent on thermometric species) iii) Wide temperature range (dependent on thermometric species) iv) Less sensitive than emission measurements to subtle LTE changes v) Use of laser excitation sources can improve detectability of weak absorption transitions from many species vi) Relatively insensitive to particulate incandescence, scattering fluorescence, and source fluctuations	i) Line-of-sight temperature ii) Measurement of small relative differences (absorption) on large signal (background transmittance) iii) Poor temporal resolution when utilizing curve of growth method iv) Self-absorption and temperature and concentration gradients errors v) Not useful in sharp temperature gradient flames
- Laser saturated Absorption	i) Three-dimensional spatial resolution achieved ii) Same as above	i) Self-absorption errors ii) Temperature profiling tedious iii) Has only been utilized for species concentrations
Profile Resolution Obtained by Excitation (PROBE)	i) Spatially resolved line-of-sight temperatures ii) Insensitive to particulate incandescence, fluorescence, and source fluctuations iii) Absorption not measured, but rather, the temporal distortions in the laser pulses iv) Corresponding weak absorption (from two-photon excitation processes) easily measured from pulse shapes	i) Not yet applied to flames ii) Difficult to experimentally set up and operate

ionization from the upper level j is negligible, and the
flame is assumed to contain only a single species, the
number density in level j can be calculated from the ideal
gas law. However, in practical flame situations, the
assumptions given are not valid.

An alternative approach to absolute measurement of the
line or band radiance is based on the observation that the
number density in the excited state j (and therefore, the
emission intensity) for the particular transition j→i will
increase with increasing temperature until a maximum is
reached at a temperature characteristic for each line. The
temperature at which the maximum intensity is attained is a
result of the balance between the Boltzmann factor on excited
state population density and ionization losses. If the
temperature distribution within the flame ranges higher than
the maximum temperature, the measurement of B(em) can be
made relative to the maximum intensity and not on an abso-
lute basis [371, 372]. Because of overlap difficulties,
this procedure is more applicable to low pressure flames
with high resolution detection of the emission.

b. Two-line ratio method. At LTE, the Boltzmann dis-
tribution describes the populations of the various energy
states at a particular temperature. The two-line (or band)
emission radiance ratio method involves the peak height
emission measurements of two lines or bands of the same
flame species. The general equations for temperature mea-
surement using the two-line ratio methods are given in

Appendix B and can be generally given for an isothermal flame as

$$\ln\left[\frac{g_j A_{ji} \nu_o}{B(em)}\right] - \ln\left[\frac{g_{j'} A_{j'i'} \nu_{o'}}{B'(em)}\right] = \frac{E_j - E_{j'}}{kT} \qquad (85)$$

where

$B(em)$ and $B'(em)$ = spectral radiances measured for transitions $j \to i$ and $j' \to i'$ ($J\ s^{-1}m^{-2}sr^{-1}$),

g_j and $g_{j'}$ = respective statistical weights for the upper levels j and j' (dimensionless),

A_{ji} and $A_{j'i'}$ = Einstein coefficients for spontaneous emission for the transitions $j \to i$ and $j' \to i'$ (s^{-1}),

ν_o and $\nu_{o'}$ = frequencies for transitions $j \to i$ and $j' \to i'$ (Hz),

E_j and $E_{j'}$ = energies of upper levels j and j' with respect to the ground state (J).

For rotational energy levels, $(E_j - E_{j'})$ can be reduced to $N_j(N_j+1) - N_{j'}(N_{j'}+1)$ in which N_j and $N_{j'}$ refer to the rotational quantum numbers for each upper level j and j' [11].

The relative ratio of transition probabilities rather than the absolute values for each transition probability is required. However, the line-ratio method is sensitive to departures from LTE for two significant reasons: i) the validity of the temperature determination is critically dependent on the measurement of the line or band radiances which are particularly sensitive to nonLTE conditions if the upper level energies are approximately the same, and

ii) transitions from nonresonance, <u>thermally</u> assisted energy
levels are generally utilized due to the severe self-absorption
difficulties associated with the use of resonance lines (espe-
cially at the concentrations of introduced thermometric species
needed to <u>detect</u> emission from several lines) [9, 14, 127, 154,
345]. In addition, this method using atomic electronic levels
is generally applicable to isothermal flame zones using Fe
[154, 373-377] and to fuel-rich isothermal flame zones using
Ti [363, 378-380]. Fe can provide excellent flame temperature
measurements since the observed emission spectrum is composed
of many lines ($\gtrsim$ 43 lines at ~ 3100 K) whose transition proba-
bilities are relatively well known [377]. If sufficient emis-
sion lines are detectable at the flame temperature, the
two-line ratio method can be applied if the detection system
is accurately calibrated. With Abel inversion techniques,
temperature distributions can be mapped across the flame
[9, 140] (see Appendix B).

IR band ratio techniques involve the measurement of
integrated band intensities in two separate IR spectral
regions for flames in the 500-2500 K temperature range.
H_2O, CO_2, OH, CH, I_2, and HCl have been utilized as thermo-
metric seeds [381-386]. The only requirement other than
the absence of temperature gradients and self-absorption of
the emitted bands is the need for a strong IR emitter. The
principal advantage of this approach is the potential for
applicability in a wide range of flames and combustors with
capability for remote sensing. Either native IR emitters

can be utilized or the thermometric species, I_2 and HCl, can be introduced into the flame (see Tables A-19 and A-20).

C. Boltzmann Plot or Slope Method

With the measurement of radiances from many lines of an internal energy distribution, a <u>Boltzmann plot</u> can be constructed to determine a slope temperature. Rotational temperatures can be derived from a plot of

$$\ln \left[B_F \lambda / A \ (2N'+1) \right] \ \text{vs.} \ BN'(N'+1) \tag{86}$$

where

B_F = emission radiance for each rotational line
$(J \ s^{-1} m^{-2} sr^{-1})$,

λ = wavelength of each transition (m),

N' = rotational quantum number of the upper state from which each transition originates (dimensionless),

A = rotational transition probability for each transition (s^{-1}),

B = rotational constant $(J \ s^{-2} g^{-1} m^{-3})$, as defined by

$$B = h/8\pi^2 Ic \tag{87}$$

where

I = moment of inertia $(g \ m^2)$,

c = speed of light (m/s).

In general, the plot of

$$\ln[B_F \lambda / gA] \ \text{vs.} \ \Delta E \tag{88}$$

where

ΔE = energy of the upper level from which the transi-
tion arises with respect to the ground state (J).

will result in a corresponding excitation temperature [3, 11].

d. Rotational temperatures. Molecular rotational tem-
peratures from species such as OH, C_2, NH, HF, and CH can be
determined from several methods (listed in Table A-22) [11,
387-391]. Serious errors due to self-absorption of the
emission lines and temperature gradients can produce inaccur-
acies in the slope temperature determination (see Appendix
B). However, the relative accuracy of the method is in-
creased over the two-line ratio accuracy because several
lines can be utilized which may be less susceptible to small
deviations from LTE. The measurement of rotational temper-
atures is especially desirable because the relative transition
probabilities are easily calculable [392-393].

The rotational temperature can also be estimated from
the position of the maximum intensity in a specific branch
of the rotational energy distribution [9, 11]. However,
this approach is quite insensitive to temperature variations
and provides relatively poor accuracy ($\geq$ 25%).

e. Iso-intensity method. In contrast, the iso-
intensity method [9, 323, 393] can be useful when self-
absorption of the emitted lines is particularly severe.
This modification of the Boltzmann plot method, which is

Table A-22
Rotational Temperatures Based on Emission

I.   Maximum intensity position in spectral energy distribution contour.

II. Boltzmann plot (slope temperature).

III. Iso-intensity method.

mainly used for OH, involves the observation for which pair
of differing rotational quantum number rotational lines of
nearly equal frequency, the line radiances are equal. The
iso-intensity method is applicable to nonoverlapping spec-
tral lines which are both equally affected by self-absorption
errors and to molecular bands which possess an intensity
peak. The chosen lines should occur at N' above and below
N'$_{max}$ in the same spectral interval. The results are inde-
pendent of the photographic plate or optical multichannel
analyzer calibration and the background continuum. Even
though the iso-intensity technique does not rely on perhaps
inaccurate quantitative intensity measurements, it does re-
quire a highly dispersive monochromator in order to resolve
the rotational fine structure and does not directly indicate ·
the occurrence of a partial Boltzmann (LTE) distribution [11].

   f. OH rotational temperatures. The monitoring of OH
emission in flames as a rotational temperature indicator has
been known for many years [9, 332, 395-401]. However, sev-
eral observations of anomalous temperature measurements have
been noted primarily in the reaction zone, i.e., straight-
line Boltzmann plots which produce a too high rotational
slope temperature or curved Boltzmann plots with two
straight-line portions near high N' and occasionally near low
N' [11, 12]. The accuracy of the OH emission rotational
temperature is also somewhat dependent on the flame

composition: straight-line plots with an apparent tempera-
ture near the adiabatic equilibrium temperature have been
reported for H_2/air, H_2/O_2, CH_2O/O_2, $CHOOH$/O_2, and moist
CO/O_2 flames, while for other organic-fueled flames, the
results vary drastically. These anomalous, nonthermal
emission temperatures are usually attributed to OH chemi-
luminescence in which OH is formed in an excited electronic
and rotational state following chemical reactions in the
primary reaction zone; i.e., $CH + O_2 \rightarrow CO + OH^*$ [2, 12, 381].
However, OH radicals do appear to deactive electronically
rather efficiently. Thermal Boltzmann plots are expected
above the reaction zone within the interzonal region.
Other molecules which show possibilities as rotational
thermometric species include NH, C_2, CH, NO, and the
Schumann-Runge bands of O_2 [11, 12].

  g. Vibrational temperatures. Boltzmann plots of inte-
grated vibrational band radiance can also be interpreted to
provide vibrational temperatures [11, 397, 402-404]. In
addition, the vibrational temperature can be estimated from
the position of the band's maximum intensity [11]. However,
not only must appropriate vibrational transition probabili-
ties be determined [405-410], but the intensity distribution
throughout specific vibrational bands must be measured in
the presence of severe overlapping from other vibrational
bands. The intensity distribution observed which is in-
duced by the underlying rotational lines is dependent upon

the particular vibrational band within the particular thermometric species and the apparent rotational temperature. With correction for the effective rotational temperature and rotational and vibrational transition probabilies of the individual lines, the vibrational temperature can be determined from a Boltzmann plot of radiances from rotational lines of the same rotational quantum number in several vibrational-rotational bands of the thermometric species [11, 12, 397, 411]. Vibrational temperatures have been deduced using CN, OH, NH, CO, and C_2 [388, 412-415]. However, effective, accurate vibrational temperatures are difficult to obtain due to inaccuracies in the determination of the needed transition probabilities, the actual measurements of the vibrational bands and the specific rotational lines, and problems due to predissociation of molecules of high vibrational and rotational quantum number [11, 416, 417]. In effect, the measurement of apparent vibrational temperatures provides indications of deviations from LTE, particularly in the reaction zone, induced by nonthermal excitation of the thermometric species.

h. Electronic temperatures. Boltzmann plots of electronic transitions in atoms and molecules can be difficult to obtain from emission radiance measurements. The strong lines of many atomic species can be readily observed, but the thermally assisted levels are practically nondetectable in flames in the temperature range of $\leq$ 1500 K to 3000 K [11].

Specifically, Fe is probably the only elemental thermometric species which can be consistently and reproducibly utilized for multiline emission measurements in most flames [127, 363]. In contrast, many molecular species are not appreciably excited to higher electronic levels at flame temperatures. The resulting measurement of the integrated electronic level radiance is severely complicated by vibrational-rotational band overlapping across the broad spectral interval of the molecular electronic emission.

3. Absorption methods

a. Basic equations. Absorption temperature techniques can also be used as well as emission-based methods [417-423]. The relative absorption, α, of continuum source irradiation by flame species within the irradiated flame volume can be described as

i) Low optical density of absorbers [419, 424, 425]:

$$\alpha = \frac{\phi_A}{\phi_o} = \frac{\pi e^2 \ell \lambda_o^2 \, n_i \, B_{ij}}{m \Delta \lambda_s c^2} \tag{89}$$

where

ϕ_A = continuum source irradiance absorbed by the thermometric species ($J \, s^{-1} m^{-2}$),

ϕ_o = incident source irradiance ($erg \, s^{-1} cm^{-2}$),

e = electron charge (esu),

m = electron mass (g),

ℓ = absorption path length (cm),

λ_o = peak wavelength of absorption (cm),

n_i = number density of absorbing species in absorption transition lower level i (cm^{-3}),

B_{ij} = Einstein coefficient of induced absorption for transition i→j (m^3 Hz J^{-1} s^{-1}),

$\Delta\lambda_s$ = monochromator spectral bandpass (cm).

ii) High optical density of absorbers [424, 426-428]:

$$\alpha = \frac{1}{\Delta\lambda_s}\left(\frac{2\pi e^2 \ell \lambda_o^2 n_i B_{ij}\delta\lambda_L}{mc^2}\right)^{1/2} \tag{90}$$

where

$\delta\lambda_L$ = Lorentz (collisional) half-width (cm).

Equation 89 is valid if $\Delta\lambda_s \geq 4 \; \delta\lambda_a$ where

$\delta\lambda_a$ = total half-width of the absorption line (cm).

Equation 90 is generally applicable when $\alpha \gtrsim 0.3$. Otherwise, the monochromator bandpass, $\Delta\lambda_s$, is too narrow to detect the absorption line wings in very high optical density flames [426]. The flame temperature can be determined from the measurement of the integrated absorption coefficient over the total absorption profile, in terms of frequency, $\int\alpha(\nu)d\nu$.

b. Two-line integrated absorption ratio method. The two-line ratio method [419, 429] can be utilized when $\int\alpha(\nu)d\nu$ for two absorption transitions, i.e., a resonance line and an excited state line whose lower level is not

the ground state, have been relatively evaluated [2, 429-431]:

$$\int \alpha(\nu_i) d\nu_i = \frac{h\nu_i}{c} B_{ij} n_i \qquad (91)$$

$$\int \alpha(\nu_{i'}) d\nu_{i'} = \frac{h\nu_{i'}}{c} B_{i'j'} n_{i'} \qquad (92)$$

where

ν_i and $\nu_{i'}$ = frequencies of absorption for the two lines, i and i' (Hz),

B_{ij} and $B_{i'j'}$ = Einstein coefficients of induced absorption (m^3 Hz J^{-1} s^{-1}),

n_i and $n_{i'}$ = number densities in lower levels of lines i and i' (m^{-3}).

The temperatures corresponding to low optical density and high optical density of the absorbing thermometric species can be given by [419, 429]

i) Low optical density:

$$T = \frac{E_i - E_{i'}}{k \ln\left(\left[\frac{g_i B_{ij}}{g_{i'} B_{i'j'}}\right]\left[\frac{\nu_i}{\nu_{i'}}\right]\left[\frac{\int \alpha(\nu_i) d\nu_i}{\int \alpha(\nu_{i'}) d\nu_{i'}}\right]\right)} \qquad (93)$$

where

k = Boltzmann constant (J K^{-1}),

g_i and g_i' = statistical weights of levels corresponding to the transitions i→j and i'→j' (dimensionless).

ii) High optical density:

$$T = \frac{E_i - E_{i'}}{k \ln \left[\frac{g_i B_{ij}}{g_{i'} B_{i'j'}} \frac{\nu_i}{\nu_{i'}} \frac{\int \alpha(\nu) d\nu}{\int \alpha(\nu_{i'}) d\nu_{i'}} \frac{\delta\lambda_L}{\delta\lambda_{L'}} \right]} \tag{94}$$

As can be seen from Equations 93 and 94, it is desirable
to measure absorption at low optical densities and with
continuum source excitation in order to avoid the necessity
of obtaining the ratio of Lorentz half-widths and the exact
profiles of the source emission and the thermometric
species' absorption lines [420, 433, 434]. However, the
$\int \alpha'(\nu_i) d\nu_i / \int \alpha'(\nu_{i'}) d\nu_{i'}$ ratio may be interpreted in terms
of the Lorentz half-widths of each absorption line as [420]

$$\frac{\delta\lambda_L}{\delta\lambda_{L'}} = \frac{\int \alpha'(\nu_i) d\nu_i}{\int \alpha'(\nu_{i'}) d\nu_{i'}} \tag{95}$$

where

$\int \alpha'(\nu_i) d\nu_i$ and $\int \alpha'(\nu_{i'}) d\nu_{i'}$ = integrated absorption

coefficients for each line (ν_i and $\nu_{i'}$) at the

absorber concentration corresponding to the inter-

section of the low and high optical density asymp-

totes of the curve of growth.

With substitution of $\int \alpha'(\nu_i) d\nu_i / \int \alpha'(\nu_{i'}) d\nu_{i'}$ for

$\delta\lambda_L / \Delta\lambda_{L'}$ in Eqn. 94, the resulting temperature expres-
sion (at high optical densities) is identical with Eqn. 93
(at low optical densities). The 451.1 nm and 410.2 nm lines
of In [420] were found to give equivalent temperatures at

low and high In concentrations (without experimentally measuring $\delta\lambda_L$ and $\delta\lambda_{L'}$). However, the necessity for constructing the relevant absorption curves of growth for the thermometric species limits severely the application of absorption temperature measurements at high optical density to turbulent flames where temporally resolved (single-shot) temperature measurements are desired.

Many thermometric species are suitable for use in absorption temperature measurements (under conventional source and laser excitations), particularly In, Ga, Tl, OH, and I_2 [420, 421].

When atomic thermometric species are utilized, the lower energy level of the nonresonance line should be within ~ 1.0 eV of the ground state [416] in order to avoid excitation disequilibrium effects [178, 435, 436]. The greatest sensitivity of the absorption temperature technique is obtained with the accurate measurement of the ratio of two widely-varying absorption lines [420, 430]. The ratio $\alpha_i/\alpha_{i'}$ may be measured precisely when the ratio occurs within the range 1.1 to 5.0 [420]. Therefore, the working temperature ranges of the atomic thermometric species are Ga: 650-2200 K, In: 1220-3500 K, and Tl: 3650-7750 K.

I_2 is a particularly useful absorption thermometric species; I_2 strongly absorbs at wavelengths that other species do not absorb at temperatures which range from room temperature to 1500 K. In addition, I_2 can be utilized as a monitor of rapidly fluctuating temperatures in internal

combustion engines [328, 419]. S and S_2 can also be used for absorption temperatures, but are relatively less inert than I_2 [419]. However, I_2 has been observed to inhibit the propagation (relative flame velocity) of some flames in the primary reaction zone by interfering with certain chain-branching combustion reactions involving H, OH, and O radicals [419, 437].

The apparent flame temperature may be anomalous if self-absorption of the transitions used is occuring and the absorption curve of growth method is not utilized. Under high optical density conditions, when time-resolved absorption measurements are desired, the errors due to self-absorption may be corrected by using small path length burners [48, 51, 418] or by detecting transitions of low absorption probability and lower level population [51]. Since absorption techniques are line-of-sight temperature measurement methods, boundary layer effects are important because of the decrease in species concentration and temperature at the flame edges [354, 419, 420]. In addition, the lower energy levels, including the ground state, of the thermometric species are more insensitive to temperature changes than excited levels which produce thermal emission [2, 419]. Therefore, absorption methods are generally not useful in flames with sharp temperature gradients [419]. In contrast, these methods are especially valuable when the selected emission lines to be used in an emission-based method suffer considerable spectral interference [420, 439]

or in flames whose temperature is below 1500 K and insufficient emission is observed for adequate temperature measurements [419].

The measurement of flame absorption temperatures in flames of low optical density of the thermometric species frequently limits α_i and α_j, to $\gtrsim 0.03$ [420]. Importantly, at these low absorption values, the error in the measured temperature is $\pm 5\%$ ($\pm \approx 120$ K) for low temperature (< 2000 K) flames and $\pm 10\%$ ($\approx \pm 240$ K) for higher temperature flames (< 4000 K). This magnitude of error limits the utility of the absorption technique. However, the utilization of high power lasers as excitation sources can improve the sensitive measurement of absorption from weak absorbers such as NH_3 [440, 441], CO [421], and NO [442].

c. Flash photolysis method. The flash photolysis technique has been utilized for the determination of radical (C_2, CH, CN, NH, C_3, and OH) concentrations on a time-resolved basis ($\gtrsim 1$ ms) [12, 443-446]. Absorption spectra are recorded as a function of time after excitation via a flashlamp background quasi-continuum source. The rise and decay of specific species absorptions can be measured over short (~ 1-10 ms) time intervals. The flash photolysis method is quite sensitive and the resulting absorption spectra could be applied to flame temperature measurements. However, flash photolysis has been primarily utilized in the detonations of acetylene and other hydrocarbons with oxygen and not in stationary-type flames [12].

d. Laser saturated absorption. Laser saturated absorp-
tion techniques could be potentially applied to the measure-
ment of flame temperatures as well as to species
concentrations [447-451]. Three-dimensional spatial
resolution is achieved by the crossing of two laser beams
at large angles. A saturating beam is used to significantly
deplete the population of an atomic or molecular ground
state, while a probing beam of lesser intensity is tuned
generally to the same resonance transition [449]. The
saturating beam perturbs the absorption of the probing beam
within the interaction volume. However, the increase in
spatial resolution ($\gtrsim$ 1 mm^3) relative to the line-of-sight
absorption techniques results in a decrease of spectral
resolution which may not be significant in atmospheric
pressure (and higher pressure) flames. The ratio of the
absorptions of the probe beam with and without the saturating
beam perturbation is directly related to the ground state
(or any energetically low-lying level) population. There-
fore, as determined via conventional source excitation, the
ratio of the relative absorptions (see Eqn. 89) for the two
absorption transitions (performed on a sequential time basis)
could provide an estimated flame temperature which is insensi-
tive to particulate incandescence, scattering, and laser
power fluctuations [449].

e. PROBE method. The Profile Resolution Obtained by Excitation (PROBE) technique may also provide spatially resolved line-of-sight flame temperatures [452]. Two counter-propagating laser beams are collinearly directed through the flame such that the pump beam is tuned to an absorption transition, while the probe beam is tuned to a transition which originates from the resonantly excited state. The probe pulse will suffer absorption proportional to the ground state density at the location where the probe and pump pulses overlap on a temporal and spatial basis. If the pump pulse saturates the resonance transition, the degree of attenuation of the probe pulse will be independent of the pump pulse's temporal and spatial characteristics. The ground state density of the thermometric species could be determined from the relative amplitude of a series of laser probe pulses or from the shape and depth of attenuation created in one temporally large probe pulse [1, 452].

Even though PROBE has not yet been applied to flames, the flame excitation temperature could be obtained from the ratio of the ground state number density of the thermometric species to the excited state number density [1]. In addition, the sensitivity and versatility of the PROBE technique allows the measurement of excited state populations via two-photon excitation processes [452].

4. Elastic (Rayleigh) scattering method

The elastic scattering of light from gas molecules at the same wavelength as the incident source wavelength is termed Rayleigh scattering [453-455]. However, the utilization of Rayleigh scattering methods for temperature measurements has been limited to very clean flames because Mie scattering from particulates and spurious laser light are serious interferences and Rayleigh scattering results in a lack of molecular specificity [7, 455]. In contrast, the Rayleigh cross section (and therefore, the sensitivity) is 1000 times greater than the vibrational Raman cross section (see Table A-22) [7, 456, 457]. Rayleigh scattering is mainly used for total density measurements [459, 460], but translational temperatures can be determined via the measurement of the Doppler-broadened line width of the scattering radiation with a Fabry-Perot interferometer [50, 458, 461]. Generally, a frequency stabilized, single mode Ar^+ laser is utilized [461]. The Doppler broadening of the incident light is due to three factors: gas flow turbulence, Brillouin scattering from laser induced density waves, and primarily, kinetic effects due to molecular thermal motion [11, 461]. Brillouin scattering may be particularly significant when probing the precombustion and reaction zones [50]. The scattering line profile is dependent on the molecular weight of the scattering species (and therefore, the flame composition) but is not susceptible to collision broadening and quenching losses. Rayleigh scattering has

Table A-22
Scattering Cross Section Values*

Scattering Process	Differential Cross Section (cm^2/sr)
Rayleigh scattering -N_2 (488 nm)	10^{-27}
Mie scattering - 1.0 μm particles - 0.1 μm particles	10^{-7} 10^{-13}
Atomic Fluorescence - strong, visible λ	10^{-13}-10^{-18}
Molecular Fluorescence - simple molecules, radicals	10^{-19}-10^{-24}
Rotational Raman scattering - N_2	6×10^{-31}-10^{-29}
Vibrational Raman scattering - N_2, Stokes Q branch (488 nm)	5×10^{-31}

*from Ref. 456.

been utilized to map the translational temperature and total
density profiles throughout an H_2/air flame [461]. In addi-
tion, the resultant temperature measurements were made on a
point (spatially resolved) basis. However, the sensitivity
of this approach is relatively poor due to the square root
dependence of the scattering line width on temperature
[11, 346]:

$$I(\nu) = K \sum_i \mu_i \frac{d\Omega_{R_i}}{d\Omega} \, f_i(\nu) \, n_T \, \ell \, \Omega \, I \qquad (96)$$

where

$I(\nu)$ = spectral scattering intensity ($J \, m^{-2} s^{-1}$),

I = incident laser intensity ($J \, m^{-2} s^{-1}$),

μ_i = mole fraction of scattering species i
(dimensionless),

$\dfrac{d\Omega_{R_i}}{d\Omega}$ = molecular Rayleigh scattering differential
cross section for species i (cm^2/sr),

$f_i(\nu)$ = fractional molecular (Doppler) velocity distri-
bution for species i (dimensionless),

ℓ = path length (cm),

K = calibration constant for the collection optics
(dimensionless),

n_T = total number density of scattering species (cm^{-3}),

Ω = solid angle of collection optics (sr)

where the Doppler velocity distribution for species i is
given by:

$$f_i(v) = f'n \left(\frac{m_i}{2\pi kT}\right)^{1/2} \exp\left(\frac{-m_i v^2}{2kT}\right) \tag{97}$$

where

$f'n$ = function of,

m_i = mass of species i (g),

T = translational temperature (K).

In addition, the Rayleigh scattering intensity can be directly related to the incident laser intensity via the Rayleigh scattering cross section [50, 462]:

$$I(v) = K \, I \, \Omega \, \ell \, \sum_i n_i \, \frac{d\Omega_{R_i}}{d\Omega} \tag{98}$$

where

I = incident laser intensity (J s^{-1} m^{-2}),

Ω = solid angle of the collection optics (sr),

ℓ = laser path length (cm),

n_i = molecular number density of species i (cm^{-3}),

$\dfrac{d\Omega_{R_I}}{d\Omega}$ = differential Rayleigh cross section at 90° from incident light for species i (cm^2/sr),

K = calibration constant (dimensionless).

The ideal gas equation can be used to relate the number density of molecular species to the gas pressure and the absolute translational temperature. Therefore, if the Rayleigh scattering cross section for the flame species can be assumed to be constant, the translational temperature can be determined from knowledge of the flame compositional

gradients throughout the flame [50, 462]. Particularly with premixed flames, the variations in Rayleigh scattering intensities (normalized to incident laser intensity) are primarily due to temperature changes [50]. The Rayleigh cross section can be evaluated as a function of the extent of chemical reaction occuring within the flame.

Utilizing this approach, time-resolved, nonintrusive, laser Rayleigh temperature measurements have been determined in premixed, laminar and turbulent flames [50, 463-465] as well as in turbulent, jet diffusion flames [460, 467]. Mie scattering from soot which is not a function of temperature is a major interference. Therefore, careful selection of the investigated flame composition is needed to avoid complications from severe particulate formation processes. Certain photon counting methods can begin to discriminate against Mie scattering and spurious light detection [50, 466]. In addition, high resolution monochromators, multipass cells, and intracavity laser arrangements have reduced the detection of background flame luminescence which may be ~ 15% of the Rayleigh intensity [467, 468]. In effect, Rayleigh scattering is applicable to flame temperature measurements only in very clean (soot-free) flames.

5. Inelastic scattering methods

a. Spontaneous Raman scattering. Raman scattering is the instantaneous ($\leq 10^{-12}$ s) inelastic scattering of light from molecules [7, 469]. The Raman effect is produced from

the induction of oscillating molecular dipoles by the laser
beam electric field interaction with the molecular polari-
zabilities at the various rotational and vibrational fre-
quencies [456]. Raman shifts corresponding to the molecular
vibrational and rotational frequencies (internal energy
distribution) produce sidebands which are displaced from
the incident laser beam frequency [456, 457]. The Raman
spectrum therefore occurs at a fixed frequency separation
from the laser line which is characteristic of the scatter-
ing molecular species. Because Raman spectroscopy is rela-
tively stronger at shorter laser wavelengths, e.g., the
Raman scattering intensity varies with $1/\lambda 4$, lasers which
produce UV-visible light (Ar$^+$ laser at 488.0 nm line) are
more advantageously utilized. In addition, the spontaneous
Raman scattering cross section is very small ($\approx 10^{-30}$ cm^2/sr)
(see Table A-22) which results in low signal-to-noise ratio
collected intensity. In effect, Raman scattering is not
only species-specific, but can be produced from many dominant
(> 0.001 mole fraction) molecular flame species; i.e., N_2
[48, 470-482], O_2 [471, 472, 474, 478, 480, 483, 484], H_2
[473, 474, 480, 484], CO [474, 483, 484], CO_2 [472, 474, 477,
484-486], H_2O [472, 474, 484, 485], CH_4 [474, 486], C_2H_2 [474],
C_3H_8 [487], and NO [478]. In addition, the Raman scattering
intensity is linearly dependent on the molecular number den-
sity and can be measured on a spatially and temporally
resolved basis [50, 474, 488-491] (see Fig. A-3).

Figure A-3. Generalized energy level diagrams depicting the basis for Raman scattering, CARS, and laser excited fluorescence spectroscopy. Real atomic or molecular energy levels are indicated by solid lines. Virtual levels are indicated by dashed lines. The heavy arrows indicate incident laser pumping transitions, while the thin arrows indicate scattering or emission transitions.
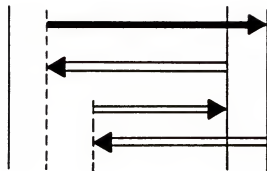
FLUORESCENCE

RAMAN SCATTERING

CARS
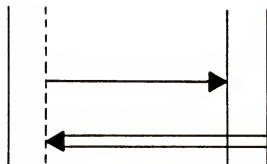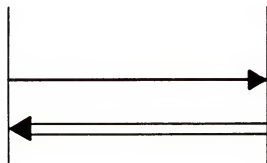
Table A-23
Figures of Merit for Scattering Processes

Method	Type of Temp. [a]	Temperature Range (K)	Temperature Precision (K)	Spatial Resolution [b] (mm³)	Temporal Resolution [c] (s)	Sensitivity [d]	Selectivity [e]	Cost [f]	Time [g]	Overall Rating [h] in Flames Laminar	Turbulent	Sooty
Rayleigh Scattering	TR	--	100-200	< 0.1	$\leq 10^{-8}$	M	F	H	M-L	F	P	P
Raman Scattering	E-VB E-RT	--	50-100	< 0.1	$\leq 10^{-8}$-cw	L	E	H	M-L	G	G	P
CARS	E-VB E-RT	--	50-100	< 0.1	$\leq 10^{-8}$	M	E	VH	L	E	E	E
Stimulated Raman Gain/Loss Spectroscopy	E-VB E-RT	--	?	< 0.1	$\leq 10^{-8}$	M	E	VH	L	F	F	F

-- = not applicable

[a] Temperature measured: TR = translational, RA = radiational, E-El = electronic excitation, E-VB = vibrational excitation, E-RT = rotational excitation, E-El = electronic excitation, vibrational excitation or rotational excitation temperature.

[b] Inversion methods not needed to obtain radially resolved temperature.

[c] Temporal resolution refers to the time interval in which the measurement can be made, not to the frequency of measurement, cw = continuous wave measurement.

[d] Sensitivity of measurement: H = high, M = moderate, L = low.

[e] Selectivity refers to freedom from spectral interferences: E = excellent, F = fair.

[f] Cost = equipment cost: VH = very high (> $100,000), H = high, M = moderate, L = low, VL = very low (< $10,000).

[g] Time = time to set up system and time for proper operation: L = long, M = moderate, S = short.

[h] Overall rating = capability to provide reproducible, accurate, and precise temperature measurements in laminar, turbulent, and sooty flames: E = excellent, G = good, F = fair, P = poor.

Table A-24
Advantages and Disadvantages of
Scattering Techniques

Method	Advantages	Disadvantages
Rayleigh Scattering	i) Translational temperature obtained ii) Stronger signals than Raman scattering iii) Relatively simple to implement iv) Measures scattering from native flame species v) Temporally and spatially resolved temperatures	i) Temperature measured from Doppler-broadened line width-poor sensitivity to temperature fluctuations ii) No species specificity iii) Mie scattering, spurious laser light, and fluorescence serious interferences
Spontaneous Raman Scattering*	i) Species-specific measurements ii) Raman scattering obtainable from many flame species iii) Not susceptible to quenching and collisional broadening effects iv) Single-pulse Raman spectra obtainable v) Relatively simple to perform vi) Point and tomographic measurements obtainable	i) Low signal-to-noise ratio collected intensities ii) Severe interferences from neighboring Raman signals, background fluorescence, and laser induced particulate incandescence and luminescence
Coherent Anti-Stokes Raman Scattering (CARS)**	i) Very intense anti-Stokes Raman signals ii) Very high collection efficiencies iii) Not sensitive to fluorescence spectral interferences iv) Single-pulse temperature measurements	i) Extremely difficult to implement ii) Best for majority flame species iii) Extensive data anlysis required iv) Background CARS signals potentially serious interference

*See Table A-25.

**See Table A-26.

Table A-24 continued

Method	Advantages	Disadvantages
Stimulated Raman Gain/loss Spectroscopy	i) Spontaneous Raman spectrum obtained ii) High background fluorescence not serious interference iii) Single-pulse temperature could potentially be obtained	i) Generated from only certain scattering species ii) Need very high pressure flames and intense excitation iii) Small signals (relative gain or loss measured)

b. Near-resonant Raman scattering. Near-resonant Raman scattering in which the incident laser is tuned close to a molecular electronic resonance transition [7, 492] can be used to increase the effective Raman scattering cross section by up to six orders of magnitude. However, most flame majority species, e.g., N_2, O_2, CO, and CO_2, can not be excited via near-resonant Raman scattering because they do not possess electronic transitions (> 200.0 nm) accessible to laser excitation [7]. In contrast, molecular species such as NO_2 and I_2 [7, 493-495] can be near-resonantly enhanced (if the resolution of very narrow Raman lines can be accomplished).

Therefore, flame temperature measurements can be deduced from the Raman spectrum of a particular species because the resulting spectral intensity distribution is directly related to the rotational and vibrational "population" temperatures. In effect, flame temperatures (see Tables A-23 and A-24) from Raman scattering spectroscopy can be determined from spectral band contours [473, 493, 496], peak height ratios [474, 484, 486, 497, 498], and peak height shifts [7, 499].

c. Rotational Raman methods. Rotational Raman techniques can be difficult to use for flame thermometry due to the possible occurrence of overlapping rotational lines [6, 7, 11, 50] because of the small rotational Raman shifts ($\sim$ 10-100 cm^{-1} from the laser line) and to the presence of rotational Raman lines from many molecular species within

the same spectral range (spectral interference) [499].
However, stronger Raman signals may be detected from rota-
tional Raman lines relative to vibrational Raman lines due
to the relatively larger Raman cross section (see Table A-22)
[456].

Rotational Raman interferometry [500-506] can be util-
ized to scan the entire rotational Raman spectrum with the
highest discrimination and resolution. The Fabry-Perot
interferogram is produced by scanning the interferometer in
the spectral regions where the free spectral range (4B) is
equal to the spectral period (or an odd integral submultiple)
between adjacent rotational Raman lines [504]. At this con-
dition, all the Raman lines are transmitted while the Ray-
leigh scattering line is not transmitted [503]. As the free
spectral range deviates from this condition, alternating
Raman and Rayleigh lines are transmitted. The interferogram
profile is sensitively dependent on the flame temperature
and the inherent multiplex advantage results in large abso-
lute detected signals [503]. With computer simulation of
the interferogram fringe profile, the rotational flame temp-
erature could be determined [504] from the ratio of the Raman
irradiances of a Stokes rotational line to an anti-Stokes
rotational line of the same rotational quantum number:

$$T = \frac{4B(N_i + \frac{3}{2})hc/k}{\ln\left[\frac{E_s(N_i)}{E_{AS}(N_i)} \frac{\omega_o + \omega(N_i)}{\omega_o - \omega(N_o)}\right]^4} \qquad (99)$$

where

$$E_S(N_i) \text{ and } E_{AS}(N_i) = \text{Stokes and anti-Stokes irradiances} \\ (J \ m^{-2} \ s^{-1}),$$

$$B = \text{rotational constant } (m^{-1}),$$

$$N_i = \text{rotational quantum number of ith} \\ \text{level (dimensionless)},$$

$$\omega_o = \text{frequency of incident laser line} \\ (cm^{-1}),$$

$$\omega(N_i) = \text{frequency shift of Nth rotational} \\ \text{Raman line from } \omega_o \ (cm^{-1}).$$

The interferogramic method could provide single-pulse temp-
erature measurements while providing insensitivity to laser
power fluctuations and variations in the number density of
the thermometric species.

The peak height ratio method can also be used from con-
ventional measurement of selected rotational lines (Stokes
and anti-Stokes) which originate from the same initial state
(same rotational quantum number) so that a Boltzmann distribu-
tion for all rotational Raman lines is not required [473, 499,
506]. If rotational lines are used which vary in rotational
quantum number, it is important to select lines from low to
high rotational quantum number in order to maximize the
energy difference between the lines and thus the sensitivity
of the technique (see section C) [499]. The temperature eval-
uated from the Boltzmann distribution of rotational Raman
lines is especially reliable below 2000 K.

d. Vibrational Raman methods. Rotational Raman scat-
tering is ~ 10 times stronger than vibrational Raman
scattering. However, vibrational Raman scattering does not,
in general, possess as serious spectral interferences due to
overlapping vibrational-rotational lines, since the vibra-
tional Raman shift is ~ 1000 cm^{-1} [6, 11, 499]. The poten-
tial temperature methods include comparison of the Stokes
band profile with the computer generated profile (spectral
band contour method)[499], the determination of the Stokes
intensity ratios for resonance transitions from the vibra-
tionally excited states [6, 7, 497-499], and the Stokes to
anti-Stokes peak intensity ratio [6, 499]. Vibrational
Raman interferometry could also be performed [504, 507].

e. Evaluation of Raman scattering methods. The major
interferences to accurate flame temperature measurements by
Raman scattering are listed in Table A-25. Raman spectral
interferences may originate from similar Raman processes at
nearly the same vibrational frequency involving an interfer-
ing molecular species and which occurs at both the Stokes
and anti-Stokes frequencies [7]. Generally, with appropriate
selection of the thermometric species, this problem may be
minimized. Fluorescence interferences [472, 485, 508] may
occur when other flame species are excited by the laser
irradiation or via chemiluminescence and subsequently emit
at the same Raman frequencies [7]. For the OH radical,
Raman interferences from H_2O may be present while

Table A-25
Advantages and Disadvantages of Spontaneous
Raman Scattering Techniques*

I. Advantages

    A. Most flame majority species can provide spontaneous Raman spectra.

    B. In nonluminous laminar flames, Raman scattering is relatively simple to apply to temperature measurements of relatively high accuracy.

    C. Accurate, single-pulse temperature measurements can be achieved even in turbulent flames and combustors.

    D. Tomographic determinations of flame temperatures can be determined.

    E. Nonintrusive, local, and temporally resolved temperatures can be measured.

    F. Experimental operation is relatively simple.

II. Disadvantages

    A. Background luminescence and laser induced particulate fluorescence can be severe interferences.

    B. Laser-modulated particulate incandescence in which the already incandescent soot particles absorb the incident light and subsequently emit significant blackbody radiation can be a particularly severe interference.

    C. Rotational Raman scattering possesses larger signal strengths than vibrational Raman scattering, but due to small rotational Raman shifts, interferences from Rayleigh scattering of major flame constituents and Mie particulate scattering may provide limited applicability of rotational Raman scattering to flame diagnostics.

    D. Feasible for only majority (> 0.1%) flame species.

    E. Low Raman signal-to-noise ratios in flames and the use of signal averaging techniques generally not desirable.

    F. Limited applicability to turbulent and sooty flames.

*from Ref. 7.

fluorescence interferences may occur at the Stokes frequencies from CN and at the anti-Stokes frequencies from CH_2O. Background flame luminescence and laser modulated particle incandescence may arise from the appearance of a graybody continuum due to soot and other particulates in hydrocarbon-fueled flames [7, 509, 510]. In addition, these interferences are typically in phase temporally with the laser pulse and are not easily minimized [7]. If spectrally well-shifted Raman lines are evaluated, complications due to Raman scattering, Mie scattering, and spurious stray light at the incident laser frequency can be avoided.

An evaluation of the practical application of Raman scattering is compiled in Table A-24. Temperature measurements by Raman scattering techniques are feasible in "clean" flames, exhausts, and combustors where the concentration of particulates is relatively low [7]. One significant advantage of Raman scattering methods is the capability to readily measure the concentrations of majority flame species.

Pulsed lasers can be employed to yield spatially and temporally resolved flame temperatures as well as to discriminate against natural flame emission. Signal averaging techniques [7, 511] may increase the Raman signal-to-noise ratios by averaging out shot noise fluctuations in stationary, laminar flames. However, signal averaging in temporally fluctuating, turbulent flames may produce ambiguous flame temperature measurements [7]. Therefore, single-pulse temperature measurements in "clean" flames from certain majority flame species, e.g., N_2, can provide the most accurate results.

f. Coherent anti-Stokes Raman scattering method. Coherent anti-Stokes Raman scattering (CARS) is a nonlinear optical technique in which two incident laser pump beams at frequencies ω_1 and ω_2 (the Stokes beam) interact through the third order nonlinear susceptibility χ $(-\omega_3, \omega_1, \omega_1, -\omega_2)$ to generate a coherent beam at frequency $\omega_3 = 2\omega_1 - \omega_2$ (the anti-Stokes beam)[7, 512, 513]. The intensity of the CARS probe beam depends upon the presence of molecular resonance transitions (Raman vibrational modes) near the frequency $\omega_1 - \omega_2$. A CARS spectrum is produced by varying ω_2 to scan the molecular resonances and by recording the CARS intensity as a function of $\omega_1 - \omega_2$ [512-519] (see Fig A-3).

The CARS signal is at least 1000 times greater than spontaneous Raman scattering. The high conversion efficiency of CARS is strongly dependent upon the presence of a Raman active resonance frequency, ω_j, very close to $\omega_1 - \omega_2$, the incident laser intensities, the resonance line width, Γ_j, and the concentration of the Raman active species, n_j. The CARS intensity can be expressed as [7]

$$\Phi_3 = \frac{4\pi^2 \omega_3^2}{c^2} I_1^2 \Phi_2 |\chi|^2 z^2 \qquad (100)$$

where

I_1 = intensity at frequency ω_1 (J m^{-2} s^{-1}),

Φ_2 = flux at frequency ω_2 (J s^{-1}),

Φ_3 = flux of CARS beam at frequency ω_3 (J s^{-1}),

χ = third order nonlinear susceptibility (m^3 J^{-1}),

z = coherence path length over which the phase-matched interaction occurs (m).

The nonlinear resonant susceptibility can be given for species i as [7]

$$\chi = K_j \frac{\Gamma_j}{2\Delta\omega_j - i\Gamma_j} \qquad (101)$$

and

$$K_j = \frac{2c^4}{\hbar\omega_2^4} n_i \Delta_j g_j \left(\frac{\partial\sigma}{\partial\Omega}\right)_i \frac{1}{\Gamma_j} \qquad (102)$$

where

$$\Delta\omega_j = \omega_j - (\omega_1 - \omega_2), \qquad (103)$$

$\Delta\omega_j$ = detuning frequency from the Raman active frequency ω_j (Hz),

Γ_j = Raman line width of the transition j (Hz),

n_i = number density of scattering species i (m^{-3}),

Δ_j = population difference between the levels involved in the Raman transition j (dimensionless),

g_j = statistical weight of upper level of the Raman transition j (dimensionless),

$\left(\frac{\partial\sigma}{\partial\Omega}\right)_i$ = differential Raman cross section for species i (m^2 sr^{-1}),

$\hbar$ = Planck's constant divided by 2π (J s).

The term $n_i\Delta_j$ corresponds to the rotational and vibrational temperature of the flame:

$$n_i\Delta_j = n_{v,j} - n_{v+1,j} \qquad (104)$$

where

$n_{v,j}$ = number density of species i populating the
excited level of vibrational quantum number v
Raman transition (m^{-3}),

$n_{v+1,j}$ = number density of species i populating the
excited level of vibrational quantum number
v+1 (m^{-3}),

and

$$(\Delta_j g_j)^2 = (2N+1)^2 \, g_I^2 \, \exp\left(-\frac{2hc}{k} \frac{G(v)}{T_v} + \frac{F_v(N)}{T_r}\right) \quad (105)$$

where

N = rotational quantum number (dimensionless),

g_I = nuclear spin degeneracy (dimensionless),

$G(v)$ = vibrational term constant (cm^{-1}),

$F_v(N)$ = rotational term constant (cm^{-1}),

T_v = vibrational temperature (K),

T_r = rotational temperature (K).

For pure rotational temperatures, the line width is
assumed to be constant for all anti-Stokes lines and the
expression BN(N+1) can be substituted for the term $F_v(N)$
where B is the rotational constant (cm^{-1}).

For most efficient CARS generation, I_1 and Φ_2 should be
on the order of 10^5-10^6 J s^{-1}; the laser beams must be care-
fully matched and aligned such that the three-wave mixing
is properly phased, and the laser line width must be narrower
than the Raman line widths which may be difficult to achieve

Table A-26
CARS Advantages and Disadvantages *

Advantages

1. $> 10^5$ increase in Raman conversion efficiencies for CARS over spontaneous Raman scattering efficiencies.

2. Generation of coherent CARS beam allows highly efficient collection of CARS compared to the collection efficiency of the 4π spontaneous Raman and fluorescence signals.

3. Under narrow band (< 0.20 cm^{-1}) Stokes excitation, spectral isolation of the CARS line (with spectral width generally determined by laser line width) not necessary.

4. Under broadband ($\gtrsim 10$ cm^{-1}) Stokes excitation, large portions of the CARS spectrum can be generated in a single laser shot.

5. The coherent and spectral properties of CARS minimize interferences from laser induced fluorescence and natural emission from flames.

Disadvantages

1. Generation of background signals due to severe nonresonant susceptibility limits detection of trace ($\gtrsim 1$ ppm) scattering species.

2. CARS not useful in strongly absorbing media or where Mie scattering is severe.

3. Difficulty in the scanning of the entire vibrational-rotational spectrum and in highly resolved observation of small Raman shifted lines.

4. CARS signals strongly dependent on laser intensities, number density of scattering species, and laser line widths.

5. Distortions in the CARS spectrum may be produced from neighboring resonances and background signals.

6. Signal averaging not desirable in turbulent flames.

7. System equipment and operation cost very high ($< \$100,000$).

*from Ref. 518.

[520, 521]. Typically, the laser beams are aligned par-
allel or colinear to each other to obtain proper phase
matching, but the result is often an ambiguous spatial
resolution [7, 50, 514-517, 522, 523]. However, very high
spatial resolution ($\gtrsim 1$ mm^3) can be achieved by employing
the BOXCARS geometry [524-531] in which CARS is generated
only at the intersection of the crossed beams. Difficulties
arise from the requirement for strict polarization purity
of the incident beams and only certain Raman modes can be
observed [524]. Folded BOXCARS can provide nonplanar,
crossed-beam phase matching [532], while polarization con-
straints are minimized [531].

Conventionally, the CARS spectrum is generated by util-
izing a narrowband Stokes beam (at ω_2) to scan across the
Raman lines. In addition, this method can provide high
spectral resolution which is limited only by the available
laser line widths [7, 50]. Very intense CARS signals can be
detected without the need for spectral isolation of the in-
dividual lines. However, many laser shots are required to
obtain a complete CARS spectrum which limits this approach
to stationary, laminar flames [519]. In contrast, if a
broadband Stokes source at ω_2 is used, the entire CARS spec-
trum can be generated with each laser pulse [533]. Broadband
CARS can therefore be applied to turbulent flames where
time-resolved temperature measurements are desired, but
weaker CARS signals are produced and the CARS lines need to
be spectrally isolated. In effect, real time temperature

measurements on a single-shot basis can be accomplished if an image detector (optical multichannel analyzer) is utilized [533-535] in conjunction with the broadband CARS approach.

As discussed by Eckbreth et al. [7, 50], CARS can be used as a thermometric method by measuring the rotational or vibrational-rotational temperature from either the rotational population distribution of the Q branch of the scattering species [400, 517, 526-528, 536-539] or from the ratio of the CARS peaks from the ground and first vibrational states [7]. The rotational CARS spectrum is desired over the vibrational-rotational spectrum if the rotational anti-Stokes Raman lines are well separated and the spectral inteferences are less severe between adjacent transitions. The spectrum analysis is therefore simplified [7, 532]. However, the advantages of the above results and the occurrence of larger spontaneous Raman cross sections for rotational CARS relative to vibrational-rotational Raman cross sections are partially offset by the relatively small rotational population differences between levels at flame temperatures [532].

The temperature technique which directly utilizes the Raman population distribution (and the CARS spectrum) can provide great accuracy (25-50 K) and less sensitivity to spectral interferences. However, computer simulation of the CARS spectrum at the apparent flame temperature is often required to confirm the experimental results. The second

temperature method is less accurate at flame temperatures, because the Raman lines corresponding to high rotational quantum number levels from the Q branch of the ground vibrational state interfere with the first vibrational levels. CARS thermometric species (concentration $\gtrsim 0.1\%$) include N_2, H_2, CO, O_2, H_2O, and CO_2 [50]. CARS has been applied to premixed, laminar flames [514-517], laminar diffusion flames [292, 528], highly sooting flames [528, 539], as well as to turbulent flames and combustors [519, 534, 535].

The major interferences (see Table A-26), as with Raman scattering, are due to background luminescence and laser modulated particle incandescence. Generally, the CARS intensity (with pulsed laser excitation) is significantly stronger than these spectral interferences. Other less severe difficulties may include stimulated Raman emission when I_1 is too intense such that the ω_2 transition undergoes gain [7] and turbulence-induced phase mismatching. Additional background signals may be due to nonresonant susceptibility and neighboring resonance contributions which may limit the detectability of certain species occurring at trace levels ($\gtrsim 10$ ppm) [517, 518, 540] by altering the shape of the CARS lines.

g. Stimulated Raman gain/loss spectroscopy. Stimulated Raman gain/loss spectroscopy refers to nonlinear optical techniques in which the pump beam at frequency ω_1 induces gain in the Stokes beam at ω_2 (stimulated Raman

gain) [7, 50, 541-545] or losses in the anti-Stokes probe beam at ω_3 [50, 546-548] via the imaginary part of the third order nonlinear susceptibility (inverse Raman scattering). The real part of the susceptibility is related to the non-linear refractive index of the medium, while the imaginary part of the susceptibility is associated with the Raman transition [518, 549, 550]. Because ω_2 corresponds to or is very close in frequency to a Raman active transition in the scattering species, these nonlinear techniques could be employed for flame temperature measurements. The flame temperature can be calculated from vibrational-rotational Raman line intensities present in the observed <u>spontaneous</u> Raman spectrum [548, 551].

However, stimulated Raman effects appear to be gener-ated from only certain scattering species such as N_2 and H_2 [542, 543, 548]. In addition, the gain or loss is very small ($\sim 10^{-4}$-10^{-5} relative difference) at atmospheric pressure [50]. Stimulated Raman gain/loss spectroscopy can generally be applied only to very high pressure environments (> 100 atm) in which the Raman active thermometric species is under very intense pulsed laser excitation. Under these conditions, broadband pulse lasers may be utilized to obtain single-pulse temperature measurements.

In contrast to CARS generation, no phase-matching of the pump and probe beams are required [50]. Nonresonant susceptibility contributions from the background may also

be less severe. Importantly, stimulated Raman gain/loss spectroscopy offers high background fluorescence rejection capabilities [545].

6. Fluoresence methods

a. Fluorescence processes. Recently, fluorescence diagnostic methods have become widely popular for the measurement of excitation temperatures in flames (see Tables A-27 and A-28)[1, 2, 6, 7, 14, 39, 40-44, 48, 50, 251, 484, 554-562]. Fluorescence is the spontaneous emission of radiation from an upper electronic state of an atomic or molecular species which had been directly excited by the previous absorption of radiation (or electron bombardment and chemical reaction) [1]. Resonance fluorescence occurs when the same upper and lower states are involved in the absorption and emission of radiation. Direct-line fluorescence occurs when only the upper excited state is identical in the radiative excitation and deexcitation processes, while stepwise fluorescence results when different upper levels are involved in the excitation-deexcitation process. Thermally assisted fluorescence (THAF) [40-44] describes the emission of radiation from excited states which had been populated via the collisional redistribution of the radiatively excited level. Other types of fluorescence, such as sensitized and multiphoton fluorescence [2, 4] are unlikely to be of significance in flame diagnostics.

If the excitation energy is greater than the fluorescence energy, the resulting process is termed Stokes

Table A-27

Figures of Merit for Fluorescence Measurements

| Method | Type of Temp.[a] | Temperature | | Spatial Resolution[b] (mm³) | Temporal Resolution[c] (s) | Sensitivity[d] | Selectivity[e] | Cost[f] | Time[g] | Overall Rating[h] in Flames | | |
		Range (K)	Precision (K)							Laminar	Turbulent	Sooty
Two-line Fluorescence												
-Conventional Source Excitation	E-El*	--	25-100	< 1.0	10^{-3}-cw	H	E	L-M	L-M	G	F	P
-Laser Excitation	E-El*	--	25-100	< 1.0	≤ 10^{-6}-cw	H	E	H	L	E	F	P
-Pulsed Laser Excitation	E-El*	--	25-100	< 1.0	≤ 10^{-8}-cw	H	E	H	L	E	F	P
Color Temperature	E-El	≥ 2000	25-100	< 1.0	10^{-3}-cw	H	E	L-M	M	G	F	F
Thermally Assisted Fluorescence	E-El*	≤ 1000	≥ 10	< 1.0	≤ 10^{-8}	H	E	H	L	E	G	P

-- = not applicable

[a] Temperature measured: TR = translational, RA = radiational, E-El = electronic excitation, E-El* = electronic excitation, vibrational excitation or rotational excitation temperature.

[b] I = inversion methods not needed to obtain radially resolved temperature.

[c] Temporal resolution refers to the time interval in which the measurement can be made, not to the frequency of measurement, cw = continuous wave measurement.

[d] Sensitivity of measurement: H = high, M = moderate, L = low.

[e] Selectivity refers to freedom from spectral interferences: E = excellent, F = fair.

[f] Cost = equipment cost: VH = very high (> $100,000), H = high, M = moderate, L = low, VL = very low (< $10,000).

[g] Time = time to set up system and time for proper operation: L = long, M = moderate, S = short.

[h] Overall rating = capability to provide reproducible, accurate, and precise temperature measurements in laminar, turbulent, and sooty flames: E = excellent, G = good, F = fair, P = poor.

Table A-28

Advantages and Disadvantages of Fluorescence

| Method	Advantages	Disadvantages
Two-line Fluorescence		
-Conventional Source Excitation	i) Spatially resolved temperature measurements and profiles with high precision and accuracy	i) Difficult to obtain adequate temporal resolution
	ii) Not susceptible to spectral interferences (if observing nonresonance lines)	ii) Need source spectral irradiance measurements at each observed λ
	iii) Large signal-to-noise ratios	iii) Optical calibration of system required
	iv) Introduced or native flame thermometric species	iv) Flame must be optically thin (self-absorption errors)
	v) Wide temperature range (dependent on thermometric species)	v) Detect only portion of 4π fluorescence generated
	vi) Some methods do not require A (transition probability) values	vi) Best results with Tl-type atomic species
	vii) Relatively simple instrumentation and procedures	
-Laser Excitation (LIF methods)	i) Temporal and spatial resolution (single-shot temperatures achievable)	i) Excitation (linear or saturated) conditions and measurement procedure must be strictly followed
	ii) Fluorescence can be observed from introduced atomic species (Tl, In, Ga, Pb, etc.) and native flame intermediates (OH, NO, etc.)	ii) A (transition probability) values generally required
	iii) Can use time-resolved and time-averaged detection	iii) Susceptible to post-filter effects and scattering interferences at resonance excitation lines
	iv) Saturated fluorescence methods generally provide temperatures independent of quenching corrections	iv) Detect only portion of 4π fluorescence generated
		v) Best results with Tl-type atomic species in atomic fluorescence methods

Table A-28 continued

Method	Advantages	Disadvantages
Color Tempera-ture	i) Null point measurement (at which source color temperature = flame temperature) provides high precision ii) Spatially resolved temperatures through-out the flame	i) Source spectral irradiances at proper wavelengths required ii) Detection system calibration required iii) Limited temperature range
Thermally-Assisted Fluorescence	i) Single-shot local flame temperatures achievable ii) Advantages of slope temperature method: accuracy and precision increased over two-line methods iii) Optimal signal-to-noise ratios observed under saturation conditions iv) Applicable to "quenching" flames and to high quantum efficiency flames v) Simultaneous temperature and trace species concentrations potentially obtained	i) Steady state partial Boltzmann distribu-tion of collisionally excited levels must be achieved ii) Sensitive to nonLTE conditions iii) Susceptible to laser induced particulate incandescence interferences iv) A (transition probability) values re-quired v) Rather elaborate experimental measurement procedures required for single-shot mea-surements vi) Detect only portion of 4π fluorescence generated vii) Best results with Tl-type atom

direct-line fluorescence. If the fluorescence energy is greater than the excitation energy, anti-Stokes direct-line fluorescence occurs. Excited state fluorescence results when the upper and lower energy levels of the fluorescence transition are both excited states. Generally, it is necessary to observe nonresonance fluorescence transitions for the highly accurate determinations of temperature and species concentrations because of the severity of Rayleigh and Mie scattering and stray light (spurious laser scattering) at the incident excitation wavelength (see Fig. A-5).

Like Raman scattering processes, fluorescence involves the inelastic scattering of a photon and is species-specific. However, fluorescence can be many times (10^7-10^5 times greater) more intense than Raman or near-resonant Raman scattering because of the corresponding increase in the fluorescence cross section compared to the Raman cross section [6, 456, 563]. In addition, unlike Raman scattering processes, the fluorescence intensity is susceptible to quenching (collisional deactivation of the excited level population to the ground state), other energy transfer collisional processes including collisional transfer to other excited states within the thermometric species, internal collisional energy transformation to other internal energy distributions within a molecular thermometric species, molecular dissociation, excited state chemical reactions, and collision induced ionization. These energy transfer processes can be designated as "losses" or competitive pathways with respect to the fluorescence

Figure A-4.   Types of fluorescence transitions (the spacing
              between levels is not indicative of any specific
              atom or molecule): a. resonance fluorescence
              (either process), b. excited state resonance
              fluorescence, c. Stokes direct-line fluores-
              cence, d. anti-Stokes direct-line fluores-
              cence, e. Stokes stepwise line fluorescence,
              f. anti-Stokes stepwise line fluorescence,
              g. thermally assisted Stokes (or anti-Stokes)
              fluorescence, and h. two-photon excitation
              fluorescence. The heavy arrows indicate the
              laser pumping transitions, while the thin
              arrows indicate the fluorescence transitions.
              The dashed line arrows represent collision-
              induced transitions. Real energy levels are
              represented by solid lines, while virtual
              levels are indicated by dashed lines.
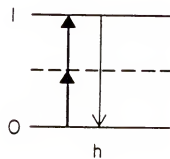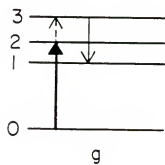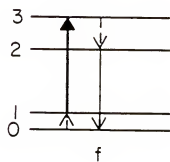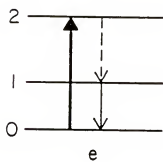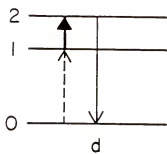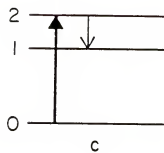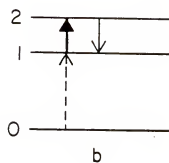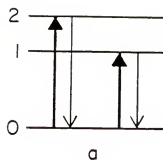
excitation-deexcitation process. Collisional redistribution
of the radiatively excited population reduces the amount of
fluorescence which can be detected from that level (fluo-
rescence quantum efficiency << 1) and can interfere with the
spectral data interpretation. Quenching corrections can be
derived if the flame gas species densities and the rates of
collisional and radiative energy transfer on a per state
basis are known or saturation techniques may be used to
eliminate potentially the need for quenching evaluation
[1, 38, 99].

The fluorescence intensity solutions based on steady
state rate equation approaches have been extensively devel-
oped with respect to source intensity, source bandwidth,
geometry, energy of the levels whose fluorescence is being
observed, and fluorescence to collisional energy transfer
rates [1, 98-112]. In order to eliminate line width decon-
volution difficulties including broadening effects, the use
of continuum source (source bandwidth >> absorption profile
line width) excitation is desired. Self-absorption of the
detected fluorescence must be avoided; this condition there-
fore necessitates the judicious selection of fluorescence
excitation wavelengths, observed fluorescence lines, and the
concentration of the atomic thermometric species which may
be introduced when utilizing atomic fluorescence temperature
methods [1, 2, 89].

b. Temperature measurement approaches. These are essentially two means of measuring flame fluorescence temperatures: an atomic species (Tl, In, Ga, Pb, Fe, etc.) can be introduced into the flame [39, 41, 43, 138, 554-560] or a native flame species (OH, NO, C_2, CH) can be utilized [42, 48, 51, 562, 565-569]. Many elements are amenable to UV-visible excitation and their fluorescence lines are generally widely separated over a broad spectral region. In addition, a variety of atomic fluorescence methods can be utilized for flame temperature measurements. The selective use of certain fluorescence transitions (nonresonance, thermally assisted lines, etc.) can minimize spectral interferences due to the detection of associated emission or fluorescence lines from other flame species as well as scattering and stray light problems associated with resonance fluorescence detection. However, the collisional energy transfer processes vary in extent depending on the observed fluorescence line of each particular thermometric species and the flame quenching characteristics. Correspondingly, the severity of self-absorption will be different for each fluorescence transition and must be determined under experimental conditions since high thermometric seed concentrations (~ 100 ppm) are often introduced into the flame in order to optimize the signal-to-noise ratios of the fluorescence signals. The useful temperature ranges for Ga, In, Tl, and Pb are, respectively, ~ 500-1000 K, ~ 800-1700 K, ~ 1400-3500 K, and ~ 1400-3000 K [39, 570].

Table A-29
Fluorescence Measurement Techniques

I. Conventional Source Excitation Methods

    A. Two-line linear methods.
    B. Boltzmann slope temperature method.
    C. Color temperature method.

II. Laser Induced Fluorescence (LIF) Methods

    A. Two-line linear (fluorescence intensity vs. laser energy) method.
    B. Saturation two level peak method.
    C. Saturation two-line method with sequential pumping.
    D. Saturation two-line method with simultaneous pumping.
    E. Thermally Assisted Fluorescence (THAF) method.

c. Conventional source excitation methods. Observa-
tion of fluorescence can be accomplished via conventional
continuum source excitation (W strip lamp, Xe arc lamp,
quartz iodine lamp, etc.) or via broadband, quasi-continuum
tunable dye laser excitation (CW, pulsed) [1, 2]. Under
conventional source excitation (and generally, under laser
excitation), several fluorescence temperature measurement
methods can be utilized (in the temperature range of 700-
3000 K) and are listed in Table A-29. Typically, as shown
in Fig. 3, a Tl-type atom can be used in which the level
2 → level 1 radiative transition is forbidden; e.g., level
2 is a metastable level and only collisional transitions
are allowed between level 1 and level 2.

i. Two-line ratio method I. The ratio between the
anti-Stokes direct-line fluorescence $(B_{F_{3 \to 1}})$ and the Stokes
direct-line fluorescence $(B_{F_{3 \to 2}})$ upon simultaneous excita-
tions of levels 2→3 and levels 1→3, respectively, can be
given by [39, 555-558]

$$T_I = \frac{5040 \; \Delta E_{12}}{\log\left[\dfrac{B_{F_{3 \to 2}}}{B_{F_{3 \to 1}}}\right] + 6\log\left[\dfrac{\lambda_{23}}{\lambda_{13}}\right] + \log\left[\dfrac{E_\lambda(\lambda_{23})}{E_\lambda(\lambda_{13})}\right]} \quad (106)$$

where

ΔE_{12} = excitation energy with respect to the
ground state of level 1 (J),

$B_{F_{3 \to 2}}$ and $B_{F_{3 \to 1}}$ = fluorescence radiances of the Stokes
and anti-Stokes lines respectively
$(J \; m^{-2} s^{-1} sr^{-1})$,

λ_{23} and λ_{13} = wavelengths of the fluorescence
lines (nm),

$E_\lambda(\lambda_{23})$ and $E_\lambda(\lambda_{13})$ = <u>source</u> spectral irradiances at
each wavelength (J s^{-1} m^{-2} nm^{-1}).

Therefore, the flame temperature can be calculated by this
two-line atomic fluorescence method (TLAF) by measuring the
source spectral irradiances at the excitation wavelengths
and the anti-Stokes and Stokes fluorescence intensities.
The precision (% relative standard deviation, % RSD), for
the measured flame temperature, assuming that the major
source of random error is the measurement of the fluores-
cence intensity ratio, can be stated as [39, 139, 561]

% RSD = (T/5040 $\Delta E_{12}/(\Delta B_F^{\prime}/B_F^{\prime})$ x 100

where

$(\Delta B_F^{\prime}/B_F^{\prime})$ = relative random error in the fluorescence
intensity ratio (dimensionless).

Therefore, for a given $\Delta B_F^{\prime}/B_F^{\prime}$, the relative error in the
temperature will decrease as the energy of the metastable
level 2 increases, ΔE_{12} [39]. Generally, the relative
errors in the temperatures obtained from Ga are too large
for the best diagnostic measurements; e.g., an error of
1% in the fluorescence radiance ratio could result in an
error of ~ 53 K in the temperature measurement, while the
corresponding error from Tl would be ~ 6 K [39].

Below the lowest usable source temperature of 700 K,
there is a large change in the ratio of the source spectral

irradiances, $E_\lambda(\lambda_{23})/E_\lambda(\lambda_{13})$, and therefore a larger change
in $B_{F_{3\to2}}/B_{F_{3\to1}}$ for a small change in the flame temperature.
Also, the anti-Stokes fluorescence line has a very low signal-
to-noise ratio. Above an upper temperature of ~ 3000 K, there
is only a small change in the ratio of the source spectral
irradiances, and so $B_{F_{3\to2}}/B_{F_{3\to1}}$ shows a small change for a
large change in the flame temperature [39]. Therefore,
under conventional low-intensity source excitation, the
random errors increase in the cool flame edges for elements
with large ΔE_{12} excitation energies, such as Tl and Pb, and
in the flame center of hot flames for elements with small
ΔE_{12} values, such as In and Ga [39]. The accurate and pre-
cise measurements of the source spectral irradiances are
difficult to obtain over a wide temperature range; i.e.,
for the best accuracy and precision, the source spectral
irradiance ratio should vary between the values 5 and 50
[570]. Importantly, the significant advantages of the TLAF
method are the increased signal intensities and signal-
to-noise ratios over the corresponding Raman scattering
intensities and even though the source spectral irradiance
ratio must be accurately measured, transition probabilities
(A-values) need not be known. In addition, optical satura-
tion of the excited levels must not occur [4, 98].

 ii. Two-line ratio method II. The fluorescence exci-
tation temperature can also be evaluated from the ratio of
the excited resonance fluorescence radiance $B_{F_{3\to2}}$ (from
excitation of level 3 after thermal excitation of level 2)

to the Stokes direct-line fluorescence radiance $B_{F_{3\to2}}$ (from excitation of levels 1→3) [39]:

$$T_{II} = \frac{5040\ \Delta E_{12}}{\log\left[\dfrac{E_\lambda(\lambda_{23})}{E_\lambda(\lambda_{13})}\right] + 3\log\left[\dfrac{\lambda_{23}}{\lambda_{13}}\right] + \log\left[\dfrac{g_2 f_{23}}{g_1 f_{13}}\right] + \log\left[\dfrac{B_{F_{3\to2}}^{2\to3}}{B_{F_{3\to2}}^{1\to3}}\right]}$$

where

(107)

g_1 and g_2 = statistical weights of levels 1 and 2 respectively (dimensionless),

f_{13} and f_{32} = oscillator strengths for the absorption transitions 1→3 and 2→3 (dimensionless),

$E_\lambda(\lambda_{23})$ and $E_\lambda(\lambda_{13})$ = source spectral irradiances for the excitation transitions 2→3 and 1→3 ($J\ s^{-1}\ m^{-2}\ nm^{-1}$),

λ_{13} and λ_{23} = wavelengths of the fluorescence transitions (nm),

$B_{F_{3\to2}}^{2\to3}$ and $B_{F_{3\to2}}^{1\to3}$ = fluorescence radiances for the transitions: 3→2 (excitation via 2→3) and 3→2 (excitation via 1→3) ($J\ s^{-1}\ m^{-2}\ sr^{-1}$).

The flame excitation temperature can be calculated from this TLAF method if the ratio of the oscillator strengths is known. For many elements, the absolute f-values are known to no better than ~ 5-10%; however, the ratio of the transition probabilities may be more accurately measured [2, 39].

iii. Color temperature method. The color temperature of the flame may be derived from the relation that the ratio of the source spectral irradiances, $E_\lambda(\lambda_{23})/E_\lambda(\lambda_{13})$, corresponds to the blackbody temperature, T_c, since at that temperature, the fluorescence spectral radiance ratio will be equivalent to the source spectral irradiance ratio [39, 554, 571, 572]:

$$\frac{B_{F_{3\to1}}}{B_{F_{3\to2}}} = \frac{E_\lambda(\lambda_{23})}{E_\lambda(\lambda_{13})} \left(\frac{\lambda_{23}}{\lambda_{13}}\right)^5 \exp(-\Delta E_{12}/kT_f) \qquad (108)$$

such that

$$\frac{B_{F_{3\to1}}}{B_{F_{3\to2}}} = \exp\left(\Delta E_{12}(T_c^{-1} - T_f^{-1})/k\right) \qquad (109)$$

where

$B_{F_{3\to1}}$ and $B_{F_{3\to2}}$ = fluorescence radiances for transitions $3\to1$ and $3\to2$, respectively ($J\ s^{-1}\ m^{-2}\ sr^{-1}$),

$E_\lambda(\lambda_{23})$ and $E_\lambda(\lambda_{13})$ = source spectral irradiances for the excitation transitions $2\to3$ and $1\to3$ ($J\ s^{-1}\ m^{-2}\ nm^{-1}$),

λ_{13} and λ_{23} = wavelengths of fluorescence transitions (nm),

T_f = flame temperature (K),

T_c = source color temperature (K).

One advantage of the color temperature method for the measurement of flame temperatures between 2000 K and 3000 K [554] is the ratio $B_{F_{3\rightarrow1}}/B_{F_{3\rightarrow2}}$ may be less than or greater than unity depending on the source color temperature. Therefore, the source color temperatures can be varied until the null point occurs; i.e., $B_{F_{3\rightarrow1}}/B_{F_{3\rightarrow2}}$ is equal to unity and the source color temperature is equal to the flame temperature. The measurement of the null point, as with Na line reversal temperature measurements, can provide quite accurate and precise results ($\lesssim 1\%$) [554]. In addition, the intercept of a plot of $\log(B_{F_{3\rightarrow1}}/B_{F_{3\rightarrow2}})$ vs. T_c^{-1} will produce the flame temperature, T_f.

The relative error in the resulting flame temperature depends on the precise determination of the source color temperature [554]:

$$\frac{\Delta T_c^2}{T_c^2} = \left(\frac{dE_\lambda'}{E_\lambda'}\right)^2 \left(\frac{0.434\ T_c}{5040\ \Delta E_{12}}\right) \tag{110}$$

where

E_λ = source spectral irradiance ratio:
$E_\lambda(\lambda_{23})/E_\lambda(\lambda_{13})$ (dimensionless),

dE_λ' = random error in the source irradiance ratio (dimensionless),

T_c = color temperature (K),

ΔT_c = error in measurement of source color temperature (K).

Therefore, even with an error in the measurement of the source spectral irradiance ratio of ~ 5%, the resulting error in the temperature may be ≳ 1-2% at ~ 2200 K [554]. If the source lamp can be accurately calibrated and the advantages of the null point method can be realized, the resulting accuracy and precision of the color temperature method can possibly be higher than the previous TLAF methods. However, these TLAF temperature techniques enjoy a significant capability to measure excitation flame temperatures over a wide temperature range.

The necessity to accurately calibrate both the detection system and the source for multiwavelength response can be circumvented if the temperature of an experimental, standard flame has been determined accurately by another technique, such as Na line reversal, and if the fluorescence radiance ratios for the "known" and the "unknown" flame can be measured [39]:

$$\log\left[\left(\frac{B_{F_{3\to 1}}}{B_{F_{3\to 2}}}\right)_{T_k} \middle/ \left(\frac{B_{F_{3\to 1}}}{B_{F_{3\to 2}}}\right)_{T_u}\right] = \frac{5040 \; \Delta E_{12}}{T_u} - \frac{5040 \; \Delta E_{12}}{T_k}$$

(111)

where

T_k = temperature of "known" temperature flame (K),

T_u = temperature of "unknown" temperature flame (K).

In effect, atomic fluorescence temperature methods with conventional continuum source excitation are quite versatile

and can be exploited in many experimental situations, typically for temperature measurement in laboratory-type flames. To obtain the most accurate flame temperature determinations, a Tl-type atom should be utilized as the thermometric seed. The fluorescence lines must be easily spectrally isolated from the incident source excitation wavelengths, and the source must provide excitation wavelengths of sufficient intensity to excite the thermometric seed over a wide temperature range. For low temperature ($\gtrsim$ 1500 K) flames, In and Ga can be used with good precision, if the total error in the evaluation of the fluorescence radiance ratio is $\gtrsim$ 5%. Pb can be used to advantage for hotter ($\gtrsim$ 2000 K) flames. However, the Pb resonance line at 280.0 nm can be difficult to excite with low-intensity conventional source irradiation and most importantly, the accurate calibration of the detection system and the source may be difficult to achieve in this spectral region [570].

   d. Laser induced fluorescence methods. Temporally-resolved temperature measurements can not be readily achieved with conventional source fluorescence techniques. However, pulsed (or chopped cw) laser excitation can provide temperature measurements with high temporal resolution (pulse widths from 5 ns to 1 μs) as well as highly intense excitation wavelengths that can produce fluorescence signals of maximal intensity [1, 6, 7, 14]. Temporal resolution can refer to both the signal averaging of many fluorescence pulses produced and detected only during the

laser excitation pulse or to actual single-pulse measurements in which a unique temperature is determined during each laser shot [114].

Several laser-based fluorescence flame temperature methods using atomic thermometric seeds have been developed [1, 40]. Like the conventional source excitation fluorescence methods, most laser-based fluorescence techniques require the measurement of the ratio of the fluorescence radiances resulting from excitation of level 3 in a Tl-type atom (three level model) [1, 4, 7, 98, 99] via levels 1 or 2 [40]. The theoretical basis of these techniques has been extensively developed and will not be repeated here [98-166]. In essence, the detected fluorescence signals are measured under _linear_ (B_F vs. laser irradiance E_ν) conditions or under _saturation_ conditions. Saturation of the laser pumped level presumes such a sufficiently intense source irradiance that the laser spectral irradiance, E_ν ($J\ m^{-2}\ s^{-1}$), is so high that the stimulated radiational excitation-deexcitation rates dominate over the spontaneous emission and collisional rate; i.e., the response time of the system is governed simply by the product of the Einstein coefficient of induced absorption for the excitation transition ($m^3\ Hz\ J^{-1}\ s^{-1}$) and the laser power density. The atomic system may reduce to a pseudo-two level model in which the laser is able to redistribute the population between the two levels. At saturation intensities for a two level system, the fluorescence signal does not depend upon the source irradiance (nor its

fluctuations) nor the fluorescence quantum efficiency of
the transition. In contrast, for the three level (or multi-
level) model used as the basis for most fluorescence temp-
erature diagnostics, at saturation, the fluorescence is
also independent of the source irradiance, but is still
dependent on the collisional coupling ratios among the
energy levels. For accurate fluorescence measurement,
especially in low fluorescence quantum efficiency (quench-
ing) flames, the signal detection system must be able to
resolved temporally the fluorescence pulse from the natural
flame emission on a $\lesssim 10^{-5}$ time scale. A careful evaluation
of the collisional processes occurring within the thermo-
metric seed upon laser irradiation is often required; in
some cases, the transition probabilities for each fluores-
cence transition is needed or the ratio of the transition
probabilities must be determined. In addition, the effect
of the measurement procedure (time-resolved vs. time-
averaged detection of the fluorescence pulse) on the result-
ing apparent flame temperature must be determined if the
laser excitation pulse duration is on the time scale of the
effective lifetimes of the excited states whose fluorescence
is being measured. Steady state fluorescence must be reached
during the laser pulse and a Boltzmann distribution of the
atomic population must be achieved.

     i. Two-line linear method: There are basically five
laser-induced fluorescence (LIF) methods, although other
techniques can be described. The two-line linear method

(see Table A-29) involves the sequential measurement of the anti-Stokes fluorescence for the 3→1 transition (via 2→3 excitation) and the Stokes fluorescence measured under linear fluorescence intensity vs. incident laser energy conditions [40]:

$$T_I = \frac{\Delta E_{12}/kT}{\ln\left[\dfrac{E_\lambda(\lambda_{23})}{E_\lambda(\lambda_{13})}\right] + 6\ln\left[\dfrac{\lambda_{23}}{\lambda_{13}}\right] + \ln\left[\dfrac{B_{F_{\substack{3\to2\\1\to3}}}}{B_{F_{\substack{3\to1\\2\to3}}}}\right]} \qquad (112)$$

where

$E_\lambda(\lambda_{23})$ and $E_\lambda(\lambda_{13})$ = source spectral irradiances for excitation transitions 2→3 and 1→3 ($J\ m^{-2}\ s^{-1}\ nm^{-1}$),

$B_{F_{\substack{3\to2\\2\to3}}}$ and $B_{F_{\substack{3\to1\\2\to3}}}$ = fluorescence radiances for transitions 3→2 (excitation via 1→3) and 3→1 (excitation via 2→3) ($J\ m^{-2}\ s^{-1}\ sr^{-1}$),

λ_{13} and λ_{23} = wavelengths of the transitions 1→3 and 2→3 (nm),

ΔE_{12} = excitation of level 2 with respect to the ground state (J).

This LIF method, like the conventional source two-line method I, requires the accurate calibration of linear fluorescence signals which results in lower fluorescence signal strengths than those obtained under saturated conditions. Possible systematic errors due to post-filter effects at 3→1 detection

may be introduced into the temperature determination. However, the accurate measurement of T_I is independent of non-radiative (collisional) and radiative rate constants; i.e., no assumptions are needed to obtain T_I.

  ii. Saturation two level peak method: The saturation two level peak method requires the sequential temporal resolution of the fluorescence pulses at the pseudo-two level steady state value [40] which is governed by the pumping time of the system $(B_{13}E_\nu(\nu_{13})/c \sim B_{31}E_\nu(\nu_{13})/c \gg$ spontaneous emission and collision induced rates, where B_{13} = Einstein coefficient of induced absorption for $1\rightarrow3$ (m^3 Hz J^{-1} s^{-1}), B_{31} = Einstein coefficient of induced emission for $3\rightarrow1$ (m^3 Hz J^{-1} s^{-1}), $E_\nu(\nu_{13})$ = source spectral irradiance (J s^{-1} m^{-2} Hz). The fluorescence radiances are measured prior to the system relaxation to its three (or more) level steady state population distribution which is controlled by the collisional and radiative rates during the laser pulse. The LIF temperature can be given by

$$T_{II} = \frac{\Delta E_{12}/k}{\ln\left[\left(\dfrac{g_1+g_3}{g_2+g_3}\right)\left(\dfrac{g_2}{g_1}\right)\right] + \ln\left[\dfrac{B_{F_{\substack{3\rightarrow1\\1\rightarrow3}}}}{B_{F_{\substack{3\rightarrow1\\2\rightarrow3}}}}\right]} \qquad (113)$$

where

    g_1, g_2, and g_3 = statistical weights of each energy
             level (dimensionless),

    $B_{F_{\substack{3\rightarrow1\\1\rightarrow3}}}$ = resonance fluorescence radiance for
            transition $3\rightarrow1$ (excitation via $1\rightarrow3$)
            (J m^{-2} s^{-1} sr^{-1}),

$B_{F_{\substack{3\to1\\2\to3}}}$ = anti-Stokes fluorescence radiance for transition $3\to1$ (excitation via $2\to3$) J m^{-2} s^{-1} sr^{-1}).

The measurement of T_{II} is independent of the transition probabilities and maximal fluorescence intensities can be observed. However, the two excitation wavelength laser pulses must be spatially homogeneous, possess the same cross sectional area, and be optically aligned to probe the same flame volume. In addition, Mie and Rayleigh scattering may be severe at the resonance $3\to1$ fluorescence line and post-filter effects may also occur [1, 40]. Most importantly, full saturation of the excited levels and temporally resolved detection of the two level peak fluorescence must be achieved for each transition.

    iii. Saturation two-line method with sequential pumping: This saturation sequential pumping LIF method [1, 40] refers to the sequential two-step excitation of the thermometric seed and the subsequent measurement of the fluorescence radiances at $3\to1$ or $3\to2$ after the system has relaxed to its three level state:

$$T_{III} = \frac{\Delta E_{12}/k}{\ln\left\{\left[\dfrac{2+\dfrac{A_{32}+k_{32}}{k_{21}}}{\frac{1}{2}\left(2+\dfrac{A_{31}+k_{31}}{k_{21}}\right)}\right]\left(\dfrac{\nu_{3j}A_{3j}}{\nu_{3i}A_{3i}}\right)\left(\dfrac{B_{F_{\substack{1\to3\\3\to1}}}}{B_{F_{\substack{3\to j\\2\to3}}}}\right) - 3\left(\dfrac{2}{2+\dfrac{A_{31}+k_{31}}{k_{21}}}\right)\right\}}$$

$$(113)$$

where

i and j = levels 1 or 2,

ν_{3j} = frequency of fluorescence line for transition from level 3→j (Hz),

ν_{3i} = frequency of fluorescence line for transition from level 3→i (Hz),

A_{3i} and A_{3j} = Einstein coefficients of spontaneous emission for transitions 3→i and 3→j (s^{-1}),

$B_{F_{3 \to i}}$ and $B_{F_{3 \to j}}$ = fluorescence radiances from transi-
$\phantom{B_{F}}_{1 \to 3}$ $\phantom{B_{F}}_{2 \to 3}$ tions 3→i (excitation via 1→3) and 3→j (excitation via 2→3) ($J\ s^{-1}\ m^{-2}\ sr^{-1}$).

k_{32}, k_{31} and k_{21} = collisional rate constants for tran-
sitions 3→2, 3→1, and 2→1 respectively.

The measurement of T_{III} is dependent on the accurate knowledge of the fluorescence transition probabilities and the attainment of three level steady state fluorescences upon sequential excitation (within ~ 1 ns) of level 3 from levels 1 and 2. If $k_{21} \gg (A_{31} + k_{31}) \approx (A_{32} + k_{32})$, then elimination of the rate constant terms, i.e., k_{31}, k_{32}, k_{21}, A_{31}, etc., within the temperature expression occurs. Post-filter and scattering effects must be minimized, while spatial filtering of the laser beams is critical.

iv. Saturation two-line method with simultaneous pumping: The LIF flame temperature can be evaluated

from the detection of resonance fluorescence for the $3 \rightarrow 1$ transition (resulting from simultaneous excitation of $1 \rightarrow 3$ and $2 \rightarrow 3$) and the fluorescence (either $3 \rightarrow 1$ or $3 \rightarrow 2$) resulting from pumping $1 \rightarrow 3$ or $2 \rightarrow 3$ as [1, 40]

$$T_{IV} = \frac{\Delta E_{12}/k}{\ln \left\{ 4 \left(\frac{{}^B F_{3 \rightarrow 1} \atop < {1 \rightarrow 3 \atop 2 \rightarrow 3} >}{{}^B F_{3 \rightarrow 1} \atop 2 \rightarrow 3} - \frac{3}{4} \right) \left[\frac{1}{1 + \frac{1}{2} \left(\frac{A_{31} + k_{31}}{k_{21}} \right)} \right] \right\}}$$

where

$\quad {}^B F_{3 \rightarrow 1} \atop < {1 \rightarrow 3 \atop 2 \rightarrow 3} >$ = fluorescence radiance resulting from the simultaneous pumping of level 3 from levels 1 and 2 ($J\ m^{-2}\ s^{-1}\ sr^{-1}$),

$\quad {}^B F_{3 \rightarrow 1} \atop 2 \rightarrow 3$ = fluorescence radiance resulting from $2 \rightarrow 3$ excitation ($J\ s^{-1}\ m^{-2}\ sr^{-1}$),

$\quad A_{31}$ = Einstein coefficient of spontaneous emission for the $3 \rightarrow 1$ transition (s^{-1}),

k_{31} and k_{21} = collisional rate constants for the $3 \rightarrow 1$ and $2 \rightarrow 1$ transitions (s^{-1}).

The advantages and disadvantages of this approach are similar to those reported for T_{III}. However, the requirement for the knowledge of A_{31}, k_{31}, and k_{21} can be circumvented if the $2 \rightarrow 3$ excitation occurs just prior to the simultaneous pumping of $1 \rightarrow 3$ and $2 \rightarrow 3$. If $k_{21} >> (A_{31} + k_{31})$ and if the fluorescence is measured at the peak of the resulting pseudo-two level system population:

$$T_{IV_{peak}} = \frac{\Delta E_{12}/k}{\ln\left[\left(\frac{8}{3}\right)\left(\frac{^BF_{3\to1}}{^BF_{1\to3}}\right/\frac{^BF_{3\to1}}{^BF_{2\to3}}\right)\right]} \qquad (115)$$

The measurement of $T_{IV_{peak}}$ is therefore independent of the collisional and radiative rate constants and possesses the same advantages and disadvantages as T_{II}.

v. Thermally assisted flourescence method: Thermally assisted fluorescence (THAF) refers to the detection of emission from collisionally excited levels close in energy to the radiatively pumped level during resonance excitation. Levels up to ~ 2 eV above the pumped level can be observed. THAF assumes the establishment of a steady state collision-dominated Boltzman population distribution over the excited levels during the laser pulse. The THAF temperature is calculated from the slope temperature equation [2, 40-44]:

$$T_V = \frac{\Delta E_{ij}/k}{\ln\left[\frac{A_i g_i}{A_j g_j}\right] + \ln\left[\frac{\lambda_j}{\lambda_i}\right] + \ln\left[\frac{^BF_{j12}}{^BF_{i12}}\right] + \ln\left[\frac{1}{D}\right]} \qquad (116)$$

where

$$D = \frac{1 + \dfrac{k_{41}}{K_1}}{1 + K_2\dfrac{k_{41}}{K_1}} \quad , \qquad (117)$$

$$K_1 = k_{42} + \frac{k_{43}}{k_{23}}\left(k_{23} + k_{24}\right) \quad , \qquad (118)$$

$$K_2 = \frac{k_{42}/k_{41}}{k_{32}/k_{31}} \quad , \qquad (119)$$

k_{41}, k_{42}, k_{43}, k_{23}, etc. = collisional rate constants for transitions 4→1, 4→2, 4→3, 2→3, etc. (s^{-1}),

$B_{F_{j12}}$ and $B_{F_{i12}}$ = fluorescence radiances for emission from levels j and i assuming 1→2 excitation $(J\ s^{-1}\ m^{-2}\ sr^{-1})$,

g_i and g_j = statistical weights of levels i and j (dimensionless),

A_i and A_j = Einstein coefficients of spontaneous emission for the transitions from levels i and j (s^{-1}),

ΔE_{ij} = energy difference between levels i and j (J).

The THAF temperature, T_V, can be determined by measuring the intensity ratios of two fluorescence lines which can be transitions from the radiatively excited level and an upper thermally assisted level, from two thermally assisted levels, or from the slope of a plot of

$$\ln(B_{F_{j12}}\lambda_j/g_jA_j) \text{ vs. } \Delta E_j/k \qquad (120)$$

where

ΔE_j = energy difference between level j and the ground state (J),

D = factor which indicates deviations from a partial Boltzmann equilibrium (dimensionless).

Invalid temperatures are measured if unbalanced colli-
sional rates resulting from significant collisional transfer
to or from lower lying levels produce deviations of level
populations from the required Boltzmann distribution, i.e.,
$D \neq 1$. Deviations may also result from system losses such
as ionization and chemical reactions or most importantly,
steady state is not being attained during the laser pulse
for the thermometric seed. A serious systematic error can
result if the A-values are inaccurate.

THAF appears to possess the most potential for versa-
tile flame temperature measurements [40]. Saturation is
not required but can occur. With only one laser excitation
wavelength, there are no difficulties due to ill-matched or
inhomogeneous laser beams. The most significant advantage
of THAF is its potential simplicity for the achievement of
single-shot temperatures. However, the A (transition prob-
ability) values must be known and the collisional energy
transfer processes within the thermometric species must be
evaluated to determine where steady state excited level
populations are achieved during the laser pulse. THAF has
been successfully applied using Tl, Ga, and OH thermometric
seeds in CH_4/air, gasoline/air, and C_2H_2/O_2/Ar premixed
laminar flames. However, Na in several C_2H_2/O_2/Ar or $/N_2$
flames, under various excitation modes, produced THAF which
indicated that thermal equilibrium was <u>not being approached</u>
during the ~ 5 ns or ~ 1 μs laser excitation pulse [36, 47,
86, 138].

e. Laser induced fluorescence of native flame species.
LIF techniques can also be applied to native flame molecular
species, such as OH [42, 48, 51, 562, 565-569]. The LIF
techniques, at least with respect to the rotational excitation
temperature, are generally classified according to whether
the temperature is calculated from the ground state popula-
tion via fluorescence detection or from the observed excited
state population distribution [569]. Boltzmann plots of the
fluorescence intensity vs. the energy of the laser pumped
lower rotational level can be constructed by scanning the
rotational excitation spectrum and measuring the fluorescence
with a (spectral) broadband detector [48, 49, 562, 565, 568].
The results of the data interpretation appear to depend on
the type of flame, the extent of collisional redistribu-
tion of the laser excited population, and self-absorption of
the various fluorescence lines (specifically, the emission
transition).

The temperature can also be deduced from the observed
excited electronic state rotational and vibrational popula-
tion distributions [566, 567]. The accuracy of the resulting
population temperature is dependent on the validity of colli-
sional energy transfer models for the excited state thermo-
metric species [51, 106, 569].

Laser excited OH fluorescence as a temperature diag-
nostic method provides several attractive features [569]:

    i)   OH is present in high concentrations ($\gtrsim$ 1 ppm) in
        flames;

ii) the (0,0) and (0,1) vibrational bands of the $A^2\Sigma^+-X^2\Pi$ electronic transition occur in the spectral region of the frequency-doubled wavelengths of the efficient rhodamine laser dyes; and

iii) the frequencies and radiative transition rates of OH rotational lines are well characterized [394, 573-575].

The earliest studies of OH LIF excitation spectra indicated, in contrast to OH absorption measurements, an apparent nonequilibrium OH ground state population distribution [51]. The anomalous excitation temperatures observed were most likely results of self-absorption errors (> 30%) of the fluorescence signals at the high OH concentrations (~ 0.5%) reported in CH_4/air and other flames [48, 51]. Appreciable data scatter was observed in the Boltzmann plot of the OH fluorescence intensity vs. the energy of the initial rotational state in the $^2\Pi(v'' = 0)$ ground electronic state even though a small path length, curved flame front burner was utilized to circumvent the self-absorption difficulties [48]. However, the apparent OH rotational energy distribution was in equilibrium with the N_2 vibrational energy distribution (from Raman scattering) throughout the experimental flame [48].

Interpretation of the excited state fluorescence spectra has indicated nonequilibrium excited state population distributions which varied with the excited state being pumped [51, 564, 576]. The excited state distribution is also sensitive to self-absorption difficulties. Differing temperature results were also reported for fluorescence detected within a wide range of spectral monochromator bandpasses [51]. With

excitation near the intense (0,0) band emission, the detection system may discriminate against high N' (excited state rotational quantum number) P and Q lines.

The weaker, less self-absorbing (1,0) vibrational band of the $A^2\Sigma^+ \rightarrow X^2\Pi$ transition can also be radiatively excited. However, in these attempts [51, 566, 567] to determine the (0,0) band fluorescence temperature after v' = 0 to v" = 0 vibrational relaxation resulted in rotational temperatures which were still quite dependent on which rotational level in the v' = 1 band was initially excited. For both (0,0) and (1,0) excitations, the vibrational collisional transfer rates to other rotational levels are strongly dependent on the rotational quantum number N' and the excited state population does not relax to a partial Boltzmann temperature before radiating. In addition, even with lesser self-absorption difficulties, the actual degree of self-absorption depends on the line whose fluorescence is being observed [51].

Excitation and observation of fluorescence in the (1,1) OH vibrational band has provided rotational temperatures which even though not affected by fluorescence self-absorption are still functions of the nonequilibrium excited state population [577]. Therefore, in general, LIF techniques which require scanning of the rotational fluorescence excitation spectrum or the observation of the rotational or vibrational excited state population distributions may provide accurate rotational temperatures, but are still likely to be affected by at least severe data scatter and possibly, nonequilibrium excited state distributions.

Through knowledge of all rotational collisional energy transfer and quenching cross sections on a per state basis as functions of the temperature and the gas composition, the translational OH temperature has been determined by exciting the (0,0) vibrational fluorescence and observing the corresponding nonequilibrated excited state rotational population distribution from that vibrational level [566, 578]. The modelling of this distribution is based on the empirical temperature dependence of the collisional transfer rates at a known gas composition when under the assumption that self-absorption is negligible.

Vibrational flame temperatures can also be obtained by exciting a specific vibrational absorption line of the (0,0) vibrational band of the $A^2\Sigma^+ \rightarrow X^2\Pi$ electronic transition [567]. Measurements of the intensities of the (0,0) and (1,0) vibrational bands can provide the ratio of the populations in the two vibrational levels from which the vibrational temperature can be deduced. This LIF method should be able to be utilized for single-shot temperature measurements under broadband detection and is independent of the laser intensity and the degree of saturation. However, as with the rotational temperature methods, the collisional rate processes must be investigated and the effect of self-absorption in the (0,0) and (1,0) band must be determined [51, 567]. Because of the nonequilibrium population distributions that may occur, the technique must be calibrated for the rotational levels whose fluorescence is being detected.

Cattolica [568] has reported a clever, two-line rotational fluorescence temperature method which is very similar to the atomic fluorescence two-line method I (linear excitation conditions). A specific rotational level is excited in the $A^2\Sigma^+$ state from <u>two different</u> levels in the $X^2\Pi$ state. The main assumption is that the ground state rotational population distribution ($X^2\Pi(v'' = 0)$) is Boltzmannian. Difficulties due to self-absorption of excited rotational lines, nonequilibrium excited state populations, and temperature sensitivity to detector spectral bandpass and to collisional energy transfer are eliminated; the rotational nonequilibrium and self-absorption effects, etc., are the same for each excitation wavelength because the same excited state is being pumped. The rotational temperature obtained from the fluorescence ratio depends only on the energy level difference and absorption probabilities of the two ground state levels [568]. This technique appears quite promising for turbulent flame measurements if two pulsed dye lasers could be used to excite the two OH lines within ~ 1-3 ns. However, linear conditions must be maintained which limits the obtainable fluorescence intensities.

To maximize fluorescence signal-to-noise ratios, saturation of the excitation transition would be desirable. Lucht et al. [569] have developed a two-line laser saturated fluorescence method which is quite similar to the atomic fluorescence LIF methods. The balanced cross-rate model is used to describe the steady state population coupling between

the lower and the excited upper levels [106, 569]. If the rotational relaxation rates in the upper and lower rotational manifolds are approximately the same and if the collisional redistribution of the rotational population is sufficiently fast such that steady state is being attained, the populations of the coupled levels will be relatively constant during the laser pulse. In this method, two different excited states are pumped from two different lower levels and fluorescence from those levels is monitored. The temperature sensitivity is directly proportional to the energy difference between the ground rotational levels. The experimental procedure can consist of the sequential excitation of the two pump transitions and the detection of each fluorescence signal or of the simultaneous pumping of the excitation lines via blended lines [569]. Lucht et al. [569] have discussed the merits of each procedure and the two-line methods of Cattolica [568] and Lucht et al. [569].

NO has also been suggested as a thermometric species [569, 579, 580] in the application of LIF to flames. NO fluorescence has been investigated as the basis for temperature measurements in low temperature (< 1000 K) flames [579, 580].

The major interferences to successful application of LIF to flame temperature measurements include Rayleigh and Mie scattering at the resonance wavelengths, laser modulated particle incandescence, and especially, laser induced particulate fluorescence [7]. In sooty flames where there are significant hydrocarbon concentrations, hydrocarbon

fluorescence (with excitation ~ 300.0-375.0 nm region) can be severe throughout the UV-visible spectrum [581, 582]. In addition, for many LIF techniques, the A (transition probability) values must be known for each observed fluorescence line. However, the potential capability of LIF techniques to provide simultaneous temperature and trace ($\gtrsim$ 1 ppm) species concentration measurements is definitely advantageous.

7. Translational and other temperatures

a. Atomic and molecular species translational temperatures.

Translational or gas kinetic temperatures can be determined from the measurement of the Doppler broadened half-width of the spectral line (emission, absorption, fluorescence, Raman scattering, etc.)[2, 9, 11, 461]. The translational temperature (see Rayleigh scattering methods) can be calculated from

$$\frac{\delta\nu_D}{\nu_o} = 7.16 \times 10^{-7} \sqrt{\frac{T}{m_i}} \tag{121}$$

where

$\delta\nu_D$ = Gaussian half-width of a purely Doppler broadened line (Hz),

ν_o = peak frequency of line (Hz),

m_i = relative mass of the species i whose transition is being observed (g),

T = translational (Doppler) temperature (K).

The radiating (absorbing, scattering, etc.) species must not significantly alter their velocities within a time interval corresponding to $(2\Pi\delta\nu_D)^{-1}$ or collisional line-narrowing (Dicke narrowing) [2] may result, the line profile will not be Gaussian, and the effective Doppler temperature will be inaccurate. The two main disadvantages to the determination of the Doppler temperature are the weak sensitivity of the square root dependence of temperature to subtle temperature variations and the presence of other line profile broadening processes at moderate (atmospheric) flame pressures, especially collisional broadening, which can severely affect the shape of the line profile. It is also difficult to isolate spectrally a particular transition from other overlapping lines and bands. Therefore, the Doppler temperature is not frequently determined in flames, even though the translational "temperature" is the flame "temperature" most likely to correspond to LTE [2]. However, Doppler temperatures have been measured in flames by spectrally scanning a particular OH line with a tunable dye laser [438, 440]. The Doppler temperature of a Rayleigh scattered line which does not suffer collisional broadening effects has also been measured [461].

The translational flame temperature corresponding to the N_2 ground state temperature was measured by Muntz [583]. A narrow beam of fast electrons (10-100 keV) was injected into the flame and the excitation spectrum of the first negative bands of N_2 (N_2^+, $B^2\Sigma_u^+ \rightarrow X^2\Sigma_g^+$) was measured. The overall

intensity of the N_2 bands is proportional to the N_2 density [11, 583] and the N_2 rotational temperature is essentially the translational temperature.

  b. Ionization temperatures. The ionization excitation temperature [2, 9, 585] can be measured from the integrated radiance of a particular ionic line in emission (and in fluorescence), from the radiance ratio of two ionic lines of the same thermometric species, from the Boltzmann plot of several ionic line intensities, and possibly from the ratio of an atomic line and an ionic line of a thermometric species (see Section 2). The expression for the Boltzmann distribution of the excited level population of a singly-ionized atomic species is equivalent to that derived for the neutral atom (see Table A-3). The partition function, Q, for an ionic species, can be determined in the same manner as the partition function for the neutral atom (see Table A-3) or can be assumed constant for all ionic lines of the same thermometric species. If the experimental flame has a sufficiently high temperature ($\gtrsim$ 3500 K) that the ionic emission can potentially be detected or the ionic fluorescence is measured, Cu or Zn can be introduced into the flame as the thermometric species [140].

    The ionization temperature may also be determined from the radiance ratio of an atomic and an ionic line of a particular species if the electron density can also be measured (see Table A-3) [9, 584-586]. To ensure accurate calibration of

the optical system, it is generally advisable to measure absolutely the radiance (emission, fluorescence) of either the atomic or ionic line [9]. Huldt [584] determined ionization temperatures in a C_2H_2/air flame via the measurements of the emission intensity ratio of Ba/Ba$^+$ lines and Sr/Sr$^+$ lines.

In addition, due to the difficulty in accurately measuring the absolute concentrations of the atomic and ionic species, ionization temperatures are not generally determined from the direct evaluation of $K_i(T)$ (see Table A-3):

$$K_i(T) = \frac{[A^+][e^-]}{[A]} \tag{122}$$

for the ionization/recombination process:

$$A \rightleftarrows A^+ + e^-$$

where

$[A]$ = number density of neutral species (cm^{-3}),

$[A^+]$ = number density of ionic species (cm^{-3}),

$[e^-]$ = electron number density (cm^{-3}),

$K_i(T)$ = temperature-dependent ionization constant (cm^{-3}).

Moreover, the assumption that <u>thermal ionization</u> exists for the particular ionization/recombination process may not be valid in certain flames [2]. The apparent ionization "temperature" may not conform to the actual flame temperature due to slow relaxation times (see Table A-5). In addition, the stringent requirements for accurate measurements of widely varying intensities of atomic and ionic lines may limit the

application of apparent ionization "temperatures" only to the evaluation of deviations from LTE in flames [585, 586].

C.   Electron Temperatures

The translational "temperature" corresponding to the flame electron "temperature" (which generally deviates from the true flame translational temperature due to the discomparable electron mass) has been measured in certain flame regions, primarily in the combustion zone [2, 175, 587-590]. The electron temperature even in an electrically neutral system like a flame can also deviate from the true translational temperature because of their reactions with other flame species which may produce excessive natural flame ionization of these flame species [2]. In the combustion zone, the electron temperature may exceed the flame gas temperature by as much as $\gtrsim$ 200 K in many low pressure N_2-diluted hydrocarbon-based flames at 2000 K and up to ~ 1000 K in atmospheric pressure C_2H_2/O_2 torch flames at 2500 K [175, 587]. However, in the post-reaction zones, the electron temperature corresponds more closely to the true flame temperature [2, 59, 173]. Assuming that systematic errors in the measurement procedure do not interfere with the data analysis, the electron temperature deviations from the flame gas temperature in the combustion zone may result from the presence of "hot" electrons possessing excess translational energy often above the ionization energy of many atomic and molecular species [2]. Metal and OH chemiluminescence may

result. Perturbations in the recombination reactions may induce deviations in Saha equilibrium [2].

Electron temperatures are generally evaluated from the current-voltage characteristic produced from the electrostatic probes used to measure the electron current. Both single probe and double probe techniques have been utilized under the assumption that the electron current follows from a Maxwellian distribution of electron velocities.

Single probe methods utilize a highly asymmetric reference electrode which is well separated from the relatively smaller probe electrode. The probe or sensing electrode is generally a thin wire (Pt, 40% Rh electrode) or a small sphere which can be biased either negatively or positively with respect to the reference electrode. Like thermocouples, radiation and conduction losses and catalytic effects must be corrected for. Other systematic errors include AC pickup, leakage currents, and the inability of the probe electrode to accurately sense the electron current in flame zones characterized by sharp temperature gradients.

The double probe techniques utilize two equal area, symmetrical probes spaced close together within the flame in addition to the reference electrode. High electron current drain within the flame, which is a significant problem in the applications of single probe methods, can be compensated for with double probe methods. The second probe electrode is used to sense shifts in the flame potential.

Correspondingly, more accurate current-voltage characteristics can be measured. In addition, the spatial resolution of the temperature measurement is improved.

Attard [592] determined the electron temperature in an atmospheric pressure C_2H_2/O_2 torch flame by measuring the electrical Johnson noise. Johnson noise occurs as a result of the random <u>thermal</u> motion of the charge carriers (electrons) within any ohmic resistor (such as a flame) [2]. The Nyquist formula gives the standard deviation of the current fluctuations, σ_i [2]:

$$\sigma_i = 4kT\Delta f/R \qquad (123)$$

where

    T = absolute temperature of the resistor (flame) (K),

    Δf = effective noise bandwidth (Hz),

    R = ohmic resistance (Ω).

This relation is valid for any linear dissipative system regardless of the state of LTE in that system [2].

D. Temperature Distributions and Tomography in Flames

1. Spatial resolution

Spatially resolved temperature measurements are often required to evaluate the dynamic combustion processes. The radial flame temperature distributions and the axial flame temperature profiles have a direct effect on the course of combustion reactions, the extent of ionization, and the formation of flame species, especially particulates and

pollutants. There are two basic approaches for the measurement of spatially resolved temperatures: the temperature distributions within the entire flame or within any particular flame zone can be mapped via a series of point temperatures or the temperature distribution can be monitored from the entire probed volume (tomographic methods).

Mathematical inversion procedures [5, 9, 593-597] are often required to determine local temperatures when utilizing a line-of-sight or tomographic method. As shown in Appendix B, temperature gradients along the line-of-sight result in apparent temperatures which are neither the average temperature nor the weighted average temperature. Therefore, if the flame is axially symmetric and optically thin, Abel inversion "onion-peeling" procedures (see Appendix C) can be utilized to obtain radially resolved measurements [2, 5,9]. Inversion procedures consist of successive temperature measurements from the outer flame zones in toward the center with the assumption that the acquired knowledge of the outermost flame zone or "shell" can be used to determine the next successive zone's properties and the temperature within the third inner shell is the new unknown and so on. The shell thickness must be chosen carefully so that the temperature contribution within each shell is an accurate evaluation of the true local flame temperature [2, 5]. In addition, the errors involved in the zone subtraction procedure propagate into the next steps resulting in a loss of accuracy as the center flame regions are approached.

Abel inversion techniques are utilized in interferometric techniques as well as in radiation pyrometry and in spectrophotometry. Nonoptical techniques such as the OLD photoacoustic method [321] and thermocouple techniques can generally provide spatially resolved temperature measurements without line-of-sight integration and subsequent application of inversion procedures.

In some limiting cases in which emission or absorption of a particular thermometric species is measured for several lines, the frequency scanning inversion procedure [5] may be applicable. This method consists of the measurements of emission at different frequencies over a given line-of-sight path. The frequencies detected are carefully selected such that the frequencies monitored are strongly absorbed near the emergence point of the scan (flame edge closest to detector), while the cumulative emission from the whole beam is detected at less strongly absorbing frequencies (optically thin flame). The frequency scanning inversion procedure posssess the advantages that each line-of-sight path is resolved separately and axisymmetric flames are not required.

Reversal temperature measurements have been performed on a somewhat spatially resolved basis with the local seeding of the flame with the thermometric species [361]. Single droplet (10-100 μm diameters) generators have also been utilized to provide local reversal temperatures [598].

Multiangular (tomographic) absorption measurements in a CH_4-diffusion jet have been performed in order to obtain spatially resolved (2 mm^3) CH_4 concentrations [597]. This computerized tomographic approach could be utilized to obtain multidimensionally resolved absorption temperatures. Absorption data were obtained from several projections (15° rotations) throughout the jet, the Fourier transforms were computed, and through the inverse transformation, the local temperature at any point in the jet could be evaluated.

Laser excited Raman scattering and CARS have been utilized to map the local temperature distributions within laminar and turbulent flames [6, 212, 499, 528]. Fluorescence methods, as well as laser saturated absorption, can provide local temperatures due to the right angle viewing arrangement. Haraguchi et al. [555-558] used Tl and In as thermometric seeds in order to measure ~ 2 mm^3 local flame temperatures under conventional source excitation. Temperature profiles of C_2H_2/air and H_2/air flames were obtained with temperature precisions which ranged from ± 20-60 K in the flame interzonal regions and from ± 50-100 K in the outer, more turbulent flame zones.

Fluorescence generation via laser excitation can provide local (< 1 mm^3) temperatures of similar accuracy and precision [41-44, 114, 569]. Flame volumes as small as 2 μm^3 have been probed via the two-line atomic fluorescence techniques and OH laser induced fluorescence methods [48, 569, 599].

Tomographic methods as well as the measurements of point temperatures [600-604] can be applied to flames with

fluorescence techniques. Two-dimensional imaging of In two-line laser induced fluorescence in a CH_4/air flame was obtained by producing loosely focused radiation which was passed through the flame 20 mm above the burner [604]. The fluorescence emitted at right angles was imaged onto an intensified-diode array rapid-scan spectrometer system (2.5 mm x 25 mm spatial resolution). The measured LTE flame temperature was 2150 K ± 200 K. In addition, two-dimensional imaging of OH laser induced fluorescence for simultaneous species concentration measurements at different points in the flame have been reported using approximately the same procedure [601, 602]. The instantaneous species concentration distributions were obtained by forming a sheet of radiation (~ 0.5 mm x 35 mm spatial resolution) which produced fluorescence at right angles to the excitation beam. The fluorescence was imaged onto a vidicon (or a diode matrix-array) detector to result in a spatial resolution of 0.35 mm x 1.75 mm x 0.5 mm [601]. This tomographic imaging procedure could be applied to flame temperature measurements using either two-line fluorescence (generally on sequential laser shots) or THAF techniques.

Previously, two-dimensional mapping of Raman scattering (for species concentrations) had been demonstrated by Hartley [605]. In this approach, "Ramanography," the Raman radiation was image-intensified to provide high spatial resolution, but still resulted in relatively weak Raman signals. An improved multipass approach incorporated an optical multichannel

analyzer for CH_4 and N_2 concentration measurements [606]. In addition, two-dimensional single-shot Mie and Rayleigh scattering measurements have been performed [607, 608] for the mapping of species concentration profiles.

It should be readily apparent that very small probed volume temperatures and temperature profiles can be measured on a point basis without the need for Abel inversion procedures. Instantaneous temperature tomographic mapping can also be accomplished. The attainment of two-dimensional temperature profiles (using an atomic or native flame thermometric species) is especially desirable in the investigation of transient flame fluctuations and other dynamic combustion processes.

2. Temporal resolution

Temporally resolved flame temperature measurements are especially valuable in highly turbulent flame environments. Temporal resolution, however, can refer to two experimental procedures: the time-averaging over many laser shots of fluorescence (scattering, absorption, etc.) signals produced during each laser pulse or the determination of single-shot temperatures in which a unique temperature is measured during each laser pulse. Both chopped cw lasers and pulsed dye lasers ($\gtrsim 10^{-8}$-10^{-6} s pulse durations) can be used to obtain temporally resolved temperatures. However, the selection of a laser of suitable pulse width is often a balance between two critical factors: significant ionization and excited state chemical reactions at longer (~ 10^{-6} s) pulse lengths

and the possibility of not achieving a partial Boltzmann distribution over the excited levels during spectrophotometric determinations or even not approaching steady state during short ($\sim 2 \times 10^{-8}$ s) laser pulses [1, 2, 4, 40, 51, 86, 138].

In Raman scattering and CARS experiments, signal averaging over several laser shots can often reduce the accuracy of the temperature measurement and the capability of the technique to follow highly fluctuating temperatures [7, 50]. In premixed, laminar flames, single-shot temperatures are not actually needed to improve the accuracy, but rather to increase the precision [40, 114, 599]. The ratioing of the detected signals to laser power fluctuations on a single-shot basis will often improve the precision of the technique, especially for longer pulse length laserswhich may have significant amplitude jitter and which, in some cases, may correspondingly affect the signals observed. However, the accuracy of single-shot techniques often depends on the experimental arrangement and measurement procedure [1, 2, 38, 111, 138]. Optical multichannel analyzers can be utilized for fluorescence, Raman scattering, and CARS temperature measurements. Therefore, on a single-shot basis, the sensitivity of the detector on a distortion-free basis must be quite high and the measurement repetition rates are limited to < 100 Hz. In addition, timing and the need for spatial homogeneity of the beams become especially critical when several laser beams are needed for the temperature measurement. Those techniques which require only one laser beam are more readily amenable to accurate single-shot temperature measurements.

Several techniques, e.g., PROBE, laser saturated absorption, and the OLD photoacoustic method, could be applicable to single-shot temperature measurements in flames. However, the first single-pulse determinations were restricted to Raman scattering [50, 456, 609] and CARS experiments [533-535, 610]. Single-shot Raman scattering temperatures have been demonstrated in a homogeneous charge gas-fueled combustion engine as well as in premixed, laminar and diffusion flames resulting in precisions of 5-7% [456, 609, 610].

Single-pulse CARS temperature measurements have been performed in a variety of flames and combustors [528, 533-535, 610, 612]. Excellent precisions of ~ 25-50 K can be achieved with the broadband CARS method if a highly dispersive mono-chromator in conjuction with an optical multichannel ana-lyzer (free from channel cross-talk) is utilized. In contrast to signal-averaged CARS spectra, the single-pulse data are generally of higher quality.

The two-line atomic fluorescence method in which the Stokes and anti-Stokes direct-line fluorescence from In is measured on a sequential basis has been used to provide pre-liminary single-shot temperature measurements [599, 604]. Two pumped dye lasers are needed to excite the thermometric seed and therefore beam homogeneity and timing are critical [40]. For the high (~ 10 kHz) data repetition rates desired, it would be necessary to operate the pump laser in conjunction with two dye laser systems and to use a four-channel analog-to digital converter data acquisition system in order to ratio out any

laser power fluctuations. The precision achieved was ± 13% at ≳ 2500 K.

Single-pulse temperature measurements using Tl THAF have been obtained in three premixed, laminar $C_2H_2/O_2/Ar$ flames which range in temperature from 2200 K to 2465 K [114]. A N_2-pumped pulsed dye laser (pulse length ~ 5 ns) pumped BBQ dye at 0.2 mJ total pulse energy to excite Tl via the resonance 377.6 nm transition. On an averaged basis, six Tl thermally assisted fluorescence transitions could be observed. For single-shot measurements, two detection channels, each consisting of a monochromator, fast photomultiplier tube, and boxcar averager, were used to detect the THAF signals. Several pairs of THAF transitions were evaluated. Depending on which pair was used, the precision of 100 single-shot temperatures at 2465 K ranged from ± 11 K with the 276 nm - 292 nm line pair to ± 32 K with the 323 nm - 292 nm pair. The temperature precisions corresponded very well to those obtained by the Na line reversal method (± 10 K) for each of the three experimental flames. The precision of the THAF single-shot temperature obtained was always much better than the precision of the time integrated (averaged) measurement, which indicates that random errors in the experiment such as laser power fluctuations, Rf noise variations, and nebulizer irregularities in aerosol production were minimized significantly. The reliability of the THAF single-shot method has been shown, suggesting that with a longer pulse length laser (to ensure steady state conditions and

Boltzmannian distributions), better optical collection and more sensitive electronic detection, further improvements in temperature precision could be obtained. For most flame diagnostic experiments, THAF via the introduction of the thermometric seed will be adequate. However, in some situations such as those involving engines and other large-scale combustors, single-shot THAF measurements with a native flame species such as OH should be investigated.

V. Conclusion

It is obvious that several diagnostic techniques are available for temperature measurements in any type of flame at any temperature or pressure [7, 613]. However, no one technique can provide temperature data over very large temperature, composition, or pressure ranges. It is generally necessary to apply several techniques or in some cases, such as the Raman scattering and fluorescence methods, different methods or thermometric seeds need to be used. Intrusive techniques such as probe thermometry can provide quick temperature measurements on an adequate spatial resolution scale, but may perturb the flame and cannot provide a fast enough response to provide temporal resolution. Even though techniques such as density-based and sound velocity-based temperature methods cannot, in general, provide high spatial or temporal resolution, these methods are nonperturbing. Difficulty in applying these methods and other line-of-sight techniques (interferometry, radiation pyrometry, and absorption

methods) to turbulent flames can be severe. Laser-based techniques are the most promising methods for totally spatially resolved, instantaneous temperature measurements in most flame environments. However, the difficulty in applying these methods conveniently and accurately on a routine basis is correspondingly greater. Tomographic methods are especially desirable because of the future potential for obtaining instantaneous, complete flame temperature mapping.

Spontaneous and near-resonant Raman scattering are mainly applicable to clean (soot-free) secondary combustion zones where the background luminosity and incandescence are at a minimum. These scattering techniques have been considerably developed and can provide spatial (point or tomographic), single-pulse temperatures using selected flame species such as N_2.

CARS appears to be an excellent technique for flame temperature determinations on a point, instantaneous basis where ease of use and instrumentation cost are not the highest priorities. CARS is much less sensitive than fluorescence, but the capability to increase the incident powers has resulted in quite large signal-to-noise ratios for several species even in turbulent, sooting flames. The nonlinear dependence of temperature on laser power and composition generally necessitates computer fitting of the observed spectrum to generated models. In general, laser induced fluorescence techniques are versatile and can be adapted to many situations. LIF has been criticized because many

flame species are not amenable to laser excitation-fluorescence detection and, in most methods, information about the transition probabilities, and quenching and collisional energy transfer is needed. However, for spatial and instantaneous flame temperatures, there are several ubiquitous flame species that can be used, or in many cases (not in engines and large scale combustors), atomic fluorescence LIF can be accurately and precisely used, potentially even at high data rates.

APPENDIX B
SPECTROSCOPIC LINE-OF-SIGHT TEMPERATURES*

The apparent temperatures determined from spectroscopic line-of-sight techniques have been derived by Reif et al. [127] for a uniform flame (no temperature nor thermometric seed concentration gradients), an isothermal flame with a nonhomogeneous thermometric seed distribution, and a non-isothermal flame with a nonhomogeneous distribution of the thermometric species and have been found to be not equal to the averaged temperature, T_{avg}, nor the weighted averaged temperature, T_{wt-avg}:

$$T_{avg} = \frac{\int_0^\ell dx T(x)}{\int_0^\ell dx} \qquad (124)$$

$$T_{wt-avg} = \frac{\int_0^\ell dx n_o(x) T(x)}{\int_0^\ell dx n_o(x)} \qquad (125)$$

where

ℓ = optical path length (m),

n_o = number density of species in the ground state (m^{-3}),

$T(x)$ = temperature determined in volume differential of length dx at a distance x from the flame edge closest to the spectrometer (K).

350

The general expressions for the radiance emitted or absorbed by a flame characterized by LTE are given by:

$$B(em) = \int_{\Delta\nu_{ji}} d\nu \int_0^\ell dx \left[\frac{1}{4\pi} A_{ji} \, h\nu \, n_j \, P(\nu) \right] \quad x \quad (126)$$

$$\exp\left[- \int_0^x dx' \, K(\nu) \right],$$

$$B(abs) = \int_{\Delta\nu_{ji}} d\nu \, B_\nu^b \, (\nu, T_b) \left[1 - \exp \, (-\int_0^\ell dx \, K(\nu)) \right] \quad (127)$$

where

$$K(\nu) = \frac{h\nu}{c} \, (B_{ij} n_i - B_{ji} n_j) P(\nu),$$

A_{ji} = Einstein coefficient of spontaneous emission for the transition from level j to level i (s^{-1}),

B_{ji} = Einstein coefficient of induced emission for transition j→i $(m^3 \, Hz \, J^{-1} \, s^{-1})$,

B_{ij} = Einstein coefficient of induced absorption for transition from level i to level j $(m^3 \, Hz \, J^{-1} \, s^{-1})$,

n_i = number density in level i (m^{-3}),

n_j = number density in level j (m^{-3}),

$B_\nu^b(\nu, T_b)$ = spectral radiance of a blackbody source at temperature T_b and at frequency ν $(J \, s^{-1} \, m^{-2} sr^{-1} \, Hz$

$\Delta\nu_{ji}$ = total width of spectral line for transition from levels j to i (Hz),

T_b = source brightness temperature at which a black-body emits the same spectral radiance as the source at frequency ν (K),

$P(\nu)$ = line shape function (Hz),

h = Planck constant (J s),

c = speed of light (m/s).

The expression $dx((\frac{1}{4\pi})A_{ji}h\nu n_j P(\nu))$ refers to the spectral radiance of a volume differential of length dx at distance x from the origin.

The factor $\exp(-\int_o^x dx' \, K(\nu))$ refers to the fraction of the energy lost to self-absorption as the radiation travels down ℓ where $x = \ell$.

A. Line Reversal Method

1. Uniform Flame

At the reversal point, the radiant energy emitted by the flame, B(em), is equal to the energy absorbed by the flame from the continuum irradiation emitted by the source, B(abs):

$$B(abs) = \int_{\Delta\nu_{ji}} d\nu \; B_\nu^b(\nu,T_r) \left[1 - \exp(-K(\nu)\ell) \right] \qquad (128)$$

$$B(em) = \int_{\Delta\nu_{ji}} d\nu \; B_\nu^b(\nu,T_f) \left[1 - \exp(-K(\nu)\ell) \right] \qquad (129)$$

If B(abs) = B(em), $T_r = T_f$.

2. Isothermal Flame with Nonhomogeneous
   Distribution of the Thermometric Species

$$B(abs) = \int_{\Delta\nu_{ji}} d\nu\ B_\nu^b\ (\nu, T_r)\ \left[1 - \exp(-\overline{K(\nu)}\ell)\right] \qquad (130)$$

$$B(em) = \int_{\Delta\nu_{ji}} d\nu\ B_\nu^b\ (\nu,\ T_f)\ \left[1 - \exp(-\overline{K(\nu)}\ell)\right] \qquad (131)$$

where

$$\overline{K(\ell)} = \frac{h\nu}{c}\ \left[B_{ij}\ \overline{n_o}\ \exp(-E_i/kT_f) - B_{ji}\ \overline{n_o}\ x \right. \qquad (132)$$

$$\left. \exp(-E_j/kT_f)\right]\ P(\nu)$$

$$\overline{n_o} = \frac{\int_0^\ell dx\ n_o(x)}{\ell}\ , \qquad (133)$$

$\overline{n_o}$ = average number density of species in the ground
     state (m^{-3}).

If $B(abs) = B(em)$, $T_r = T_f$.

3. Nonisothermal Flame with Nonhomogeneous
   Distribution of Thermometric Species

Self-absorption in a nonisothermal source does not
affect the emission and absorption line profiles in the same
way. The extent of the difference depends on the line shape
which is determined from Doppler, collisional, and natural
broadening effects. Assume:

self-absorption is negligible $(K(\nu,x) \sim 0)$,

$\exp[-\int_0^x dx'\ K(\nu,x')] \simeq 1$

$[1 - \exp(-\int_0^\ell dx\ K(\nu,x))] \simeq \int_0^\ell dx\ K(\nu,x),$

$$B(\text{abs}) = \int_{\Delta\nu_{ji}} d\nu \left[\frac{c}{4\pi} \; \frac{8\pi h\nu^3}{c^3} \; \frac{1}{\exp(h\nu/kT_r)-1} \right] \times$$

$$\int_0^{\ell} \frac{h\nu}{c} \; (B_{ij}n_0(x) \frac{g_i}{g_0} \; \exp[-E_i/kT(x)] \; -$$

$$B_{ji}n_0(x) \frac{g_j}{g_0} \exp[-E_j/kT(x)])P(\nu) \qquad (134)$$

$$B(\text{em}) = \int_{\Delta\nu_{ji}} d\nu \int_0^{\ell} dx \frac{1}{4\pi} A_{ji}h\nu n_0(x) \frac{g_j}{g_0} \exp$$

$$[-E_j/kT(x)]P(\nu) \qquad (135)$$

where

E_i = energy of level i above the ground state (J),

E_j = energy of level j above the ground state (J),

g_i = statistical weight of level i (dimensionless),

g_j = statistical weight of level j (dimensionless),

g_0 = statistical weight of ground level (dimensionless).

The weighted average of the function $\exp(-E/kT(x))$ over the optical path, ℓ, is defined as

$$\overline{\exp(-E/kT)} = \frac{\int_0^{\ell} dx n_0(x) \; \exp(-E/kT(x))}{\int_0^{\ell} dx n_0(x)} \qquad (136)$$

The parameter, $\dot{T}$, can be defined from

$$\exp(-E/k\dot{T}) = \overline{\exp(-E/kT)}. \qquad (137)$$

$\dot{T}$ depends on the temperature profile, the concentration distribution of the thermometric species, and on the excitation energy, E_j.

At the reversal point:

$$\frac{E_j - E_i}{kT_r} = \frac{E_j}{k\dot{T}_{(E_j)}} - \frac{E_i}{k\dot{T}_{(E_i)}} \qquad (138)$$

if $E_i = 0$ (level i is the ground state),

$$T_r = \dot{T}_{(E_j)}$$

B. Emission-Absorption Method

1. Uniform Flame

The ratio of the flame emission, $B(em)$, to the flame absorption, $B(abs)$, for a selected spectral line is given by:

$$\frac{B(em)}{B(abs)} = \frac{B_\nu^b(\nu_o, T_f)}{B_\nu^b(\nu_o, T_b)} = \frac{\exp(h\nu_o/kT_b)-1}{\exp(h\nu_o/kT_f)-1} \qquad (139)$$

2. Isothermal Flame with Nonhomogeneous Distribution of the Thermometric Species

$$\frac{B(em)}{B(abs)} = \frac{B_\nu^b(\nu_o, T_f)}{B_\nu^b(\nu_o, T_b)} = \frac{\exp(h\nu_o/kT_b)-1}{\exp(h\nu_o/kT_f)-1} \qquad (140)$$

3. Nonisothermal Flame with Nonhomogeneous Thermometric Seed Distribution

$$\frac{B(em)}{B(abs)} = \frac{\exp[(E_j-E_i)/kT_b]-1}{\exp[(E_j-E_i)/kT_{em-abs}]-1} \qquad (141)$$

where

$$T_{em-abs} = \text{emission-absorption temperature (K)},$$

and

$$\frac{E_j - E_i}{kT_{em-abs}} = \frac{E_j}{k\dot{T}_{(E_j)}} - \frac{E_i}{k\dot{T}_{(E_i)}} \tag{142}$$

Therefore, for nonisothermal flames for the same species and line being observed, $T_{em-abs} = T_r$.

C. The Slope Method

1. Uniform Flame

When self-absorption is negligible, the measurement of integrated line intensities, B(em), for several transitions can give T_f, if B(em) for each line is plotted versus the energy of the level, E:

$$\ln\left[\frac{g_j A_{ji} \nu_o}{B(em)}\right] = \frac{E_j}{kT_f} + \ln\left[\frac{4\pi g_o}{h \ell n_o}\right] \tag{143}$$

where

$$B(em) = \frac{1}{4\pi} A_{ji} h\nu_o n_o \ell, \tag{144}$$

g_o = statistical weight of the ground level (dimensionless).

The slope of the plot will be $1/kT_f$.

2. Isothermal Flame with Nonhomogeneous Distribution of Thermometric Species

$$B(em) = \frac{1}{4\pi} A_{ji} h\nu_o \frac{g_j}{g_o} \exp(-E_j/kT_f) \int_o^\ell dx n_o(x) \tag{145}$$

$$\ln\left[\frac{g_j A_{ji} \nu_o}{B(em)}\right] = E_j/kT_f + \ln\left[\frac{4\pi g_o}{h \ell n_o}\right] \tag{146}$$

The slope will be $1/kT_f$.

3. Nonisothermal Flame with Nonhomogeneous
   Distribution of Thermometric Species

$$B(em) = \frac{1}{4\pi} A_{ji} \, h\nu_o \, \frac{g_j}{g_o} \exp[-E_j/k\dot{T}_{(E_j)}]\overline{n_o} \, \ell \, , \quad (147)$$

$$\ln\left[\frac{g_j A_{ji}\nu_o}{B(em)}\right] = \frac{E_j}{k\dot{T}_{(E_j)}} + \ln\left[\frac{4\pi g_o}{h\ell n_o}\right] \quad (148)$$

where

$$\frac{\partial}{\partial E_j}\left(\frac{E_j}{k\dot{T}_{(E_j)}}\right) = \frac{1}{kT_{slope(E_j)}} \quad , \quad (149)$$

$$\frac{1}{kT_{slope}} = \frac{\int_o^\ell dxn_o(x)\frac{1}{T(x)} \exp[-E_j/kT(x)]}{\int_o^\ell dxn_o(x) \exp[-E_j/kT(x)]} \quad (150)$$

for a given value of E_j.

The plot may not produce a straight line whose slope is $1/kT_{slope}$ and which is a function of E_j.

D. Two-line Method

1. Uniform Flame

If only two lines are measured, then the slope method can be reduced to

$$\ln\left[\frac{g_j A_{ji}\nu_o}{B(em)}\right] - \ln\left[\frac{g_{j'} A_{j'i'}\nu_{o'}}{B'(em)}\right] = \frac{E_j-E_{j'}}{kT_f} \quad (151)$$

where

g_j and $g_{j'}$ = respective statistical weights for the
upper levels j and j' of transitions j→i
and j'→i' (dimensionless),

A_{ji} and $A_{j'i'}$ = Einstein coefficients for spontaneous emission for the transitions $j{\to}i$ and $j'{\to}i'$ (s^{-1}),

$B(em)$ and $B'(em)$ = spectral radiances measured for transitions $j{\to}i$ and $j'{\to}i'$ (J m^{-2} s^{-1} sr^{-1} Hz),

ν_o and $\nu_{o'}$ = frequencies for transitions $j{\to}i$ and $j'{\to}i'$ (Hz),

E_j and $E_{j'}$ = energies of upper levels j and j' with respect to the ground state (J).

2. <u>Isothermal Flame with Nonhomogeneous Distribution of Thermometric Species</u>

$$\ln\left[\frac{g_j A_{ji}\nu_o}{B(em)}\right] - \ln\left[\frac{g_{j'}A_{j'i'}\nu_{o'}}{B'(em)}\right] = \frac{E_j - E_{j'}}{kT_f} \tag{152}$$

3. <u>Non-isothermal Flame with Nonhomogeneous Distribution of Thermometric Species</u>

$$\ln\left[\frac{g_j A_{ji}\nu_o}{B(em)}\right] - \ln\left[\frac{g_{j'}A_{j'i'}\nu_{o'}}{B'(em)}\right] = \frac{E_j}{k\dot{T}_{(E_j)}} - \frac{E_{j'}}{k\dot{T}_{(E_{j'})}} , \tag{153}$$

$$\frac{E_j - E_{j'}}{k\dot{T}_{two-line}} = \frac{E_j}{k\dot{T}_{(E_j)}} - \frac{E_{j'}}{kT_{(E_{j'})}} \tag{154}$$

If the two-line excitation energies are equal to the reversal method's upper and lower energy levels of the transition used:

$E_j{}_{\text{two-line}} = E_j{}_{\text{reversal}}$ and $E_{j'}{}_{\text{two-line}} = E_i{}_{\text{reversal}}$,

then $T_{\text{two-line}} = T_r$.

E. Absolute Measurement of Spectral Radiance of a Spectral Line

$$B(em) = \frac{h\nu_o A_{ji}}{4\pi} \frac{g_j}{g_o} \overline{n_o} \, \ell \, [\exp(-E_j/k\dot{T}_{(E_j)})] \qquad (155)$$

The apparent temperature measured, $\dot{T}_{(E_j)}$, is therefore dependent on the temperature profile, the thermometric species distribution, and on the excitation energy, E_j, of the line whose radiance, $B(em)$, is being measured.

APPENDIX C
ABEL INVERSION TECHNIQUES

The radially resolved temperature distribution across
the flame can be determined from line-of-sight temperature
measurements if the flame is axially symmetric and no self-
absorption occurs (see Fig. C-1). The relationship between
the local radiation intensity $I(r)$ as a function of the radial
distance r and the distribution of the radiance $B(x)$ measured
by scanning the flame in the horizontal x direction perpen-
dicular to the optical axis (and parallel to the y direction)
can be given by the Abel integral equation [2, 9]:

$$B(x) \alpha\ 2 \int_x^{r_0} I(r) r\ (n^2 - x^2)^{-\frac{1}{2}}\ dr$$

where

r_0 = radial distance to the flame border closest to
the detector from the origin (m),

$I(r)$ = intensity at distance r from the origin ($J\ s^{-1}\ m^{-2}$),

$B(x)$ = radiance at horizontal distance x ($J\ s^{-1}\ m^{-2}\ sr^{-1}$).

Abel inversion yields the function [2]:

$$J(r) \alpha\ \frac{1}{\pi} \int_r^{r_0} \frac{dB}{dx}\ (x^2 - r^2)^{-\frac{1}{2}}\ dx$$

Figure C-1. Horozontial cross section of a cylindrical
            flame. The radius of the inner seeded flame
            is denoted by r_0. The flame volume corres-
            ponding to the cross-hatched area is viewed
            by the spectrometer. The distance of an
            arbitrary volume element within this area is
            denoted by r.
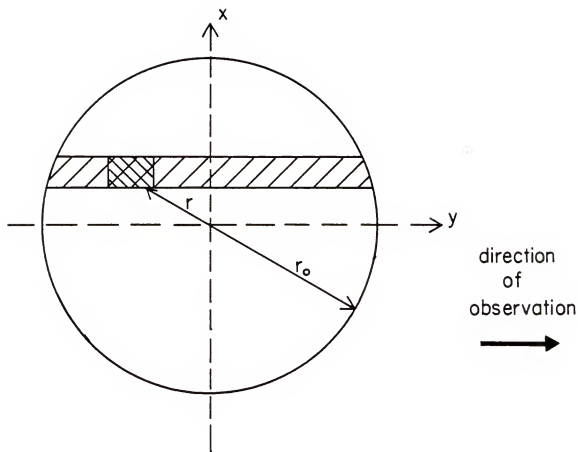
Generally, B(x) is not an analytical function and only certain forms of B(x) lead to an integral that can be evaluated [2]. In applying the Abel inversion, the boundary radius r_o and the x-axis are each divided into n equal increments of length Δ :

$$x_k = k\Delta, \; r_k = k\Delta, \; r_o = n\Delta$$

where

$$k = 0, \; 1, \; 2, \; . \; . \; . \; n-1.$$

The input data for the inversion are B(x) measured at x = 0, 1, . . . $k\Delta$, . . . $(n-1)\Delta$ [9]. The radial radiance distribution, B(r), is therefore derived. For a given r, each value of B(r) must correspond to an isothermal region or "shell."

Once the local intensities have been derived, the local temperature can be determined. If the single line/band radiance ratio method is utilized, the local intensity distribution yields the relative temperature distribution if a homogeneous distribution of thermometric species concentration occurs. The absolute temperature distribution can be determined if the local temperature in one flame region is absolutely known.

However, the temperature distribution can be directly evaluated if the two-line method or the slope method is utilized. Because the radiance for each line measured is a function of the thermometric seed concentration and two or more lines are being measured, the concentration distribution is not required.

REFERENCES

1. N. Omenetto and J. D. Winefordner, _Prog. Anal. At. Spectrosc._, 2, 1 (1979).

2. C. Th. J. Alkemade, Tj. Hollander, W. Snelleman, and P. J. Th. Zeegers, _Metal Vapours in Flames_, Pergamon Press, Oxford, 1982.

3. R. Mavrodineau and H. Boiteux, _Flame Spectroscopy_, Wiley, New York, 1965.

4. N. Omenetto, Editor, _Analytical Laser Spectroscopy_, Wiley, New York, 1979.

5. R. Goulard, Editor, _Combustion Measurements, Modern Techniques and Instrumentation_, Academic Press, New York, 1976.

6. D. R. Crosley, Editor, _Laser Probes for Combustion Chemistry_, American Chemical Society, Washington, D.C., 1980.

7. A. C. Eckbreth, P. A. Bonczyk, and J. F. Verdieck, _Appl. Spectrosc. Rev._, 13, 15 (1977).

8. B. Lewis, R. N. Pease, and H. S. Taylor, _Physical Measurements on Gas Dynamics_, Princeton University Press, Princeton, NJ, 1956.

9. R. H. Tourin, _Spectroscopic Gas Temperature Measurement, Pyrometry of Hot Gases and Plasmas_, Elsevier Publishing Company, New York, 1966.

10. B. Lewis and G. Von Elbe, _Combustion, Flames, and Explosions_, 2nd Ed., Academic Press, New York, 1961.

11. A. G. Gaydon and H. G. Wolfhard, _Flames: Their Structure, Radiation, and Temperature_, 4th Ed., Chapman and Hall, London, 1979.

12. A. G. Gaydon, _The Spectroscopy of Flames_, 2nd Ed. Chapman and Hall, London, 1974.

13. H. R. Greim, _Plasma Spectroscopy_, McGraw-Hill, New York, 1964.

14. J. W. Hastie, Editor, _Characterization of High Temperature Vapors and Gases_, Proc. 10th Materials Research Symp., National Bureau of Standards Special Publication No. 561, Washington, DC, 1979.

15. J. Lawton and F. J. Weinberg, _Electrical Aspects of Combustion_, Clarendon Press, Oxford, 1969.

16. A. Walsh, _Spectrochim. Acta_, _7_, 108 (1955).

17. C. Th. J. Alkemade and J. M. W. Milatz, _Appl. Sci. Res_, _4B_, 289 (1955).

18. C. Th. J. Alkemade, 10th Colloq. Spectrosc. Int., College Park, MD, 1962; Spartan Books, Washington, DC, p. 143.

19. J. D. Winefordner and T. J. Vickers, _Anal. Chem._, _36_, 161 (1976).

20. R. F. Browner, _Analyst_, _99_, 517 (1974).

21. J. D. Winefordner, _Chem. Tech._, 123 (1975).

22. S. J. Weeks, H. Haraguchi, and J. D. Winefordner, _Anal. Chem._, _46_, 1419 (1974).

23. H. P. Hooymayers and C. Th. J. Alkemade, _J. Quant. Spectrosc. Radiat. Transfer_, _6_, 501 (1966).

24. D. R. Jenkins, _Spectrochim. Acta_, _25B_, 47 (1970).

25. J. D. Weide and M. L. Parsons, _Anal. Chem._, _45_, 2417 (1973).

26. D. J. Johnson, F. W. Plankey, and J. D. Winefordner, _Anal. Chem._, _46_, 1898 (1974).

27. G. F. Kirkbright and M. Sargent, _Atomic Absorption and Atomic Fluorescence Spectroscopy_, Academic Press, New York, 1971.

28. D. J. Johnson and J. D. Winefordner, _Anal. Chem._, _48_, 341 (1976).

29. C. G. James and T. M. Sugden, _Proc. Roy. Soc._, _227A_, 312 (1955).

30. L. De Galan and J. D. Winefordner, _J. Quant. Spectrosc. Radiat. Transfer_, _7_, 251 (1967).

31. C. Woodward, _Spectrosc. Lett._, _4_, 191 (1971).

32. D. J. Halls, _Spectrochim. Acta_, _32B_, 397 (1977).

33. R. E. Russo and G. M. Hieftje, _Spectrochim. Acta_, _36B_, 231 (1981).

34. J. D. Winefordner, in _New Applications of Lasers to Chemistry_, ACS Symposium Series No. 85, G. M. Hieftje, Editor, American Chemical Society, Washington, DC, 1978.

35. J. D. Winefordner, Editor, _Spectrochemical Methods of Analysis_, Wiley, New York, 1971.

36. C. A. Van Dijk, Ph. D. Thesis, Utrecht, 1978.

37. E. H. Piepmeier, _Spectrochim. Acta_, _27B_, 431 (1972).

38. C. Th. J. Alkemade, 20th Colloq. Spectrosc. Int. and 7th Int. Conf. on Atomic Spectroscopy, Prague, 1977; "Invited Lectures," Prague, Sbornik VSCHT, p. 93.

39. N. Omenetto, P. Benetti and G. Rossi, _Spectrochim. Acta_, _27B_, 453 (1972).

40. J. D. Bradshaw, N. Omenetto, G. Zizak, J. N. Bower, and J. D. Winefordner, _Appl. Opt._, _19_, 2709 (1980).

41. G. Zizak, J. D. Bradshaw, and J. D. Winefordner, _Appl. Spectrosc._, _35_, 59 (1981).

42. G. Zizak, J. J. Horvath, and J. D. Winefordner, _Appl. Spectrosc._, _35_, 488 (1981).

43. G. Zizak, J. J. Horvath, C. A. Van Dijk, and J. D. Winefordner, _J. Quant. Spectrosc. Radiat. Transfer_, _25_, 525 (1981).

44. G. Zizak and J. D. Winefordner, _Combust. Flame_, _44_, 35 (1982).

45. C. A. Van Dijk, P. J. Th. Zeegers, G. Nienhuis, and C. Th. J. Alkemade, _J. Quant. Spectrosc. Radiat. Transfer_, _20_, 55 (1978).

46. C. A. Van Dijk, P. J. Th. Zeegers, and C. Th. J. Alkemade, _J. Quant. Spectrosc. Radiat. Transfer_, _21_, 115 (1979).

47. C. A. Van Dijk and C. Th. J. Alkemade, _J. Quant. Spectrosc. Radiat. Transfer_, _23_, 445 (1980).

48. J. H. Bechtel, _Appl. Opt._, _18_, 2100 (1979).

49. D. R. Crosley and G. P. Smith, Appl. Opt., 19, 517 (1980).

50. A. C. Eckbreth, Proc. 18th Symp. (Int.) on Combust., University of Waterloo, 1980, The Combustion Institute, Pittsburgh, PA, p. 1471.

51. G. P. Smith and D. R. Crosley, Proc. 18th Symp. (Int.) on Combust., University of Waterloo, 1980, The Combustion Institute, Pittsburgh, PA, p. 1511.

52. H. P. Hooymayers and C. Th. J. Alkemade, J. Quant. Spectrosc. Radiat. Transfer, 6, 847 (1966).

53. P. L. Lijnse and R. J. Elsenaar, J. Quant. Spectrosc. Radiat. Transfer, 12, 1115 (1972).

54. P. L. Lijnse and C. J. Van Der Maas, J. Quant. Spectrosc. Radiat. Transfer, 13, 741 (1973).

55. P. L. Lijnse, J. Quant. Spectrosc. Radiat. Transfer, 14, 1143 (1974).

56. J. R. Barker and R. E. Weston, Jr., J. Chem. Phys., 65, 1427 (1976).

57. F. Biraben, B. Cagnac, E. Giacobino, and G. Grynberg, J. Phys. B, 10, 2369 (1977).

58. P. L. Lijnse, Ph.D. Thesis, Utrecht, 1973.

59. J. D. Bradshaw, Ph.D. Thesis, University of Florida, 1980.

60. P. L. Lijnse, Chem. Phys. Lett., 18, 73 (1972).

61. T. F. Gallagher, W. E. Cooke, and S. A. Edelstein, Phys. Rev. A, 17, 125 (1978).

62. N. S. Ham and P. Hannaford, J. Phys. B, 12, 499 (1979).

63. R. E. Russo and G. M. Hieftje, Appl. Spectrosc., 36, 92 (1982).

64. G. P. Copley, B. P. Kibble, and L. Krause, Phys. Rev., 163, 34 (1967).

65. T. F. Gallagher, S. A. Edelstein, and R. M. Hill, Phys. Rev. Lett., 35, 644 (1975).

66. H. A. Wilson, Phil. Mag., 24, 118 (1912).

67. H. A. Wilson, Rev. Mod. Phys., 3, 156 (1931).

68. J. A. Smit and A. J. H. Vendrik, _Physica_, 14, 505 (1948).

69. R. S. Berry, in _Ionization in High-Temperature Gases_, K. E. Shuler and J. B. Fenn, Editors, Academic Press, New York, 1963.

70. A. N. Hayhurst, _IEEE Trans. Plasma Sci._, PS-2, 3, 115 (1974).

71. Tj. Hollander, Ph.D. Thesis, Utrecht, 1964.

72. M. D. Amos and J. B. Willis, _Spectrochim. Acta_, 22, 1325 (1966).

73. C. Th. J. Alkemade, in _Analytical Flame Spectroscopy_ (Selected Topics), Philips Technical Library, McMillan, London, 1970.

74. R. B. Green, R. A. Keller, C. G. Luther, P. K. Schenck, and J. C. Travis, _Appl. Phys. Lett._, 29, 727 (1976).

75. R. B. Green, R. A. Keller, P. K. Schenck, J. C. Travis, and C. G. Luther, _J. Am. Chem. Soc._, 98, 8517 (1976).

76. R. B. Green, J. C. Travis, and R. A. Keller, _Anal. Chem._, 48, 1954 (1976).

77. G. C. Turk, J. C. Travis, J. R. DeVoe, and T. C. O'Haver, _Anal. Chem._, 51, 1890 (1974).

78. C. A. Van Dijk and C. Th. J. Alkemade, _Combust. Flame_, 38, 37 (1980).

79. J. C. Travis, _J. Chem. Ed._, 59, 909 (1982).

80. C. H. Muller, K. Schofield, and M. Steinberg, _J. Chem. Phys._, 72, 6620 (1980).

81. M. Lino, H. Yano, Y. Takubo, and M. Shimazu, _J. Appl. Phys._, 52, 6025 (1981).

82. E. Speller, B. Staudenmayer, and V. Kempter, _Z. Physik A_, 291, 311 (1979).

83. B. P. Kibble, G. Copley, and L. Krause, _Phys. Rev._, 159, 11 (1967).

84. B. L. Earl and R. R. Herm, _Chem. Phys. Lett._, 22, 95 (1973).

85. B. L. Earl and R. R. Herm, _J. Chem. Phys._, 60, 4568 (1974).

86. J. E. Allen, Jr., W. R. Anderson, D. R. Crosley, and T. O. Fansler, Proc. 17th Symp. (Int.) on Combust., Leeds, UK, 1978, The Combustion Institute, Pittsburgh, PA, p. 945.

87. I. N. Siara and L. Krause, Can. J. Phys., 51, 257 (1973).

88. N. Omenetto and G. Rossi, Spectrochim. Acta, 25B, 297 (1970).

89. N. Omenetto, R. Browner, J. D. Winefordner, G. Rossi, and P. Benetti, Anal. Chem., 44, 1683 (1972).

90. J. Bradshaw, J. Bower, S. Weeks, K. Fujiwara, N. Omenetto, H. Haraguchi, and J. D. Winefordner, in Characterization of High Temperature Vapors and Gases, Proc. of the 10th Materials Research Symposium, National Bureau of Standards, Special Publication No. 561, J. W. Hastie, Editor, Washington, DC, 1979, p. 945.

91. C. H. Corliss and W. R. Bozman, NBS Monograph, 53 (1962).

92. A. Gallagher and A. Lurio, Phys. Rev., 136, A87 (1964).

93. P. T. Cunningham and J. K. Link, J. Opt. Soc. Am., 57, 1000 (1967).

94. M. Norton and A. Gallagher, Phys. Rev., A3, 913 (1971).

95. T. Anderson and G. Sorenson, Phys. Rev., A5, 2447 (1972).

96. L. L. Shimon and N. M. Erdevdi, Opt. Spectrosc., 42, 137 (1977).

97. J. Migdalek and W. E. Baylis, J. Phys. B, 12, 2595, (1979).

98. G. D. Boutilier, M. B. Blackburn, J. M. Mermet, S. J. Weeks, H. Haraguchi, J. D. Winefordner, and N. Omenetto, Appl. Opt., 17, 2291 (1978).

99. D. Olivares and G. M. Hieftje, Spectrochim. Acta, 33B, 79 (1978).

100. G. Zizak, J. D. Bradshaw, and J. D. Winefordner, Appl. Opt., 19, 3631 (1980).

101. D. Olivares and G. M. Hieftje, Spectrochim. Acta, 36B, 1059 (1981).

102. R. M. Measures, _J. Appl. Phys._, _39_, 5232 (1968).

103. J. L. Carlsten, _J. Phys. B_, _7_, 1620 (1974).

104. M. A. Bolshov, A. V. Zybin, B. G. Koloshinkov, and K. N. Koshelev, _Spectrochim. Acta_, _32B_, 279 (1977).

105. N. M. Lawandy, _Appl. Opt._, _18_, 189 (1979).

106. R. P. Lucht and N. M. Laurendeau, _Appl. Opt._, _18_, 856 (1979).

107. J. Kuhl, S. Neumann, and M. Kriese, _Z. Naturforsch_, _A28_, 273 (1973).

108. B. L. Sharp and A. Goldwasser, _Spectrochim. Acta_, _31B_, 431 (1976).

109. B. Smith, J. D. Winefordner, and N. Omenetto, _J. Appl. Phys._, _48_, 2676 (1977).

110. R. A. Van Calcar, M. J. M. Van de Ven, B. K. Van Uitert, K. J. Biewenga, Tj. Hollander, and C. Th. J. Alkemade, _J. Quant. Spectrosc. Radiat. Transfer_, _21_, 11 (1979).

111. N. Omenetto and J. D. Winefordner, _Laser Diagnostics in Flames and Plasmas at Atmospheric Pressure_, Internal Report, University of Florida, 1982.

112. J. W. Daily, _Appl. Opt._, _18_, 360 (1979).

113. C. A. Van Dijk, N. Omenetto, and J. D. Winefordner, _Appl. Spectrosc._, _35_, 389 (1981).

114. Melanie L. Elder, G. Zizak, D. L. Bolton, J. J. Horvath, and J. Winefordner, _Appl. Spectrosc._, in press.

115. J. Stupar and J. B. Dawson, _Appl. Opt._, _7_, 1351 (1968).

116. N. C. Clampitt and G. M. Hieftje, _Anal. Chem._, _44_, 1211 (1972).

117. G. J. Bastiaans and G. M. Hieftje, _Anal. Chem._, _46_, 701 (1974).

118. H. P. Hooymayers, _Spectrochim. Acta_, _23B_, 567 (1968).

119. C. Th. J. Alkemade, _Pure Appl. Chem._, _23_, 73 (1970).

120. P. J. Th. Zeegers and J. D. Winefordner, _Spectrochim. Acta_, _26B_, 161 (1971).

121. V. Svoboda, R. F. Browner, and J. D. Winefordner, *Appl. Spectrosc.*, 26, 505 (1972).

122. N. Omenetto, L. P. Hart, P. Benetti, and J. D. Winefordner, *Spectrochim. Acta*, 28B, 301 (1973).

123. F. van Geel, E. Voigtman, and J. D. Winefordner, *Appl. Spectrosc.*, submitted.

124. N. Omenetto, J. D. Winefordner, and C. Th. J. Alkemade, *Spectrochim. Acta*, 30B, 335 (1975).

125. A. B. Rodrigo and R. M. Measures, *IEEE J. Quantum Electron.*, 9, 972 (1973).

126. J. W. Daily, *Appl. Opt.*, 17, 225 (1978).

127. I. Reif, V. A. Fassel, and R. N. Kniseley, *Spectrochim. Acta*, 28B, 105 (1973).

128. J. J. Horvath, M.S. Thesis, University of Florida, 1979.

129. J. J. Horvath, J. D. Bradshaw, J. N. Bower, M. S. Epstein, and J. D. Winefordner, *Anal. Chem.*, 53, 6 (1981).

130. W. Snelleman, Ph.D. Thesis, Utrecht, 1965.

131. L. M. Fraser and J. D. Winefordner, *Anal. Chem.*, 44, 1444 (1972).

132. G. Nienhuis and F. Schuller, *Physica*, 94C, 394 (1978).

133. B. Cagnac, G. Grynberg, and F. Biraben, *J. Physique*, 34, 845 (1973).

134. T. F. Gallagher, S. A. Edelstein, and R. M. Hill, *Phys. Rev. A*, 15, 1945 (1977).

135. A. M. F. Lau, W. K. Bishel, C. K. Rhodes, and R. M. Hill, *Appl. Phys. Lett.*, 29, 245 (1976).

136. R. T. V. Kung and I. Itzkam, *IEEE J. Quantum Electron.*, QE-13, 73 (1977).

137. J. M. Daily and C. Chan, *Combust. Flame*, 33, 47 (1978).

138. Melanie L. Elder, C. A. Van Dijk, and J. D. Winefordner, *Spectrochim. Acta*, in press.

139. G. Zizak, F. Cignoli, and S. Benecchi, *Appl. Spectrosc.*, 33, 179 (1979).

140. P. W. J. M. Boumans, _Theory of Spectrochemical Excitation_, Hilger and Watts, London, 1966.

141. K. J. Laidler, _Reaction Kinetics, Vol 1: Homogeneous Gas Reactions_, Pergamon Press, Oxford, 1963.

142. J. Richter, in _Plasma Diagnostics_, W. Lochte-Holtgreven, Editor, North-Holland, Amsterdam, 1968.

143. A. B. Cambel, D. P. Duclos, and T. P. Anderson, _Real Gases_, Academic Press, New York, 1963.

144. C. Th. J. Alkemade and R. Herrmann, _Fundamentals of Flame Spectroscopy_, Adam Hilger, Bristol, 1979.

145. L. M. Bollinger and D. T. Williams, Proc. 3rd Symp. (Int.) on Combust., Madison, WI, 1948, The Williams and Wilkins Company, MD, p. 176.

146. P. T. Gilbert, _ASTM Spec. Tech. Publ._, _269_, 73 (1959).

147. J. D. Winefordner, C. T. Mansfield, and T. J. Vickers, _Anal. Chem._, _35_, 1611 (1963).

148. M. D. Fox and F. J. Weinberg, _Proc. Roy. Soc._, _268_, 22 (1962).

149. L. de Galan and J. D. Winefordner, _J. Quant. Spectrosc. Radiat. Transfer_, _7_, 703 (1967).

150. G. F. Kirkbright, M. K. Peters, M. Sargent, and T. S. West, _Talanta_, _15_, 663 (1968).

151. G. Dixon-Lewis, N. M. Sutton, and A. Williams, _Proc. Roy. Soc._, _317_, 227 (1970).

152. K. H. Parker and O. Guillon, Proc. 13th Symp. (Int.) on Combust., Salt Lake City, UT, 1970, The Combustion Institute, Pittsburgh, PA, p. 667.

153. A. Roshko, Paper No. 76-68, AIAA 14th Areospace Sciences Meeting, Washington, DC, 1976.

154. H. P. Broida and K. E. Shuler, _J. Chem. Phys._, _27_, 933 (1957).

155. P. J. Padley and T. M. Sugden, Proc. 7th Symp. (Int.) on Combust., London and Oxford, UK, 1958, Butterworths, London, p. 235.

156. T. M. Sugden, _Ann. Rev. Phys. Chem._, _13_, 369 (1962).

157. M. A. A. Clyne and B. A. Thrush, Proc. 9th Symp. (Int.) on Combust., Ithaca, NY, 1962, Academic Press, New York, p. 177.

158. T. M. Sugden, Proc. 10th Symp. (Int.) on Combust. Cambridge, UK, 1964, The Combustion Institute, Pittsburgh, PA, p. 33.

159. M. J. McEwan and L. F. Phillips, Combust. Flame, 9, 420 (1965).

160. P. J. Th. Zeegers, Ph.D. Thesis, Utrecht, 1966.

161. M. G. Davies, Ph.D. Thesis, University of Tennessee, 1968.

162. J. F. Alder, K. C. Thompson, and T. S. West, Anal. Chim. Acta, 50, 383 (1970).

163. C. Th. J. Alkemade and P. J. Th. Zeegers, in Spectro-chemical Methods of Analysis, J. D. Winefordner, Editor, Wiley-Interscience, New York, 1971.

164. E. M. Bulewicz, C. G. James, and T. M. Sugden, Proc. Roy. Soc., A235, 89 (1956).

165. P. J. Padley and T. M. Sugden, Trans. Faraday Soc., 54, 830 (1958).

166. P. J. Padley and T. M. Sugden, Trans. Faraday Soc., 56, 449 (1959).

167. C. W. Hand and G. B. Kistiakowski, J. Chem. Phys., 37, 1239 (1962).

168. C. P. Fenimore, Chemistry in Premixed Flames, Pergamon Press, Oxford, 1964.

169. E. M. Bulewicz and T. M. Sugden, Proc. Roy. Soc., A277, 143 (1964).

170. C. A. Arrington, W. Brennen, G. P. Glass, J. V. Michael, and H. Nike, J. Chem. Phys., 43, 525 (1965).

171. P. J. Th. Zeegers and C. Th. J. Alkemade, Combust. Flame, 9, 247 (1965).

172. R. Bleekrode and W. C. Nieuwpoort, J. Chem. Phys., 43, 3680 (1965).

173. A. von Engel and J. R. Cozens, in Fundamental Studies of Ions and Plasmas, H. D. Wilsted, Editor, Pisa, Italy, 1965, AGARD Conf. Proc. Ser. No. 8, Vol. 1 and 2, 1965.

174. P. J. Th. Zeegers and C. Th. J. Alkemade, <u>Combust.</u> <u>Flame</u>, <u>15</u>, 193 (1970).

175. J. C. Bell and D. Bradley, <u>Combust. Flame</u>, <u>14</u>, 225 (1970).

176. A. Fontijn, <u>Pure Appl. Chem.</u>, <u>39</u>, 287 (1974).

177. A. N. Haghurst and D. B. Kittleson, <u>Combust. Flame</u>, <u>31</u>, 37 (1978).

178. D. R. Jenkins, <u>Proc. Roy. Soc.</u>, <u>A239</u>, 493 (1966).

179. H. P. Hooymayers, Ph.D. Thesis, Utretch, 1966.

180. J. A. Fiorizo, R. N. Kinseley, and V. A. Fassel, <u>Spectrochim. Acta</u> <u>23B</u>, 413 (1968).

181. H. P. Hooymayers and P. L. Lijnse, <u>J. Quant. Spectrosc.</u> <u>Radiat. Transfer</u>, <u>9</u>, 995 (1969).

182. A. P. Thorne, <u>Spectrophysics</u>, Chapman and Hall, London, 1974.

183. W. S. Benedict and E. K. Plyler, <u>NBS Circ. No. 523</u>, 57 (1954).

184. R. H. Tourin and B. Krakow, <u>Appl. Opt.</u>, <u>4</u>, 237 (1965).

185. R. C. M. Learner, <u>Proc. Roy. Soc.</u>, <u>A269</u>, 311 (1962).

186. W. B. Zinman and S. I. Bogdan, <u>J. Chem. Phys.</u>, <u>40</u>, 588 (1964).

187. R. M. Fristrom and A. A. Westenberg, <u>Flame Structure</u>, McGraw-Hill, New York, 1965.

188. W. J. Waggener, <u>Ann. Physik</u>, <u>58</u>, 579 (1896).

189. E. L. Nichols, <u>Phys. Rev.</u>, <u>10</u>, 234 (1900).

190. A. Smithhells, <u>Trans. Inst. Gas. Eng.</u>, <u>117</u> (1905).

191. E. Griffiths and J. H. Awbery, <u>Proc. Roy. Soc.</u>, <u>123</u>, 401 (1929).

192. H. C. Hottel and F. P. Broughton, <u>Ind. Eng. Chem.</u>, <u>Anal. Ed.</u>, <u>4</u>, 166 (1932).

193. H. Klaükens and H. G. Wolfhard, <u>Proc. Roy. Soc.</u>, <u>193</u>, 512 (1948).

194. A Smeeton-Leah and N. Carpenter, Proc. 4th Symp. (Int.) on Combust., Cambridge, MA, 1952, The Williams and Wilkins Company, Baltimore, MD, p. 272.

195. R. Freidman and E. Burke, J. Chem. Phys., 22, 824 (1954).

196. W. E. Kaskan, Proc. 6th Symp. (Int.) on Combust., New Haven, CT, 1956, Reinhold Publishing Company, New York, p. 134.

197. V. Saners, Rev. Sci. Inst., 29, 917 (1958).

198. M. Kunugi and J. Hiroshi, Proc. 7th Symp. (Int.) on Combust., London and Oxford, UK, 1958, Butterworths, London, p. 942.

199. A. Yoshida and H. Tsugi, Proc. 7th Symp. (Int.) on Combust., London and Oxford, UK, 1958, Butterworths, London, p. 945.

200. C. M. Stover, Rev. Sci. Inst., 31, 605 (1960).

201. D. B. Thomas, J. Nes. NBS, 66C, 225 (1962).

202. R. M. Fristrom, Experimental Techniques for the Study of Flame Structure, Bumblebee Rept. 300, The John Hopkins University, 187 (1963).

203. G. F. Blackburn and F. R. Caldwell, J. Res. NBS, 68C, 41 (1964).

204. R. Smith, C. M. Stafford, and J. D. Winefordner, Anal. Chem., 41, 946 (1969).

205. R. Smith, Thermocouples for High Temperature Measurement, Internal Report, University of Florida, 1969.

206. J. Chedaille and Y. Braud, Industrial Flames, 1, Measurements in Flames, Arnold, London, 1972.

207. J. H. Kent and R. W. Bilger, 1st Australasian Conf. on Heat and Mass Transfer, Monash University, 1973, p. 39.

208. F. C. Lockwood and A. O. Odidi, Combustion Institute, European Symposium, University of Sheffield, UK, 1973, p. 501.

209. A. Sato, K. Hashita, M. Hasatoni, S. Sugiyama and J. Kimura, Combust. Flame, 24, 35 (1975).

210. R. M. Fristrom, in Combustion Measurements, Modern Techniques and Instrumentation, R. Goulard, Editor, Academic Press, New York, 1976.

211. O. I. Smith, Combust. Flame, 40, 187 (1981).

212. R. L. Farrow, P. L. Mattern, and L. A. Rahn, Appl. Opt., 21, 3119 (1982).

213. M. Gilbert and J. H. Lobdell, Proc. 4th Symp. (Int.) on Combust, Cambridge, MA, 1952, The Williams and Wilkins Company, Baltimore, MD, p. 285.

214. M. W. Thring, The Sciences of Flames and Furnaces, 2nd Ed., Chapman and Hall, London, 1962.

215. C. M. Ho, K. Jakus, and K. H. Parker, Combust. Flame, 27, 113 (1976).

216. A. A. Ahmed, Ph.D. Thesis, McGill University, 1971.

217. R. W. Bilger, in Combustion Measurements, Modern Techniques and Instrumentation, R. Goulard, Academic Press New York, 1976.

218. D. W. Moore, Aeron. Eng. Rev., 7, 5 (1948).

219. R. M. Fristrom, C. Grunfelder, and S. Farin, J. Phys. Chem., 64, 1386 (1960).

220. J. M. Beér and N. A. Chigier, Combustion Aerodynamics, Wiley, New York, 1972.

221. A. Maestre and A. Benoit, Proc. 14th Symp. (Int.) on Combust., University Park, PA, 1972, The Combustion Institute, Pittsburgh, PA, p. 719.

222. n.a., Appl. Opt., 20, 3103 (1981).

223. n.a., Appl. Opt., 21, A194 (1982).

224. G. Tiné, Gas Sampling and Chemical Analysis in Combustion Processes, AGARD 47, Pergamon Press, 1961.

225. A. Vranos, J. E. Faueher, and W. E. Curtis, Proc. 12th Symp. (Int.) on Combust., Poiters, France, 1968, The Combustion Institute, Pittsburgh, PA, p. 1051.

226. B. Lenze, Chemie Ing. Tech., 42, 287 (1970).

227. R. Fristrom, Int. J. Mass Spectrom. Ion Phys., 16, 15 (1975).

228. R. W. Bilger and R. E. Beck, Proc. 15th Symp. (Int.) on Combust., Tokyo, 1974, The Combustion Institute, Pittsburgh, PA, p. 341.

229. C. A. Stearns, F. J. Kohl, G. C. Fryburg, and R. A. Miller, in <u>Characterization of High Temperature Vapors and Gases</u>, Proc. 10th Materials Research Symp., National Bureau of Standards Special Publication No. 561, J. W. Hastie, Editor, Washington, DC, 1979.

230. W. J. Miller, in <u>Characterization of High Temperature Vapors and Gases</u>, Proc. 10th Materials Research Symp., National Bureau of Standards Special Publication No. 561, J. W. Hastie, Editor, Washington, DC, 1979, p. 443.

231. G. C. Eltenton, <u>J. Chem. Phys.</u>, <u>10</u>, 403 (1942).

232. S. N. Foner and R. L. Hudson, <u>J. Chem. Phys.</u>, <u>21</u>, 1374 (1954).

233. P. F. Knewstubb and T. M. Sugden, Proc. 7th Symp. (Int.) on Combust. London and Oxford, UK, 1958, Butterworths, London, p. 247.

234. P. F. Knewstubb and T. M. Sugden, <u>Nature</u>, <u>196</u>, 1311 (1962).

235. A. N. Hayhurst and T. M. Sugden, <u>Proc. Roy. Soc.</u>, <u>A239</u>, 36 (1966).

236. W. S. Young and E. L. Kuth, <u>Entropie</u>, <u>30</u>, 25 (1969).

237. R. V. Serauskas, G. R. Brown, and R. Petel, <u>Int. J. Mass Spectrom. Ion Phys.</u>, <u>16</u>, 69 (1975).

238. J. Deckers and A. Van Tiggelen, Proc. 7th Symp. (Int.) on Combust., London and Oxford, UK, 1958, Butterworths, London, p. 254.

239. R. M. Fristrom, <u>Science</u>, <u>140</u>, 297 (1963).

240. R. M. Fristrom, Proc. 6th Symp. (Int.) on Combust., New Haven, CT, 1956, Reinhold Publishing Company, New York, p. 96.

241. F. Smith, <u>Chem. Rev.</u>, <u>21</u>, 389 (1932).

242. H. Neubert, <u>Z. Tech. Phys.</u>, <u>24</u>, 180 (1949).

243. B. Lewis and G. Von Elbe, <u>J. Chem. Phys.</u>, <u>11</u>, 75 (1943).

244. J. W. Anderson and R. S. Fein, <u>J. Chem. Phys.</u>, <u>17</u>, 1268 (1949).

245. R. M. Fristrom and R. Prescott, Proc. 4th Symp. (Int.) on Combust., Cambridge, MA, 1952, The Williams and Wilkes Company, Baltimore MD, p. 268.

246. R. M. Fristrom, W. H. Avery, R. Prescott, and A. Mattuck, _J. Chem. Phys._, 22, 106 (1954).

247. C. Th. J. Alkemade, Ph.D. Thesis, Utrecht, 1954.

248. A. J. Borgers, M. J. Jongerius, and Tj. Hollander, _Appl. Spectrosc._, 34, 46 (1980).

249. A. Levy and F. J. Weinberg, _Combust. Flame_, 3, 229 (1959).

250. T. P. Pandya and F. J. Weinberg, _Proc. Roy. Soc._, 279, 554 (1964).

251. R. Kelly and P. J. Padley, _Proc. Roy. Soc._, A327, 345 (1972).

252. A. N. Hayhurst and N. R. Telford, _Combust. Flame_, 28, 67 (1977).

253. F. J. Weinberg, _Optics of Flames_, Butterworths, Washington, DC, 1963.

254. V. Dvorak, _Ann. Phys. Pz._, 9, 502 (1880).

255. H. Schardin, _Ergebn. exakt. Naturw._, 20, 303 (1942).

256. W. R. Keagy and H. H. Ellis, Proc. 3rd Symp. (Int.) on Combustion, Madison, WI, 1948, The Williams and Wilkins Company, Baltimore, MD, p. 667.

257. G. Dixon-Lewis and M. Wilson, _Trans. Faraday Soc._, 47, 1106 (1951).

258. J. W. Linnett, Proc. 4th Symp. (Int.) on Combust., Cambridge, MA, 1952, The Williams and Wilkins Company, Baltimore, MD, p. 20.

259. A. van Tiggelen and J. van Wonterghem, _Bull. Soc. Chim Belg._, 63, 235 (1954).

260. J. H. Burgoyne and F. J. Weinberg, _Proc. Roy. Soc._, A224, 286 (1954).

261. F. G. Weinberg, Proc. 6th Symp. (Int.) on Combust., New Haven, CT, 1956, Reinhold Publishing Company, New York, p. 765.

262. D. Simon, Proc. 7th Symp. (Int.) on Combust., London and Oxford, UK, 1958, Butterworths, London, p. 413.

263. J. Thovert, _Ann. Phys. Lpz._, 2, 369 (1914).

264. J. S. L. Philpot, *Nature, Lond.*, *141*, 283 (1938).

265. H. Svensson, *Arkiv. Kemi. Min. Geol.*, *22*, 1 (1946).

266. H. Gilbert, Proc. 6th Symp. (Int.) on Combust., New Haven CT, 1956, Reinhold Publishing Company, New York, p. 74.

267. D. R. Lintin and E. R. Wooding, *Brit. J. Appl. Phys.*, *10*, 159 (1959).

268. G. Dixon-Lewis and G. L. Isles, Proc. 8th Symp. (Int.) on Combust., Pasadena, CA, 1960, The Williams and Wilkins Company, Baltimore, MD, p. 448.

269. V. Ronchi, *La Prova dei Sisteme Ottici*, Zanichelli, Bolonga, 1925.

270. J. Euler and W. Hüppner, *Optik, Stuttgart*, *6*, 332 (1950).

271. H. Jeffree, *J. Sci. Inst.*, *33*, 29 (1956).

272. O. Kafri, *Opt. Lett.*, *5*, 555 (1980).

273. E. Keren, E. Bar-Ziv, I. Glatt, and O. Kafri, *Appl. Opt.*, *20*, 4263 (1981).

274. Z. Karny and O. Kafri, *Appl. Opt.*, *21*, 3326 (1902).

275. D. Marcuse, *Light Transmission Optics*, Van Nostrand, New York, 1972.

276. K. Bockasten, *J. Opt. Soc. Am.*, *51*, 943 (1961).

277. J. D. Algeo and M. B. Denton, *Appl. Spectrosc.*, *35*, 35 (1981).

278. L. Mach, *Anz. Akad. Wiss., Wien*, *28*, 223 (1891).

279. L. Mach, *Z. Instrumkde*, *12*, 89 (1892).

280. L. Zehnder, *Z. Instrumkde*, *11*, 275 (1891).

281. G. Hansen, *Z. Instrumkde*, *60*, 325 (1940).

282. M. M. El Wakil, in *Combustion Measurements: Modern Techniques and Instrumentation*, R. Goulard, Academic Press, New York, 1976.

283. S. I. Abdel-Khalik, Ph.D. Thesis, University of Wisconsin, 1973.

284. H. L. Olsen, Proc. 3rd Symp. (Int.) on Combust., Madison, WI, 1948, The Williams and Wilkins Company, Baltimore, MD, p. 663.

285. R. Ladenberg and D. Bershader, Physical Measurements in Gas Dynamics and Combustion, Oxford University Press, 1955.

286. C. L. Jaeck and M. M. El-Wakil, J. Heat Transfer, 86, 464 (1964).

287. F. J. Weinberg and N. B. Wood, Rev. Sci. Inst., 36, 227 (1959).

288. R. Kraushaar, J. Opt. Soc. Am., 40, 480 (1950).

289. J. R. Sterrett and J. R. Erwin, N. A. C. A. Tech. Note, 2827 (1952).

290. A. K. Oppenheim, P. A. Urtiew, and F. J. Weinberg, Proc. Roy. Soc., 291, 279 (1966).

291. M. J. R. Schwar and F. J. Weinberg, Nature, 221, 357 (1969).

292. M. J. R. Schwar and F. J. Weinberg, Proc. Roy. Soc., 311, 469 (1969).

293. D. W. Sweeney and C. M. Vest, Appl. Opt., 12, 2649 (1973).

294. D. W. Sweeney and C. M. Vest, Int. J. Heat Mass Transfer, 17, 1443 (1974).

295. D. T. Attwood, L. W. Coleman, and D. W. Sweeney, Appl. Phys. Lett., 26, 616 (1974).

296. E. N. Leith and J. Upatnieks, J. Opt. Soc. Am., 57, 975 (1967).

297. M. Kato and T. Suzuki, J. Opt. Soc. Am., 59, 303 (1969).

298. T. Tsuruta in Applications of Holography, E. S. Barrekette, W. E. Kock, T. Ose, J. Tsujiuchi, and G. W. Stroke, Editors, Plenum Press, New York, 1971.

299. L. D. Siebert and D. E. Gesiter, AIAA J., 6, 214 (1968).

300. D. A. Ansley, in Applications of Holography, F. S. Barrekette, W. E. Kock, T. Ose, J. Tsujiuchi, and G. W. Stroke, Editors, Plenum Press, New York, 1971,

301. G. O. Reynolds, in Combustion Measurements, Modern Techniques and Instrumentation, R. Goulard, Editor, Academic Press, New York, 1976.

302. C. M. Vest, in Combustion Measurements, Modern Techniques and Instrumentation, R. Goulard, Editor, Academic Press, New York, 1976.

303. D. W. Sweeney, in Combustion Measurements, Modern Techniques and Instrumentation, R. Goulard, Editor, Academic Press, New York, 1976.

304. C. M. Vest, Appl. Opt., 14, 601 (1975).

305. D. L. Reuss, Paper 81-16, Spring Meeting, Western States Section, Combustion Institute, Pullman Press, Washington, 1981.

306. G. P. Montgomery, Jr. and D. L. Reuss, Appl. Opt., 21, 1373 (1982).

307. L. O. Heflinger, R. F. Wuerker, and R. E. Brooks, J. Appl. Phys., 37, 642 (1966).

308. R. N. Bracewell, Aust. J. Phys., 9, 198 (1956).

309. W. Hauf and U. Grigull, in Advances in Heat Transfer, J. P. Hartnett and T. F. Irvine, Jr., Editors, Academic Press, New York, 1970.

310. D. Bershader and S. G. Prakash, in Combustion Measurements, Modern Techniques and Instrumentation, R. Goulard, Editor, Academic Press, New York, 1976.

311. A. Shirodkar, Phil. Mag., 15, 426 (1973).

312. R. M. Delaney and A. H. Weber, St. Louis University Report, 1962.

313. R. N. Weltmann and P. W. Kuhns, N.A.C.A. Tech. Note, 2580 (1951).

314. G. J. Mulhaney, Rev. Sci. Inst., 29, 87 (1958).

315. M. Camac, J. Chem. Phys., 34, 488 (1961).

316. D. G. Marlow, C. R. Nisewanger, and W. M. Cady, J. Apply. Phys., 20, 771 (1949).

317. J. E. Allen, Jr., W. R. Anderson, and D. R. Crosley, Opt. Lett., 1, 118 (1977).

318. Y. H. Pao, Editor, Optoacoustic Spectroscopy and Detection, Academic Press, New York, 1977.

319. W. R. Anderson, J. E. Allen, Jr., T. D. Fansler, and D. R. Crosley, in Characteristics of High Temperature Vapors and Gases, J. W. Hastie, Editor, Proc. 10th Materials Research Symp., National Bureau of Standards Special Publication No. 561, Washington, DC, 1979.

320. K. Tennal, G. J. Salamo, and R. Gupta, Appl. Opt., 21, 2135 (1982).

321. W. Zapka, P. Pokrowsky, and A. C. Tam, Opt. Lett., 7, 477 (1982).

322. H. Schmidt, Ann. Physik, 29, 971 (1909).

323. S. Silverman, J. Opt. Soc. Am., 39, 275 (1949).

324. National Bureau of Standards, Appl. Spect., 12, 126 (1958).

325. R. H. Tourin, Paper 63-WA-252, American Society of Mechanical Engineers, New York, 1963.

326. H. J. Babrov, J. Opt. Soc. Am., 56, 171 (1961).

327. L. A. Young, AIAA J., 3, 610 (1965).

328. S. Silverman, Proc. 3rd Symp. (Int.) on Combust., Madison, WI, 1948, The Williams and Wilkins Company, Baltimore, MD, p. 498.

329. W. S. Benedict and E. K. Plyler, NBS Circ. No. 523, 57 (1954).

330. V. V. Kandyba, Izv. Akad. Nauk. SSSR., 12, 387 (1948).

331. H. F. Quinn, Can. J. Res., 28, 411 (1951).

332. S. S. Penner, J. Chem. Phys., 19, 272 (1951).

333. G. H. Millar, J. G. Winans, O. A. Uyehara, and P. S. Myers, J. Opt. Soc. Am., 43, 609 (1953).

334. A. G. Sviridov and N. N. Sobolev, Zh. Eksperim i Teor. Fiz., 24, 93 (1953).

335. R. B. Lindsay, Introduction to Physical Statistics, Wiley, New York, 1941.

336. D. A. Dows, J. Chem. Phys., 27, 1430 (1957).

337. R. M. Goody, Atmospheric Radiation, Oxford University Press, Condon, 1964.

338. R. G. Siddall and I. A. McGrath, Proc. 9th Symp. (Int.) on Combust., Ithaca, NY, 1962, Academic Press, p. 102.

339. H. P. Broida, in Temperature, Its Measurements and Control in Science and Industry, Vol. 2, H. C. Wolfe, Editor, Reinhold Publishing Company, New York, 1955, p. 265.

340. E. E. Bell, P. B. Burnside, and F. P. Dickey, J. Opt. Soc. Am., 50, 1286 (1960).

341. G. N. Harding, M. F. Kimmit, J. H. Ludlow, P. Porteous, A. C. Prior, and V. Roberts, Proc. Phys. Soc., 77, 1069 (1961).

342. J. K. Roberts and A. R. Miller, Heat and Thermodynamics, Interscience, New York, 1960.

343. J. A. Sanderson, J. A. Curcio, and D. V. Estes, Phys. Rev., 74, 1221 (1948).

344. F. Rössler and H. Behrens, Optik, 6, 145 (1950).

345. N. N. Sobolev and T. I. Shchetinin, J. Exp. Theo. Phys. USSR, 20, 356 (1950).

346. F. Kurlbaum, Phys. Z., 3, 187 (1902).

347. C. Féry, Compt. Rend., 137, 909 (1903).

348. F. Henning and C. Tingwaldt, Z. Phys., 48, 805 (1928).

349. G. W. Jones, B. Lewis, J. B. Fraiut, and G. St. J. Perrott, J. Am. Chem. Soc., 53, 869 (1931).

350. F. P. Bundy and H. M. Strong, Proc. 3rd Symp. (Int.) on Combust., Madison, WI, 1948, The Williams and Wilkins Company, Baltimore, MD, p. 647.

351. H. M. Strong, F. P. Bundy, and R. A. Larson, Proc. 3rd Symp. (Int.) on Combust., Madison, WI, 1948, The Williams and Wilkins Company, Baltimore, MD, p. 641.

352. H. M. Strong and F. P. Bundy, J. Appl. Phys., 25, 1521 (1954); 25, 1527 (1954); 25, 1531 (1954).

353. J. R. Greig, Brit. J. Appl. Phys., 16, 957 (1965).

354. W. Snelleman, Combust. Flame, 11, 453 (1967).

355. W. Snelleman and J. A. Smit, *Metrologia*, **4**, 123 (1968).

356. W. Snelleman, in *Flame Emission and Atomic Absorption Spectrometry*, Vol. 1, J. A. Dean and T. C. Rains, Editors, Marcel Dekker, New York, 1969.

357. D. L. Thomas, *Combust. Flame*, **12**, 541 (1968).

358. I. A. Vasilieva, L. V. Deputatova, and A. P. Nefedov, *Combust. Flame*, **23**, 305 (1974).

359. J. W. Daily and C. H. Kruger, *J. Quant. Spectrosc. Radiat. Transfer*, **17**, 327 (1977).

360. R. M. Kowalik and C. H. Kruger, *J. Quant. Spectrosc. Radiat. Transfer*, **18**, 627 (1977).

361. H. Kohn, *Ann. Phys.*, **44**, 749 (1914).

362. H. G. Wolfhard and W. G. Parker, *Proc. Phys. Soc.*, **A65**, 2 (1952).

363. I. Reif, V. A. Fassel, and R. N. Kinseley, *Spectrochim. Acta*, **30B**, 163 (1975).

364. G. Kuhn and R. S. Tankin, *J. Quant. Spectrosc. Radiat. Transfer*, 8, 1281 (1968).

365. P. English and M. G. W. Dingle, *J. Sci. Inst.*, **43**, 121 (1966).

366. J. G. Clouston, A. G. Gaydon, and I. I. Glass, *Proc. Roy. Soc.*, 248, 429 (1958).

367. A. G. Gaydon and I. R. Hurle, *The Shock Tube in High Temperature Chemical Physics*, Chapman and Hall, London, 1963.

368. E. H. Carnevale, S. Wolnik, G. Larson, C. Carey, and G. W. Wares, *Phys. Fluids*, **10**, 1459 (1967).

369. D. L. Thomas, *Combust. Flame*, **12**, 569 (1968).

370. W. Lochte-Holtgreven, *Rept. Prog. Phys.*, **21**, 312 (1958).

371. R. H. Fowler and E. A. Milne, *Monthly Not. Roy. Astron. Soc.*, **83**, 403 (1923).

372. R. H. Fowler and E. A. Milne, *Monthly Not. Roy. Astron Soc.*, **84**, 499 (1924).

373. H. M. Crosswhite, The Spectrum of FeI, Johns Hopkins Spectrosc. Rept. No. 13, 1958.

374. J. O'M. Bockris, J. L. White, J. D. MacKenzie, Physiochemical Measurements at High Temperatures, Butterworths, London, 1959.

375. J. D. Winefordner, C. T. Mansfield, and T. J. Vickers, Anal. Chem., 35, 1611 (1963).

376. L. De Galan and J. D. Winefordner, J. Quant. Spectrosc. Radiat. Transfer, 7, 703 (1967).

377. I. Reif, V. A. Fassel, R. N. Kinseley, and D. J. Kalnicky, Spectrochim. Acta, 33B, 807 (1978).

378. T. G. Cowley, V. A. Fassel, and R. N. Kinseley, Spectrochim. Acta, 23B, 771 (1968).

379. J. B. Willis, J. O. Rasmuson, R. N. Kinseley, and V. A. Fassel, Spectrochim. Acta, 23B, 725 (1968).

380. V. A. Fassel, J. O. Rasmuson, R. N. Kinseley, and T. G. Cowley, Spectrochim. Acta, 25B, 559 (1970).

381. A. G. Gaydon and H. G. Wolfhard, Proc. Roy. Soc., 194A, 169 (1948).

382. J. C. Breeze and C. C. Ferriso, J. Chem. Phys., 40, 1276 (1964).

383. P. J. Hommert, R. Viskanta, and A. M. Mellor, Combust. Flame, 30, 295 (1977).

384. L. Bernath, H. N. Powell, G. A. Robinson, F. Weltz, and K. Wohl, Proc. Gen. Disc. Heat Transfer, 315 (1951).

385. E. T. Child and K. Wohl, Proc. 7th Symp. (Int.) on Combust., London and Oxford, UK, 1958, Butterworths, London, p. 215.

386. C. C. Ferriso, C. B. Ludwig, and F. P. Boynton, Proc. 10th Symp. (Int.) on Combust., Cambridge, UK, 1964, The Combustion Institute, Pittsburgh, PA, p. 161.

387. R. E. Furgenson and H. P. Broida, Proc. 5th Symp. (Int.) on Combust., Pittsburgh, PA, 1954, Reinhold Publishing Company, New York, p. 754.

388. P. F. Jessen and A. G. Gaydon, Proc. 12th Symp. (Int.) on Combustion, Poitiers, France, 1968, The Combustion Institute, Pittsburgh, PA, p. 481.

389. J. C. Cros, A. Bouvier, and J. Chevalegre, Combust. Flame, 16, 205 (1971).

390. F. Simmons, AIAA J., 5, 778 (1967).

391. H. P. Broida and J. H. Kostkowski, J. Chem. Phys., 25, 676 (1956).

392. R. C. M. Learner and A. G. Gaydon, Nature, 183, 292 (1959).

393. R. C. M. Learner, Proc. Roy. Soc., 269, 311 (1962).

394. G. Dieke and H. Crosswhite, J. Quant. Spectrosc. Radiat. Transfer, 2, 97 (1962).

395. H. P. Broida, J. Chem. Phys., 19, 1383 (1951).

396. K. E. Shuler, J. Chem. Phys., 19, 888 (1951).

397. K. E. Shuler and H. P. Broida, J. Chem. Phys., 20, 1383 (1952).

398. H. P. Broida and K. E. Shuler, J. Chem. Phys., 20, 168 (1952).

399. W. R. Kane and H. P. Broida, J. Chem. Phys., 21, 347 (1953).

400. H. J. Kostkowski and H. P. Broida, J. Opt. Soc. Am., 46, 246 (1956).

401. D. B. Vaidya, J. J. Horvath, and A. E. S. Green, Appl. Opt., 21, 3357 (1982).

402. L. S. Ornstein, Physica, 1, 797 (1934).

403. K. E. Shuler, J. Chem. Phys., 18, 1221 (1950).

404. N. Thomas, A. G. Gaydon, and C. Brewer, J. Chem. Phys., 20, 369 (1952).

405. G. Herzberg, Infrared and Raman Spectra, Van Nostrand, New York, 1945.

406. G. Herzberg, Molecular Spectra and Molecular Structure, Van Nostrand, New York, 1950.

407. M. E. Pillow, Proc. Phys. Soc., 68A, 547 (1955).

408. R. W. Nicholls, Proc. Phys. Soc., 69A, 741 (1956).

409. D. C. Jain, J. Quant. Spectrosc. Radiat. Transfer, 4, 427 (1964).

410. R. Watson and W. R. Ferguson, Proc. Phys. Soc., A69, 741 (1965).

411. J. E. Mentall and R. N. Nicholls, Proc. Phys. Soc., 86, 878 (1965).

412. K. E. Shuler, J. Chem. Phys., 18, 1221 (1950).

413. K. E. Shuler, J. Chem. Phys., 21, 340 (1953).

414. G. V. Marr, Can. J. Phys., 35, 1265 (1957).

415. A. Jones and P. J. Padley, Combust. Flame, 25, 1 (1975).

416. A. G. Gaydon and H. G. Wolfhard, Proc. Roy. Soc., 208, 63 (1951).

417. R. A. Durie, Proc. Phys. Soc., A65, 125 (1952).

418. J. U. White, J. Opt. Soc. Am., 32, 285 (1942).

419. N. J. Beck, S. K. Chen, O. A. Uyehara, J. S. Winans, and P. J. Myles, Proc. 5th Symp. (Int.) on Combust., Pittsburgh, PA, 1954, Reinhold Publishing Company, New York, p. 754.

420. R. F. Browner and J. D. Winefordner, Anal. Chem., 44, 247 (1972).

421. R. K. Hanson, P. L. Varghese, S. M. Schoenug, and P. K. Falcone, in Laser Probes for Combustion Chemistry, D. R. Crosley, Editor, American Chemical Society, Washington, DC, 1980.

422. J. Y. Wang, Appl. Opt., 14, 768 (1976).

423. R. K. Hanson, P. A. Kuntz, and C. H. Kruger, Appl. Opt., 16, 2045 (1977).

424. R. K. Hanson and P. K. Falcone, Appl. Opt., 17, 2477 (1978).

425. P. J. Th. Zeegers, R. Smith, and J. D. Winefordner, Anal. Chem., 40, 13 (1968).

426. P. J. Th. Zeegers, R. Smith, and J. D. Winefordner, Anal. Chem., 26A (1968).

427. E. Hinnov and H. Kohn, J. Opt. Soc. Am., 47, 156 (1957).

428. M. L. Parson, W. J. McCarthy, and J. D. Winefordner, _Appl. Spectrosc._, _20_, 233 (1966).

429. C. Th. J. Alkemade, _Appl. Opt._, _7_, 1261 (1968).

430. M. C. Drake, L. H. Grabner, and J. W. Hastie, in _Characterization of High Temperature Vapors and Gases_, J. W. Hastie, Editor, Proc. 10th Materials Research Symp., National Bureau of Standards, Special Publication No. 561, Washington, DC, 1979, p. 1105.

431. G. Fuchtbauer, _Phys. Z._, _21_, 322 (1920).

432. R. Ladenburg, _Z. Phys._, 4, 451 (1921).

433. F. H. Hoffman and H. Kohn, _J. Opt. Soc. Am._, _51_, 512 (1961).

434. W. W. McGee and J. D. Winefordner, _J. Quant. Spectrosc. Radiat. Transfer_, _7_, 261 (1967).

435. J. L. J. Rosenfeld and T. M. Sugden, _Combust. Flame_, _8_, 44 (1964).

436. L. de Galan and G. F. Samaey, _Spectrochim. Acta_, _25 B_ 245 (1970).

437. W. L. Garstang and C. N. Hinshelwood, _Proc. Roy. Soc._, _A130_, 640 (1931).

438. K. C. Lück and W. Thielen, _J. Quant. Spectrosc., Radiat. Transfer_, _20_, 71 (1978).

439. G. F. Kirkbright, M. Sargent, and S. Vetter, _Spectrochim. Acta_, _25B_, 465 (1970).

440. K. C. Lück and F. J. Müller, _J. Quant. Spectrosc. Radiat. Transfer_, _17_, 403 (1977).

441. R. M. Green and J. A. Miller, _J. Quant. Spectrosc. Radiat. Transfer_, _26_, 313 (1981).

442. P. K. Falcone, R. K. Hanson, and C. H. Kruger, Paper No. 79-53, Western States Section, The Combustion Institute Meeting, Berkeley, CA, 1979.

443. W. A. Bone, R. P. Fraser, and D. A. Winter, _Proc. Roy. Soc._, _114_, 402 (1927).

444. D. A. Ramsay, _J. Chem. Phys._, _20_, 1920 (1952).

445. R. G. W. Norrish, _Disc. Faraday Soc._, _14_, 16 (1953).

446. R. G. W. Norrish, G. Porter, and B. A. Thrush, <u>Proc. Roy. Soc.</u>, <u>227</u>, 423 (1955).

447. V. S. Letokhov, in <u>High-Resolution Laser Spectroscopy</u>, K. Shimada, Editor, Springer-Verlag, Berlin, 1976.

448. R. L. Farrow and L. A. Rahn, <u>Opt. Lett.</u>, <u>6</u>, 108 (1981).

449. J. E. M. Goldsmith, <u>Opt. Lett.</u>, <u>6</u>, 525 (1981).

450. J. E. M. Goldsmith and R. L. Farrow, <u>Opt. Lett.</u>, <u>7</u>, 215 (1982).

451. P. E. Walters, J. Lanauze, and J. D. Winefordner, <u>Spectrochim. Acta B</u>, submitted.

452. R. M. Measures, <u>Appl. Spectrosc.</u>, <u>32</u>, 381 (1978).

453. Lord Rayleigh, <u>Phil. Mag.</u>, <u>41</u>, 274 (1871).

454. M. Kerker, <u>The Scattering of Light</u>, Academic Press, New York, 1969.

455. R. W. Dibble and R. E. Hollenbach, Proc. 18th Symp. (Int.) on Combust., University of Waterloo, 1980, The Combustion Institute, Pittsburgh (PA), p. 1489.

456. M. Lapp, in <u>Laser Probes for Combustion Chemistry</u>, D. R. Crosley, Editor, American Chemical Society, Washington, DC, 1980.

457. M. Lapp and C. M. Penney, in <u>Advances in IR and Raman Spectroscopy</u>, Vol. 3, R. J. H. Clark and R. E. Hester, Editors, Heyden and Son, 1977.

458. F. Robben, in <u>Combustion Measurements: Modern Techniques and Instrumentation</u>, R. Goulard, Editor, Academic Press, New York, 1976

459. S. C. Graham, A. J. Grant, and J. M. Jones, <u>AIAA J.</u>, <u>12</u>, 1140 (1974).

460. T. M. Dyer, <u>AIAA J.</u>, <u>17</u>, 912 (1978).

461. R. W. Pitz, R. Cattolica, F. Robben, and L. Talbot, <u>Combust. Flame</u>, <u>27</u>, 313 (1976).

462. R. W. Dibble, R. E. Hollenbach, and G. D. Rambach, in <u>Laser Probes for Combustion Chemistry</u>, D. R. Crosley, Editor, American Chemical Society, Washington, DC, 1980.

463. I. Namer, V. Agrawal, R. K. Cheng, F. Robben, R. Schefer, and L. Talbot, Western States Section, The Combustion Institute, Stanford, CA, 1977.

464. G. D. Rambach, R. W. Dibble, and K. E. Hollenbach, Paper No. 79-51, Western States Section, The Combusttion Institute, Berkeley, CA, 1979.

465. R. W. Schefer, F. Robben, and R. K. Cheng, Combust. Flame, 38, 51 (1979).

466. R. W. Pitz and J. W. Daily, 2nd Int. Symp. on Turbulent Shear Flows, London, 1979.

467. R. A. Hill and D. L. Hartley, Appl. Opt., 13, 186 (1974).

468. G. O. Neeley, L. Y. Nelson, and A. B. Harvey, Appl. Spectrosc., 26, 553 (1972).

469. C. V. Raman, Ind. J. Phys., 2, 387 (1928).

470. D. L. Hartley, AIAA J., 12, 816 (1974).

471. W. D. Williams and J. W. L. Lewis, AIAA J., 13, 1269 (1975).

472. R. Bailly, M. Pealat, and J. P. E. Taran, Opt. Commun., 16, 68 (1976).

473. M. C. Drake and G. M. Rosenblatt, Chem. Phys. Lett., 44, 313 (1976).

474. W. Stricker, Combust. Flame, 27, 133 (1976).

475. R. S. Hickman, A. E. Kassem, and L. H. Liang, Appl. Spectrosc., 30, 179 (1976).

476. M. Pealat, R. Bailly, and J.P.E.Taran, Opt. Commun., 22, 91 (1977).

477. A. A. Boiarski, R. H. Barnes, and J. F. Kircher, Combust. Flame, 32, 111 (1978).

478. R. E. Setchell and J. A. Miller, Combust. Flame, 33, 23 (1978).

479. D. A. Stephens and W. R. Aiman, Combust. Flame, 31, 85 (1978).

480. D. P. Aeschliman, J. C. Cummings, and R. A. Hill, J. Quant. Spectrosc. Radiat. Transfer, 21, 293 (1979).

481. S. M. Schoenung and R. E. Mitchell, <u>Combust. Flame</u>, <u>35</u>, 207 (1979).

482. R. A. Hill, A. J. Mulac, D. P. Aeschliman, and W. L. Flower, <u>J. Quant. Spectrosc. Radiat. Transfer</u>, <u>21</u>, 213 (1979).

483. L. R. Sochet, M. Lucquin, M. Bridoux, M. Crunell-Cros, F. Grase, and M. Delahaye, <u>Combust. Flame</u>, <u>36</u>, 109 (1979).

484. J. H. Becthel, R. J. Blint, C. J. Dasch, and D. A. Weinberger, <u>Combust. Flame</u>, <u>42</u>, 197 (1981).

485. M. Lapp and D. L. Hartley, <u>Combust. Sci. Tech.</u>, <u>13</u>, 199 (1976).

486. S. Lederman, A. Celentano, and J. Glaser, <u>J. Phys. Fluids</u>, <u>22</u>, 1065 (1979).

487. D. A. Stephenson, Proc. 17th Symp. (Int.) on Combust., Leeds, UK, 1978, The Combustion Institute, Pittsburgh PA, p. 993.

488. P. F. Jessen, Gas Council Tech. Note, LRSTN, 207 (1971).

489. G. F. Widhopf and S. Lederman, <u>AIAA J.</u>, <u>9</u>, 309 (1971).

490. M. Lapp, L. M. Goldman, and C. M. Penney, <u>Science</u>, <u>175</u>, 1112 (1972).

491. C. J. Vear, P. J. Hendra, and J. J. MacFarlane, <u>JCS Chem. Commun.</u>, 381 (1972).

492. H. A. Szymanski, <u>Raman Spectroscopy, Theory and Practice</u>, Plenum Press, New York, 1974.

493. Y. Agarwal, T. Hadishi, and F. Robben, Paper No. 76-136, AIAA 14th Aerospace Sciences Meeting, Washington, DC, 1976.

494. W. Holzer, W. F. Murphy, and H. J. Bernstein, <u>J. Chem. Phys.</u>, <u>52</u>, 399 (1970).

495. D. G. Fouche and R. K. Cheng, <u>Phys. Rev. Lett.</u>, <u>29</u>, 536 (1972).

496. M. Lapp, C. M. Penney, and R. L. St. Peters, Project SQUID Tech. Rept. GE-1-PU, 1973.

497. S. Lederman and J. Bornstein, Project SQUID Tech. Rept. P1B-31-PU, 1973.

498. S. Lederman, *Prog. Energy Combust. Sci.*, <u>31</u>, 1 (1977).

499. M. Lapp, in *Laser Raman Gas Diagnostics*, M. Lapp and C. M. Penney, Editors, Plenum Press, New York, 1974.

500. J. J. Barrett and S. A. Myers, *J. Opt. Soc. Am.*, <u>61</u>, 1246 (1971).

501. V. G. Cooper, *Appl. Opt.*, <u>10</u>, 525 (1971).

502. R. L. Armstrong, *J. Opt. Soc. Am.*, <u>64</u>, 871 (1974).

503. R. L. Armstrong, *Appl. Opt.*, <u>14</u>, 383 (1975).

504. J. J. Barrett, *J. Opt. Soc. Am.*, <u>66</u>, 801 (1976).

505. M. C. Drake, *Opt. Lett.*, <u>7</u>, 440 (1982).

506. W. D. Williams, H. M. Powers, R. L. McGuire, J. H. Jones, L. L. Price, and J. W. L. Lewis, Paper No. 77-211, AIAA 15th Aerospace Sciences Meeting, Washington, DC, 1977.

507. W. H. Smith, *Opto-elect.*, <u>4</u>, 161 (1972).

508. D. P. Aeschliman and R. E. Setchell, *Appl. Spectrosc.*, <u>29</u>, 426 (1975).

509. B. T. Zinn, Editor, *Experimental Diagnostics in Gas Phase Combination Systems*, American Institute of Aeronautics and Astronautics, New York, 1977.

510. A. C. Eckbreth, *J. Appl. Phys.*, <u>48</u>, 4473 (1977).

511. A. C. Eckbreth, Project SQUID Tech. Rept. UTRC-4-PU, 1976.

512. R. W. Terhune, *Bull. Am. Phys. Soc.*, <u>8</u>, 359 (1963).

513. P. D. Maker and R. W. Terhune, *Phys. Rev.*, <u>137</u>, A801, (1965).

514. P. R. Regnier and J. P. E. Taran, *Appl. Phys. Lett.*, <u>23</u>, 340 (1973).

515. P. R. Regnier, F. Moya, and J. P. E. Taran, *AIAA J.*, <u>12</u>, 826 (1974).

516. F. Moya, S. A. J. Druet, and J. P. E. Taran, *Opt. Commun.*, <u>13</u>, 169 (1975).

517. F. Moya, S. Druet, M. Pealat, and J. P. E. Taran, Paper No. 76-29, AIAA 14th Aerospace Sciences Meeting, Washington, DC, 1976.

518. W. M. Tolles, J. W. Nibler, J. R. McDonald, and A. B. Harvey, Appl. Spectrosc., 31, 253 (1977).

519. I. A. Stenhouse, D. R. Williams, J. B. Cole, and M. D. Swords, Appl. Opt., 18, 3819 (1979).

520. T. W. Hansch, Appl. Opt., 11, 895 (1972).

521. R. Wallenstein and T. W. Hansch, Appl. Opt., 13, 1625 (1974).

522. A. B. Harvey, R. L. Byer, and B. S. Hudson, J. Chem. Phys., 61, 2466 (1974).

523. J. W. Nibler, W. M. Shaub, J. R. McDonald, and A. B. Harvey, Vib. Spectra. Struct., 6, 173 (1977).

524. A. C. Eckbreth, Appl. Phys. Lett., 32, 421 (1978).

525. G. Laufer, K. B. Miles, and D. Santavicca, Opt. Commun., 31, 242 (1979).

526. K. A. Marko and L. Rimai, Opt. Lett., 4, 211 (1979).

527. R. J. Hall, Combust. Flame, 35, 47 (1979).

528. A. C. Eckbreth and R. J. Hall, Combust. Flame, 36, 87 (1979).

529. G. Laufer and R. B. Miles, Opt. Commun., 28, 250 (1979).

530. A. Compaan and S. Chandra, Opt. Lett., 4, 170 (1979).

531. Y. Prior, Appl. Opt., 19, 1741 (1980).

532. J. A. Shirley, R. J. Hall, and A. C. Eckbreth, Opt. Lett., 5, 380 (1980).

533. W. B. Roh, P. W. Schreiber, and J. P. E. Taran, Appl. Phys. Lett., 29, 174 (1976).

534. G. L. Switzer, L. P. Goss, W. M. Roquemore, R. P. Bradley, P. W. Schreiber, and W. B. Roh, Appl. Opt., 18, 2343 (1979).

535. A. C. Eckbreth, Combust. Flame, 39, 133 (1980).

536. L. A. Rahn, L. J. Zych, and P. L. Mattern, Opt. Commun., 30, 249 (1979).

537. J. A. Shirley, A. C. Eckbreth, and R. J. Hall, Proc. 16th JANNAF Combust. Meeting, Monterey, CA, 1979.

538. R. J. Hall, J. A. Shirley, and A. C. Eckbreth, Opt. Lett., 4, 87 (1979).

539. I. R. Beattie, J. D. Black, and T. R. Gilson, Combust. Flame, 33, 101 (1979).

540. R. T. Lynch, Jr., S. D. Kramer, H. Lotem, and N. Bloembergen, Opt. Commun., 16, 372 (1976).

541. R. W. Minck, R. W. Terhune, and W. G. Rado, Appl. Phys. Lett., 3, 181 (1963).

542. N. Bloembergen, Am. J. Phys., 11, 989 (1967).

543. M. Maier, Appl. Phys., 11, 209 (1976).

544. F. A. Korolev, O. M. Vokhnik, and V. I. Odintsov, Sov. Tech. Phys. Lett., 2, 86 (1976).

545. S. A. Borman, Anal. Chem., 54, 1021A (1982).

546. W. J. Jones and B. P. Stoicheff, Phys. Rev. Lett., 13, 657 (1964).

547. A. Lau, W. Wernicki, M. Pfeiffer, K. Lenz, and H. J. Weigmann, in Advances in Raman Spectroscopy, Vol. 1, J. P. Mathieu, Editor, Heyden and Son, London, 1973.

548. Y. R. Shen, Rev. Mod. Phys., 48, 1 (1978).

549. P. L. Mattern and L. A. Rahn, Proc. Am. Chem. Soc. Meet., Houston, TX, 1980.

550. R. H. Pantell and H. E. Putoff, Fundamentals of Quantum Electronics, Wiley, New York, 1969.

551. P. Lallemand, in The Raman Effect, A. Anderson, Editor, Dekker, New York, 1971.

552. A. Owyoung and L. A. Rahn, IEEE J. Quantum Electron. QE-15, 25D (1979).

553. P. E. Perkins, Appl. Spectrosc., 34, 617 (1980).

554. N. Omenetto, R. Browner, J. D. Winefordner, G. Rossi, and P. Benetti, Anal. Chem., 44, 1683 (1972).

555. H. Haraguchi, B. Smith, S. Weeks, D. J. Johnson and J. D. Winefordner, Appl. Spectrosc., 31, 156 (1977).

556. H. Haraguchi and J. D. Winefordner, *Appl. Spectrosc.*, 31, 195 (1977).

557. H. Haraguchi and J. D. Winefordner, *Appl. Spectrosc.*, 31, 340 (1977).

558. H. Haraguchi, S. Weeks, and J. D. Winefordner, *Can. J. Spectrosc.*, 22, 61 (1977).

559. N. H. Wrobel and N. H. Pratt, Proc. 17th Symp. (Int.) on Combust., Leeds, UK, 1978, The Combustion Institute, Pittsburgh, PA, p. 957.

560. R. M. Kowalik and C. H. Kruger, *Combust. Flame*, 34, 135 (1979).

561. G. C. Alessandretti, S. Benecchi, and F. Cignoli, *Appl. Opt.*, 20, 2765 (1981).

562. W. R. Anderson, R. J. Decker, and A. J. Kotlar, *Combust. Flame*, 48, 163 (1982).

563. N. Omenetto and J. D. Winefordner, *Crit. Rev. Anal. Chem.*, 13, 59 (1981).

564. J. O. Berg and W. L. Shackelford, *Appl. Opt.*, 18, 2093 (1979).

565. C. C. Wang and L. I. Davis, Jr., *Appl. Phys. Lett.*, 25, 34 (1974).

566. C. Chan and J. W. Daily, *Appl. Opt.*, 19, 1963 (1980).

567. D. R. Crosley and G. P. Smith, *Appl. Opt.*, 19, 517, (1980).

568. R. Cattolica, *Appl. Opt.*, 20, 1156 (1981).

569. R. P. Lucht, N. M. Laurendeau, and D. W. Sweeney, *Appl. Opt.*, 21, 3729 (1982).

570. J. D. Bradshaw, J. Bower, S. Weeks, K. Fujiwara, N. Omenetto, H. Haraguchi, and J. D. Winefordner, in Characterization of High Temperature Vapors and Gases, J. W. Hastie, Editor, Proc. 10th Materials Research Symp., National Bureau of Standards Special Publication No. 561, Washington, DC, 1979, p. 1079.

571. G. Ribaud, *Traité de Pyrométrie*, Ed. l'Optique, Paris, 1931.

572. C. Th. J. Alkemade, *Pure Appl. Chem.*, 23, 73 (1970).

573. W. L. Dimpfl and J. L. Kinsey, J. Quant. Spectrosc. Radiat. Transfer, 21, 233 (1979).

574. I. L. Chidsey and D. R. Crosley, J. Quant. Spectrosc. Radiat Transfer, 23, 187 (1980).

575. A. Goldman and J. R. Gillis, J. Quant. Spectrosc. Radiat. Transfer, 25, 111 (1981).

576. D. R. Crosley and G. P. Smith, Combust. Flame, 44, 27 (1982).

577. W. R. Anderson, Paper 3, Eastern States Meeting of the Combustion Institute, Atlanta, 1979.

578. C. Chan, Ph.D. Thesis, University of California at Berkeley, 1979.

579. R. L. MacKenzie and K. P. Gross, Appl. Opt., 20, 2153 (1981).

580. T. Ozaki, Y. Matsui, and T. Ohsawa, J. Appl. Phys., 52, 2593 (1981).

581. D. A. Leonard, Tech. Rept. AFAPL-Tr-74-100, 1974.

582. H. G. Wagner, Proc. 17th Symp. (Int.) on Combust., Leeds, UK, 1978, The Combustion Institute, Pittsburgh, PA, p. 3.

583. E. P. Muntz, Phys. Fluids, 5, 80 (1962).

584. L. Huldt, Spectral Investigation of Electric Arc and Air-Acetylene Flame with Special Emphasis on Their Utilization as Excitation Sources in Quantitative Spectral Analysis (in German), Uppsala, Almqvist och Wiksells, 1948.

585. H. Belcher and T. M. Sugden, Proc. Roy. Soc., 201, 480 (1950).

586. H. Belcher and T. M. Sugden, Proc. Roy. Soc., 202, 17 (1950).

587. R. F. Porter, Combust. Flame, 14, 275 (1970).

588. H. Silla and T. J. Dougherty, Combust. Flame, 18, 65 (1972).

589. G. Brule, P. Michaud, and A. Barassin, Combust. Flame, 21, 33 (1973).

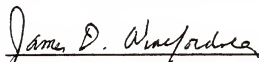590. D. Bradley and S. M. A. Ibrahim, Combust. Flame, 24, 169 (1975).

591. J. R. Cozens, J. Electron., 19, 61 (1965).

592. M. C. Attard, Ph.D. Thesis, Oxford, 1966.

593. R. N. Ramachandran and Lakshmenarayanan, Proc. Nat.
Acad. Sci. U.S., 68, 2236 (1971).

594. L. A. Shep and B. F. Logan, IEEE Trans. Nucl. Sci.,
21, 21 (1974).

595. R. Gordon, G. T. Herman, and S. A. Johnson, Sci. Am.,
233, 56 (1976).

596. R. A. Brooks and G. Dichiro, Phys. Med. Bio., 21, 689,
(1976).

597. R. J. Santoro, H. G. Semerjian, P. J. Emmerman,
R. Goulard, and R. Shabahang, in Laser Probes for
Combustion Chemistry, D. R. Crosley, Editor, American
Chemical Society, Washington, DC, 1980.

598. M. A. Fernandez and G. J. Bastiaans, Appl. Spectrosc.,
33, 145 (1979).

599. R. G. Joklik and J. W. Daily, Appl. Opt., 21, 4158
(1982).

600. M. J. Dyer and D. R. Crosley, Opt. Lett., 7, 382
(1982).

601. G. Kychakoff, R. D. Howe, R. K. Hanson, and J. D.
McDaniel, Appl. Opt., 21, 3225 (1982).

602. M. Aldén, H. Edner, G. Holmstedt, S. Svanberg, and
T. Högberg, Appl. Opt., 21, 1236 (1982).

603. M. Aldén, H. Edner, and S. Svanberg, Appl. Phys.,
29B, 93 (1982).

604. M. Aldén, P. Grafström, H. Lundberg, and S. Svanberg,
Opt. Lett., 8, 241 (1983).

605. D. L. Hartley, in Laser Probes for Combustion Chemistry,
D. R. Crosley, Editor, American Chemical Society, Wash-
ington, DC, 1980.

606. M. B. Long, B. F. Webber, and R. K. Chang, Appl. Phys.
Lett., 34, 22 (1979).

607. B. F. Webber, M. B. Long, and R. K. Chang, Appl. Phys.
Lett., 34, 22 (1979).

608. M. C. Escorda and M. B. Long, AIAA J., in press.

609. J. K. Smith, Paper 80-0137, SAE Automotive Engineering Congress and Exposition, 1980.

610. S. Warsaw, M. Lapp, C. M. Penney, and M. C. Drake, in Laser Probes for Combustion Chemistry, D. R. Crosley, Editor, American Chemical Society, Washington, DC, 1980.

611. G. L. Switzer, W. H. Roquemore, R. P. Bradley, P. W. Schreiber, and W. R. Roh, in Laser Probes for Combustion Chemistry, D. R. Crosley, Editor, American Chemical Society, Washington, DC, 1980.

612. S. Fuji, M. Gomi, and Y. Jin, Combust. Flame, 48, 232 (1982).

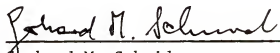613. J. H. Bechtel and A. R. Charplyry, Proc. IEEE, 70, 658 (1982).

BIOGRAPHICAL SKETCH

Melanie Louise Elder was born on August 28, 1955, at Nellis Air Force Base, Nevada. She graduated from Wagner High School at Clark Air Base, Philippines in June, 1973. She attended Agnes Scott College in Decatur, Georgia, for two years and then transferred to the Florida State University in Tallahassee, Florida, where she graduated in December, 1977, with Bachelor of Science degrees in both chemistry and biological sciences. After working with the U.S. Geological Survey as a hydrologic chemist, Melanie entered the graduate program of the Department of Chemistry at the University of Florida in September, 1978. She is currently a candidate for the Ph.D. degree specializing in analytical spectroscopy.
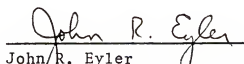
I certify that I have read this study and that in my opinion it conforms to acceptable standards of scholarly presentation and is fully adequate, in scope and quality, as a dissertation for the degree of Doctor of Philosophy.

James D. Winefordner, Chairman
Graduate Research Professor of
  Chemistry

I certify that I have read this study and that in my opinion it conforms to acceptable standards of scholarly presentation and is fully adequate, in scope and quality, as a dissertation for the degree of Doctor of Philosophy.

Gerhard M. Schmid
Associate Professor of Chemistry

I certify that I have read this study and that in my opinion it conforms to acceptable standards of scholarly presentation and is fully adequate, in scope and quality, as a dissertation for the degree of Doctor of Philosophy.
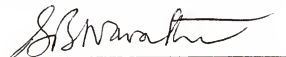
John R. Eyler
Associate Professor of Chemistry

I certify that I have read this study and that in my opinion it conforms to acceptable standards of scholarly presentation and is fully adequate, in scope and quality, as a dissertation for the degree of Doctor of Philosophy.

Leslie H. Oliver
Associate Professor of Computer
and Information Sciences

I certify that I have read this study and that in my opinion it conforms to acceptable standards of scholarly presentation and is fully adequate, in scope and quality, as a dissertation for the degree of Doctor of Philosophy.

Shamkant B. Navathe
Associate Professor of Computer
and Information Sciences

This dissertation was submitted to the Graduate Faculty of the Department of Chemistry in the College of Liberal Arts and Sciences and to the Graduate Council, and was accepted as partial fulfillment of the requirements for the degree of Doctor of Philosophy.

August 1983.

Dean for Graduate Studies and
Research